AD-A134 726 RADIATIVE PROPERTIES OF A NUCLEAR THERMAL SOURCE SIMULATOR(U) INFORMATION SCIENCE INC SANTA BARBARA CA W F DUDZIAK ET AL. 31 DEC 80 RM80-ISI101 DNA-5790F 1/2

UNCLASSIFIED DNA001-79-C-0393 F/G 14/2 NL

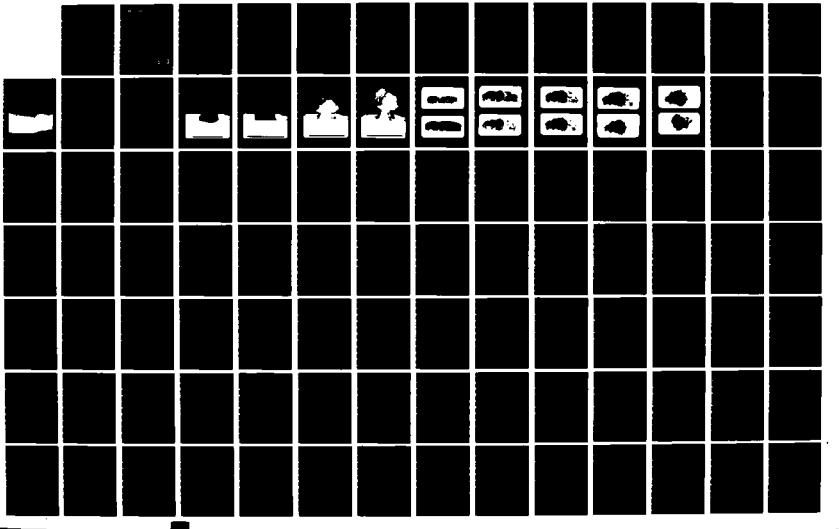

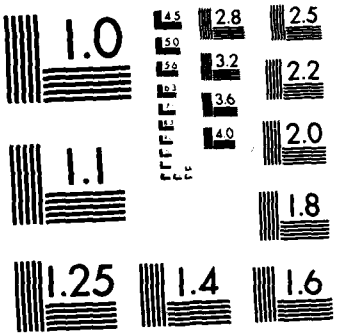

(12)

DNA 5790F

# RADIATIVE PROPERTIES OF A NUCLEAR THERMAL SOURCE SIMULATOR

Information Science, Inc.
123 West Padre Street
Santa Barbara, California 93105

31 December 1980

Final Report for Period 1 August 1979—31 December 1980

CONTRACT No. DNA 001-79-C-0393



THIS WORK WAS SPONSORED BY THE DEFENSE NUCLEAR AGENCY
UNDER RDT&E RMSS CODE B344079462 H53BAXSX37722 H2590D.



Prepared for
Director
DEFENSE NUCLEAR AGENCY
Washington, DC 20305

UNCLASSIFIED

SECURITY CLASSIFICATION OF THIS PAGE *(When Data Entered)*

| REPORT DOCUMENTATION PAGE | | READ INSTRUCTIONS BEFORE COMPLETING FORM |
|---|---|---|
| 1. REPORT NUMBER<br>DNA 5790F | 2. GOVT ACCESSION NO.<br>AD-A134 726 | 3. RECIPIENT'S CATALOG NUMBER |
| 4. TITLE *(and Subtitle)*<br>RADIATIVE PROPERTIES OF A NUCLEAR THERMAL SOURCE SIMULATOR | | 5. TYPE OF REPORT & PERIOD COVERED<br>Final Report for Period 1 Aug 79—31 Dec 80<br>6. PERFORMING ORG. REPORT NUMBER<br>RM80 - ISI101 |
| 7. AUTHOR(s)<br>Walter F. Dudziak<br>Pradip V. Lad | | 8. CONTRACT OR GRANT NUMBER(s)<br>DNA 001-79-C-0393 |
| 9. PERFORMING ORGANIZATION NAME AND ADDRESS<br>Information Science, Inc.<br>123 West Padre Street<br>Santa Barbara, California 93105 | | 10. PROGRAM ELEMENT, PROJECT, TASK AREA & WORK UNIT NUMBERS<br>Subtask H53BAXSX377-22 |
| 11. CONTROLLING OFFICE NAME AND ADDRESS<br>Director<br>Defense Nuclear Agency<br>Washington, DC 20305 | | 12. REPORT DATE<br>31 December 1980<br>13. NUMBER OF PAGES<br>146 |
| 14. MONITORING AGENCY NAME & ADDRESS*(if different from Controlling Office)* | | 15. SECURITY CLASS *(of this report)*<br>UNCLASSIFIED<br>15a. DECLASSIFICATION/DOWNGRADING SCHEDULE<br>N/A since UNCLASSIFIED |

16. DISTRIBUTION STATEMENT *(of this Report)*
Approved for Public Release; Distribution Unlimited.

17. DISTRIBUTION STATEMENT *(of the abstract entered in Block 20, if different from Report)*

18. SUPPLEMENTARY NOTES
This work was sponsored by the Defense Nuclear Agency under RDT&E RMSS Code B344079462 H53BAXSX37722 H2590D.

19. KEY WORDS *(Continue on reverse side if necessary and identify by block number)*

| | |
|---|---|
| Thermal Radiation Devices | Film Measurement Methods |
| TRS (Gas Filled) | Black Body Radiation |
| LOX TRS | Spectral Power |
| Thermal Nuclear Simulator | Spectral Temperature |

20. ABSTRACT *(Continue on reverse side if necessary and identify by block number)*
This report summarizes some of the thermal properties of an SAI thermal radiation source (TRS). Its purpose is to illustrate some of the significant time dependent surface fluctuations that do exist in such a radiator which are not present in a nuclear device. These surface fluctuations should be considered in planning experiments, as well as in the interpretation of the collected data. The report also illustrates the courseness of the approximation of the actual source by current computer codes. In these

DD FORM 1 JAN 73 1473 EDITION OF 1 NOV 65 IS OBSOLETE

UNCLASSIFIED

SECURITY CLASSIFICATION OF THIS PAGE *(When Data Entered)*

20. ABSTRACT (Continued)

codes each module is represented by a linear array of constant point source radiators along the axis of symmetry of the module.

Summarized are the thermal flux, fluence and spectral data derived from two film records of a typical gas filled SAI thermochemical simulator that releases energy through aluminum oxidation reactions. From this summary an estimate is made of the total emissivity of this aluminum oxidation reaction.

Also presented in the Annex are preliminary measurements and analysis of thermal data of a liquid oxygen system. These measurements were made during the development tests of this LOX TRS source for the MILLRACE program. Spectral surface measurements show that this source radiates at a significantly higher temperature and may possess a spectral emissivity that differs significantly from the gas module TRS source.

## SUMMARY

This report summarizes some of the thermal properties of an SAI Thermal Radiation Source (TRS). Its purpose is three fold. First, it illustrates some of the significant time dependent surface fluctuations that do exist in such a radiator which do not exist in a nuclear device that the TRS intends to simulate. These surface fluctuations should be considered in planning experiments, as well as, in the interpretation of the collected data. Second, it preserves through documentation some of the previously collected unreduced TRS data which was contained on film records which no longer exist. Third, it illustrates the courseness of the approximation of the actual source by computer codes. In these codes each module is represented by a linear array of constant point source radiators along the axis of symmetry of the module.

Summarized are the thermal flux, fluence, and spectral temperature data derived from two film records of a typical gas module SAI thermochemical nuclear simulator that releases energy through aluminum oxidation reactions. From this summary an estimate is made of the total emissivity of this aluminum oxidation reaction.

Also presented in an Annex are preliminary analysis of thermal data of a liquid oxygen TRS system. These measurements were made during the December 1980 development tests of the LOX TRS source in preparation for the MILLRACE program. Spectral surface measurements show that this source radiates at a significantly higher temperature and may possess a spectral emissivity that differs significantly from the gas module TRS source.

# PREFACE

Many individuals from various research organizations contributed to the success of this study. To these individuals we are very grateful. It is a pleasure to acknowledge various useful discussions with John Dishon and Burton Chambers III of Science Applications Inc. These had a direct bearing on the content of this report. Special thanks are given to Dr. George Ullrich, SPSS, and Mr. R. C. Webb, SPTD, of the Defense Nuclear Agency for their suggestions and helpful guidance.

Mr. Dale Fastle of Sandia Laboratories permitted use of the films he collected and provided the calibration information. For these and the many valuable discussions we are especially grateful.

Conversion Factors For U.S. Customary Units
To Metric (SI) Units Of Measurement And
Black Body Constants

| TO CONVERT FROM | TO | MULTIPLY BY |
|---|---|---|
| erg | joule (J) | 1.000 000 x E -07 |
| erg/second | watt(W) | 1.000 000 x E -07 |
| calories(thermochemical) | joules(J) | 4.184 000 |
| cal(thermochemical)/$cm^2$ | mega joule/$m^2$($MJ/m^2$) | 4.184 000 x E -02 |
| foot | meter(m) | 3.048 000 x E -01 |
| inch | meter(m) | 2.540 000 x E -02 |
| kiloton | tera joules | 4.184 |

$k$ = 1.380 622 x E -23 ($J/^0K$)

$h$ = 6.626 196 x E -34 (Js)

$c$ = 2.997 925 x E +08 (m/s)

$\frac{hc}{k}$ = 1.438 800 x E -02 ($m^0K$)

$\sigma$ = 5.669 606 x E -08 ($W/(m^2-^0K^4)$)

TABLE OF CONTENTS

## LIST OF ILLUSTRATIONS

LIST OF ILLUSTRATIONS
(continued)

LIST OF ILLUSTRATIONS
(continued)

LIST OF ILLUSTRATIONS
(continued)

# SECTION 1

## INTRODUCTION

1.0 During the summer of 1979 seven independent Thermal Radiation Sources (TRS) were assembled at the Air Force Weapon Laboratory test facility at Kirtland AFB New Mexico. In these seven tests the TRS consisted of sixteen modules. For orientation, the TRS device is shown in Figures 1 and 2. As illustrated the assembled device[1-2] consisted of individual modules of inflated plastic cylinders with length to diameter ratios of 4. The 6 mil wall plastic cylinder was filled with oxygen to an overpressure of 0.1 psi. When inflated to this overpressure the TRS module became a cylinder with a length of 6 meters and a diameter of 1.52 meters. Prior experiments[1] proved that the fluidizer could easily spray powdered aluminum pressured by nitrogen and mix aluminum with oxygen over a distance of 6 meters. Each cylinder[2] provided an $Al/O_2$ weight ratio in the TRS module of 3.5 which was capable of peak power output that could vary from $4 \times 10^7$ watts to $1.5 \times 10^8$ watts. The total energy output of a module[2] is approximately $9 \times 10^6$ calories (i.e., $3.8 \times 10^7$ joules)

As illustrated in Figure 2 the fluidized sprays in the aluminum powder which on mixing with the oxygen is ignited to create a rapid exothermic oxidation of aluminum through the chemical reaction:

$$2Al + 1.5O_2 \rightarrow Al_2O_3 \qquad \ldots 1$$

This reaction will release $3.89 \times 10^6$ calories/mole (or $7.21 \times 10^3$ calories per gram of metal). Since in this reaction the specific energy release of this metallic salt is relatively high, most of the chemical energy is released in the form of visible and near infra red light.

To produce a thermal burst of high intensity through this oxidation process, large quantities (> 1.0 kilograms) of fine powdered aluminum must be ignited and burned in a relatively short time ( < 1 second ). This can only be accomplished by thorough intermixing of aluminum with oxygen. A more detail description of this TRS source is presented in references 1 and 2.

An overview of a typical TRS ignition is illustrated in color photographs presented in Figures 3 through 6. Figures 7 through 11 illustrate in black and

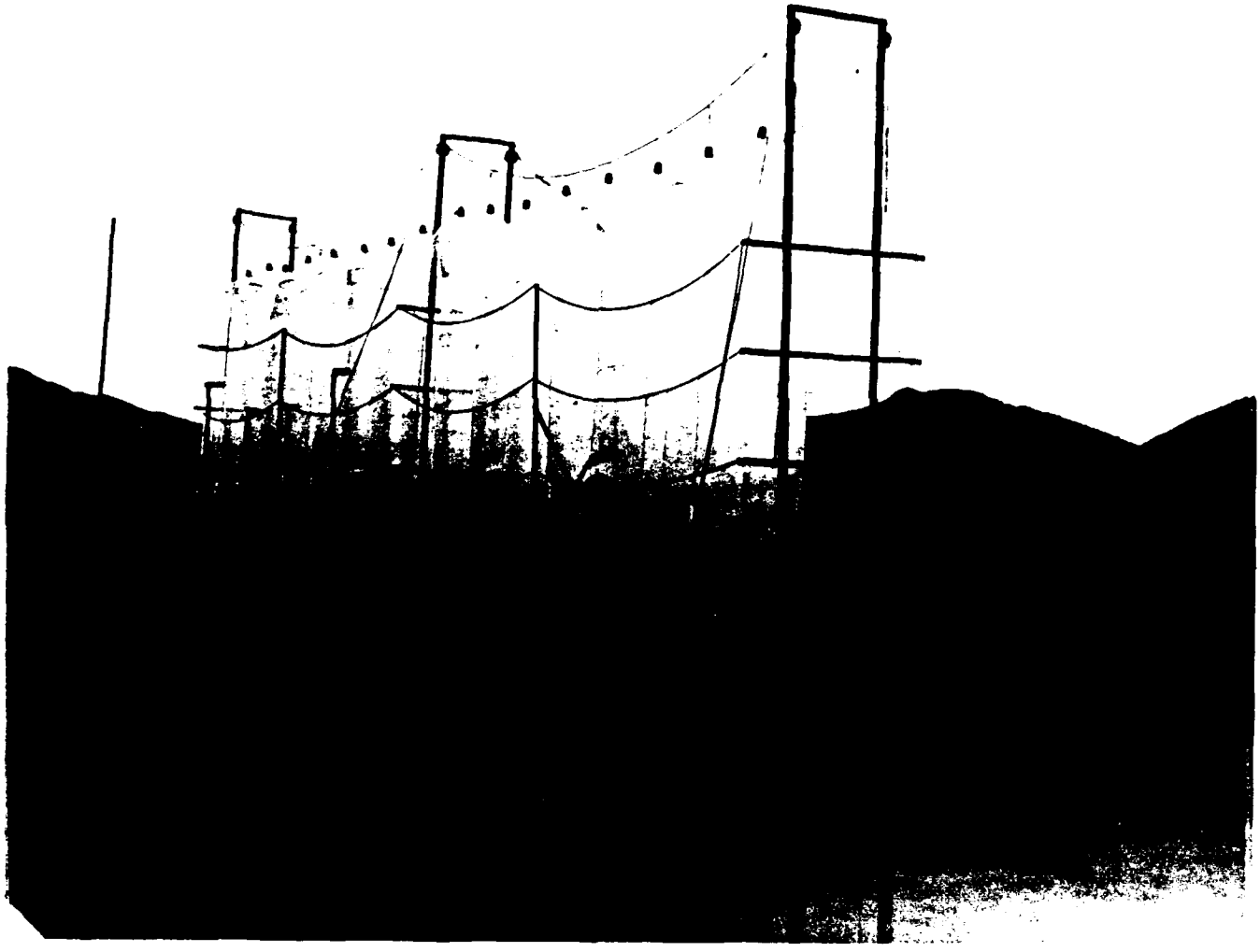

FIGURE 1. Pre-Detonation 16-Module Vertical C-System TRS Array

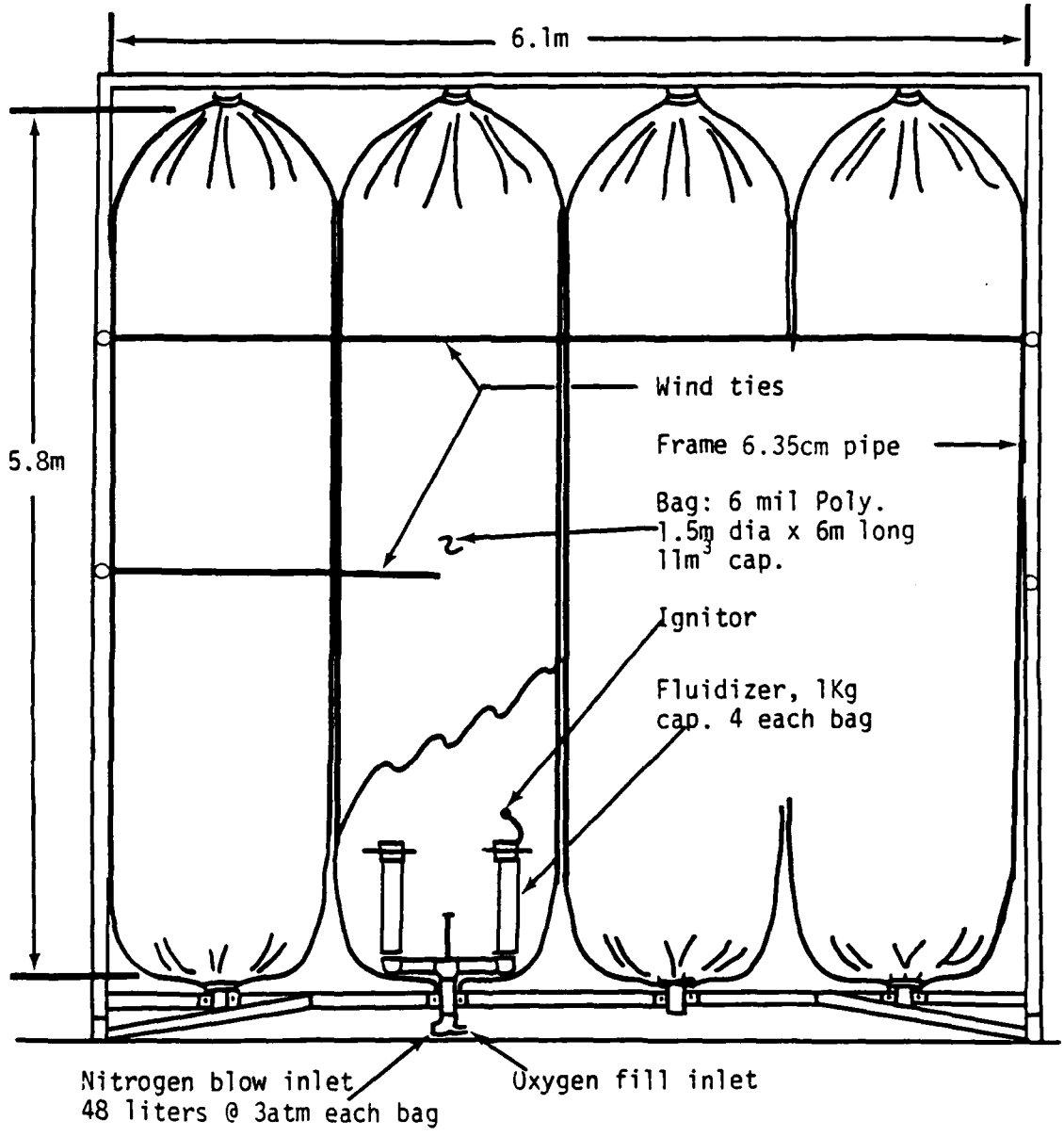


**FIGURE 2. A 4 Module Verticle C - System TRS Array**

white photographs the growth of the thermal source through the first second in 0.1 second intervals.

To characterize the thermal output of this TRS source two precision cameras were used. These two cameras were positioned 454 feet ( 138.4 meters) from the center of the source along a line perpendicular to the 16 module surface area. One camera having a focal length of 82.6 mm recorded the morphology of the TRS source on a 35 mm black and white film format at a framing speed of 100 frames per second. The data resulting from an analysis of selected frames from this film is presented in Section 3.0. The second camera recorded on 35 mm black and white film the spectral dispersed light from the TRS source by a refraction grating system. The analysis of this data is presented in Section 4.0.

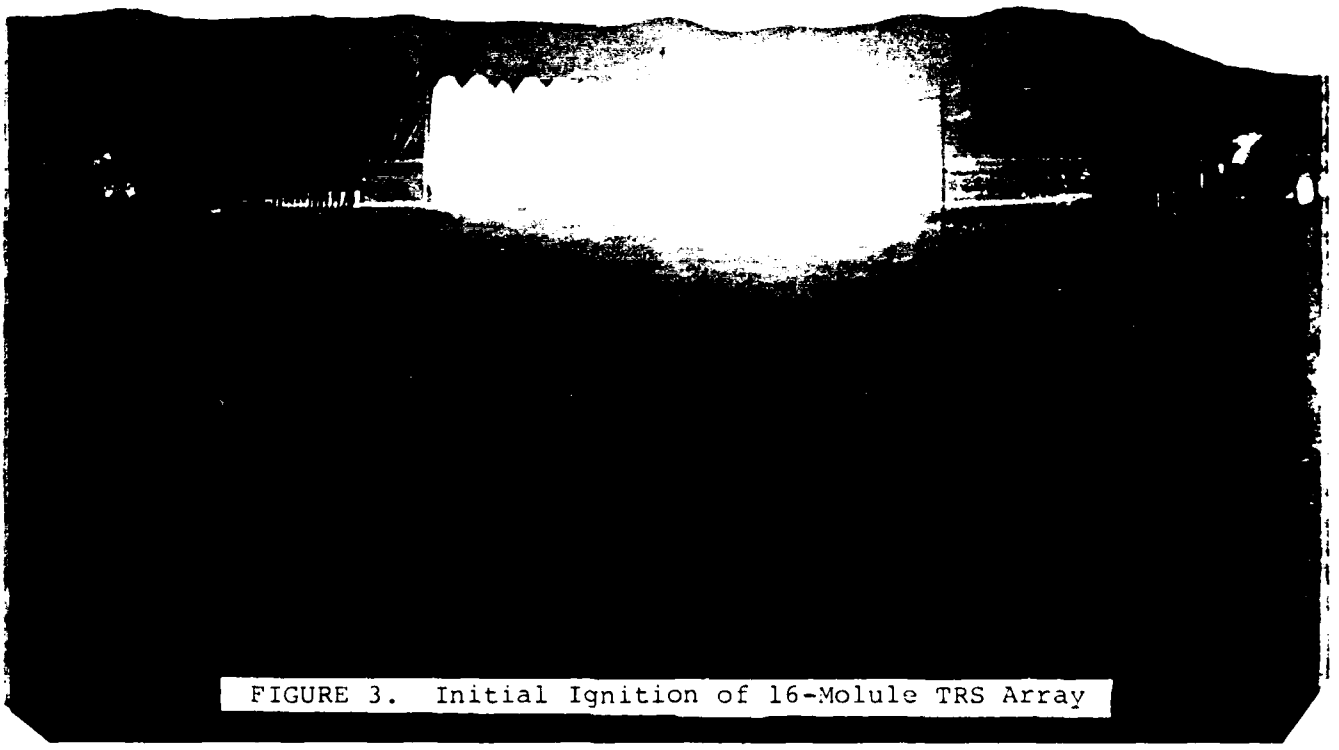

FIGURE 3. Initial Ignition of 16-Molule TRS Array

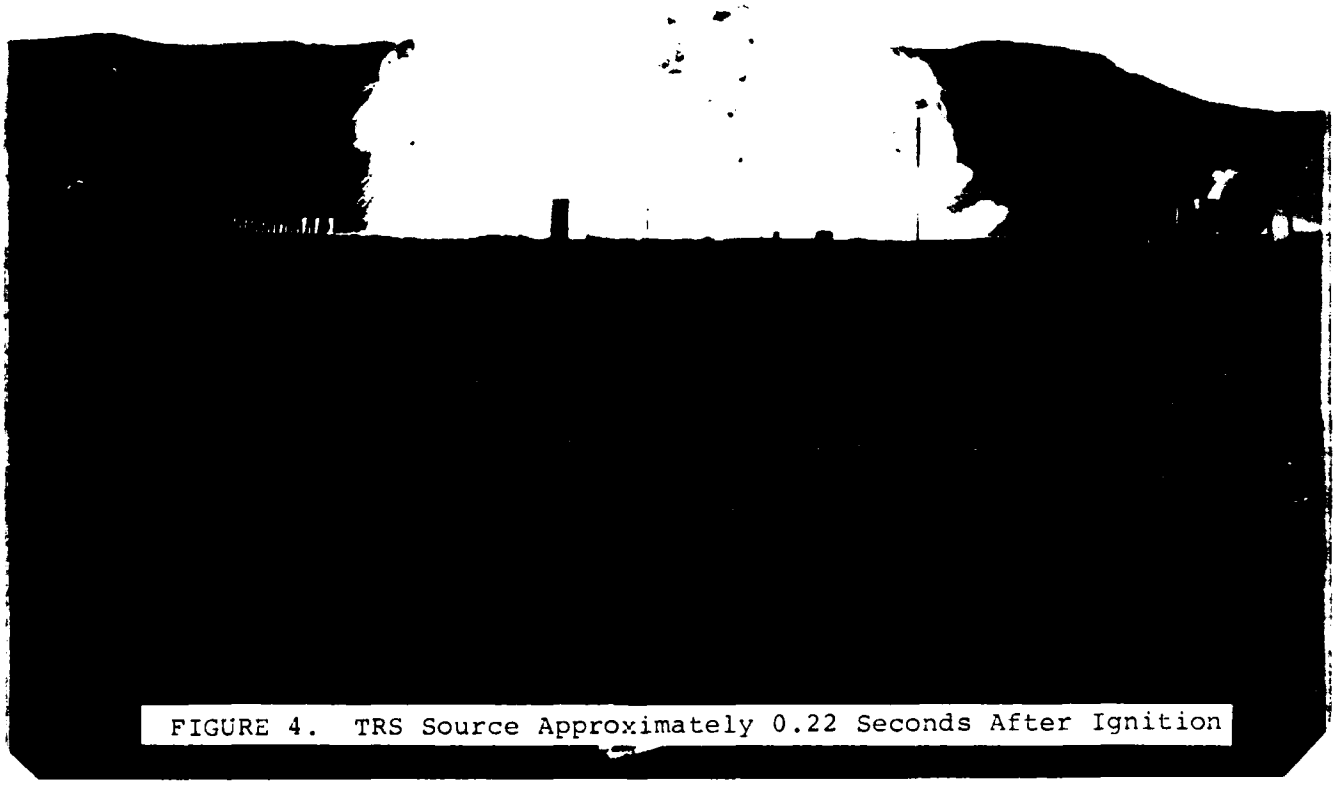

FIGURE 4. TRS Source Approximately 0.22 Seconds After Ignition

FIGURE 5. TRS Source Approximately 5 Seconds After Ignition

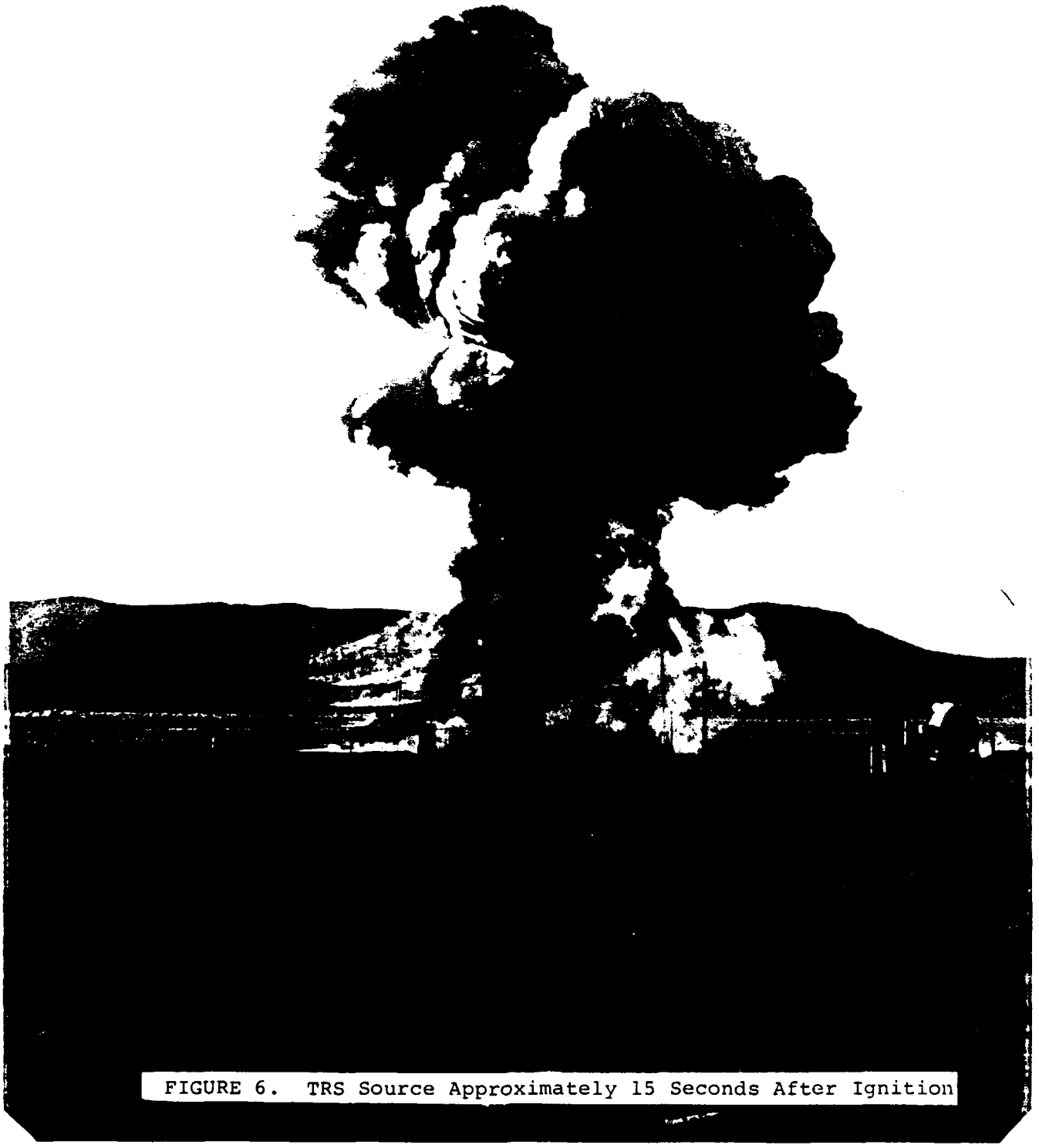

FIGURE 6. TRS Source Approximately 15 Seconds After Ignition

Time 0.01 Seconds

Time 0.2 Seconds

FIGURE 7. TRS Source at 0.1 and 0.2 Seconds After Ignition

Time 0.3 Seconds

Time 0.4 Seconds

FIGURE 8. TRS Source at 0.3 and 0.4 Seconds After Ignition

Time 0.5 Seconds

TIME 0.6 Seconds

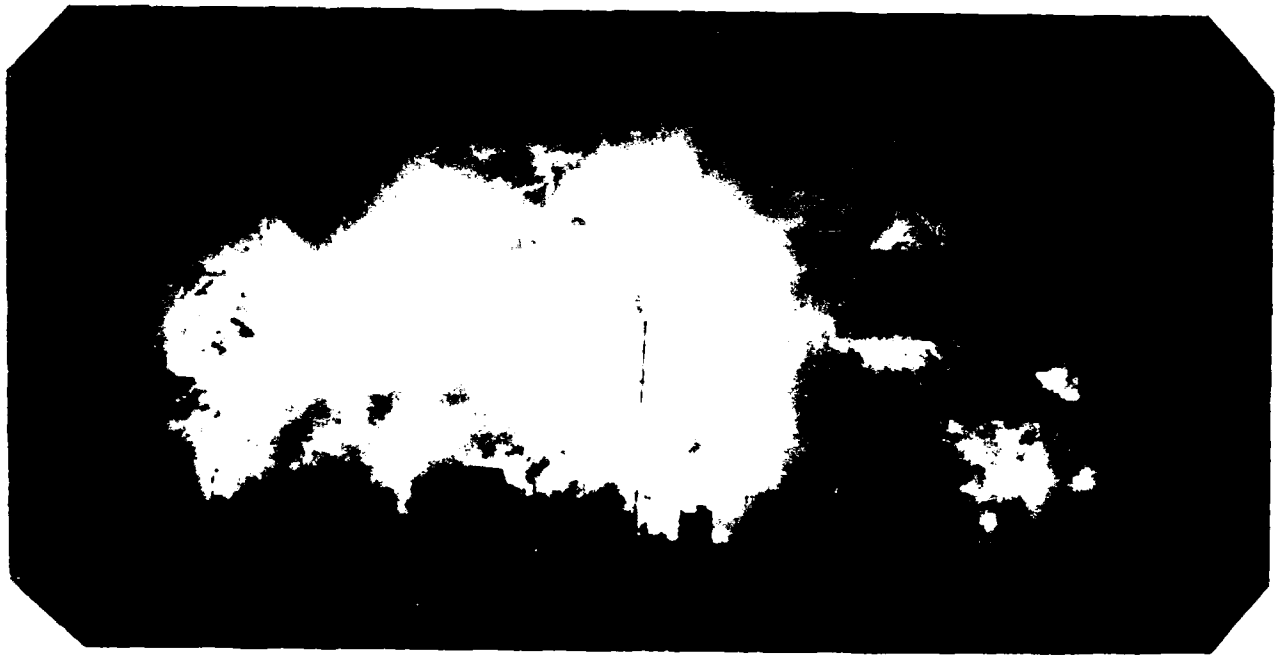

FIGURE 9. TRS Source at 0.5 and 0.6 Seconds After Ignition

Time 0.7 Seconds

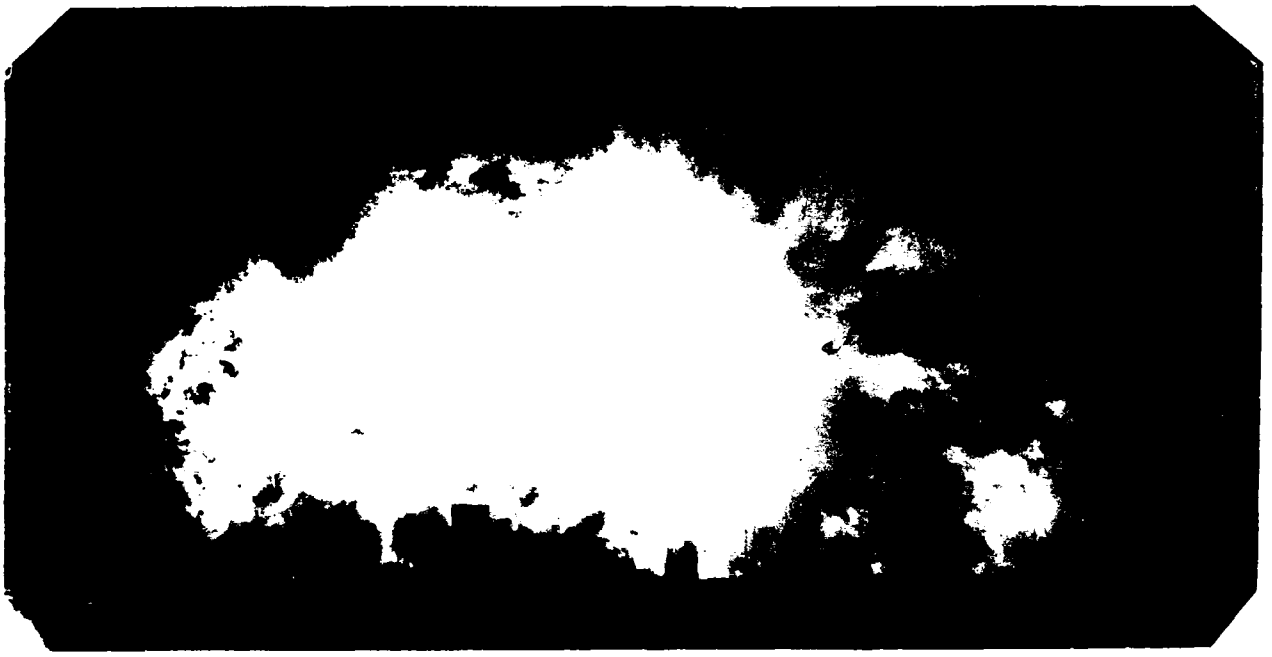

Time 0.8 Seconds

FIGURE 10. TRS Source at 0.7 and 0.8 Seconds After Ignition

Time 0.9 Seconds

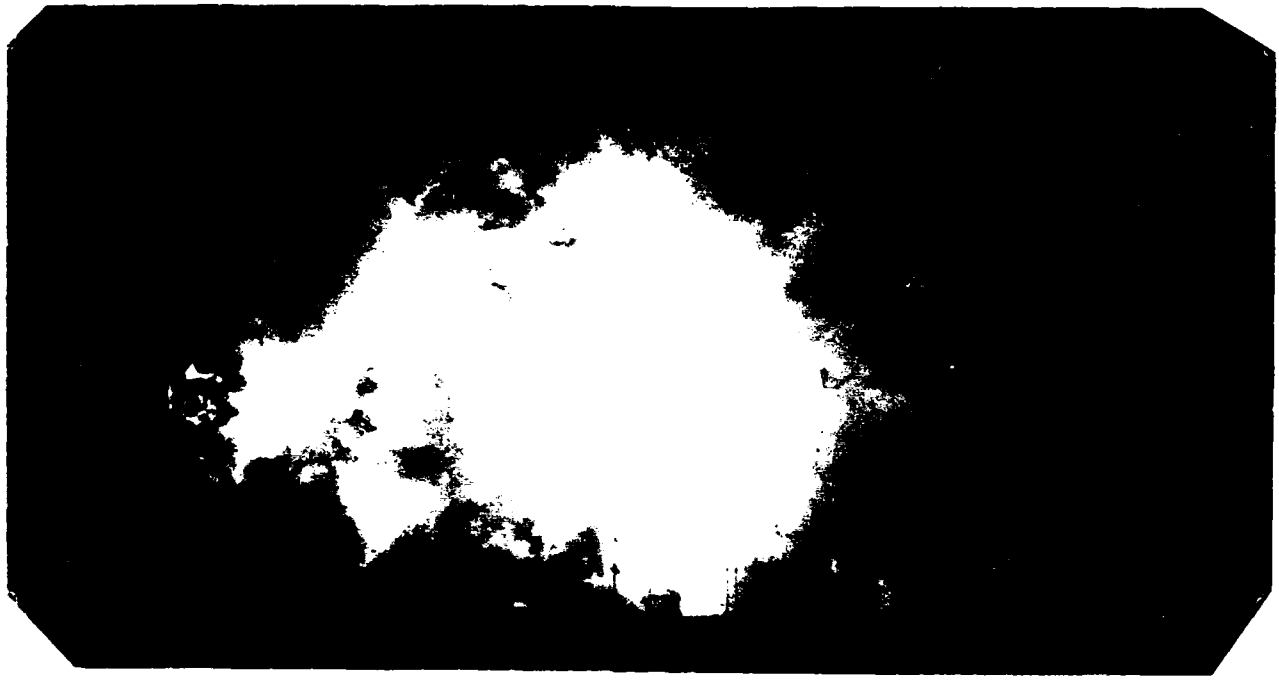

Time 1.0 Seconds

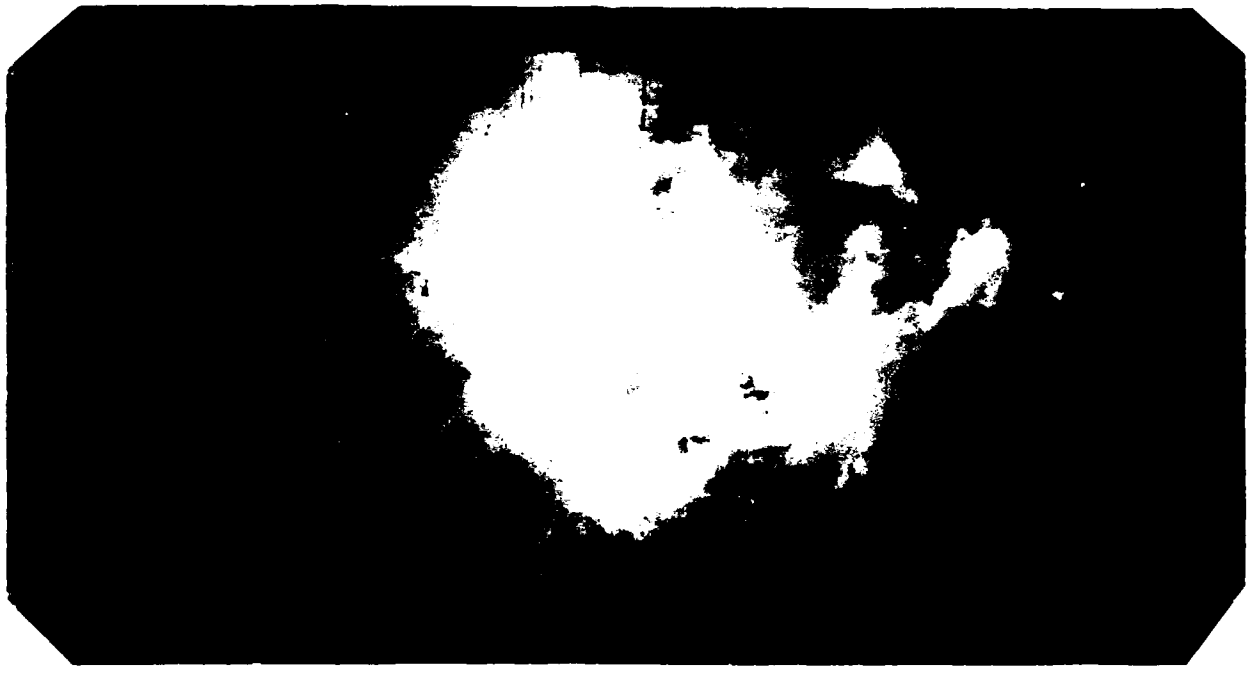

FIGURE 11. TRS Source at 0.9 and 1.0 Seconds After Ignition

SECTION 2

## 2.0 Radiometric Calibration

The radiometric process which yielded the presented information consisted of two phases. The first phase involves the film calibration process. This consists of determining the film's response (formation of silver halide) to known levels of incident energy. This response is quantified by measurement of film density, $d = \log_{10}(1/\text{tansmission})$ by a computer driven PSD microdensitometer system. Thus, the film calibration takes the form of a relationship between density and film exposure (incident energy/area) which "created" that density (after film development).

The second phase of the radiometric process is "real-world" related; it involves "backtracking" from the energy which finally reached the film through the entire imaging system (i.e., lenses, filters, windows, rotating mirrors, atmosphere, etc.) to evaluate the energy actually emitted by the radiating source. The details of this two-phase calibration/radiance conversion process, as it was implemented in these experiments, are presented below.

## 2.1 Density Versus Exposure Calibration

In principle,[3,4] exposure calibration requires detailed knowledge of the parameters governing the exposure process -- as implied by the equation below which defines "effective exposure" [3,4]:

$$E_i = \int_0^\infty U(\lambda)S(\lambda)T_i(\lambda)T'(\lambda)d\lambda \qquad \ldots 2$$

where:

$E_i$ = "effective exposure" on the film created by calibration source $U(\lambda)$ attenuated by i th attenuator (energy/area),

$U(\lambda)$ = spectral energy profile of the calibration source, measured at the film (energy/area/wavelength),

$T_i(\lambda)$ = spectral transmission of attenuators used to vary the calibration exposures,

$T'(\lambda)$ = net spectral transmission of all other attenuators between source and film,

$S(\lambda)$ = relative spectral sensitivity of film (energy/area/wavelength)$^{-1}$. This parameter measures the efficiency of different wavelengths of light in creating film density - i.e., it is the reciprocal of the amount of exposure required to achieve some constant density on the film.

The exposure calibration information is normally contained in sensitometric "step wedges" created by imaging a known source $U(\lambda)$ on the film through a calibrated stepped attenuator $T_i(\lambda)$, prior to (and after) exposure in the field. Upon development, densitometric measurements of the printed step wedge provide the necessary relationship between film (density) response and incident energy, so that image density created by the source radiation can be related to source output.

For this experiment 26 spectrally calibrated transmission attenuators, $T_i(\lambda)$, were obtained from Eastman Kodak laboratories in the form of a step wedge of constant areas of diffuse density. The density of each of these attenuators differed from each other by a constant density increment such that the total density span of these 26 attenuators was 4.0 (i.e., they covered four decades of exposure). The spectral sensitivity of the film, $S(\lambda)$, at a diffuse density of 1.0 above gross film fog, was also supplied by Eastman Kodak.

After the field test the camera systems were moved to the laboratory and positioned to record a calibrated National Bureau of Standards, $U(\lambda)$, tungsten light source. The voltage across the tungsten filament was set to raise it to a temperature of $2600^0$K. This produced a radiance of 8872 microwatts per $cm^2$ per nanometer (88.72 watts/$m^2$/nm) at a wavelength of 660 nanometers. A 24 inch achromatic lens was inserted into the optical path to permit proper imaging of this source on the film in the laboratory with the field optics system. This added lens system introduced a 10 percent additional attenuation (into $T'(\lambda)$, equation 2) of the incident flux in the laboratory over that used in the field (equation 3). Thus by compensating for all wavelength dependent transmission modifications of the field optics system, use can be made of the NBS ligth source, $U(\lambda)$, to determine the amount of energy that is collected by this lens system in the field.

The degree of contrast response over the exposure latitude of the recording film is illustrated in Figure 12. Shown in this figure are the density variations on the data film of the printed equally spaced constant density 26 step attenuators. The noisy unsmoothed data was produced by using a small square sampling aperture (50 by 50 microns) in the microdensitometer.

FIGURE 12

SANDIA 26-STEP KODAK WEDGE FILE 4 TAPE E673

MANN DENSITY VS FILM COORDINATE

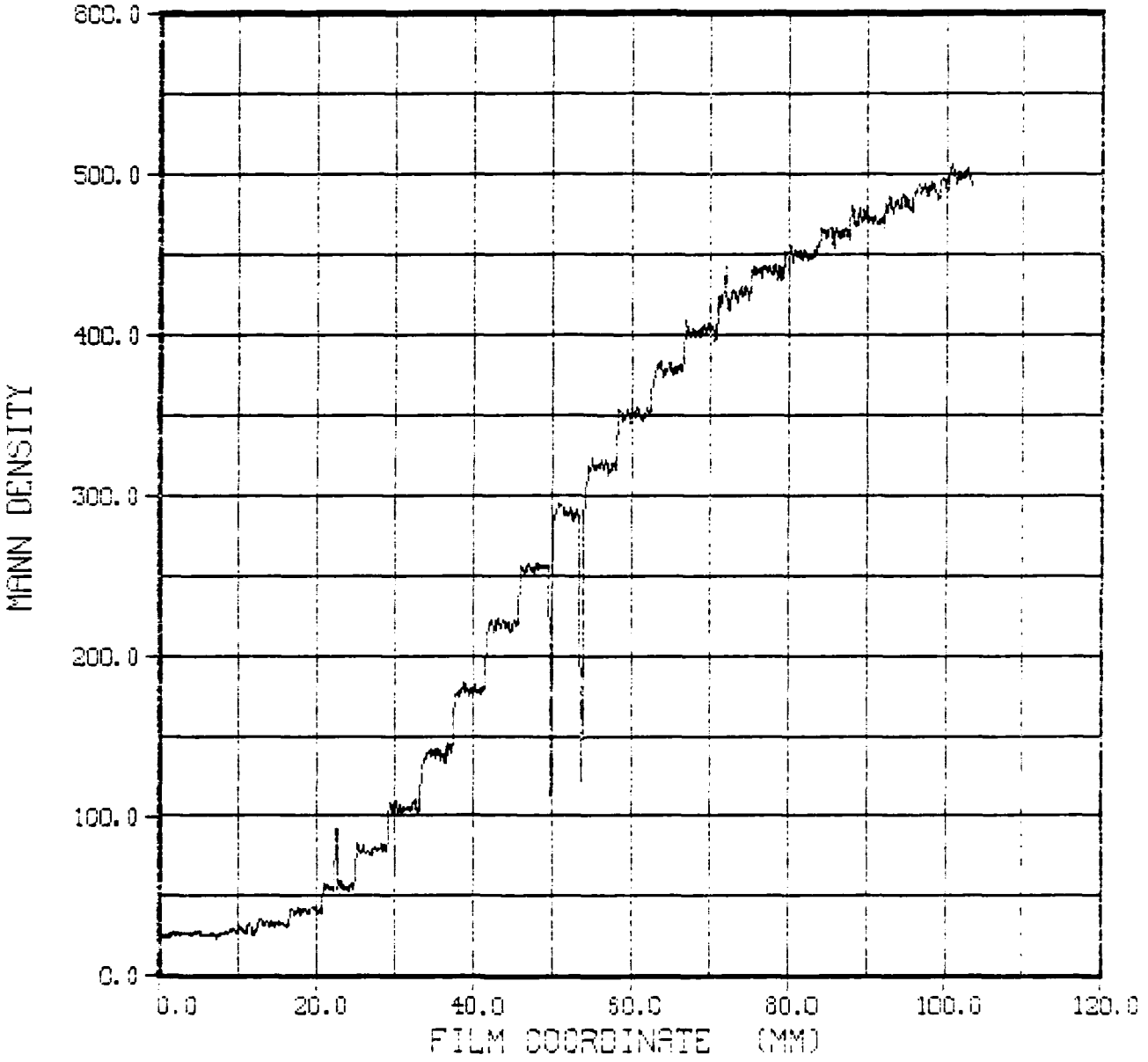

Scribe lines were purposely made at the edges of the 13 th step of the calibration wedge prior to printing. They serve as reference and illustrate how the film sensitivity deteriates at very low and very high exposure energy levels.

## 2.2 Exposure To Radiance Conversion

The general form for the relationship between the radiance of a point on the source surface and the exposure of this point on the film image is given by the "effective exposure method" equation[3,4] below:

$$R_{ab}(X,Y) = \frac{E(x,y) \int_a^b \hat{R}(\lambda,X,Y)d\lambda}{\kappa \int_0^\infty \hat{R}(\lambda,X,Y)S(\lambda)T(\lambda,X,Y)d\lambda} \quad \ldots 3$$

where: $R_{ab}(\lambda)$ = source radiance at source point (X,Y) in the waveband a → b (watts/cm$^2$/steradian),

$E(x,y)$ = film "effective exposure" at film image point (x,y) (ergs/cm$^2$)

$\hat{R}(\lambda,X,Y)$= relative source spectrum (shape measured or assumed),

$S(\lambda)$ = film spectral sensitivity as described in equation 2,

$T(\lambda,X,Y)$= combined spectral transmission of all attenuators between source and film,

$\kappa$ = factor determining the amount of energy that is collected by a lens of a given diameter,

$\kappa$ = $10^7\pi t \cos^4(\theta_{x,y})/4(f/n)^2$, where $10^7$ is the conversion factor from ergs to watts; t is image exposure time; $\theta(x,y)$ is the off optic axis angle; f/n is the camera f-stop.

The calibration method used in this experiment reduces equation 3 to

$$R_{ab}(X,Y) = E(x,y)/\kappa \quad \ldots 4$$

Because of this relation the value $\kappa$ is combined with exposure and an absolute density to radiance curve (instead of the normal exposure curve) is produced. This curve has built into it the correction for the transmission of the field lens system.

For Kodak film 2496 this curve is presented in Figure 13. As noted the calibration curve yields radiance measurement from density at a particular wavelength.

To check the validity of this calibration curve two images of the NBS

FIGURE 13

SANDIA DENSITY-RADIANCE CURVE

FLASH SIMULATOR NO. 2

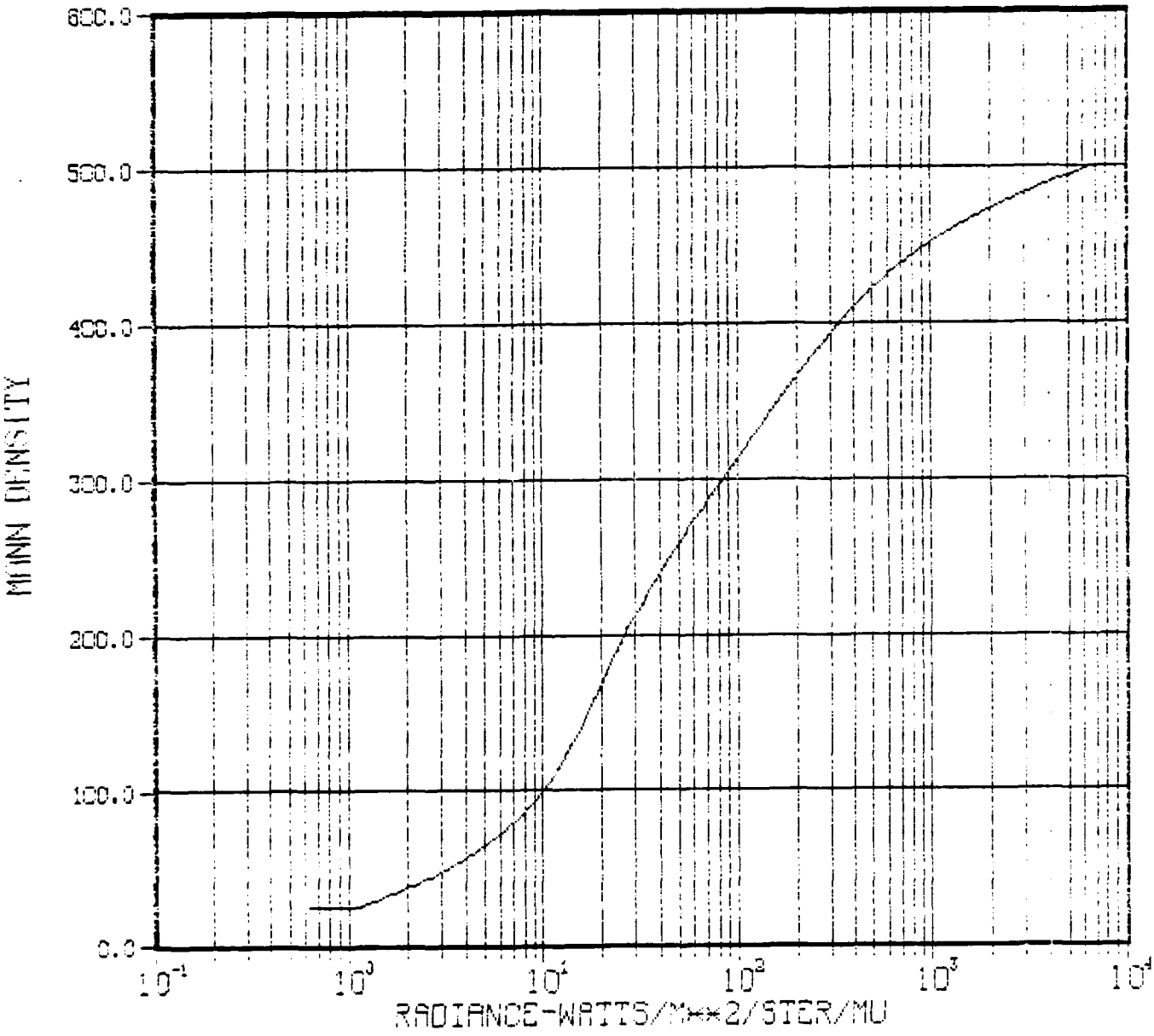

calibration light source were digitized and their density versus distance on film were converted to radiance. The results of this conversion are summarized in Figure 14 and 15. As observed these figures reproduce the calibration value of 79.85 watts/$m^2$/nm stated above (i.e., 88.72 attenuated by 10 percent).

SANDIA CALIBRATION LIGHT SOURCE SET 1 FOR TRS ..

SOURCE RADIANCE VS DISTANCE ON FILM IMAGE

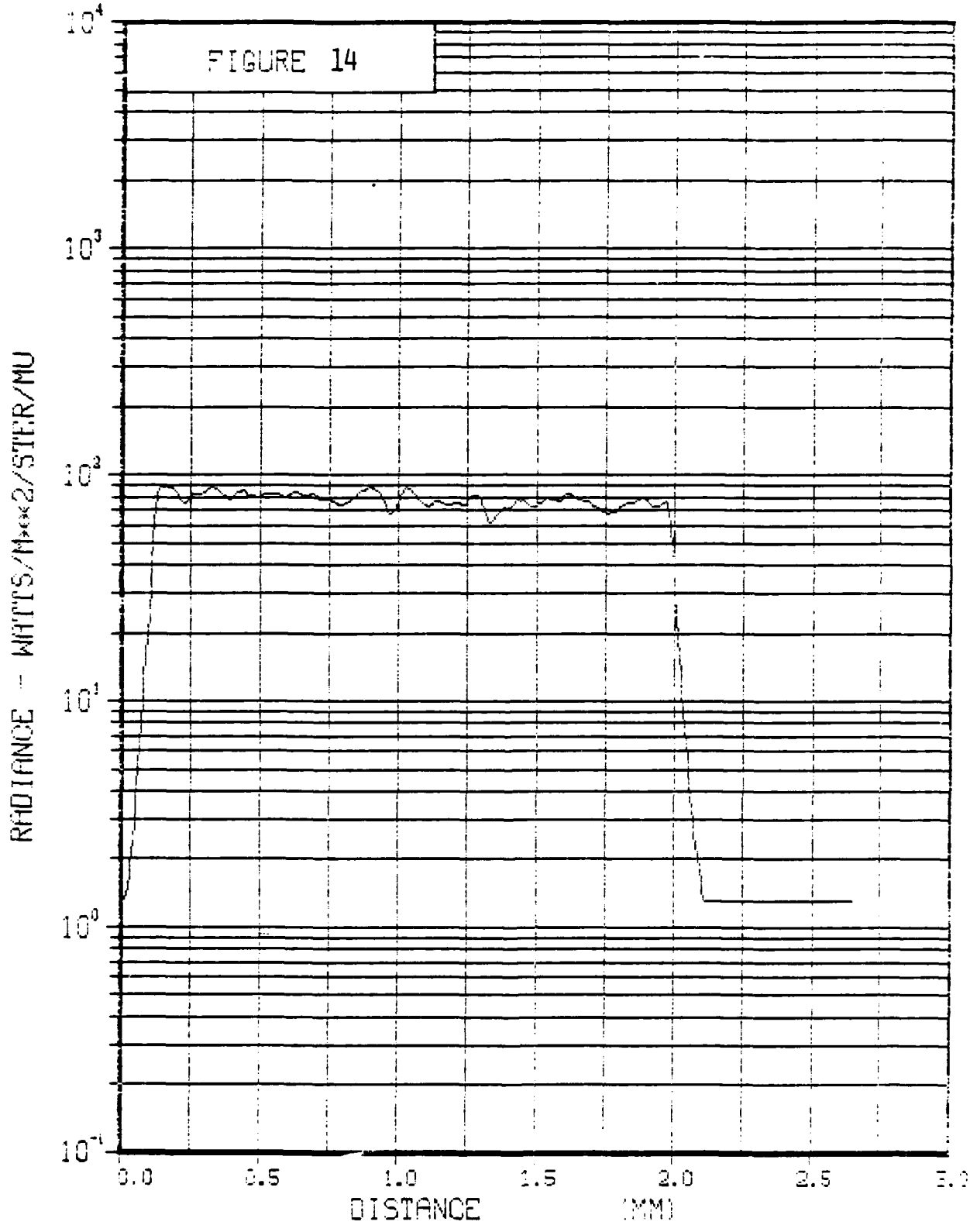

SANDIA CALIBRATION LIGHT SOURCE SET 2 FOR [illegible]

SOURCE RADIANCE VS DISTANCE ON FILM IMAGE

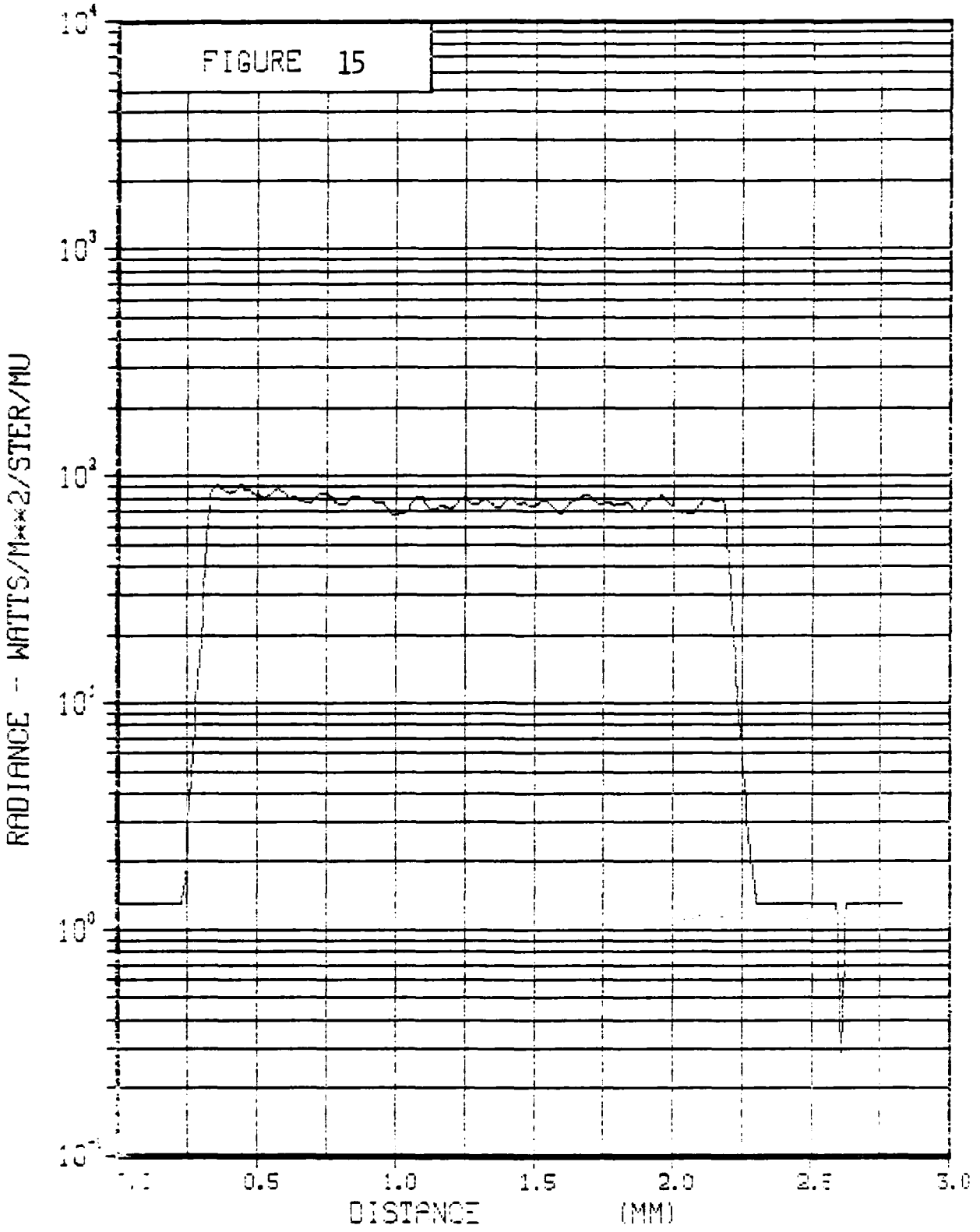

## SECTION 3

## RADIOMETIC MEASUREMENTS

3.0 Three types of radiometric measurements from the TRS source are presented: (1) estimated radiance (watts/$m^2$/steradian/nm) along horizontal and vertical profiles across the fireball; (2) radiated power (watts/nm) as a function of time; (3) peak radiance as a function of time.

To allow estimates of surface temperature the field conditions were purposely set to record the surface brightness in a very narrow waveband (deep red). This was accomplished by a Kodak Wratten 92 filter in the optical path which is opaque to all wavelengths less than 620 nanometers. The selected film emulsion -- Kodak 2496, has a very sharp spectral sensitivity cut-off at 700 nanometers and does not respond to higher wavelengths. Thus the recorded surface brightness as illustrated in Plates 6 through 10 is limited to the small waveband of 620 to 700 nanometers with a peak effective wavelength of 660 nanometers.

Of the many recorded film images (nominal camera speed was 100 frames per second) twenty were selected to describe the surface brightness of the TRS No. 2 event over a time span of 3 seconds. From these selected images the density variations over the entire fireball image were determined by overlap raster scanning with a computer driven microdensitometer. Each density sample was obtained by determining the transmittance on the film image of an area (a single pixel) of 50 by 50 microns. Each pixel corresponds to a 3.3 by 3.3 inch square surface area on the TRS source. The corresponding surface radiance of each pixel at an effective wavelength of 660 nanometers was determined from this density by a Chebychev polynomial expression which represented the calibration curve shown in Figure 3.

The luminous TRS surface area within these twenty selected frames which covered the first 3 seconds after ignition varied from 20,000 to 40,000 pixels with each pixel representing a radiance measurement. This sea of radiance data can be presented in many different ways. For this report it is presented as horizontal and vertical radiance profiles which can be transformed to profiles of black body temperature. All pixel data is also integrated to yield total power.

As stated above, the data was purposely measured in a very narrow "bell shaped" wavelength pass band of 620 to 700 nanometers with a peak at 660 nanometers. Hence the only assumption that is made in this analysis is that the radiating source has a flat spectrum over this bandwidth and therefore the measured pass band (620 to 700nm) represents the equivalent monochromatic radiance at 660 nm.

The radiation present in any region of empty space at thermodynamic equilibrium, at temperature T, is known as black body radiation, or thermal radiation. It is of practical importance as being the maximum amount of radiation that can be emitted by hot solid bodies. Hence at any temperature it radiates more energy, both in the total spectrum and also for each wavelength interval, per unit time, per unit area, than any other thermal radiator at the same temperature.

The radiant energy was observed in terms of the flux of energy radiated by the TRS source. The total black body flux across a unit area of the TRS surface can be derived from the Planck law defining the spectral distribution of thermal energy at temperature T :

$$R(\nu)d\nu = \frac{2\pi\nu^2 d\nu}{c^2} \frac{h\nu}{(\exp(h\nu/kT) - 1)} \quad \ldots 7$$

$$= \sigma T^4 (15/\pi^4 \; u^3 du/(\exp(u) - 1))$$

where $u = h\nu/kT$

The total black body radiant energy is the integral of this expression over all frequencies. Thus the black body radiation crossing unit area of the TRS source in unit time in all directions in one hemisphere is:

$$E(\text{ergs/cm}^2) = \sigma T^4 \quad \ldots 8$$

where $\sigma = 2\pi^5/15 \; \kappa^4/h^3c^2 = 5.672 \times 10^5 \; \text{ergs/cm}^2/\text{deg}^4$

For practical calculations it is convenient to note that the total radiant black body flux in watts/cm$^2$ can be expressed as:

$$R = (T/648)^4 \quad \ldots 9$$

measured power (watts/nm). Likewise an effective black body temperature is determined from which total emitted black body power is calculated.

At each time in this analysis, the first horizontal radiance profile was selected at a height 0.1 meters above the ground surface. Each additional horizontal radiance profile is displaced from its neighbor by approximately 0.8 meters. Each horizontal profile represents TRS surface radiance values of a 3.3 by 3.3 inch (8.4 by 8.4 cm) square area as these occurred as a function of time and height above the ground surface.

The vertical plotted data shows two different profiles. One of these represents the vertical profile along a line at the source center prior to ignition. The second profile presents the highest measured radiance reported by a single pixel anywhere on the surface at that height above the ground. Thus it is a measure of the maximum source radiance as a function of height.

Figures 16 through 74 present these horizontal and vertical radiance profiles as a function of time in properly identified displays.

## 3.1 Radiance To Black Body Temperature And Energy Conversion

An estimate can be obtained from these radiance values of the black body temperature. For convenience Figure 75 presents a conversion scale at a spectral wavelength of 660 nanometers for measured radiance (watts/$m^2$/nm/ster) to black body temperature. The conversion scale is based on the Planck relationship between monochromatic emissive power and the equivalent absolute temperature of a black body which leads to the expression:

$$T(^0K) = (hc/\lambda k)/\ln(2c^2h/R_m\lambda^5 + 1) \quad \ldots 5$$

$$= (1.439 \times 10^7/\lambda)/\ln(1.911 \times 10^{20}/R_m\lambda^5 + 1)$$

where: $\lambda$ = the spectral wavelength (in nanometers)

$R_m$ = spectral radiance (in watts/$m^2$/ster/nm)

For a spectral wavelength of 660 nanometers

$$T(^0K) = (2.180 \times 10^4)/(13.77 - \ln R_m) \quad \ldots 6$$

This simplified form is plotted in Figure 75.

These relationships have been used below because radiation from a non black body such as the TRS source may be represented in terms of the radiation laws given above by the use of factors that give the relative intensity of radiation of the non black body and of the black body at the same temperature. Such factors -- less than unity -- are called emissivities and may be either for the total energy radiated -- total emissivity -- or for the radiation of any spectral interval -- spectral emissivities.

As stated above each pixel of each photograph represented a radiance measurement. By equation 5 (Figure 75) these were converted to a black body temperature and by equation 9, to black body power. The radiance, temperature and black body power of each pixel were added. This yielded the data summarized in Table 1 which presents total power radiated in the measured waveband (column 3), the estimated average black body temperature of the TRS source (column 4), and the estimated black body power (column 5).

Also shown (column 6) in Table 1 is the wavelength, $\lambda_m$, at which maximum power would be emitted had the TRS source been a black body. This arises from the following simple expression which can be derived from equation 7:

$$\lambda_m T = \text{constant } (=2.898 \times 10^6 \text{for } \lambda_m \text{in nanometers}) \ldots 10$$

A plot can be made of black body power (column 5) versus time (column 2). The power time curve from this plot, when integrated over time, gives a value for the integral of $2.58 \times 10^6$ joules/$m^2$ or $6.17 \times 10^5$ calories/$m^2$. From the dimensions given above each module has a surface area of 28.65 $m^2$ and releases approximately $9 \times 10^6$ calories[2] or $3.1 \times 10^5$ calories/$m^2$. This indicates that the derived black body power is twice this value.

It bas been stated above that no known substance has the radiating characteristics of a black body and that it is customary to characterize material by an effective emissivity, e, defined such that $e\sigma T^4$ is the actual rate of radiation of unit area in unit time at temperature T. Unfortunately the emissivity of the TRS source is unknown.

If one accepts the $9 \times 10^6$ calories[2] as a measure of the output of

TABLE 1

DATA SUMMARY FOR A GAS FILLED TRS EVENT

| FRAME | TIME (seconds) | POWER 620-700 watts/nm | TEMPERATURE Average Black Body $^{\delta}K$ | POWER Black-Body watts/$m^2$ | $\lambda_m$ Nanometers |
|---|---|---|---|---|---|
| 1 | 0.00 | 1.87E2 | 1618 | 3.89E5 | 1791 |
| 5 | 0.04 | 2.41E3 | 1798 | 5.92E5 | 1612 |
| 10 | 0.09 | 7.03E4 | 2561 | 2.44E6 | 1132 |
| 13 | 0.12 | 1.04E5 | 2634 | 2.73E6 | 1100 |
| 15 | 0.14 | 1.10E5 | 2594 | 2.57E6 | 1117 |
| 19 | 0.18 | 9.26E4 | 2538 | 2.35E6 | 1142 |
| 22 | 0.21 | 6.87E4 | 2444 | 2.02E6 | 1186 |
| 25 | 0.24 | 5.48E4 | 2375 | 1.80E6 | 1220 |
| 30 | 0.29 | 3.70E4 | 2238 | 1.42E6 | 1295 |
| 35 | 0.34 | 2.91E4 | 2192 | 1.31E6 | 1322 |
| 40 | 0.39 | 2.14E4 | 2117 | 1.14E6 | 1369 |
| 50 | 0.49 | 1.64E4 | 2026 | 9.55E5 | 1430 |
| 70 | 0.69 | 1.58E4 | 2020 | 9.45E5 | 1435 |
| 90 | 0.89 | 1.44E4 | 2003 | 9.12E5 | 1447 |
| 120 | 1.19 | 1.41E4 | 1998 | 9.03E5 | 1450 |
| 150 | 1.49 | 9.24E3 | 1933 | 7.91E5 | 1499 |
| 200 | 1.99 | 6.02E3 | 1898 | 7.36E5 | 1527 |
| 250 | 2.49 | 3.34E3 | 1735 | 5.13E5 | 1670 |
| 300 | 2.99 | 1.37E3 | 1617 | 3.87E5 | 1792 |

where 1.37E3 = $1.37 \times 10^3$

each module, then one would estimate an emissivity of 0.51 for the TRS source at these temperatures. This value for emissivity appears very high since the emissivity of tungsten[5] (Figure 5A) at these temperatures is about 0.43. It has also been shown[6] that at lower temperatures ($875^0$K) the typical total emissivity of oxidized aluminum is 0.2. Tungsten's emissivity[5] increases with lower temperature.

The estimated emissivity could be lowered by extending the black body curve in time. How much would be gained by performing this task is unknown. It can be said (Table 1) that after 3 seconds the TRS source does not radiate very much in the visible.

The estimated emissivity could also be lowered by decreasing the stated[2] output of $9 \times 10^6$ calories per module. If this is a good value and the black body output cannot significantly be changed, then it must be said that the finely powdered aluminum can achieve an emissivity of 0.5 at these temperatures in the TRS oxidizing process.

FIGURE 16

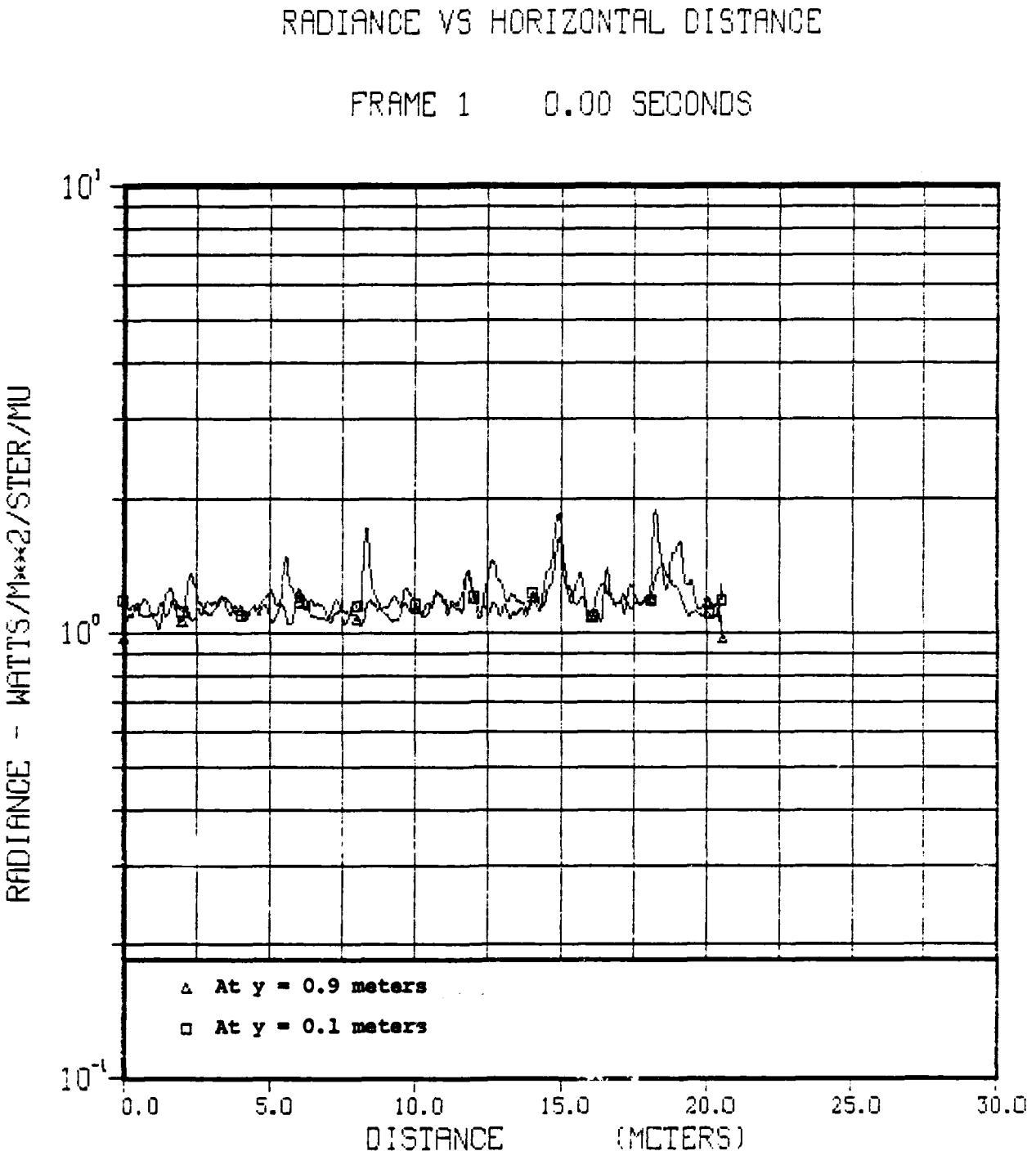
RADIANCE VS HORIZONTAL DISTANCE
FRAME 1 0.00 SECONDS
RADIANCE - WATTS/M**2/STER/MU
10^1
10^0
10^-1
At y = 0.9 meters
At y = 0.1 meters
0.0
5.0
10.0
15.0
20.0
25.0
30.0
DISTANCE (METERS)

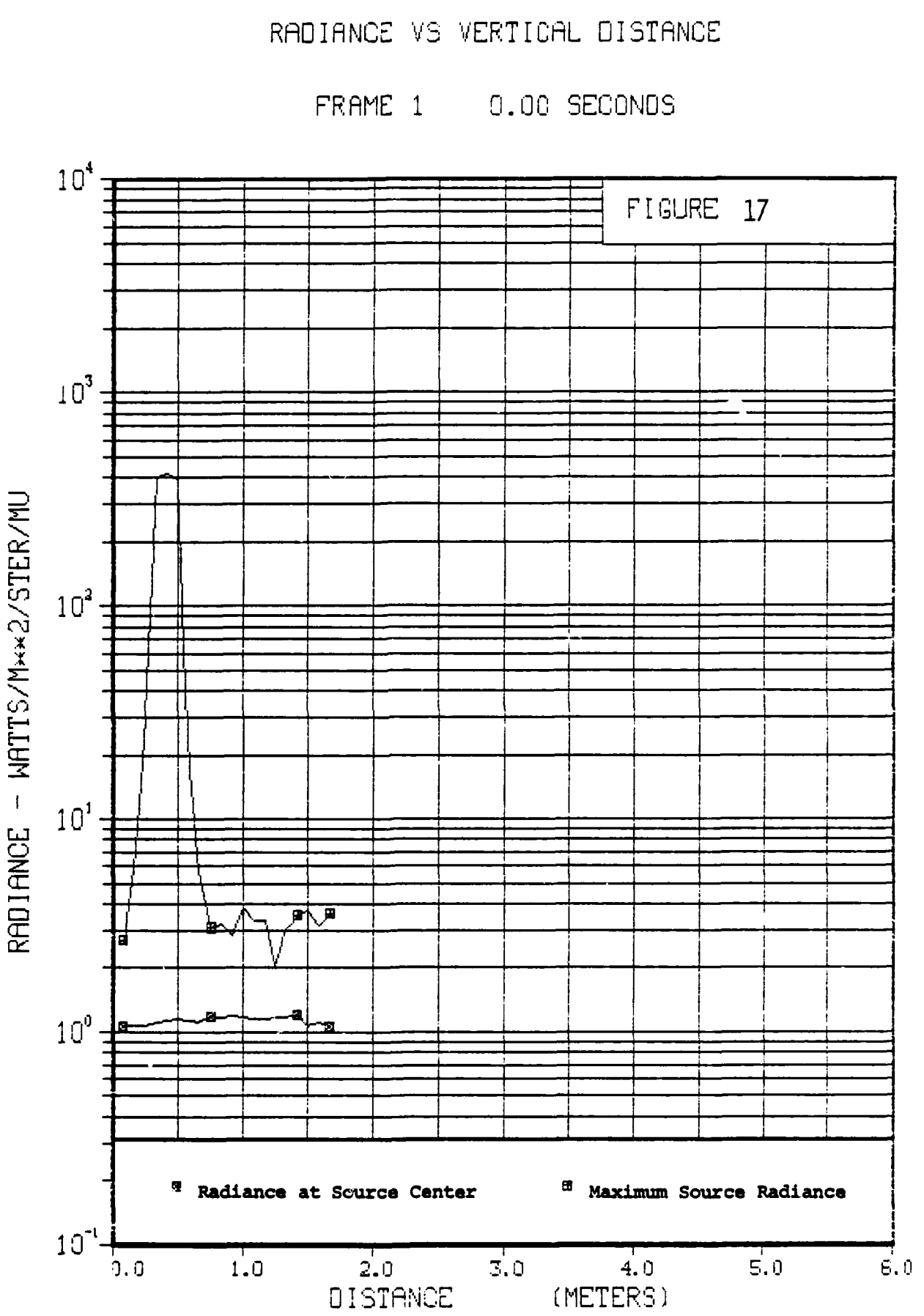
RADIANCE VS VERTICAL DISTANCE
FRAME 1 0.00 SECONDS
FIGURE 17
RADIANCE - WATTS/M**2/STER/MU
$10^4$
$10^3$
$10^2$
$10^1$
$10^0$
$10^{-1}$
0.0
1.0
2.0
3.0
4.0
5.0
6.0
DISTANCE (METERS)
Radiance at Source Center
Maximum Source Radiance

RADIANCE VS HORIZONTAL DISTANCE

FRAME 5 0.04 SECONDS

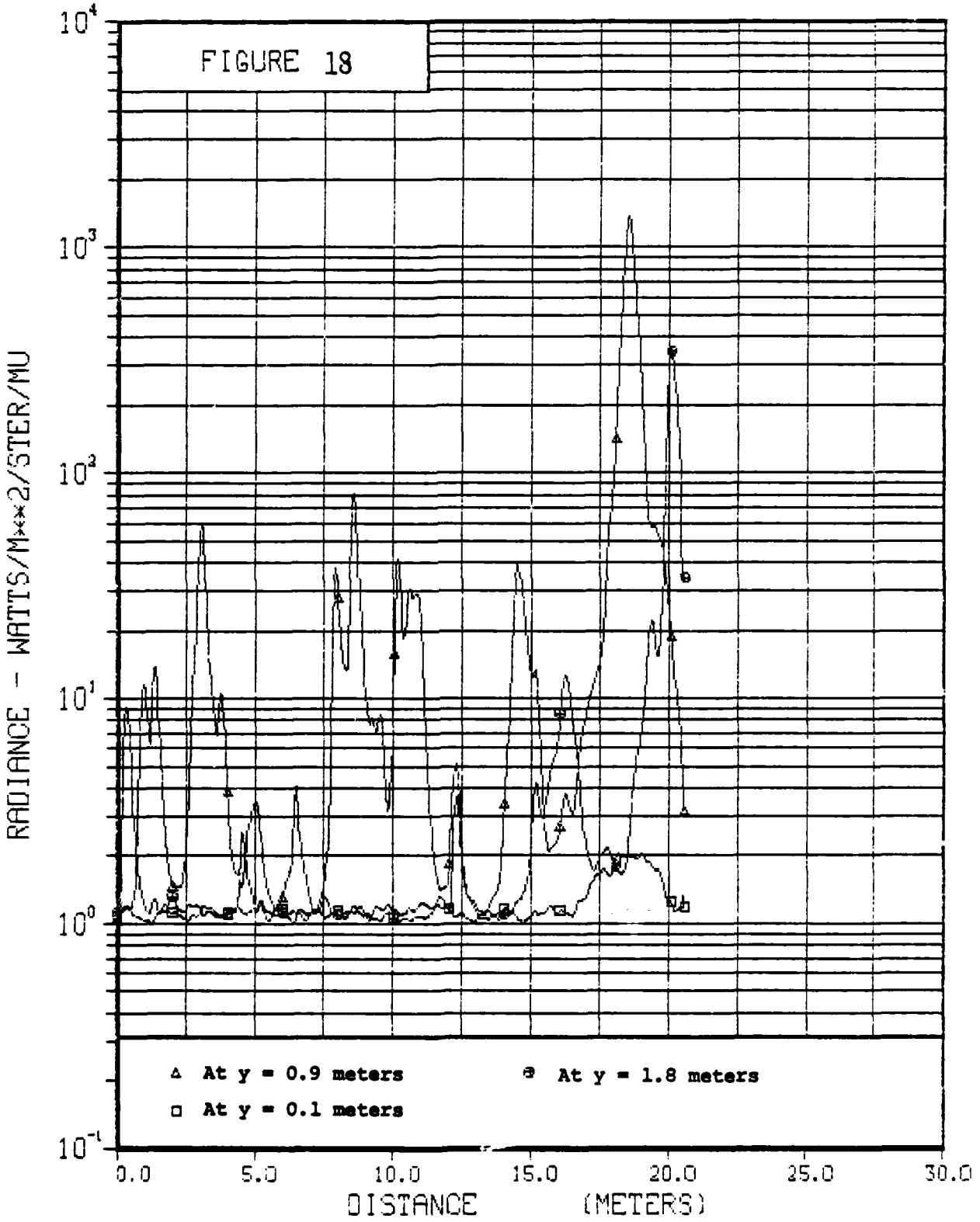

RADIANCE VS HORIZONTAL DISTANCE

FRAME 5 0.04 SECONDS

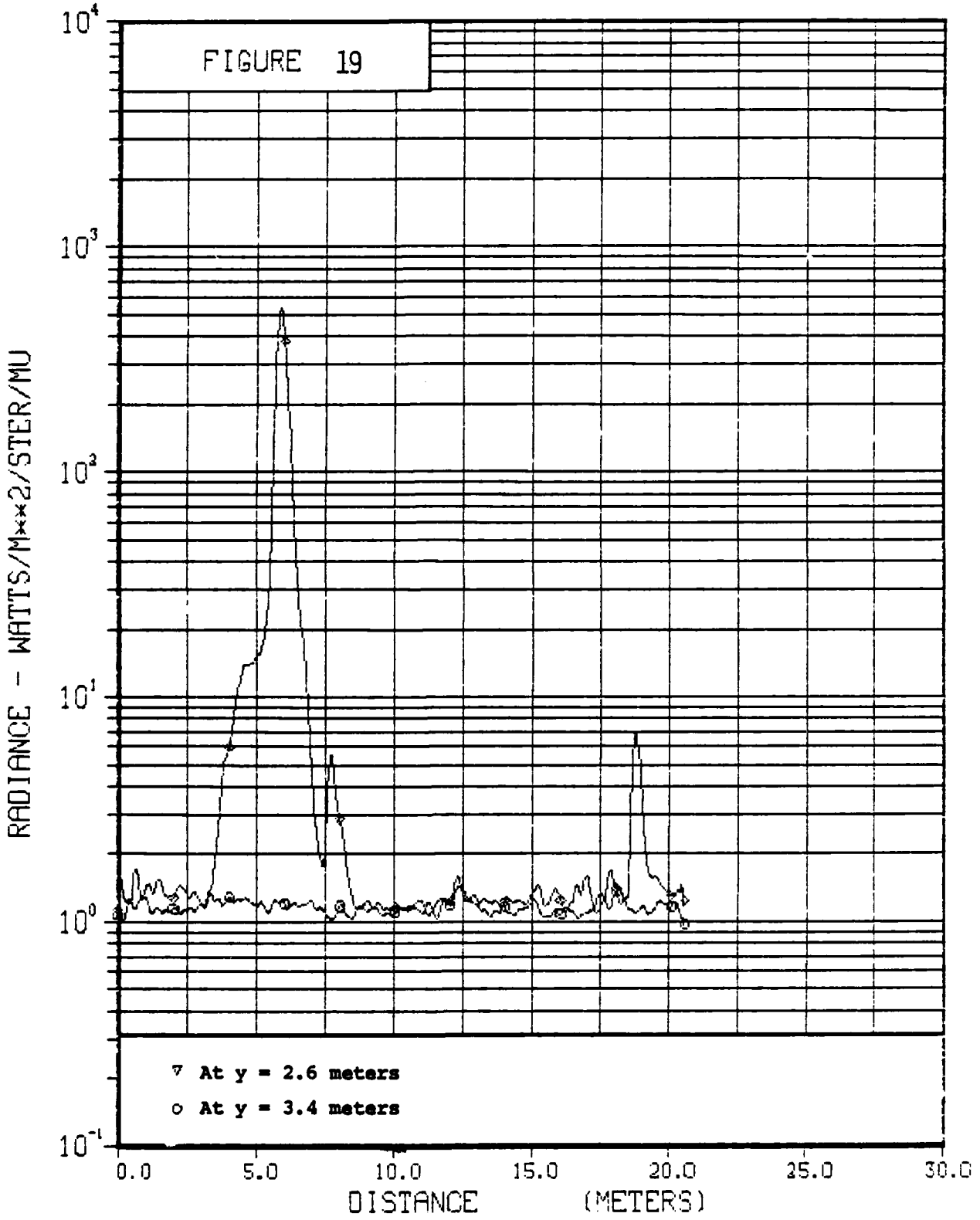

RADIANCE VS VERTICAL DISTANCE

FRAME 5 0.04 SECONDS

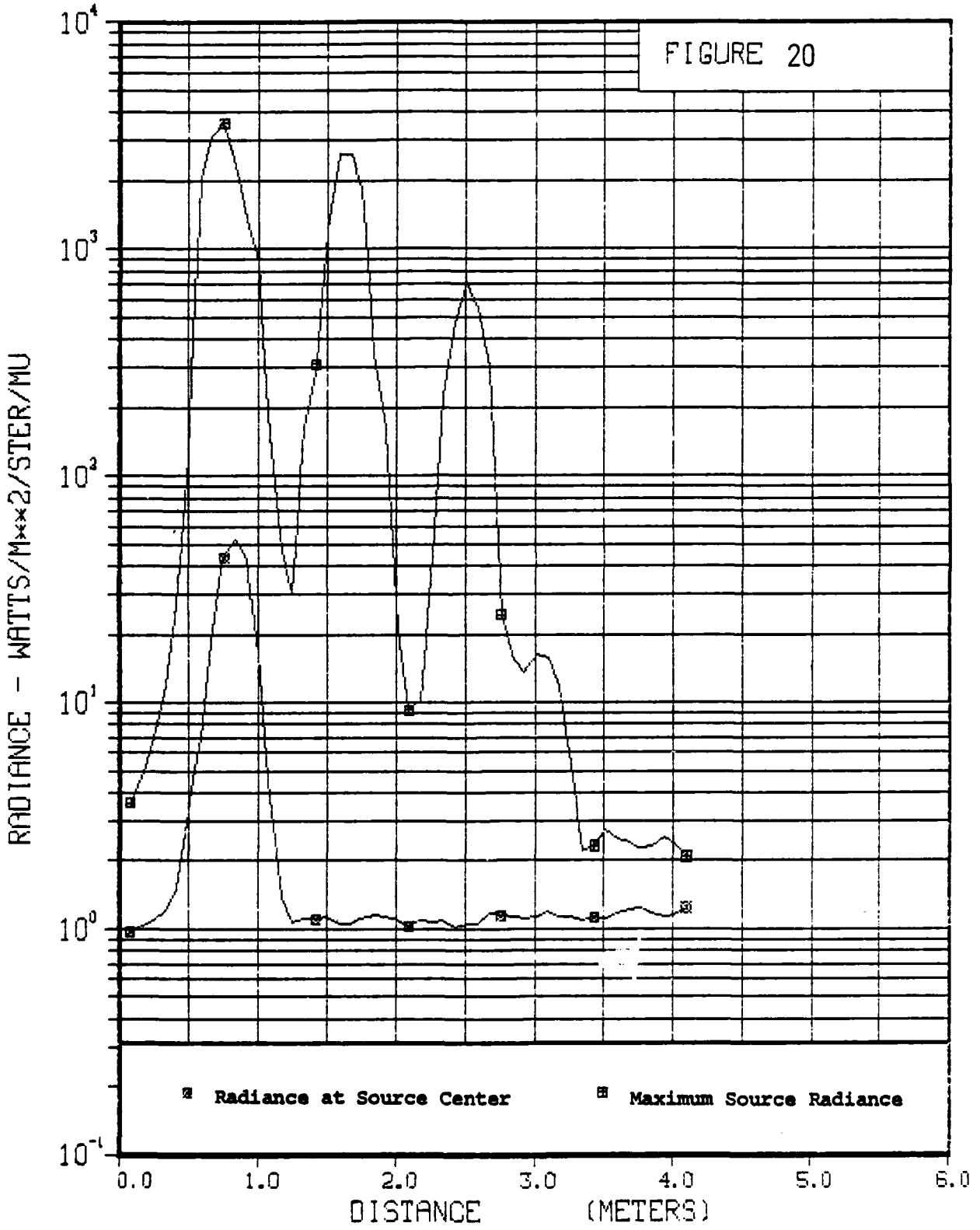

RADIANCE VS HORIZONTAL DISTANCE

FRAME 10  0.08 SECONDS

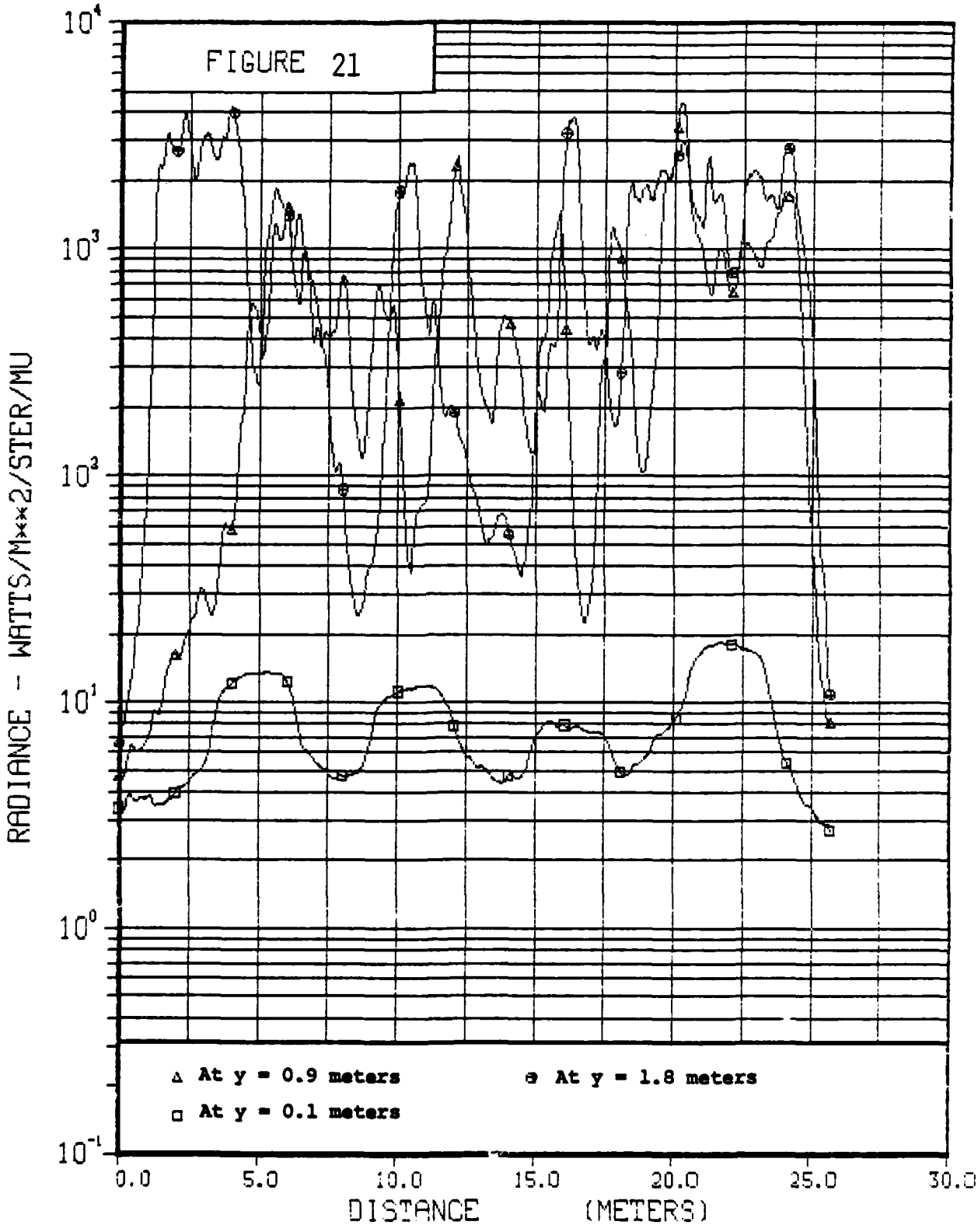

RADIANCE VS HORIZONTAL DISTANCE

FRAME 10  0.08 SECONDS

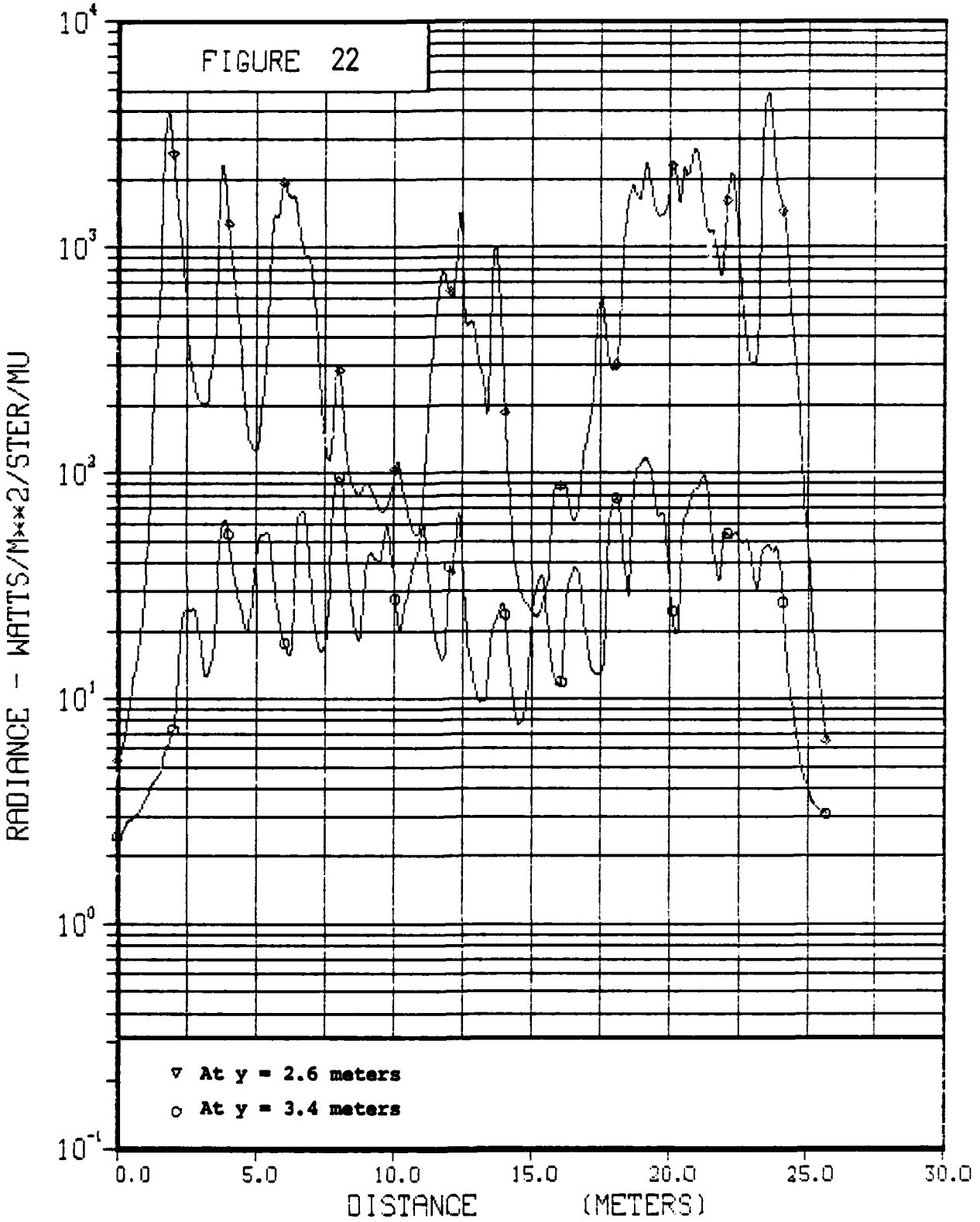

RADIANCE VS VERTICAL DISTANCE

FRAME 10  0.08 SECONDS

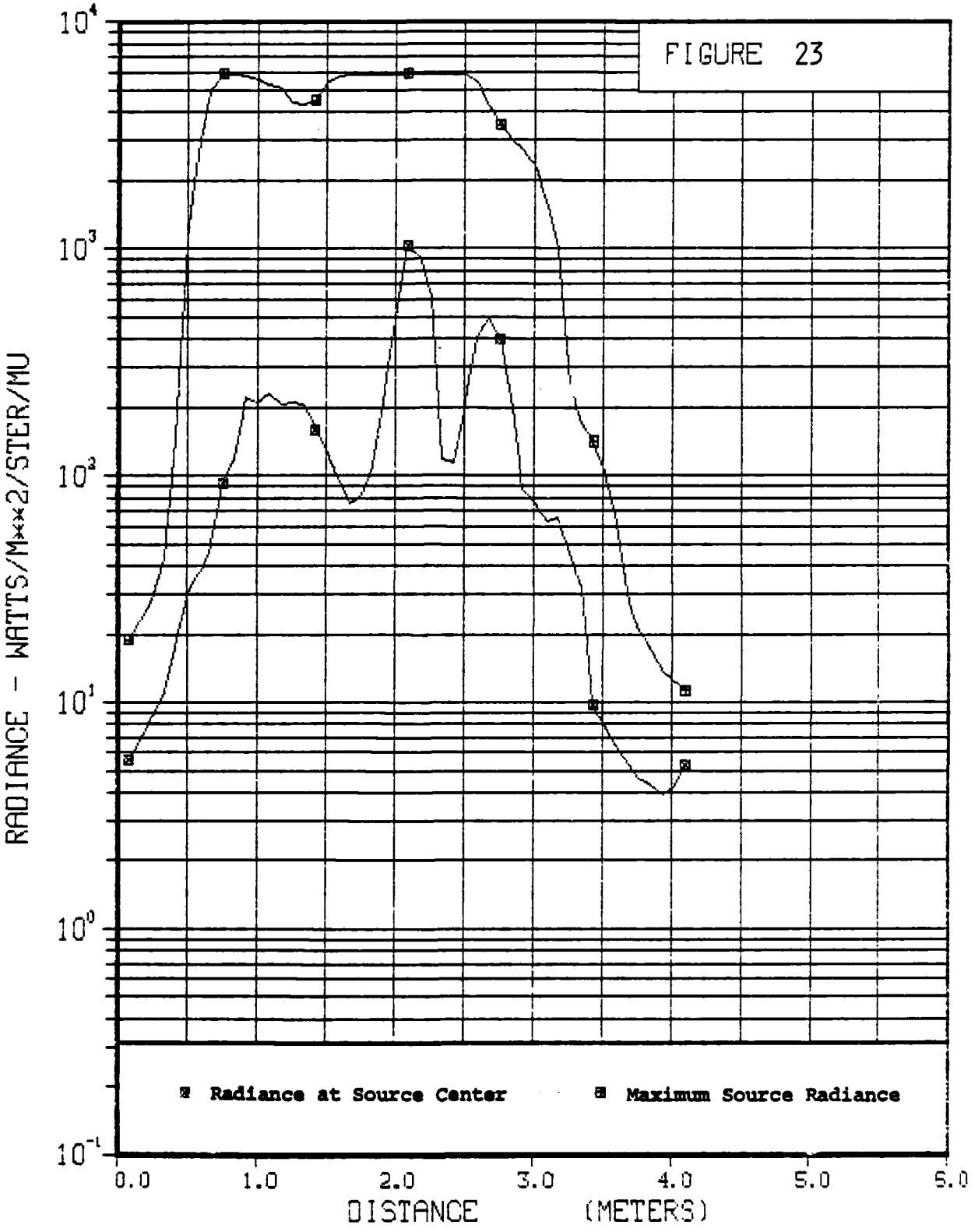

RADIANCE VS HORIZONTAL DISTANCE

FRAME 13  0.12 SECONDS

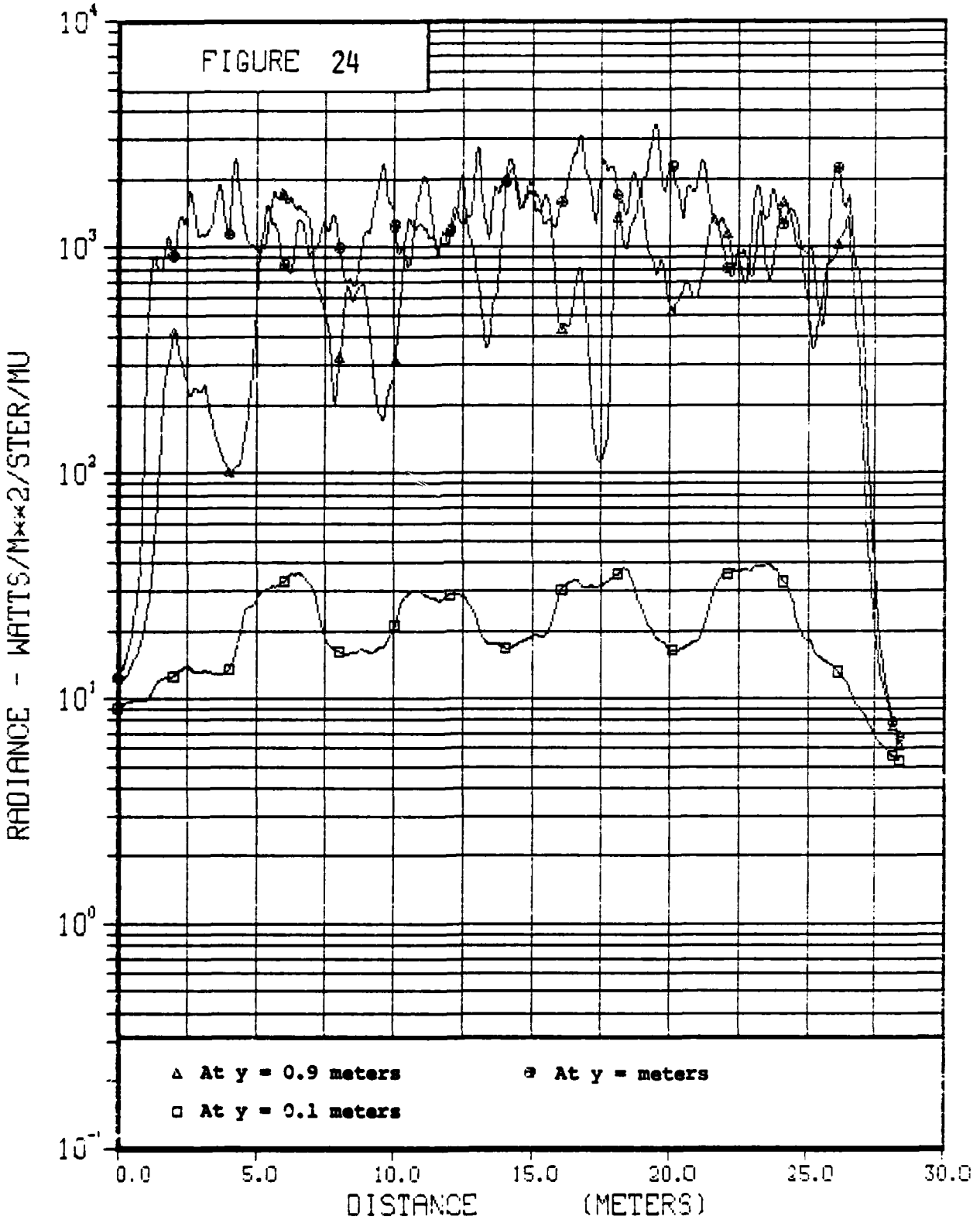

RADIANCE VS HORIZONTAL DISTANCE

FRAME 13  0.12 SECONDS

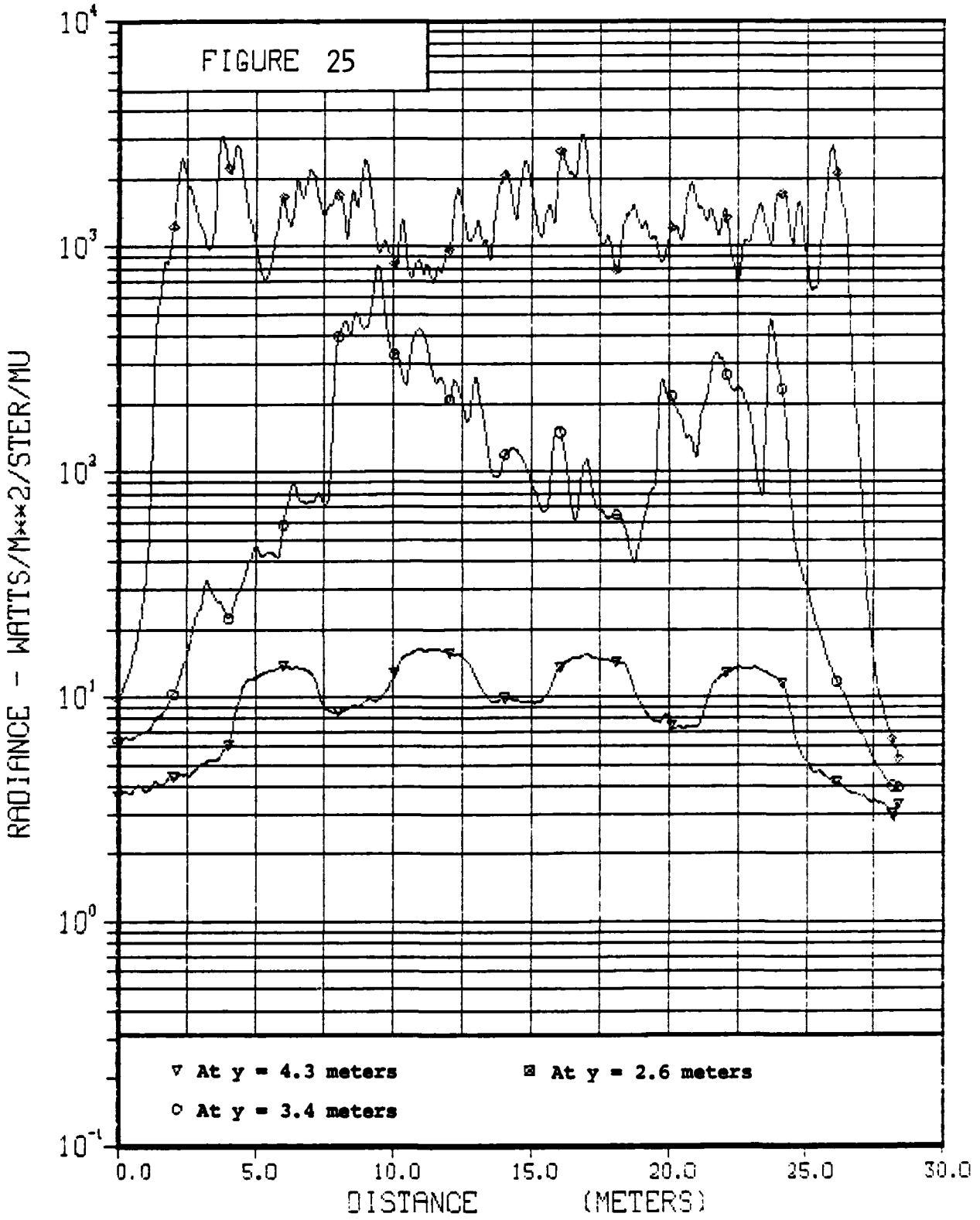

RADIANCE VS VERTICAL DISTANCE

FRAME 13  0.12 SECONDS

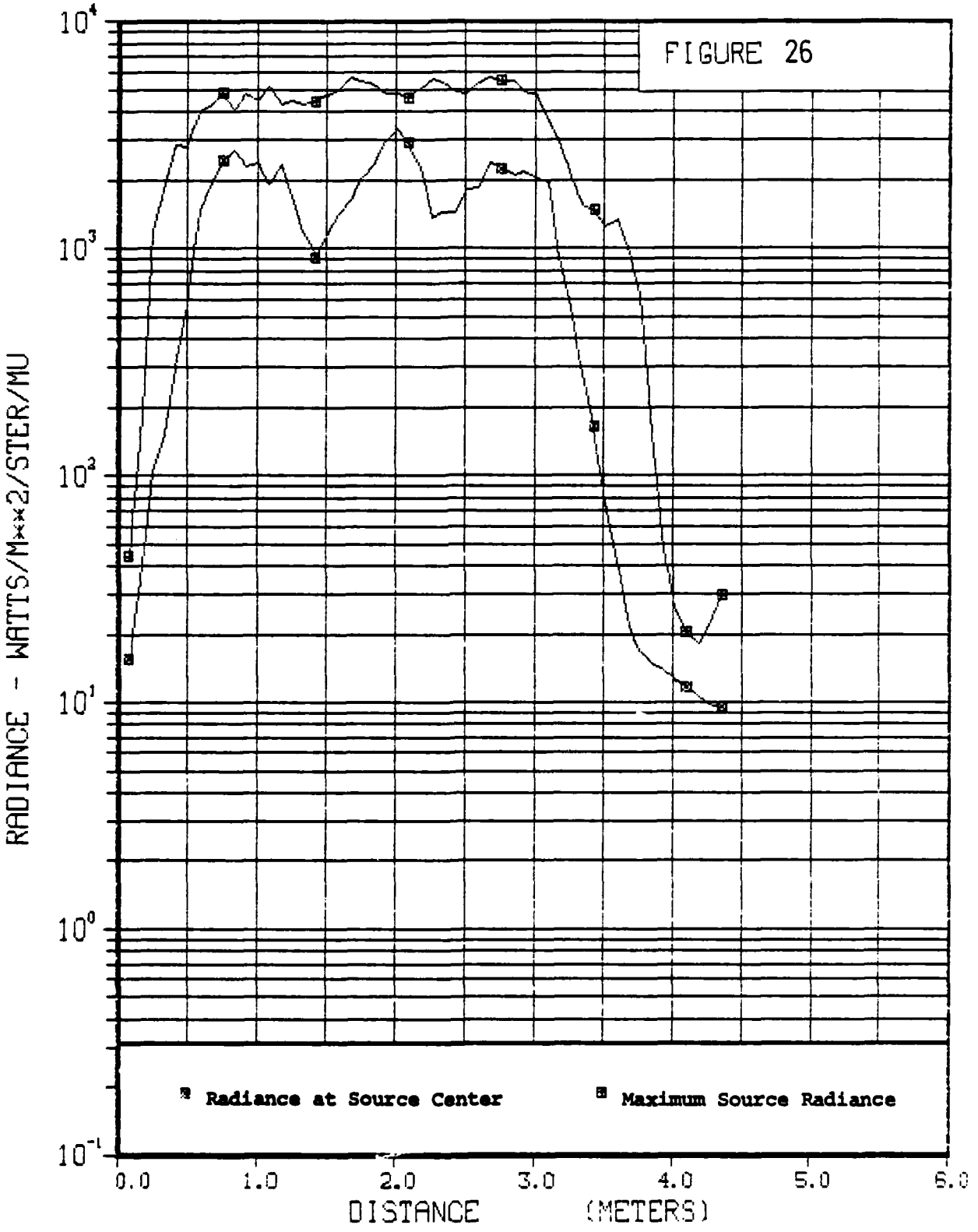

RADIANCE VS HORIZONTAL DISTANCE

FRAME 15  0.14 SECONDS

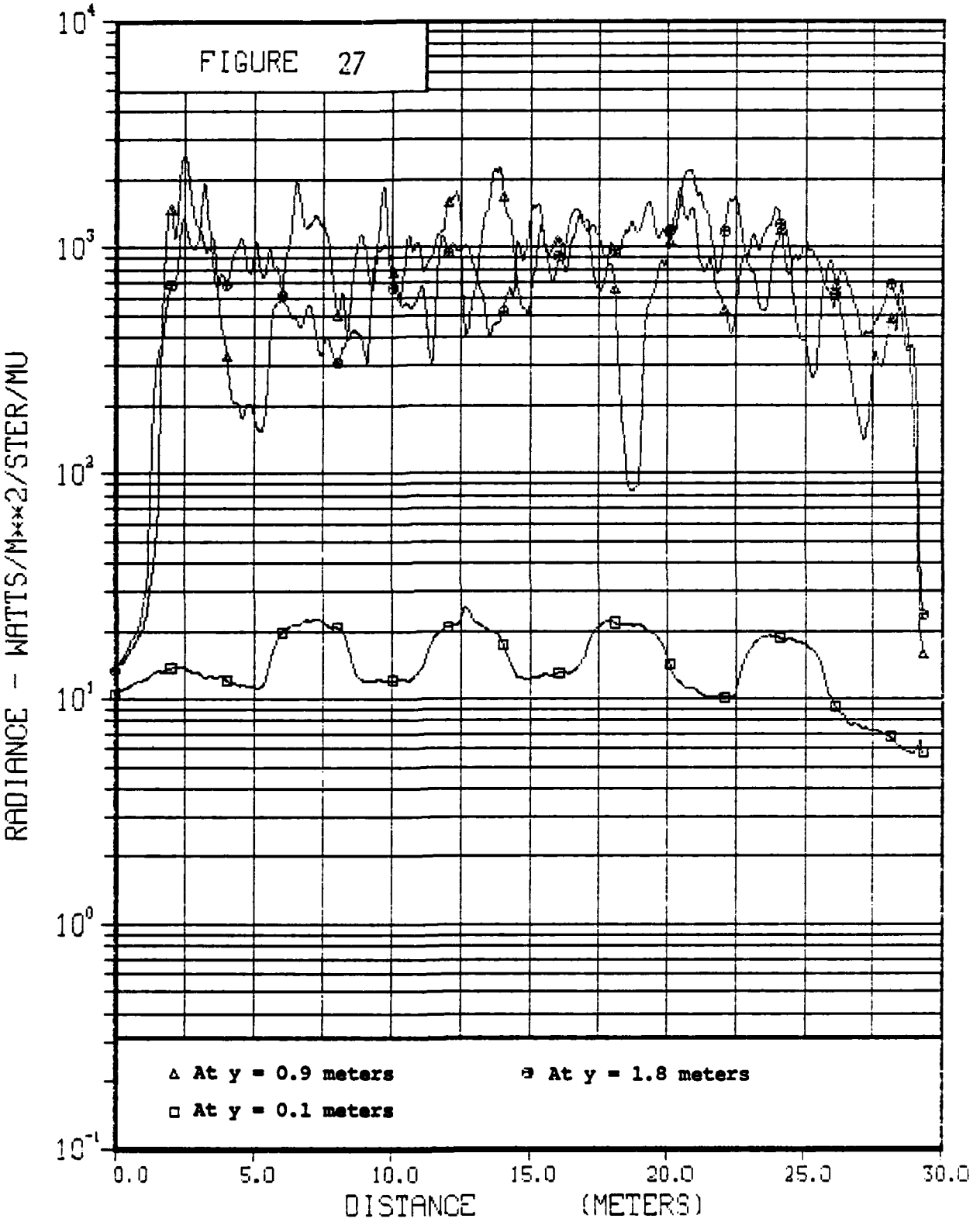

RADIANCE VS HORIZONTAL DISTANCE

FRAME 15  0.14 SECONDS

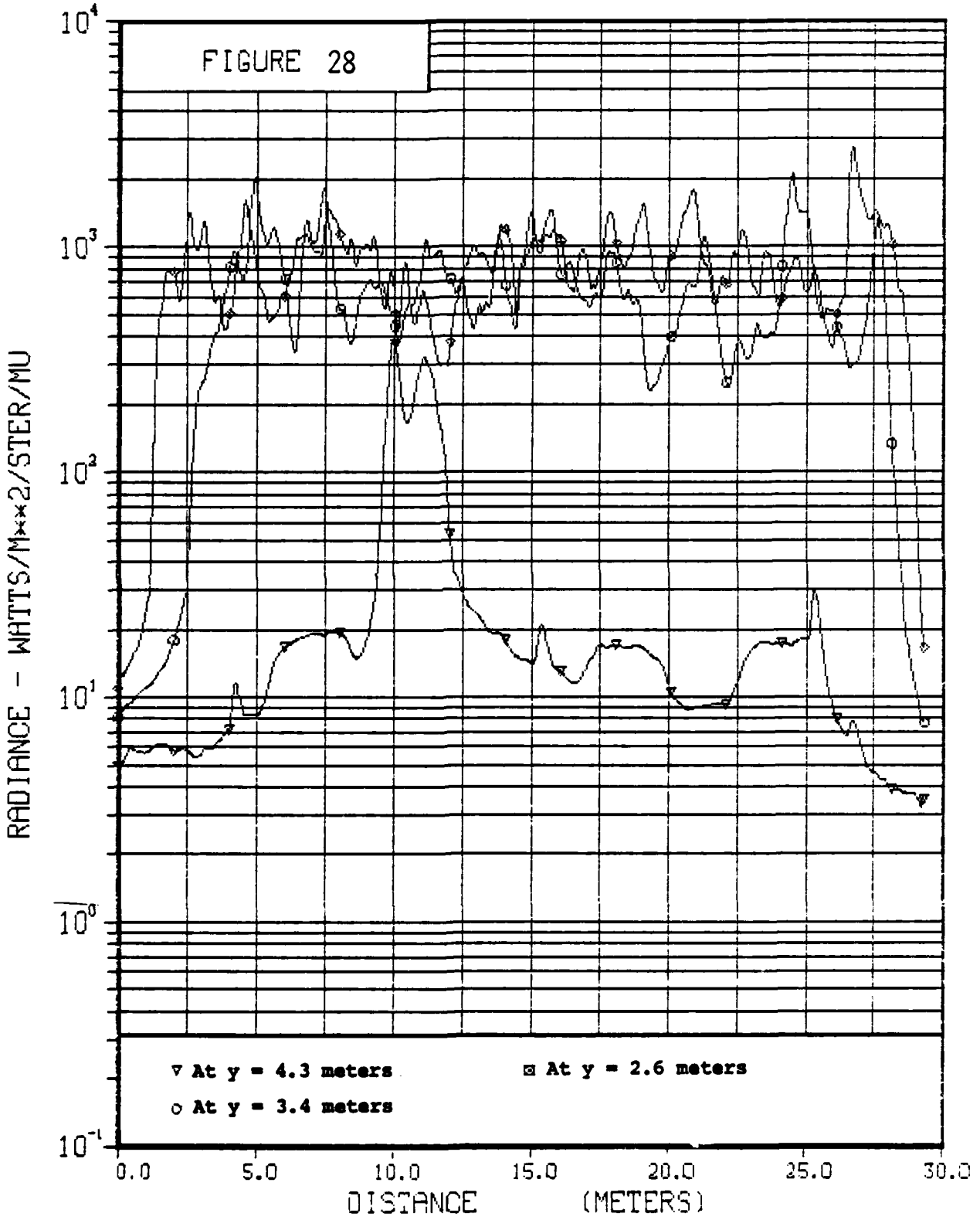

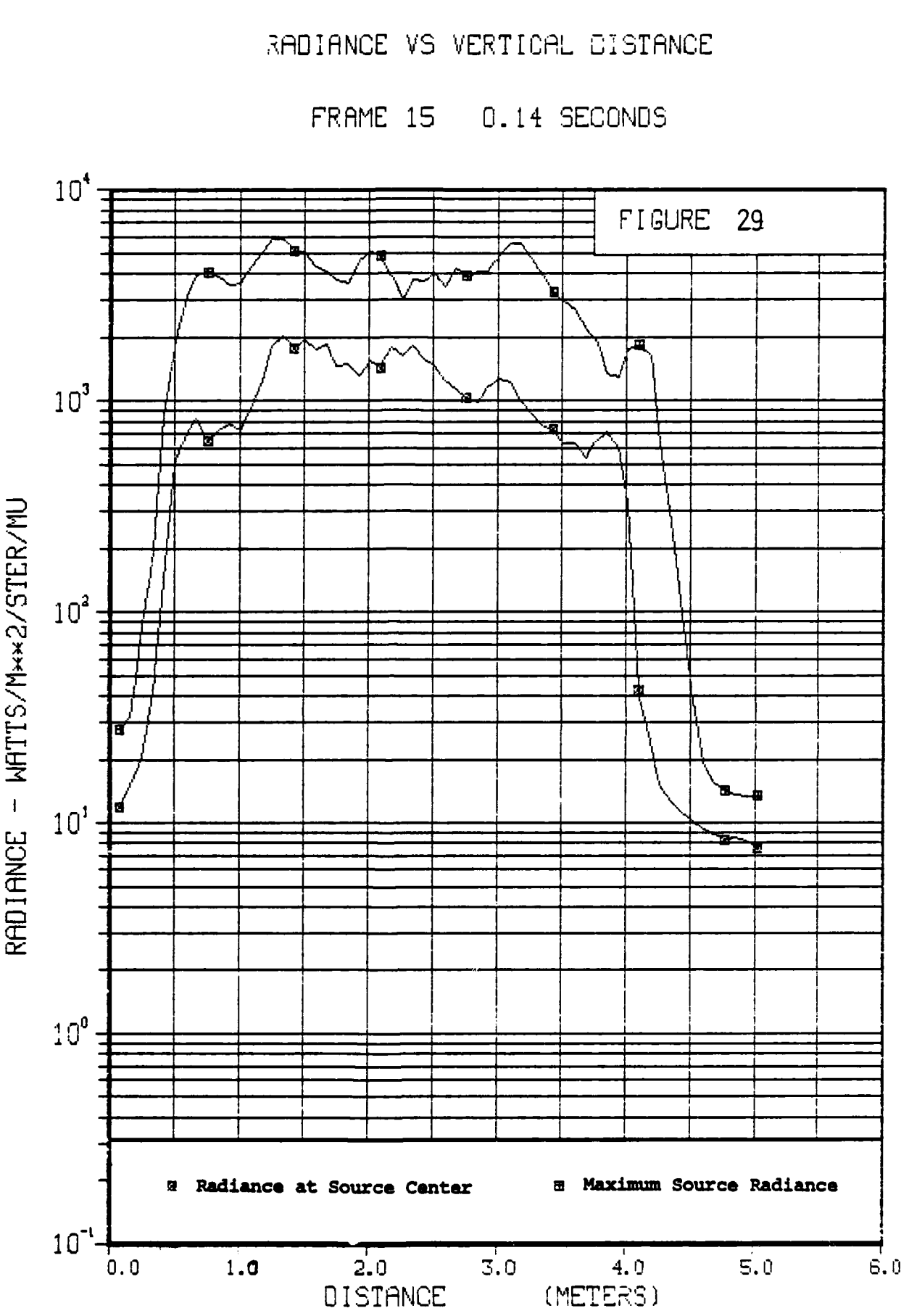
RADIANCE VS VERTICAL DISTANCE
FRAME 15 0.14 SECONDS
FIGURE 29
RADIANCE - WATTS/M**2/STER/MU
$10^4$
$10^3$
$10^2$
$10^1$
$10^0$
$10^{-1}$
0.0
1.0
2.0
3.0
4.0
5.0
6.0
DISTANCE (METERS)
Radiance at Source Center
Maximum Source Radiance

RADIANCE VS. HORIZONTAL DISTANCE

FRAME 17  0.16 SECONDS

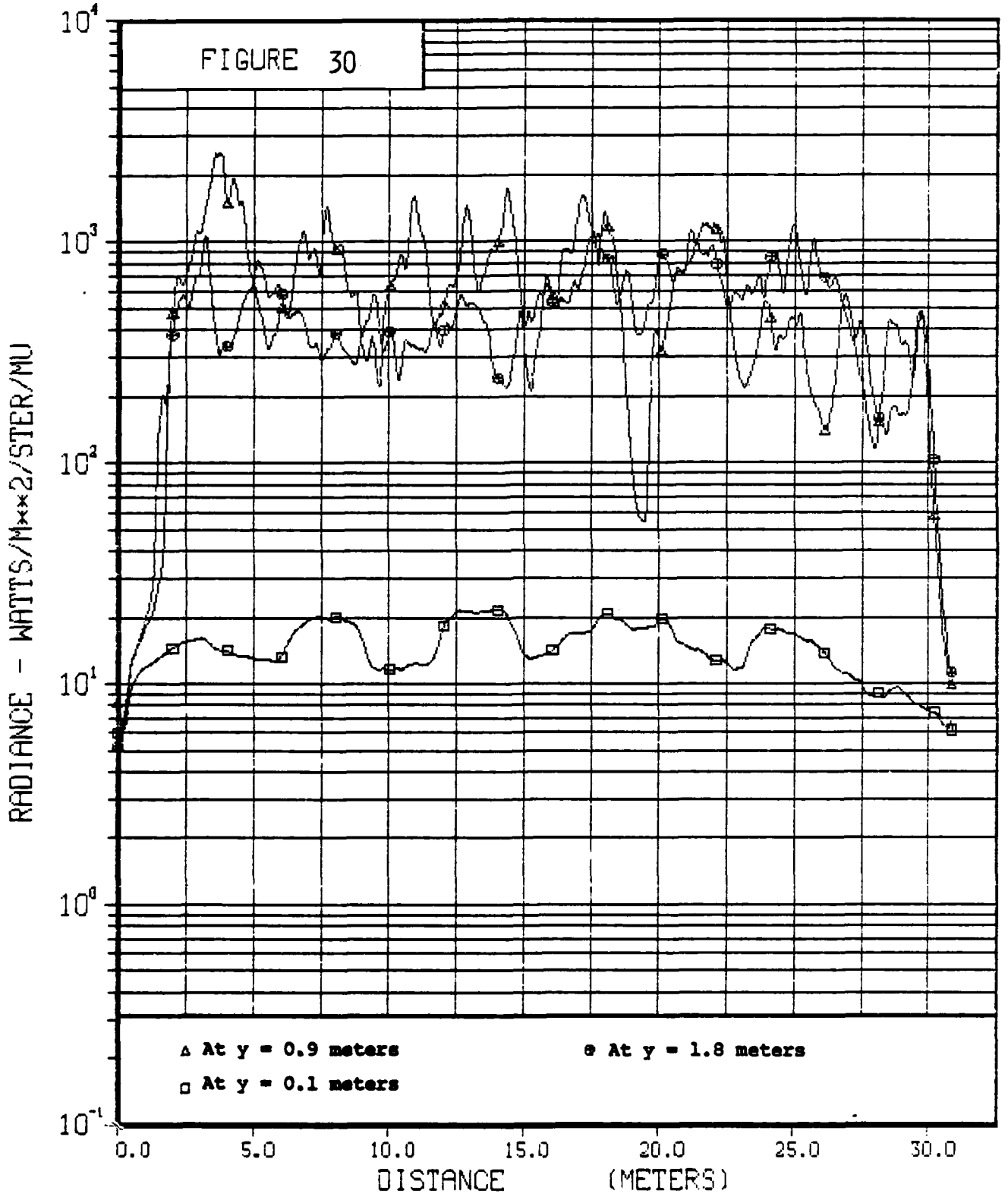

RADIANCE VS HORIZONTAL DISTANCE

FRAME 17  0.16 SECONDS

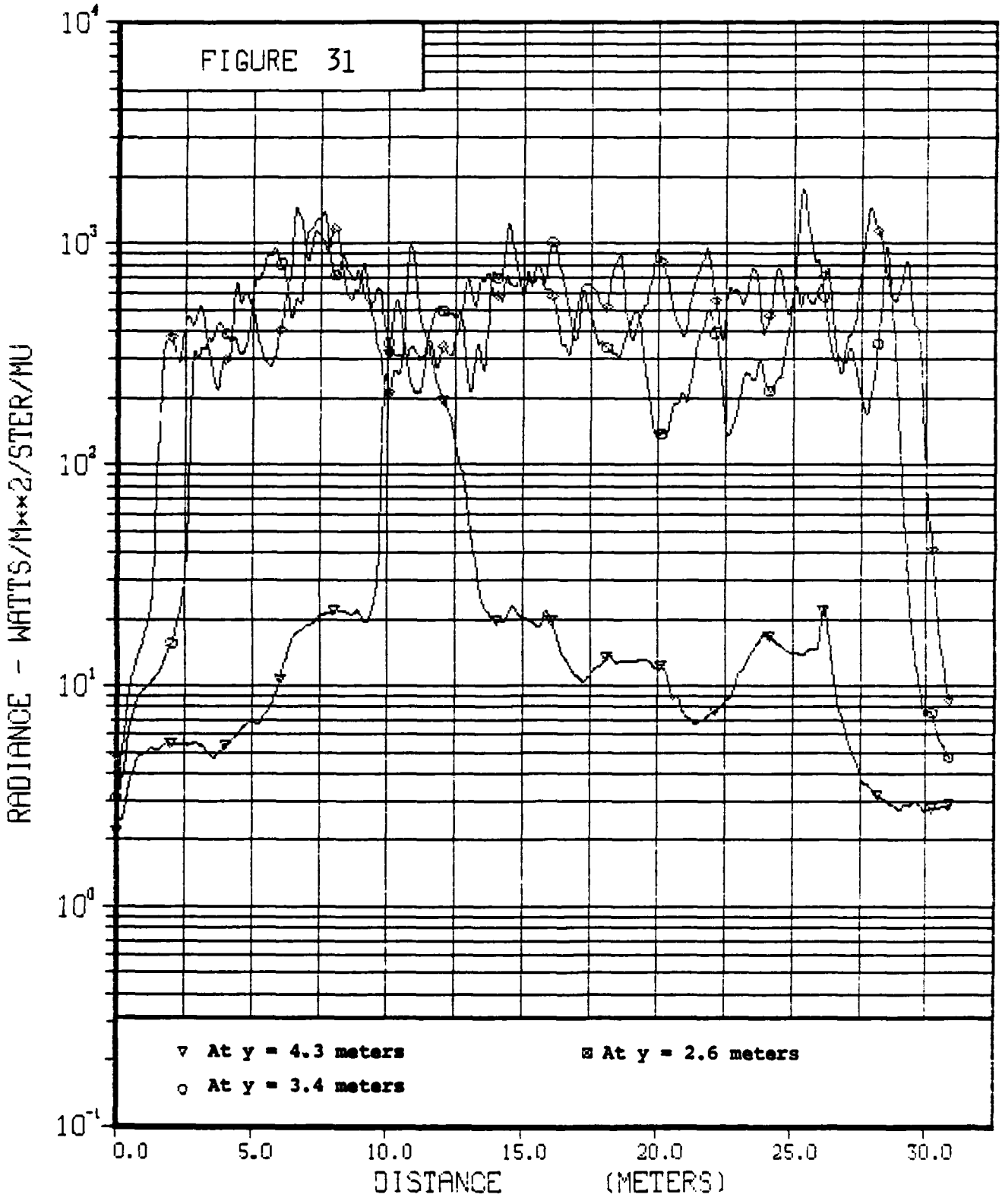

RADIANCE VS VERTICAL DISTANCE

FRAME 17  0.16 SECONDS

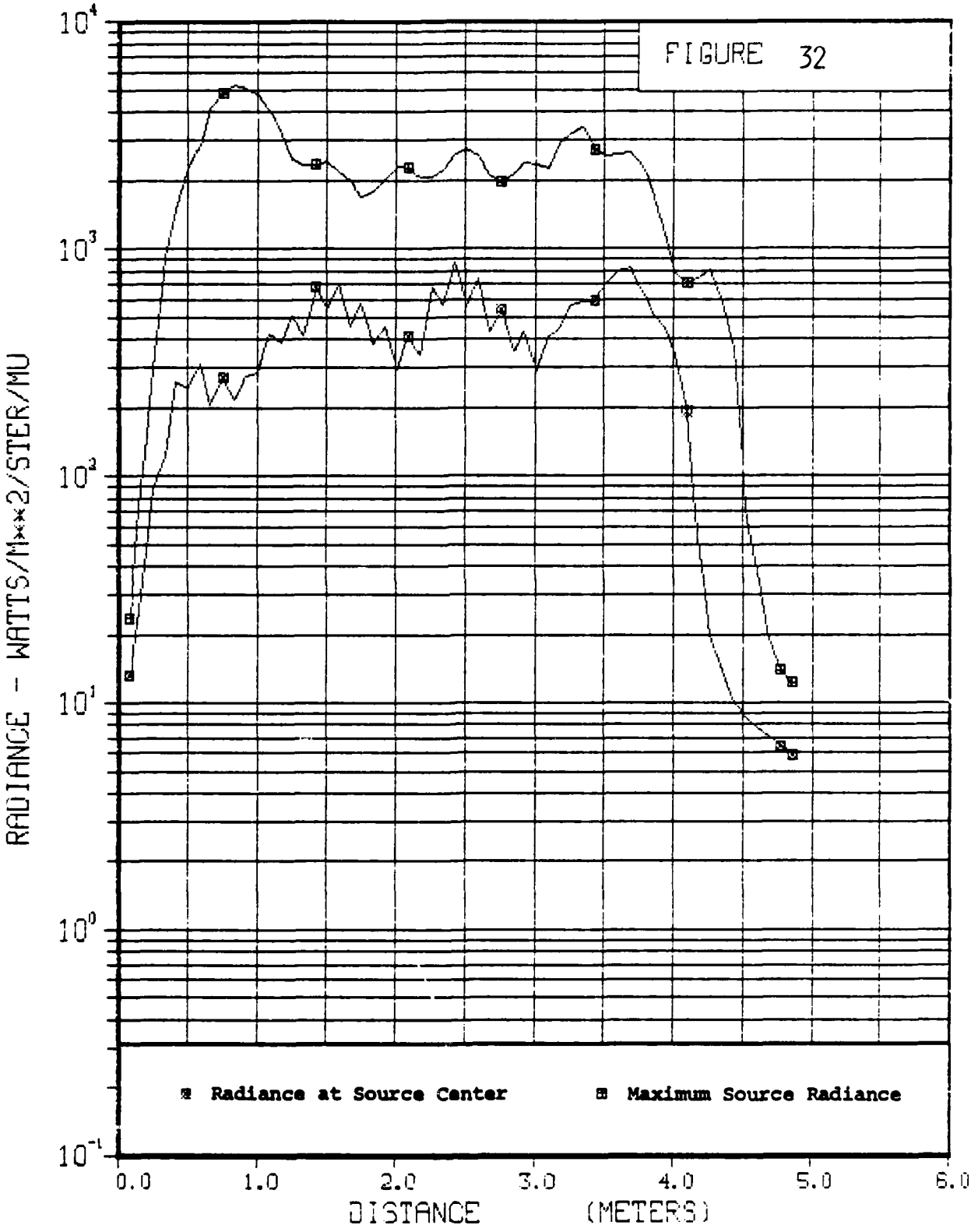

RADIANCE VS HORIZONTAL DISTANCE

FRAME 19  0.18 SECONDS

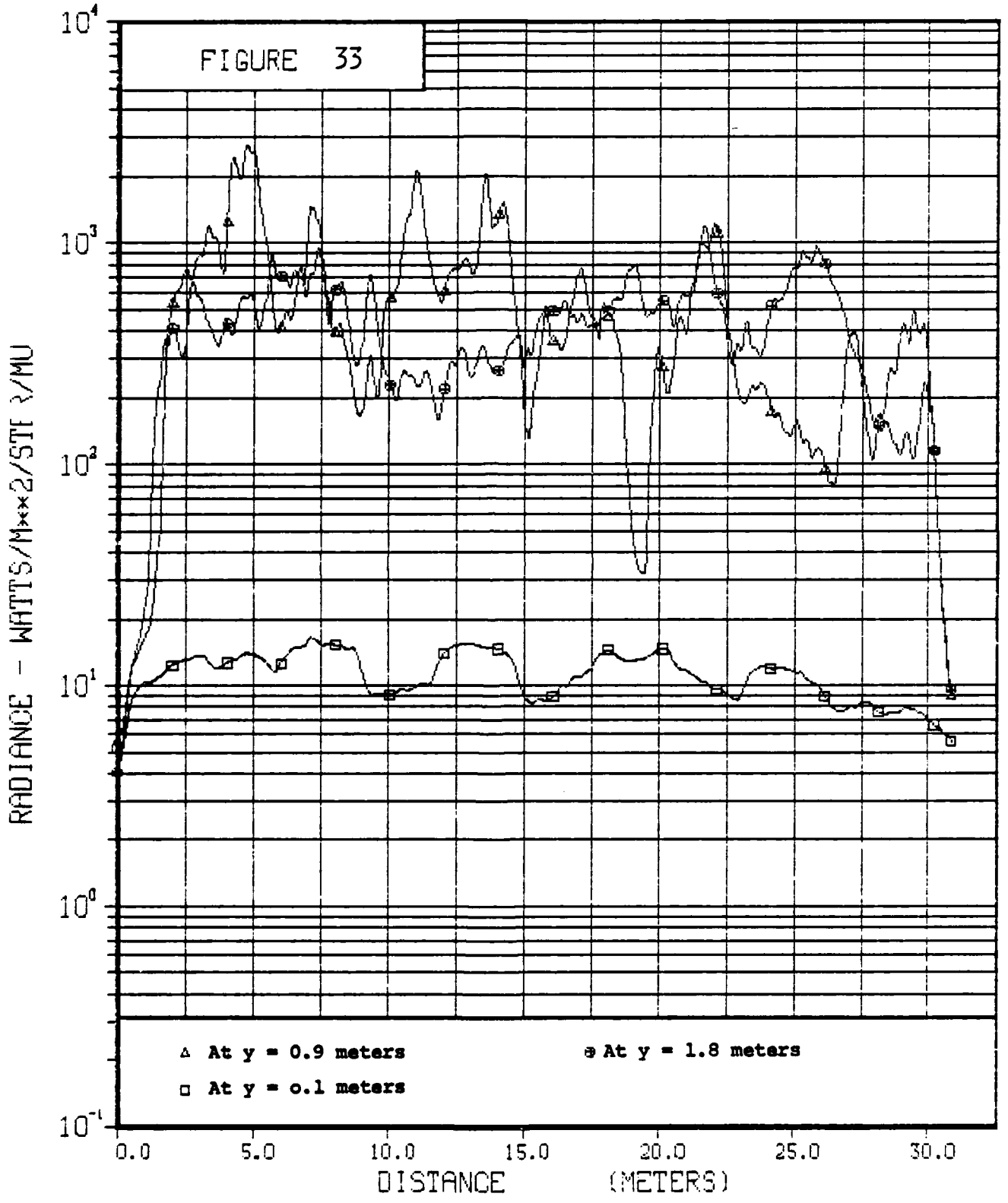

RADIANCE VS HORIZONTAL DISTANCE

FRAME 19  0.18 SECONDS

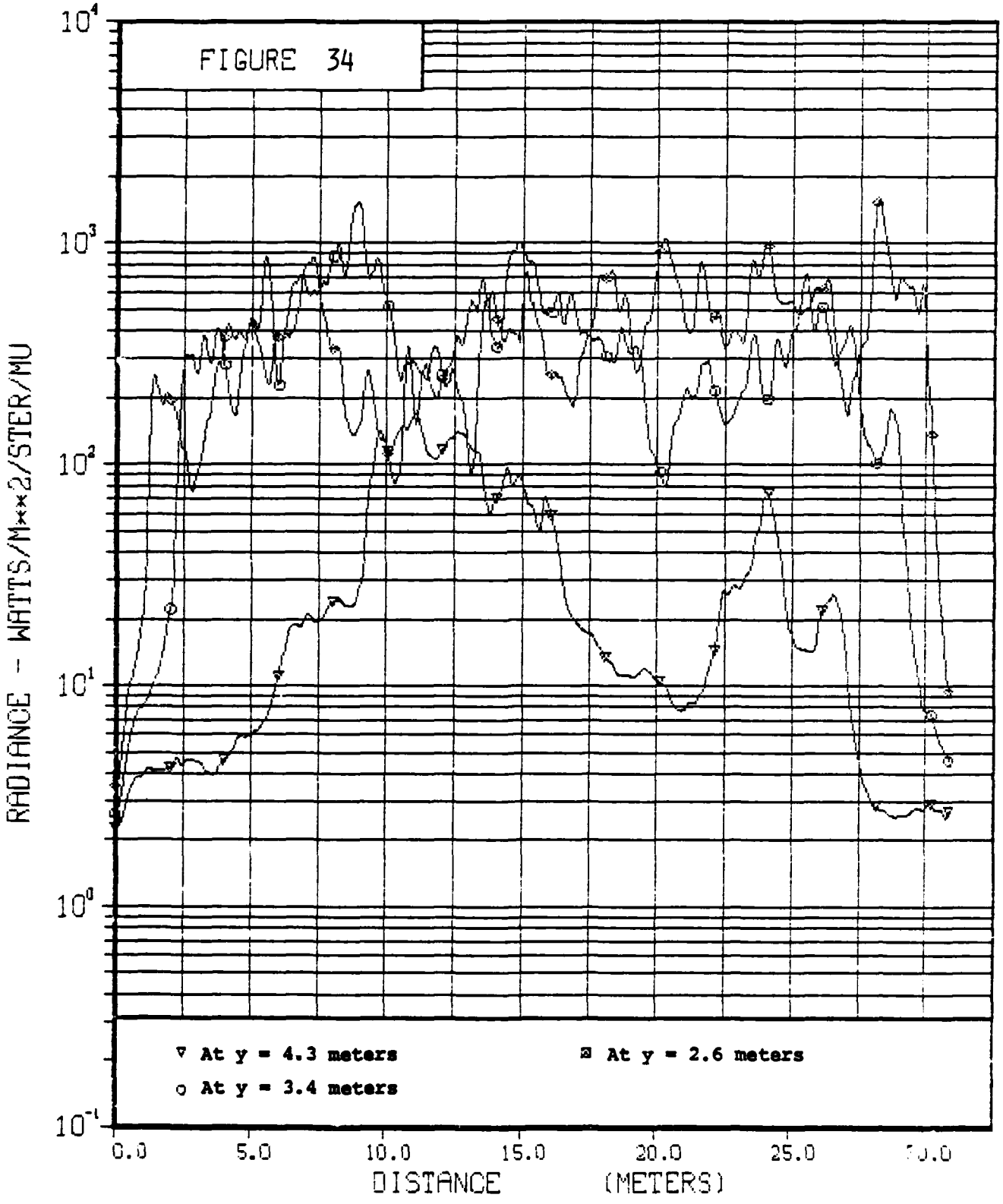

RADIANCE VS VERTICAL DISTANCE

FRAME 19  0.18 SECONDS

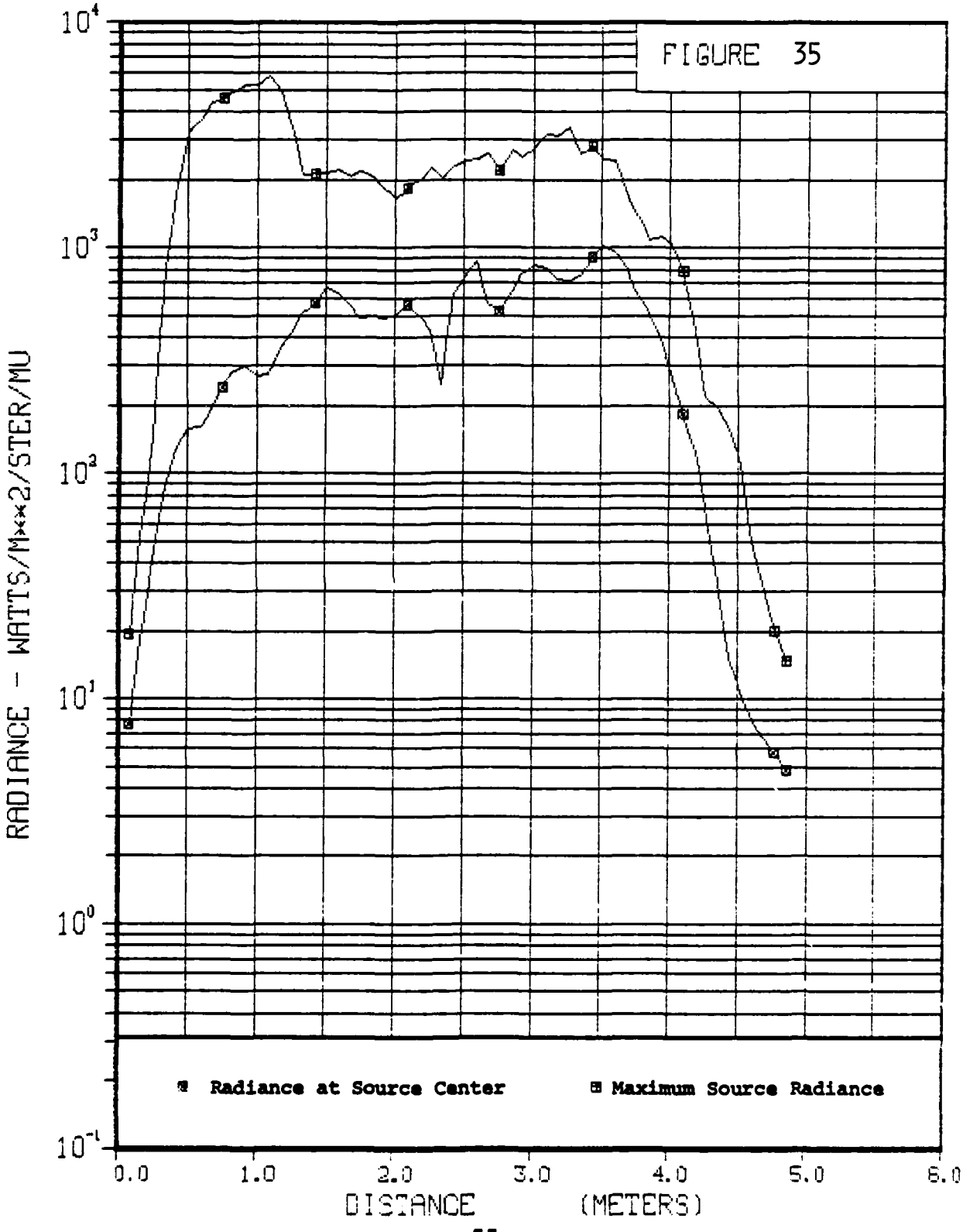

RADIANCE VS HORIZONTAL DISTANCE

FRAME 22  0.21 SECONDS

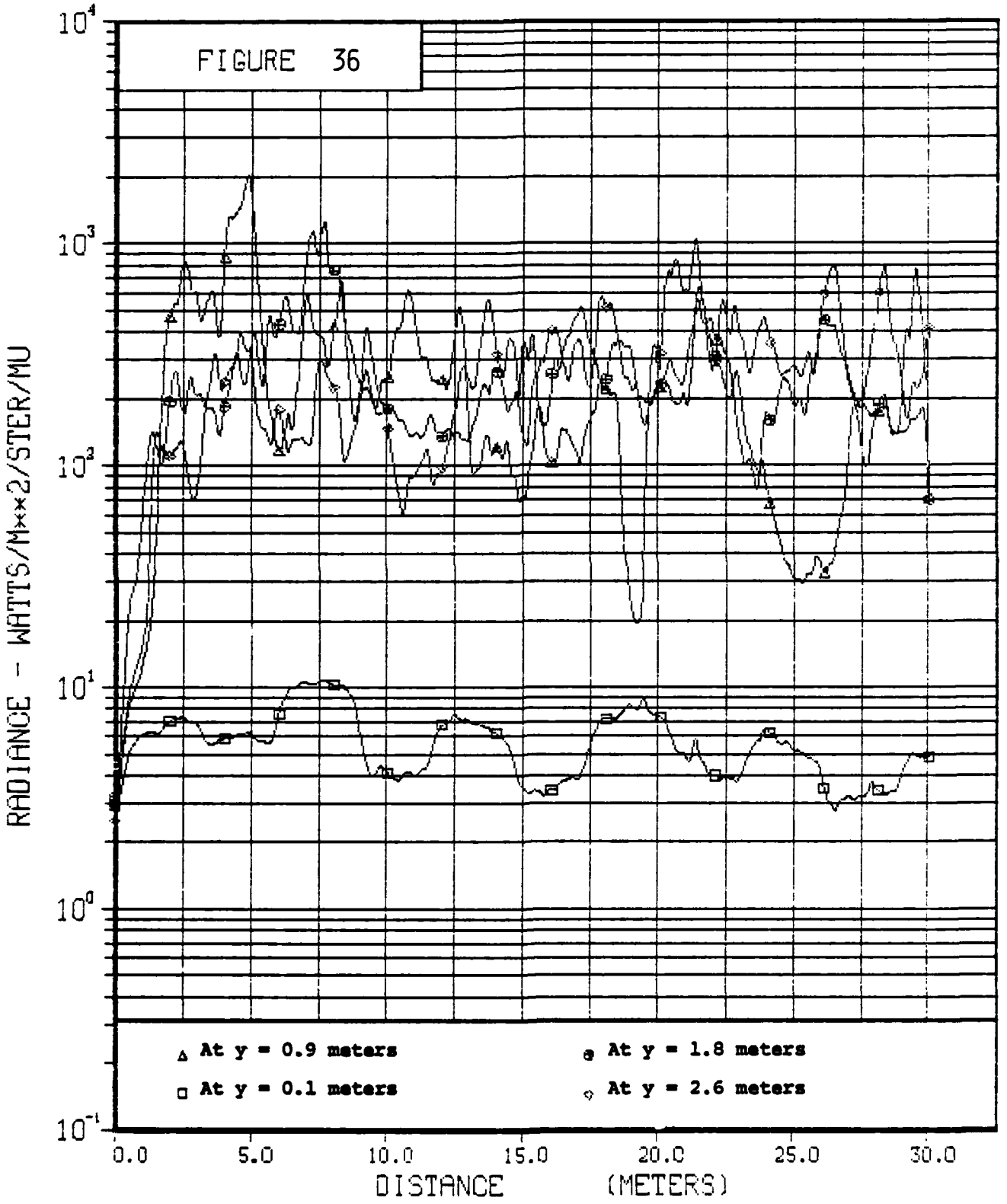

RADIANCE VS HORIZONTAL DISTANCE

FRAME 22  0.21 SECONDS

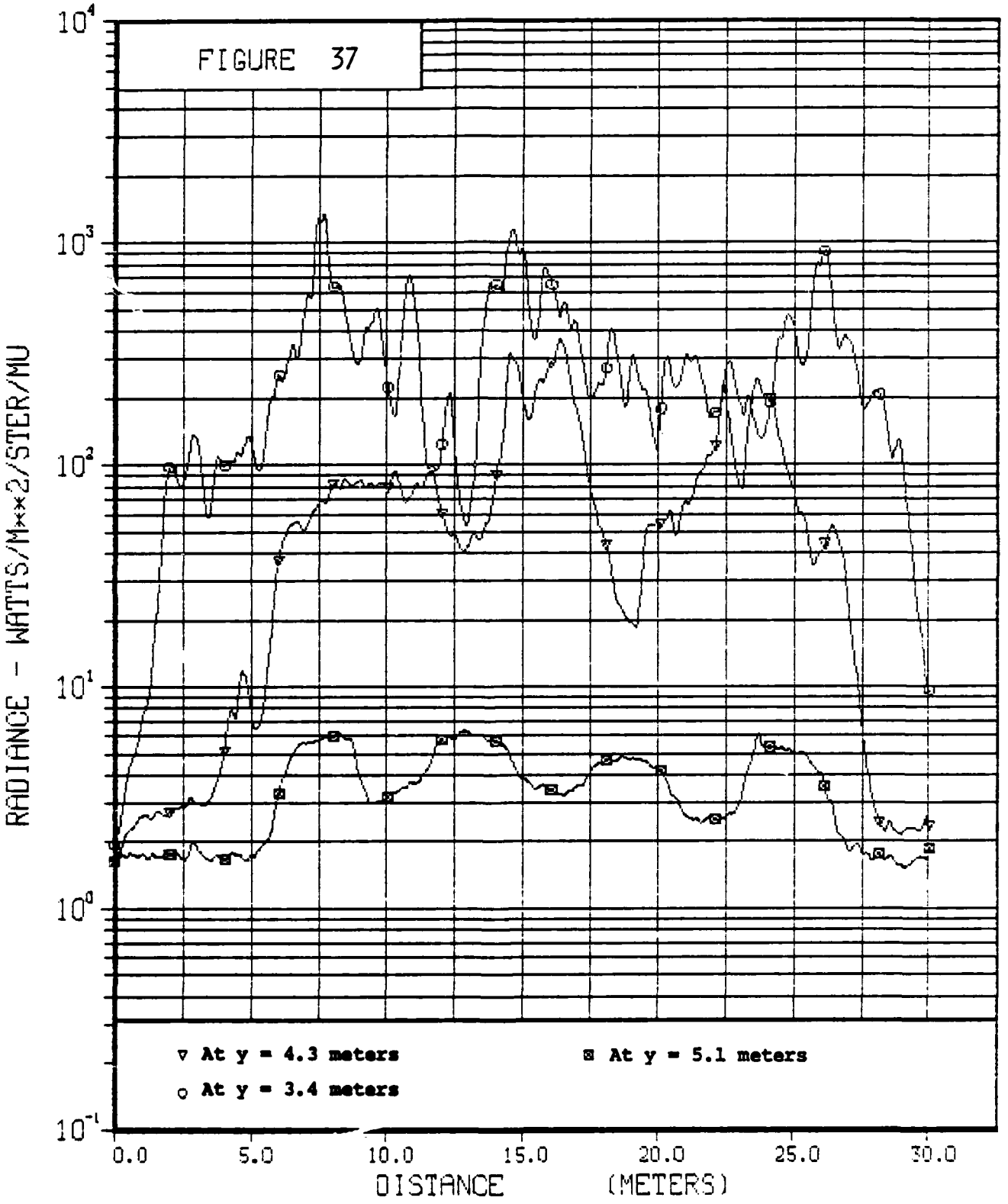

RADIANCE VS VERTICAL DISTANCE

FRAME 22  0.21 SECONDS

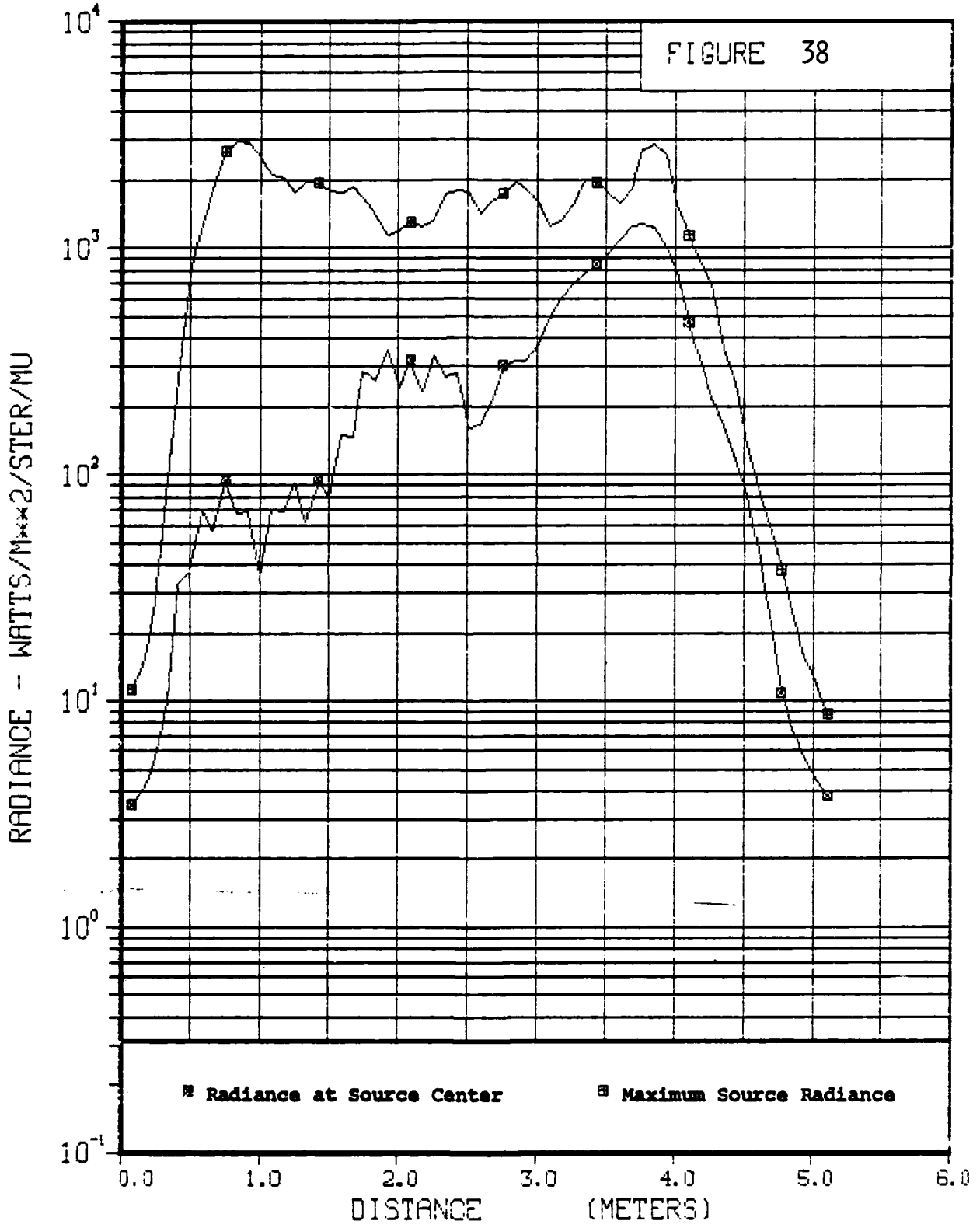

RADIANCE VS HORIZONTAL DISTANCE

FRAME 25  0.24 SECONDS

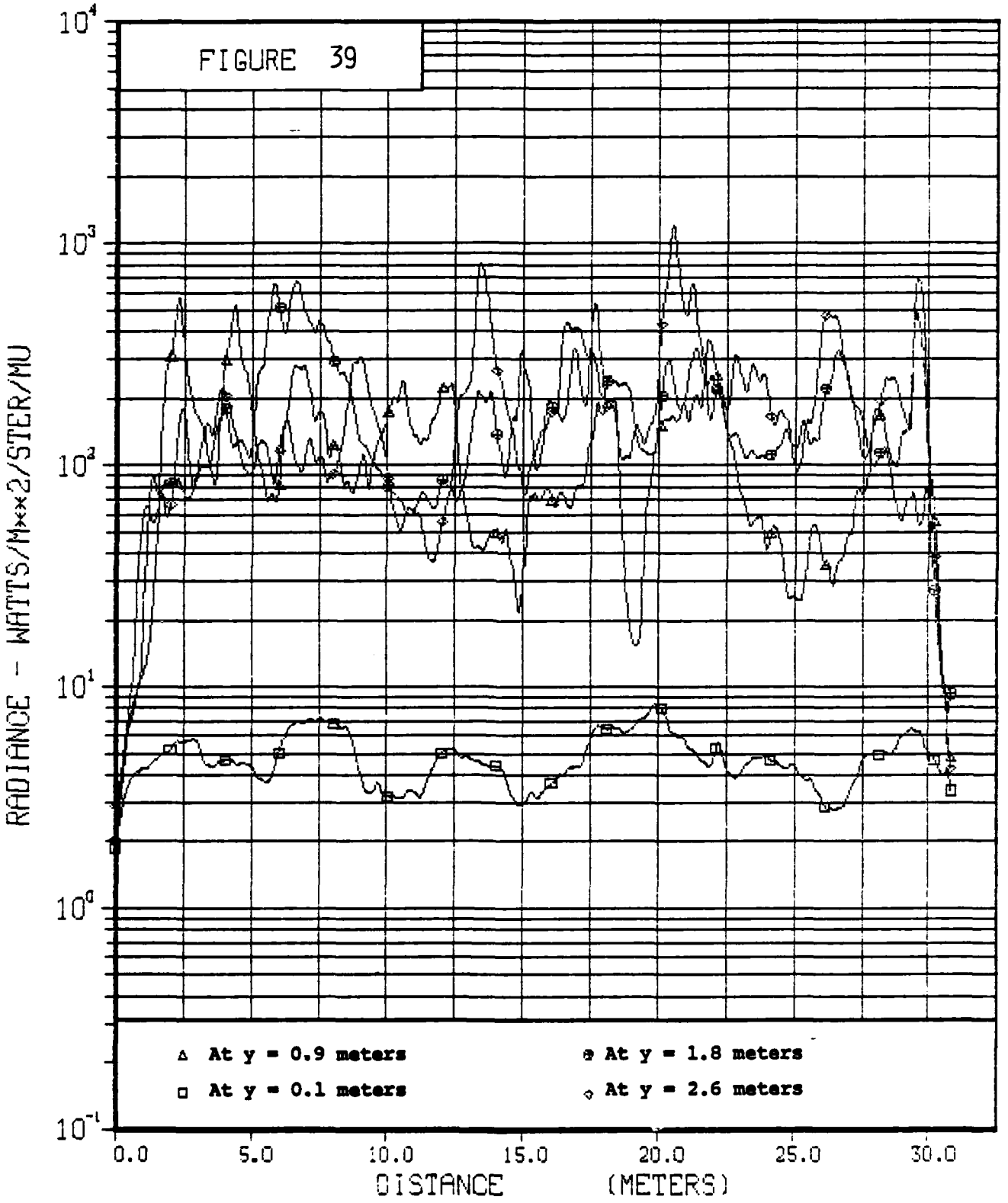

RADIANCE VS HORIZONTAL DISTANCE

FRAME 25  0.24 SECONDS

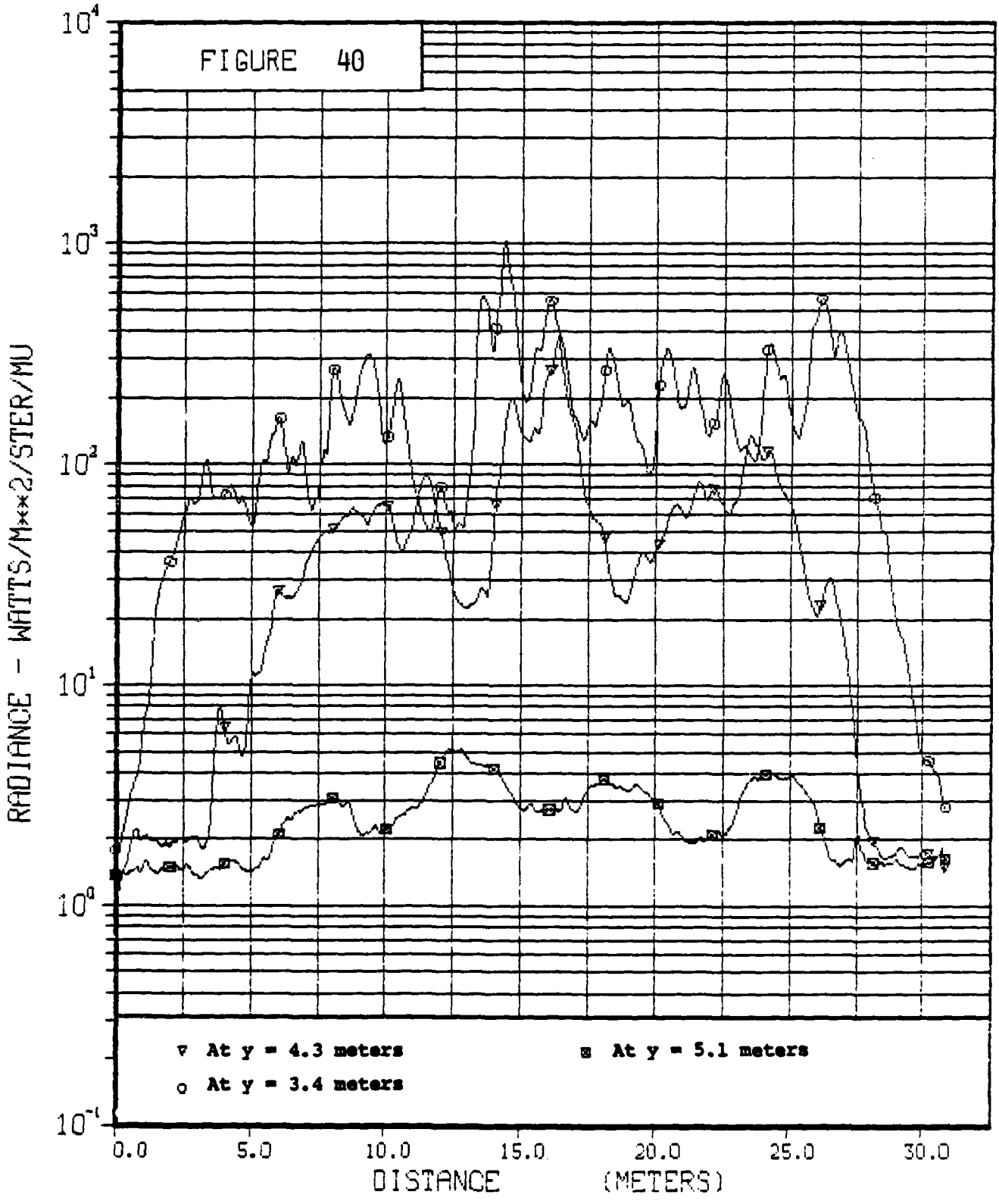

RADIANCE VS VERTICAL DISTANCE

FRAME 25  0.24 SECONDS

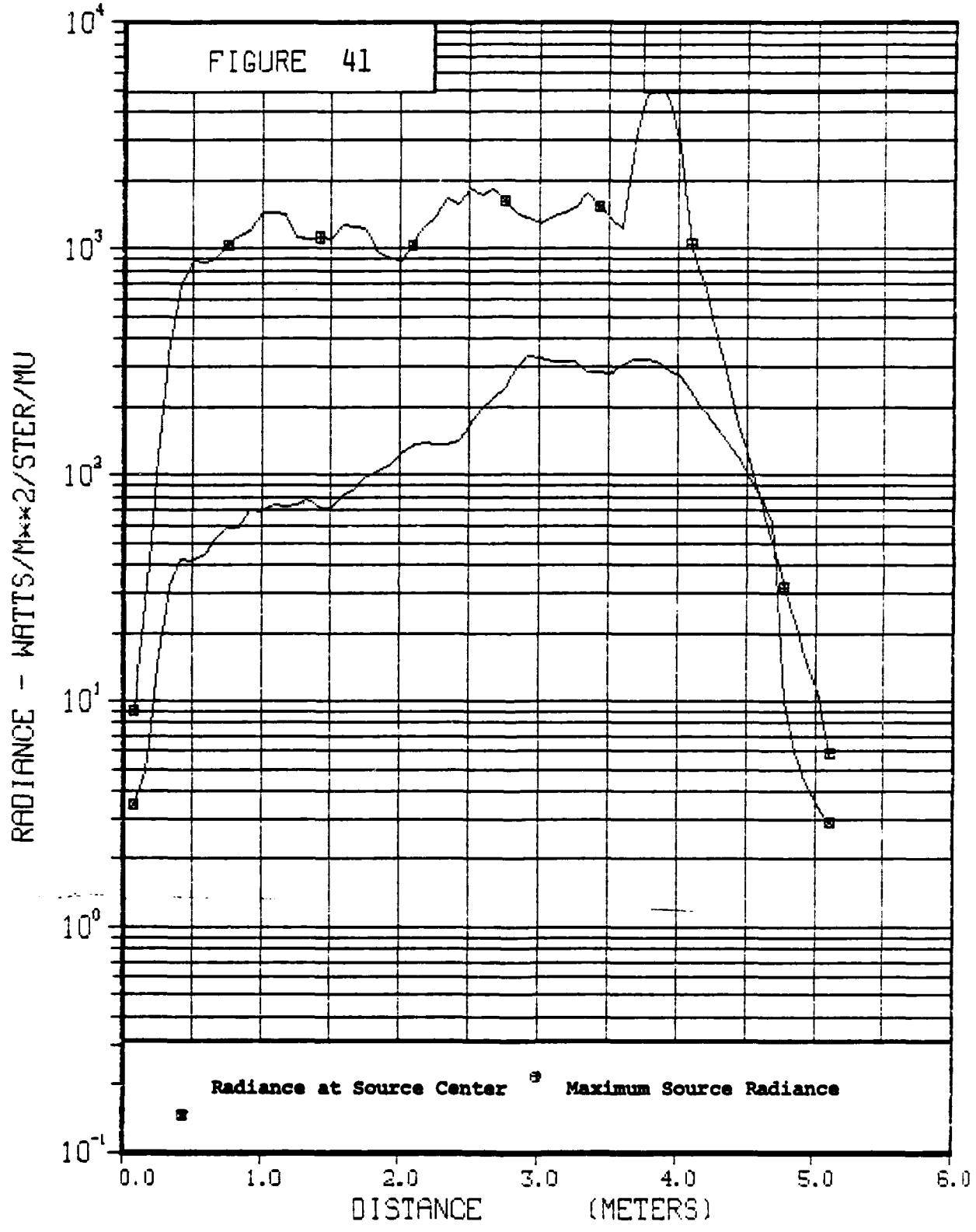

RADIANCE VS HORIZONTAL DISTANCE

FRAME 30  0.29 SECONDS

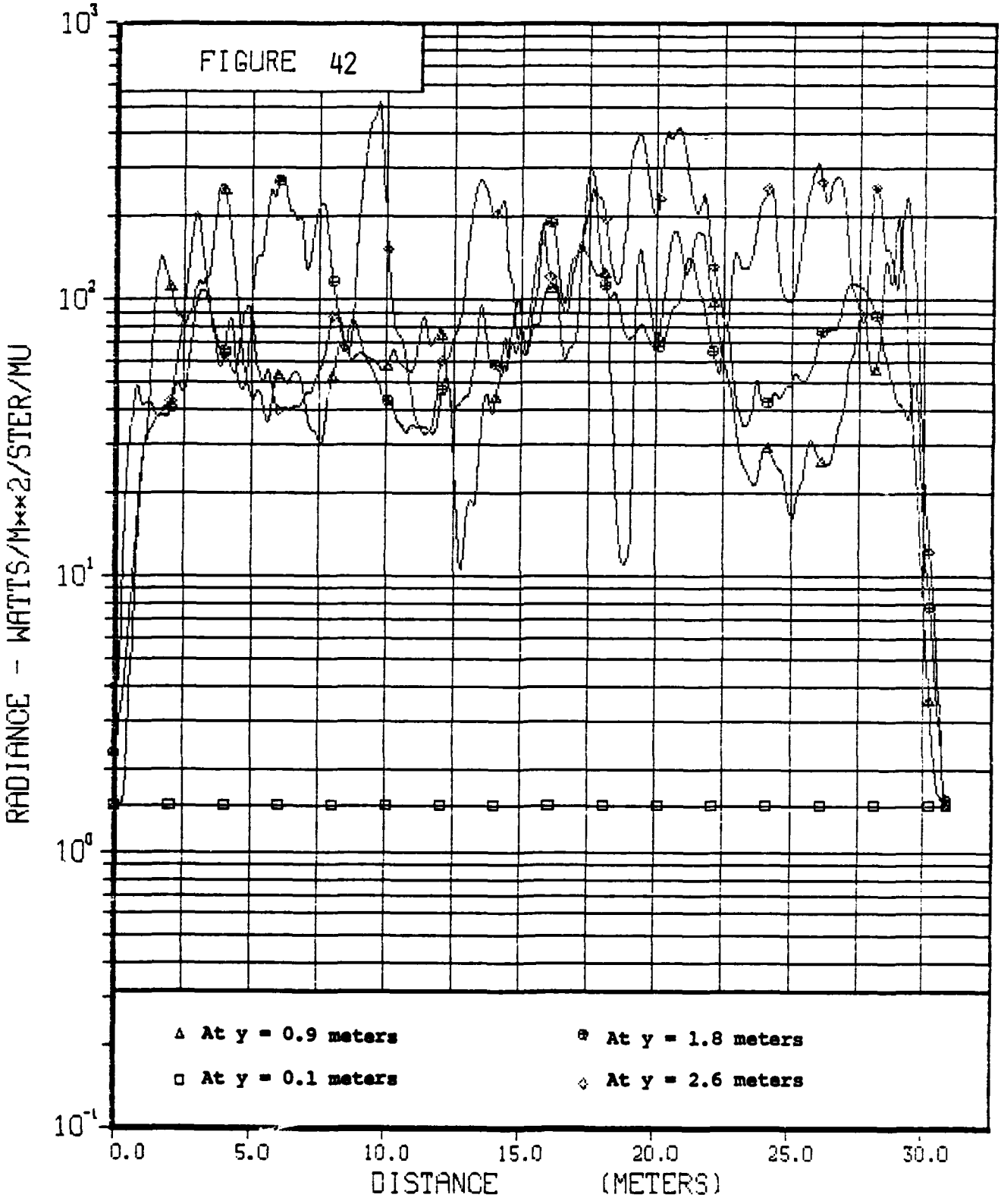

RADIANCE VS HORIZONTAL DISTANCE

FRAME 30  0.29 SECONDS

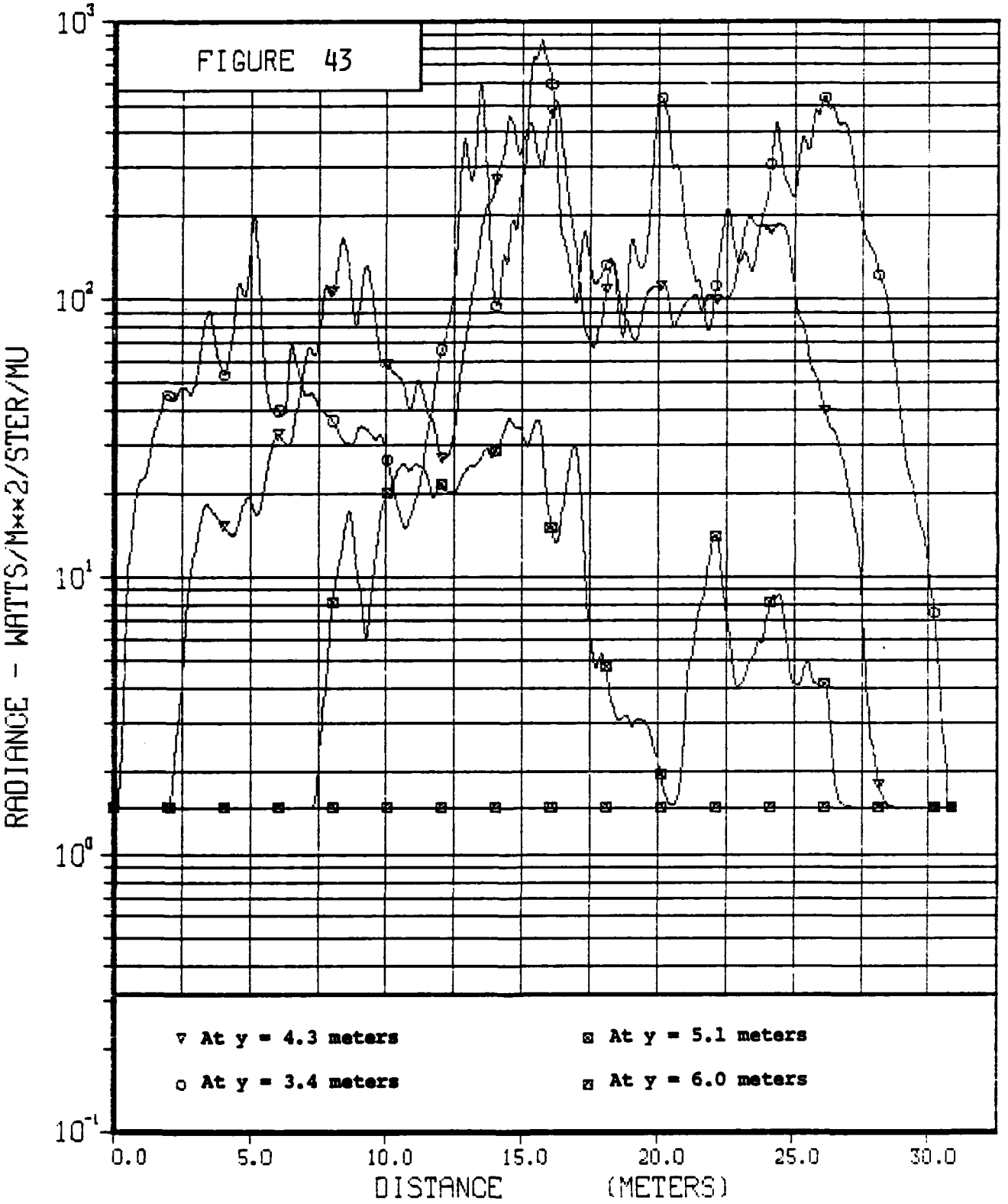

RADIANCE VS VERTICAL DISTANCE

FRAME 30  0.29 SECONDS

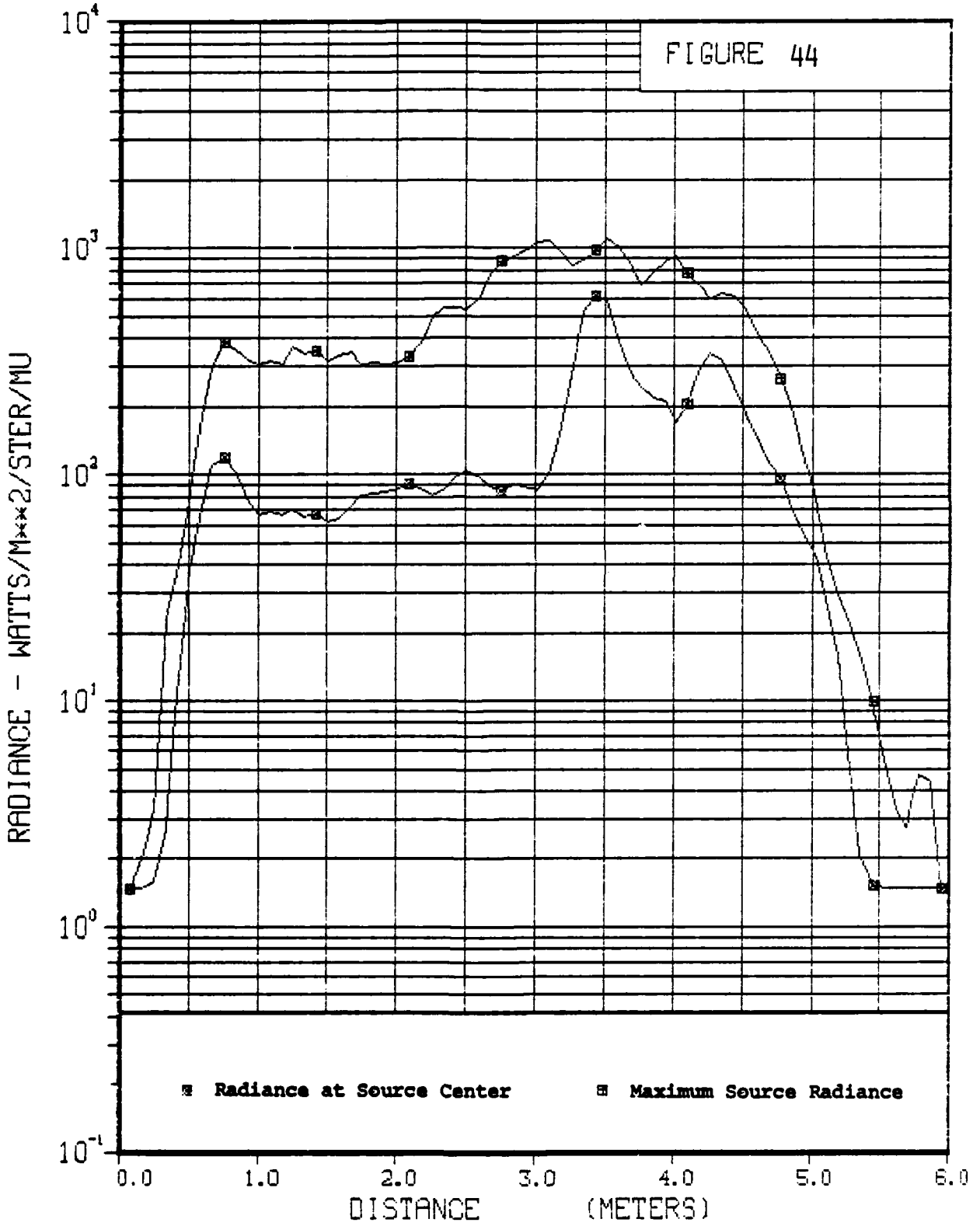

RADIANCE VS HORIZONTAL DISTANCE

FRAME 35 0.34 SECONDS

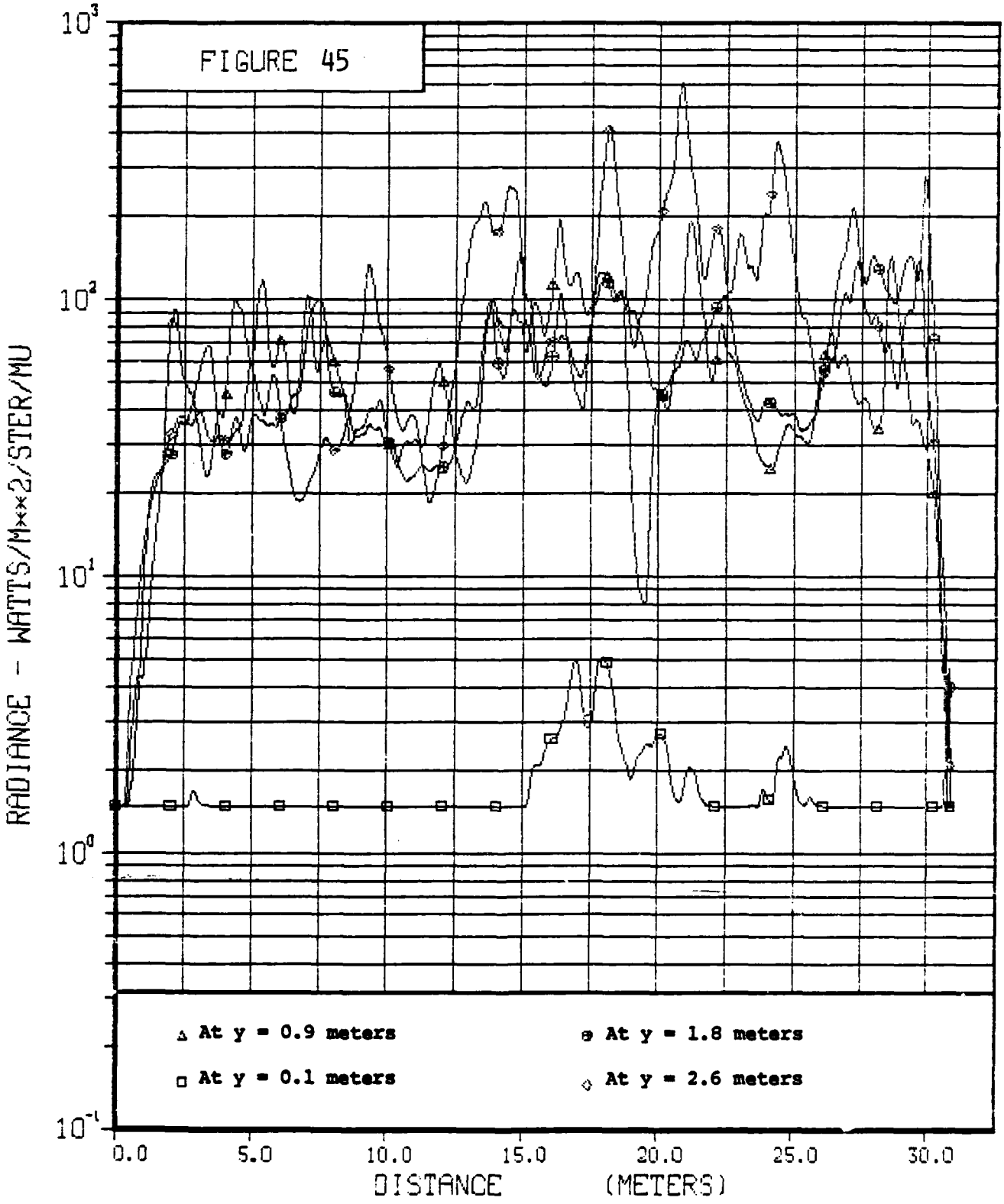

RADIANCE VS HORIZONTAL DISTANCE

FRAME 35  0.34 SECONDS

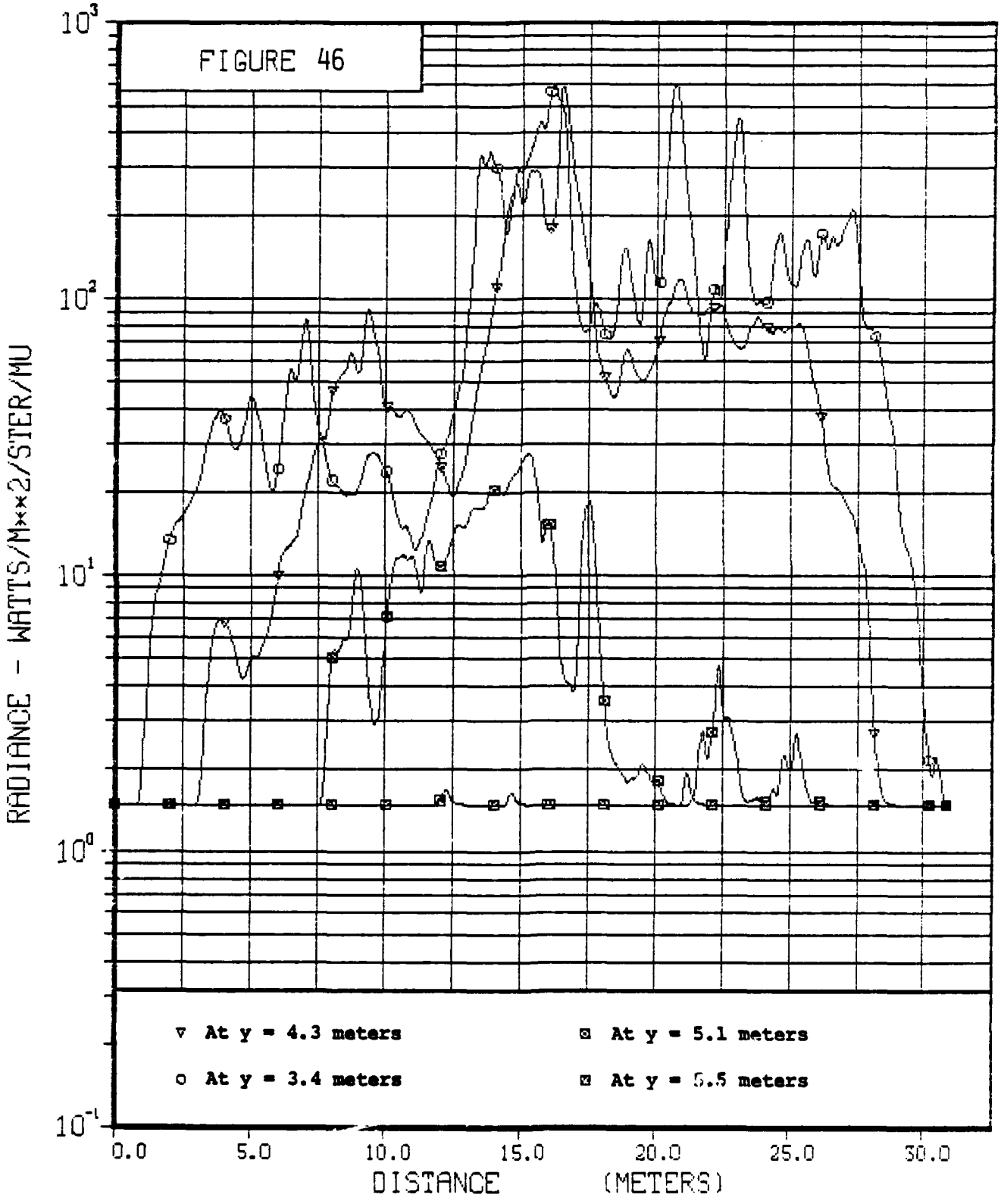

RADIANCE VS VERTICAL DISTANCE

FRAME 35  0.34 SECONDS

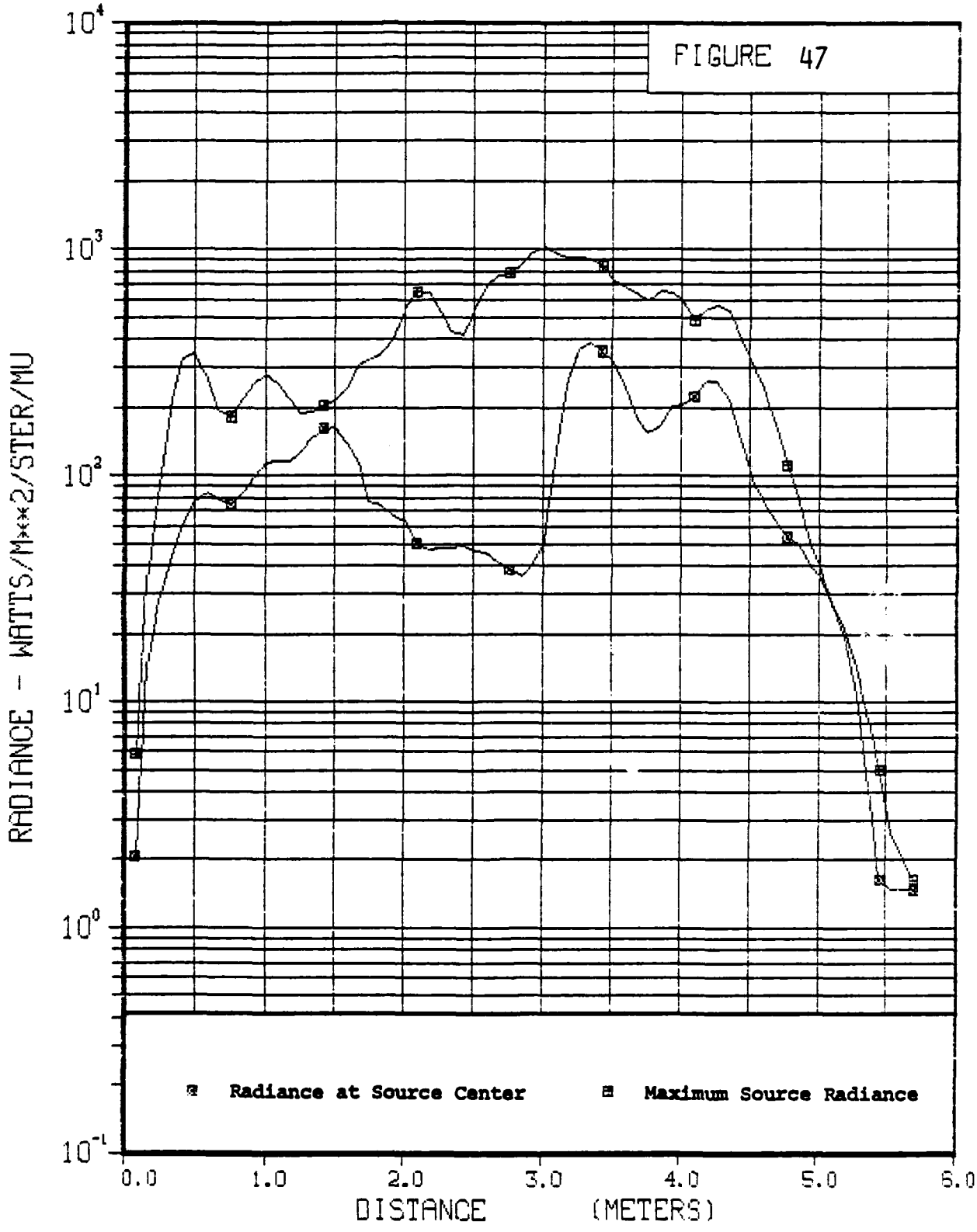

RADIANCE VS HORIZONTAL DISTANCE

FRAME 40  0.39 SECONDS

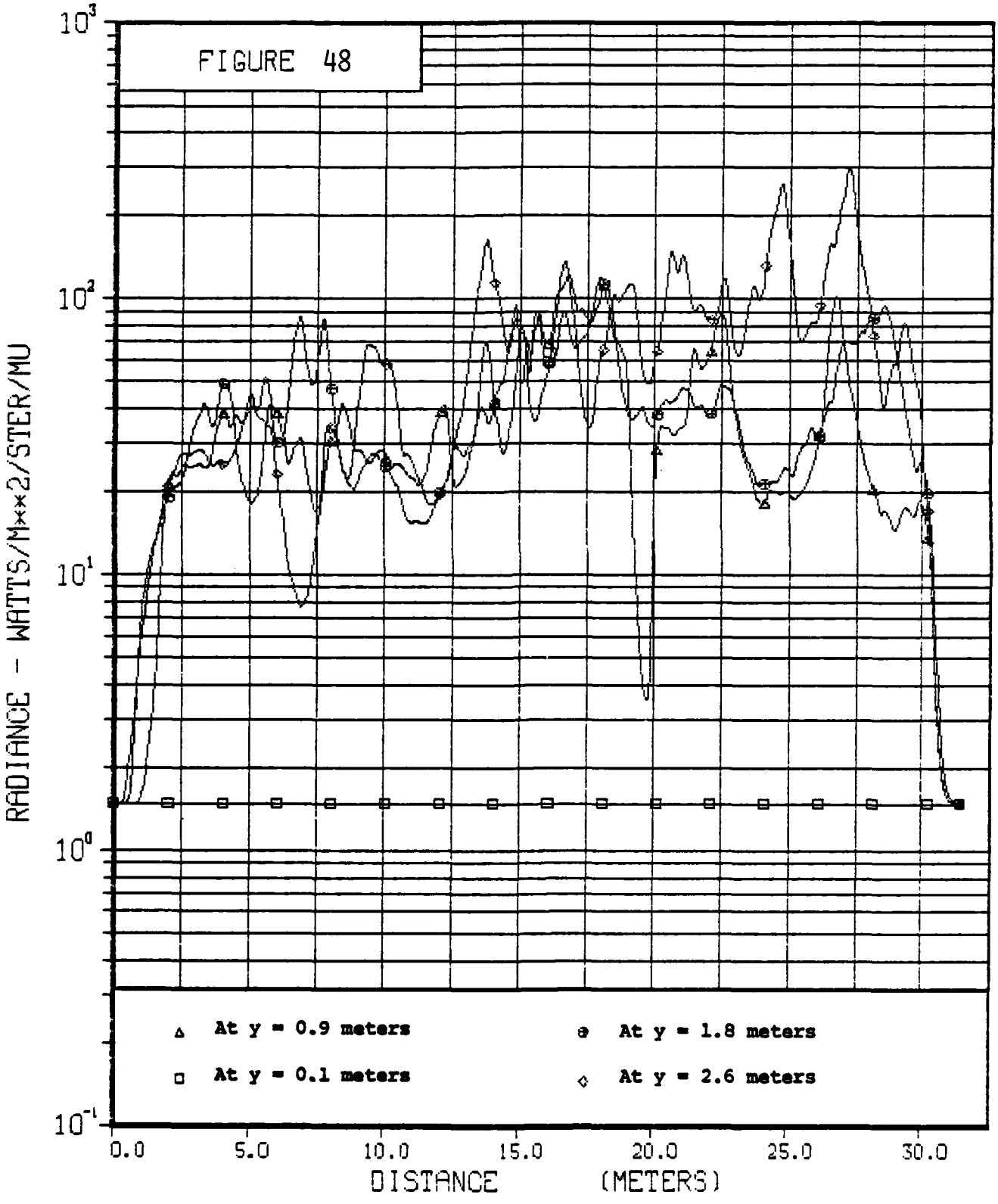

RADIANCE VS HORIZONTAL DISTANCE

FRAME 40  0.39 SECONDS

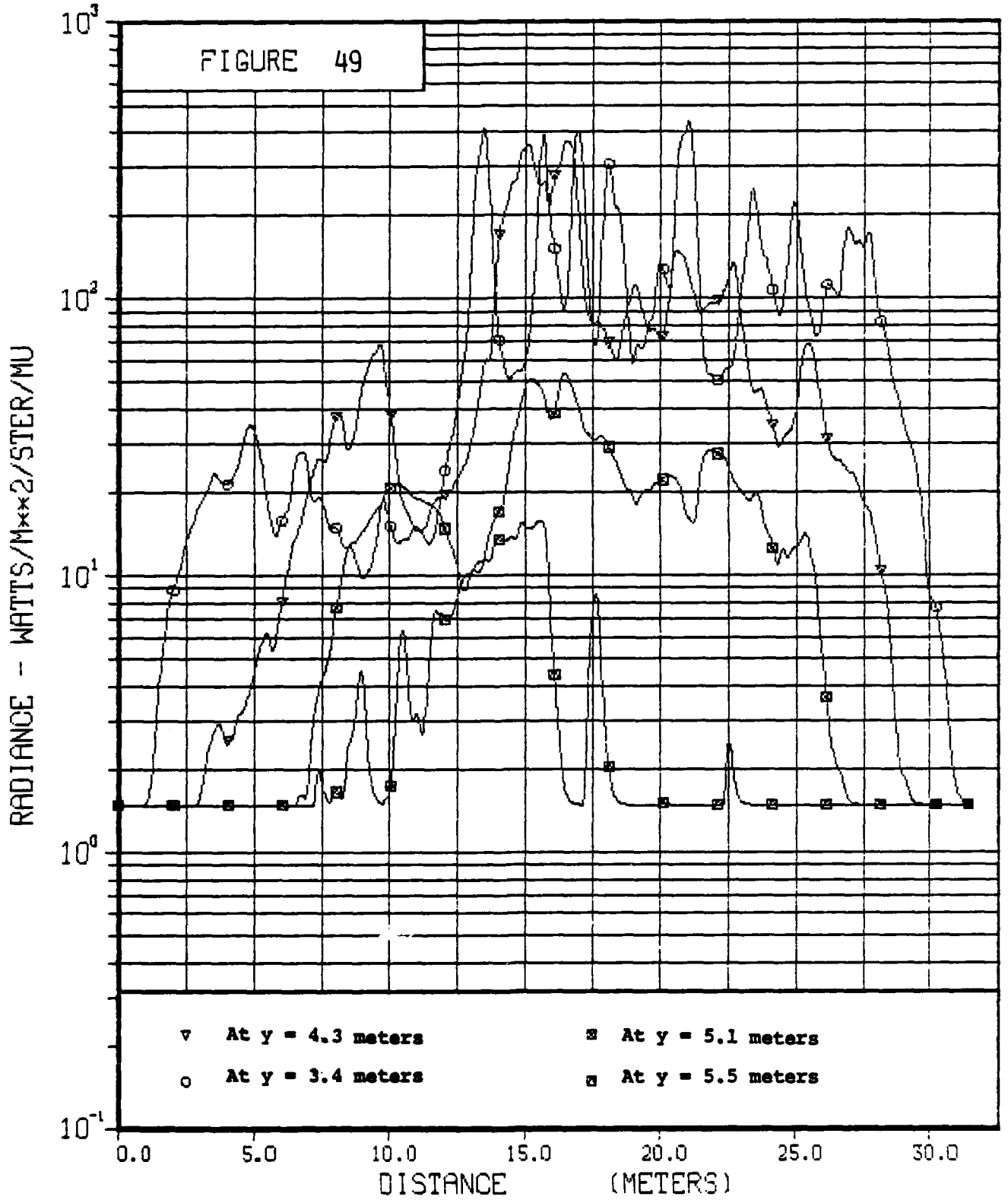

RADIANCE VS VERTICAL DISTANCE

FRAME 40  0.39 SECONDS

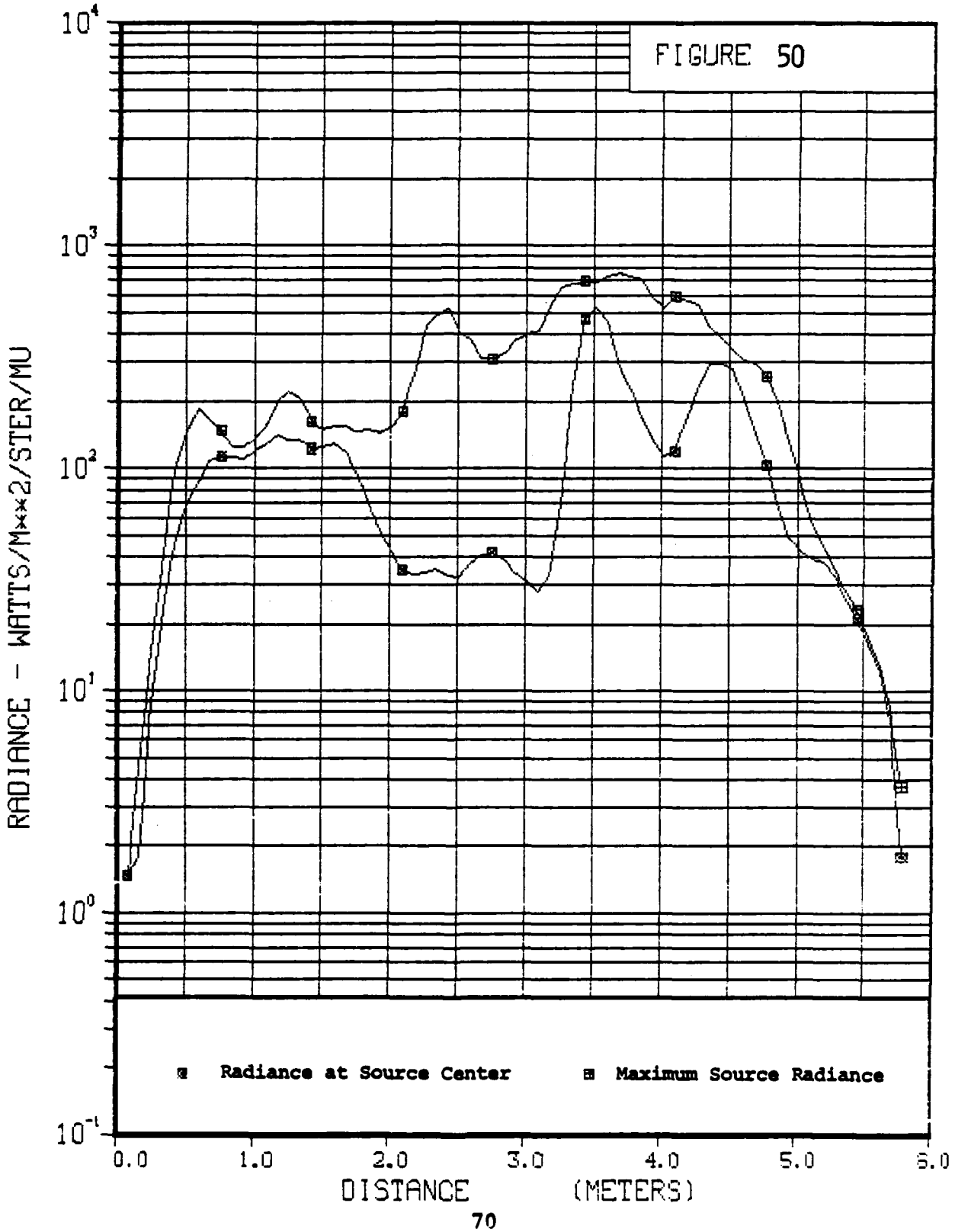

RADIANCE VS HORIZONTAL DISTANCE

FRAME 50  0.49 SECONDS

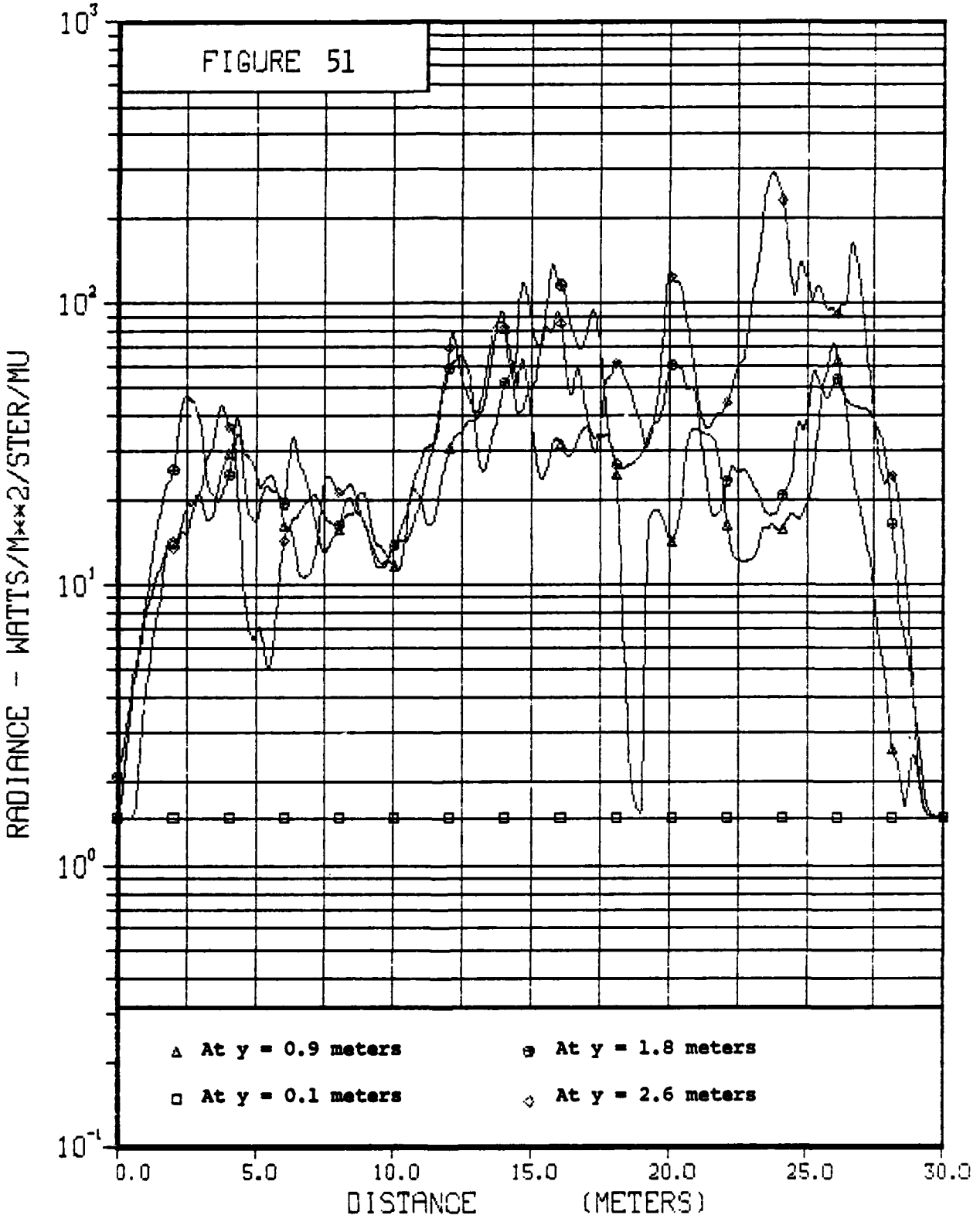

RADIANCE VS HORIZONTAL DISTANCE

FRAME 50  0.49 SECONDS

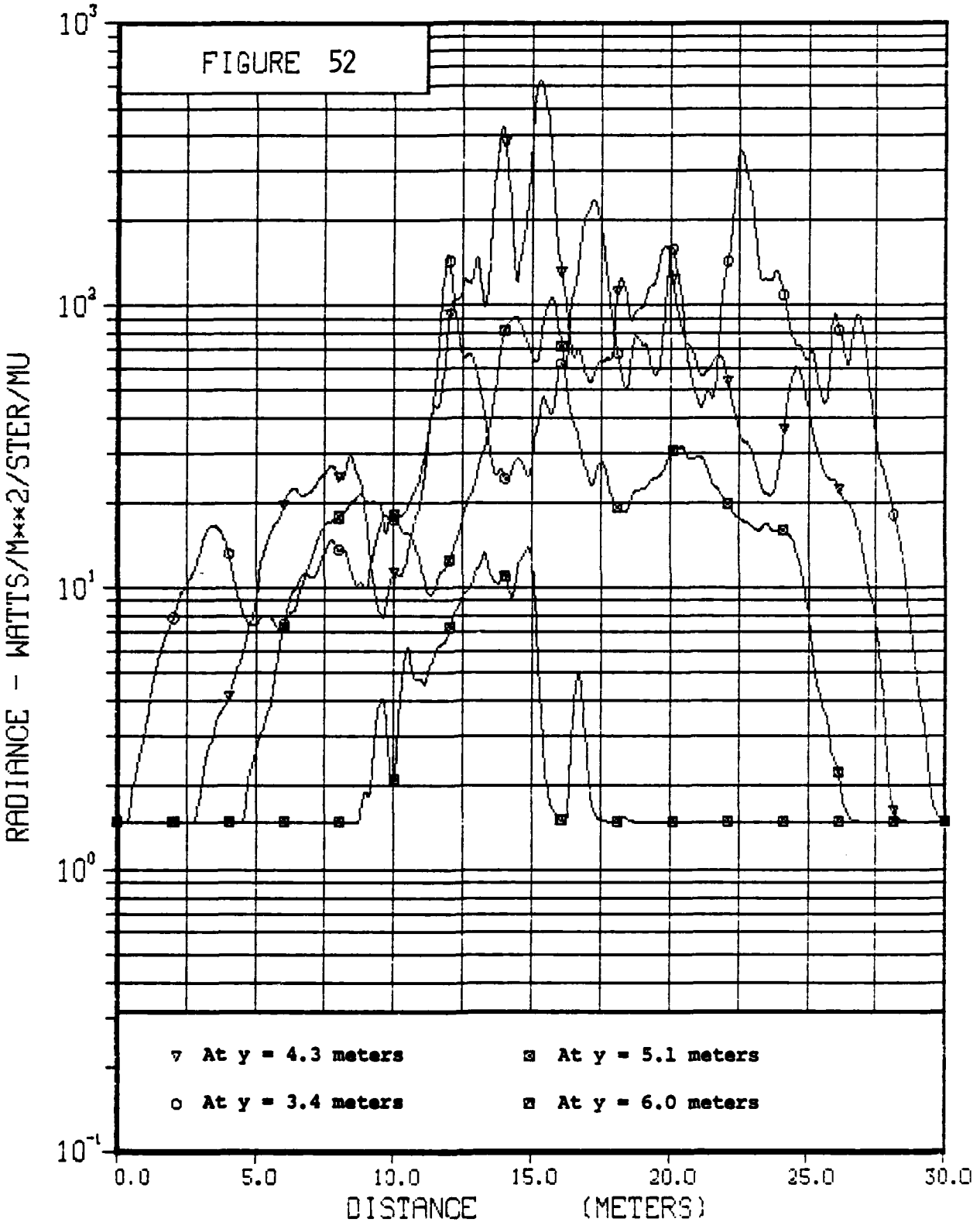

RADIANCE VS VERTICAL DISTANCE

FRAME 50  0.49 SECONDS

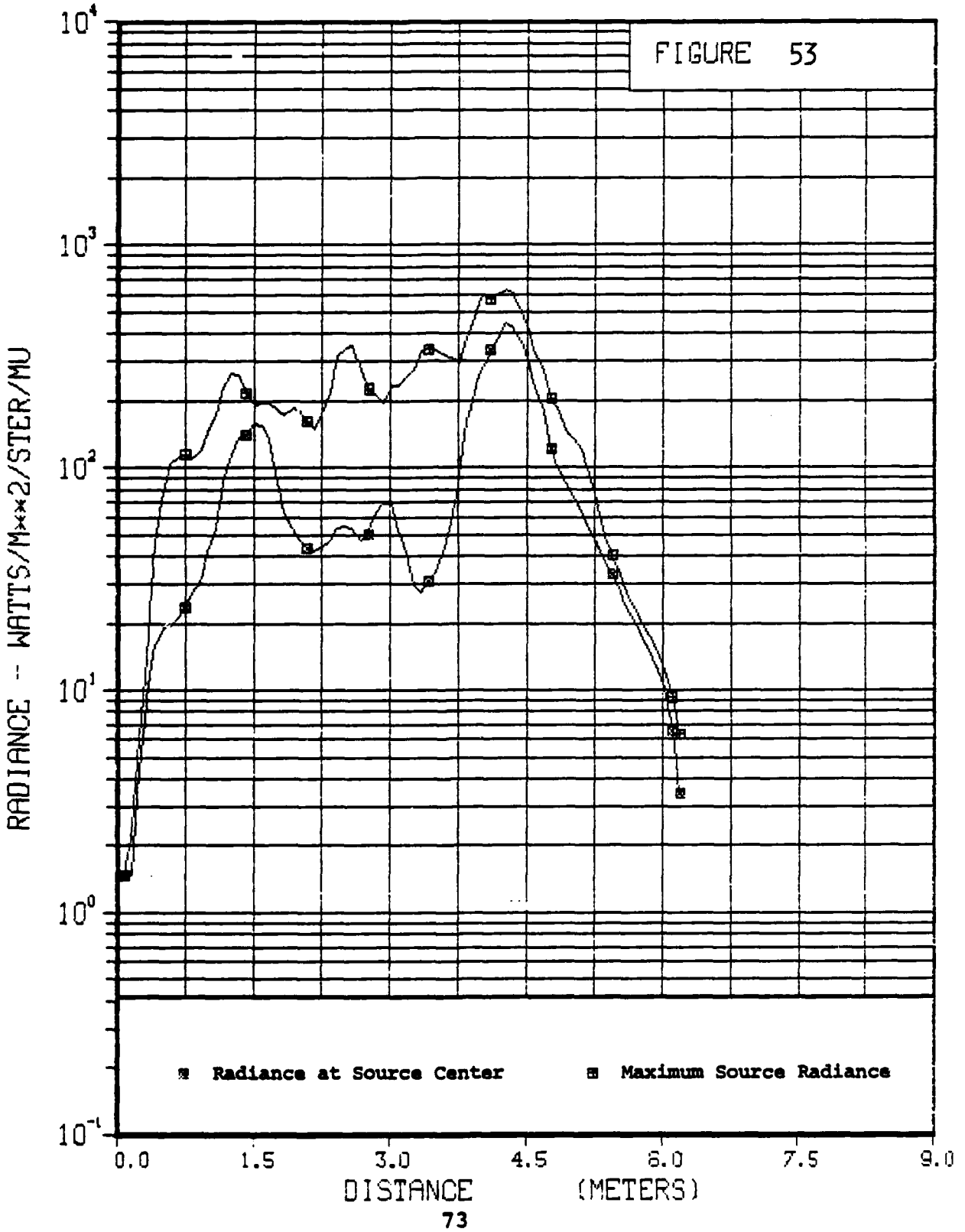

RADIANCE VS HORIZONTAL DISTANCE

FRAME 70  0.69 SECONDS

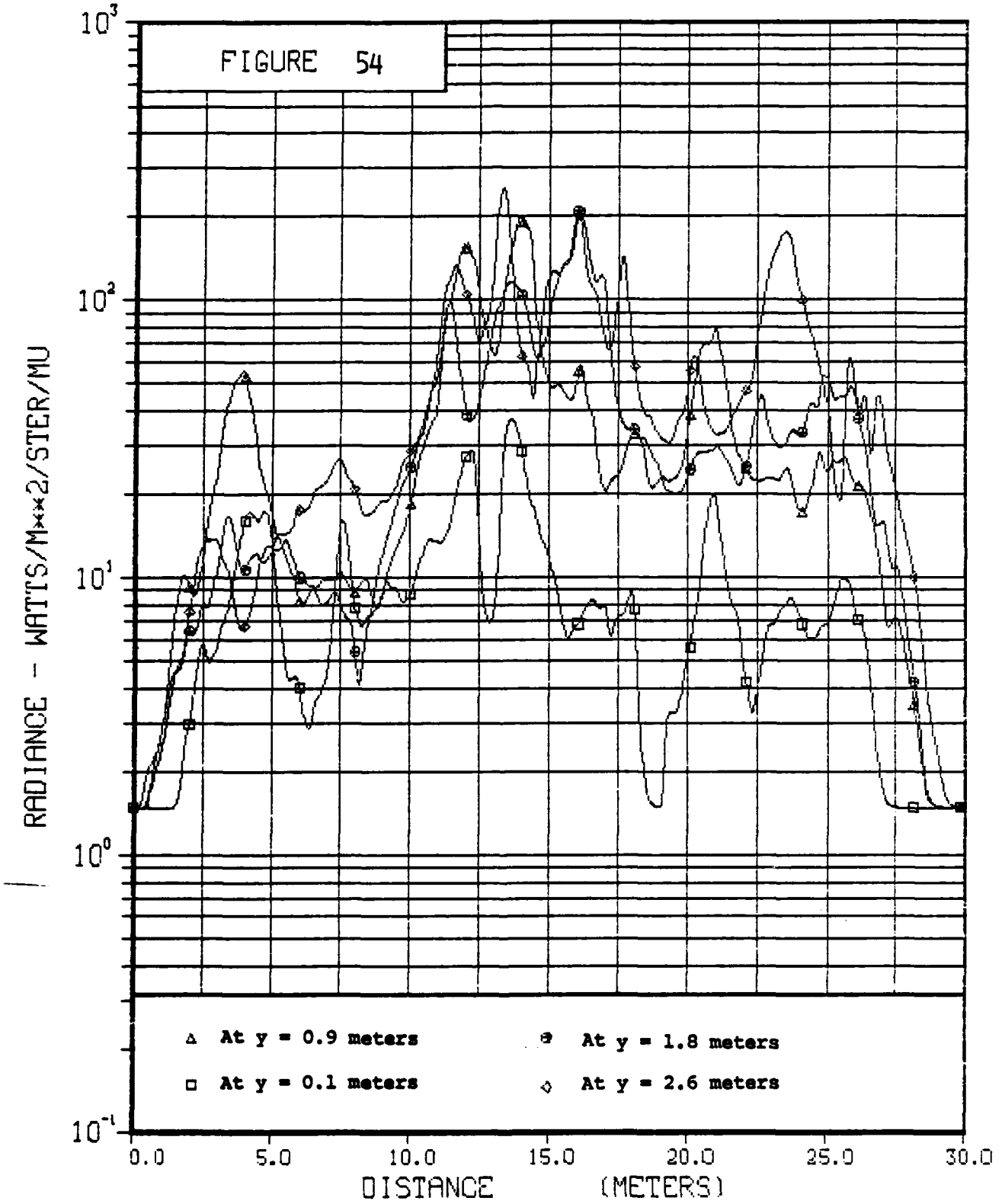

RADIANCE VS HORIZONTAL DISTANCE

FRAME 70  0.69 SECONDS

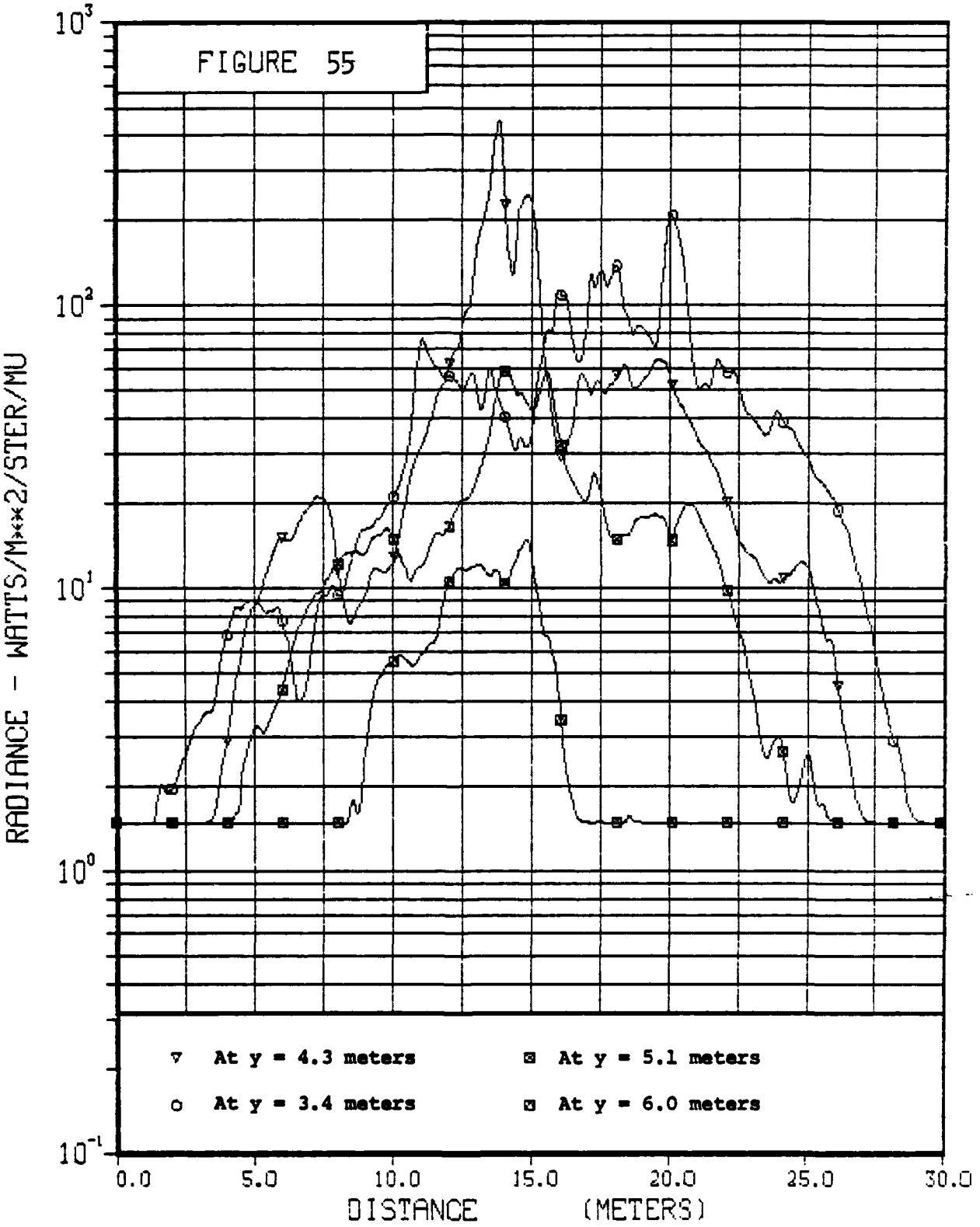

RADIANCE VS VERTICAL DISTANCE

FRAME 70  0.69 SECONDS

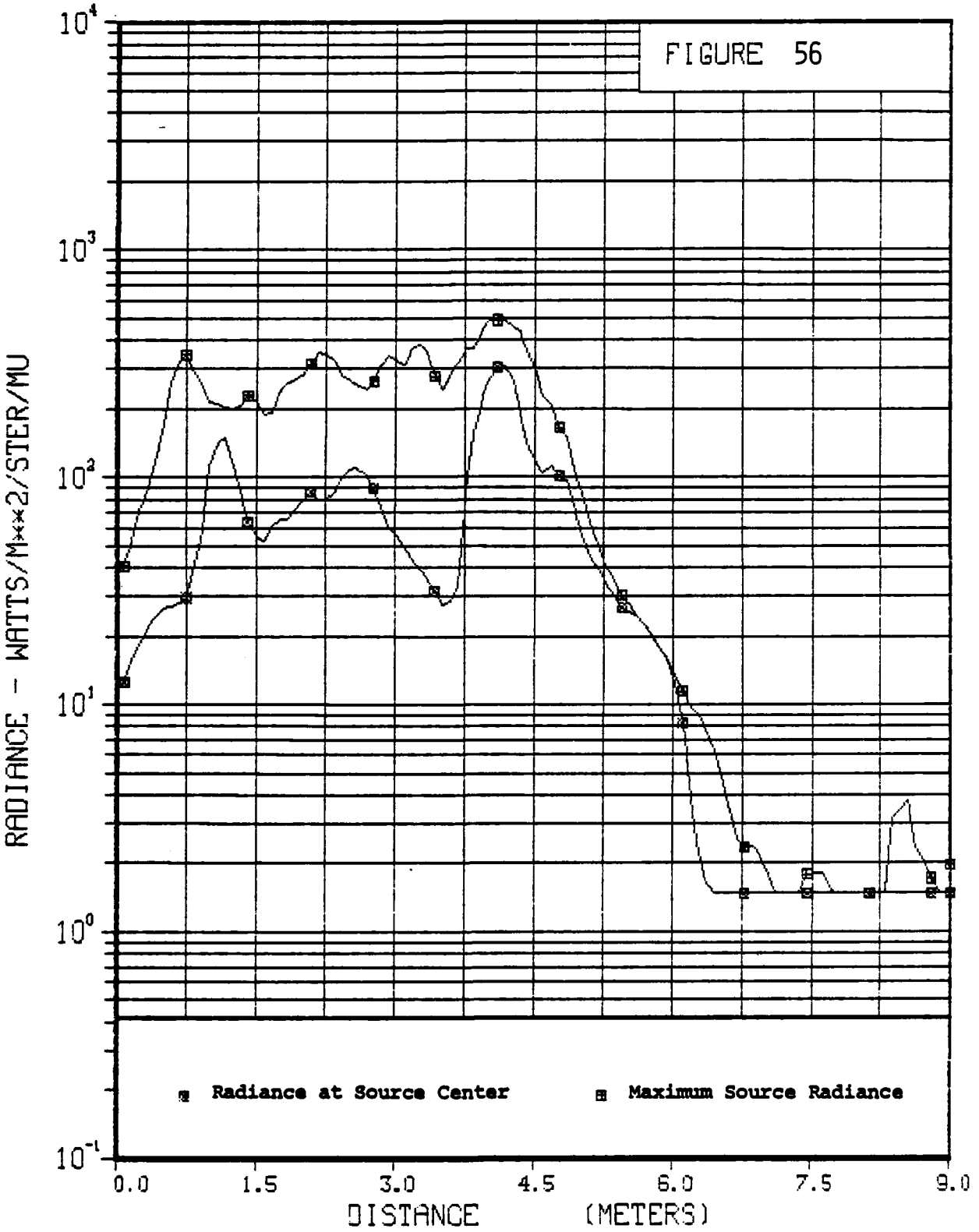

RADIANCE VS HORIZONTAL DISTANCE

FRAME 90 0.89 SECONDS

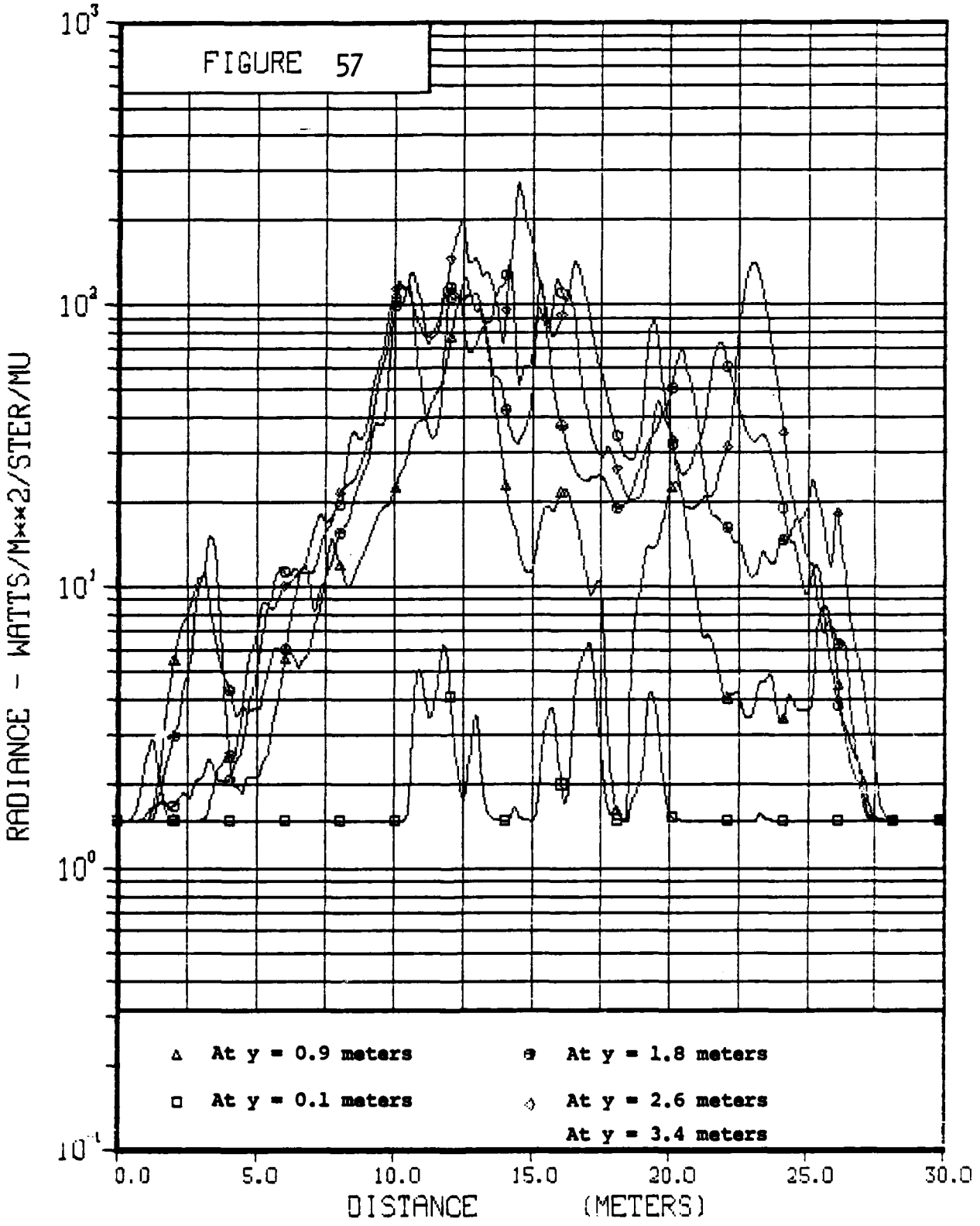

RADIANCE VS HORIZONTAL DISTANCE

FRAME 90  0.89 SECONDS

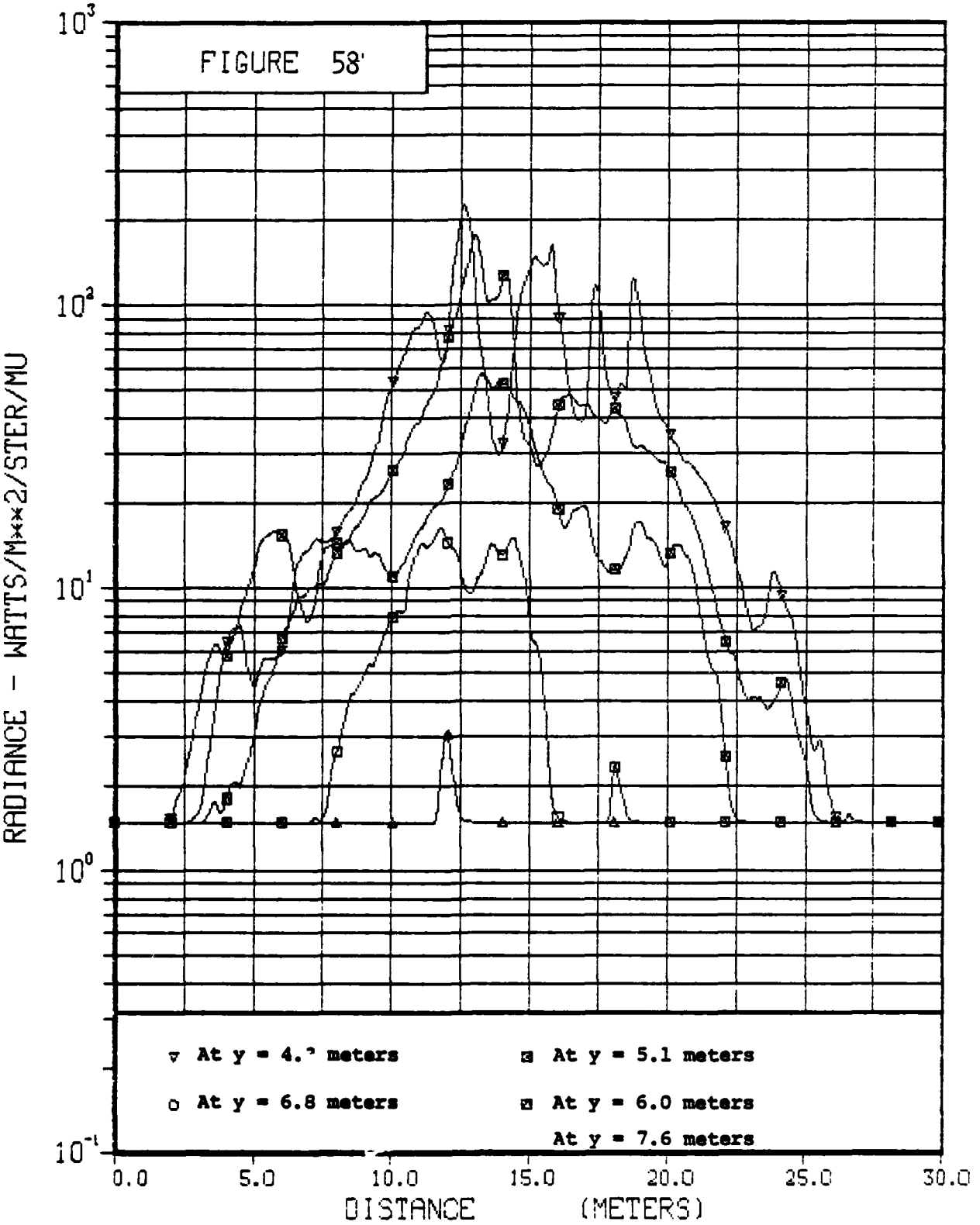

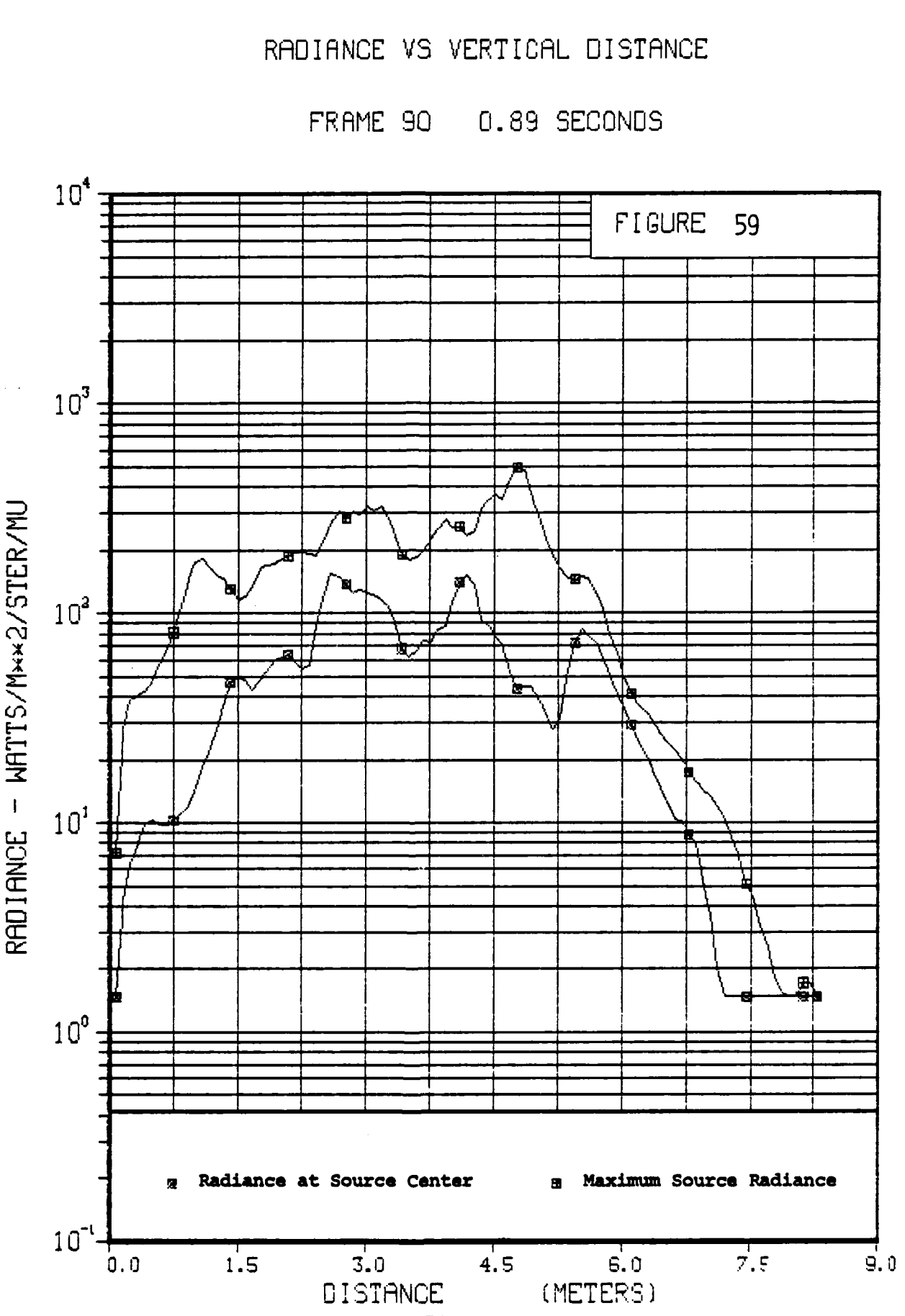
RADIANCE VS VERTICAL DISTANCE
FRAME 90 0.89 SECONDS
FIGURE 59
RADIANCE - WATTS/M**2/STER/MU
$10^4$
$10^3$
$10^2$
$10^1$
$10^0$
$10^{-1}$
0.0
1.5
3.0
4.5
6.0
7.5
9.0
DISTANCE (METERS)
Radiance at Source Center
Maximum Source Radiance

RADIANCE VS HORIZONTAL DISTANCE

FRAME 120 1.19 SECONDS

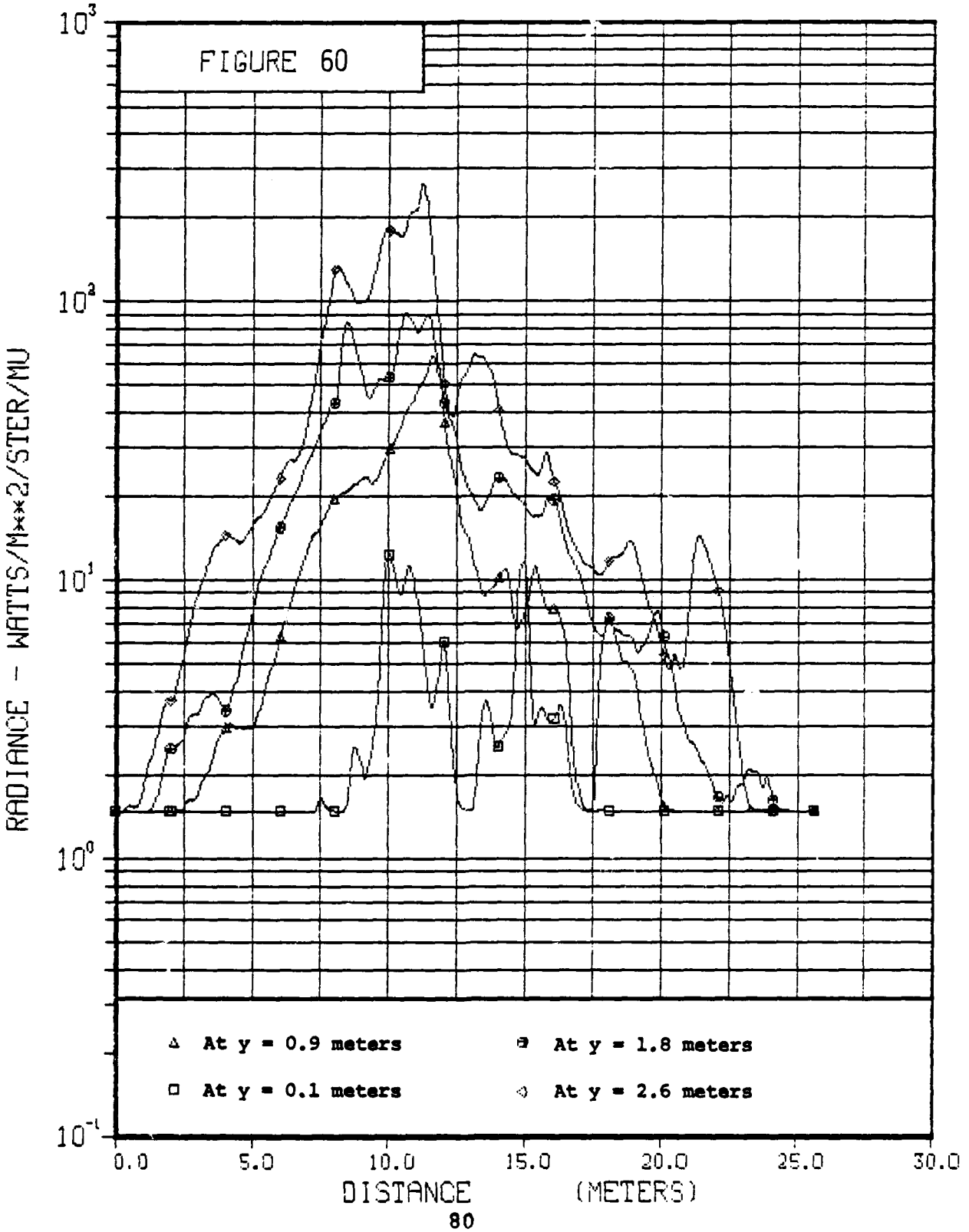

RADIANCE VS HORIZONTAL DISTANCE

FRAME 120 1.19 SECONDS

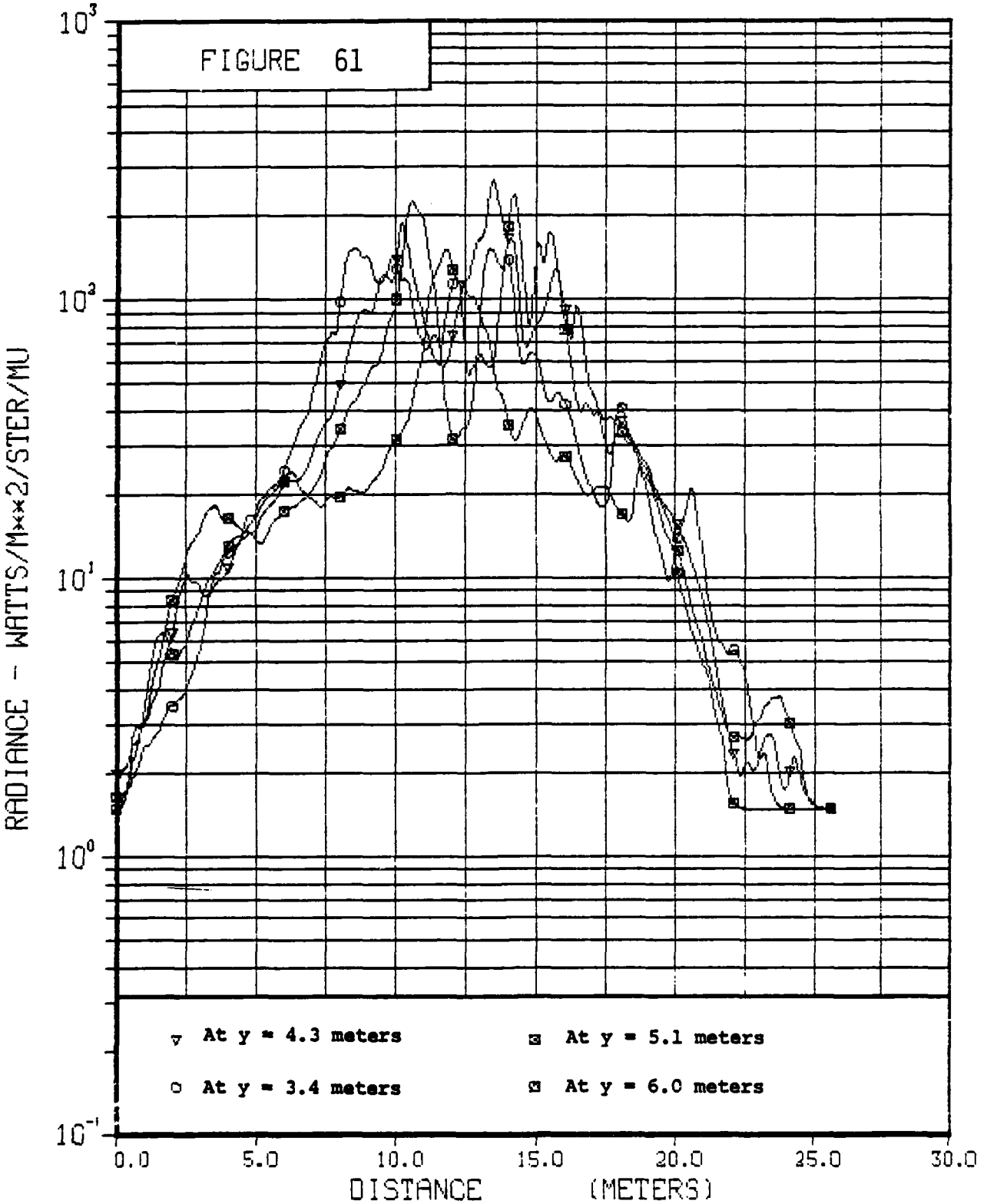

RADIANCE VS HORIZONTAL DISTANCE

FRAME 120 1.19 SECONDS

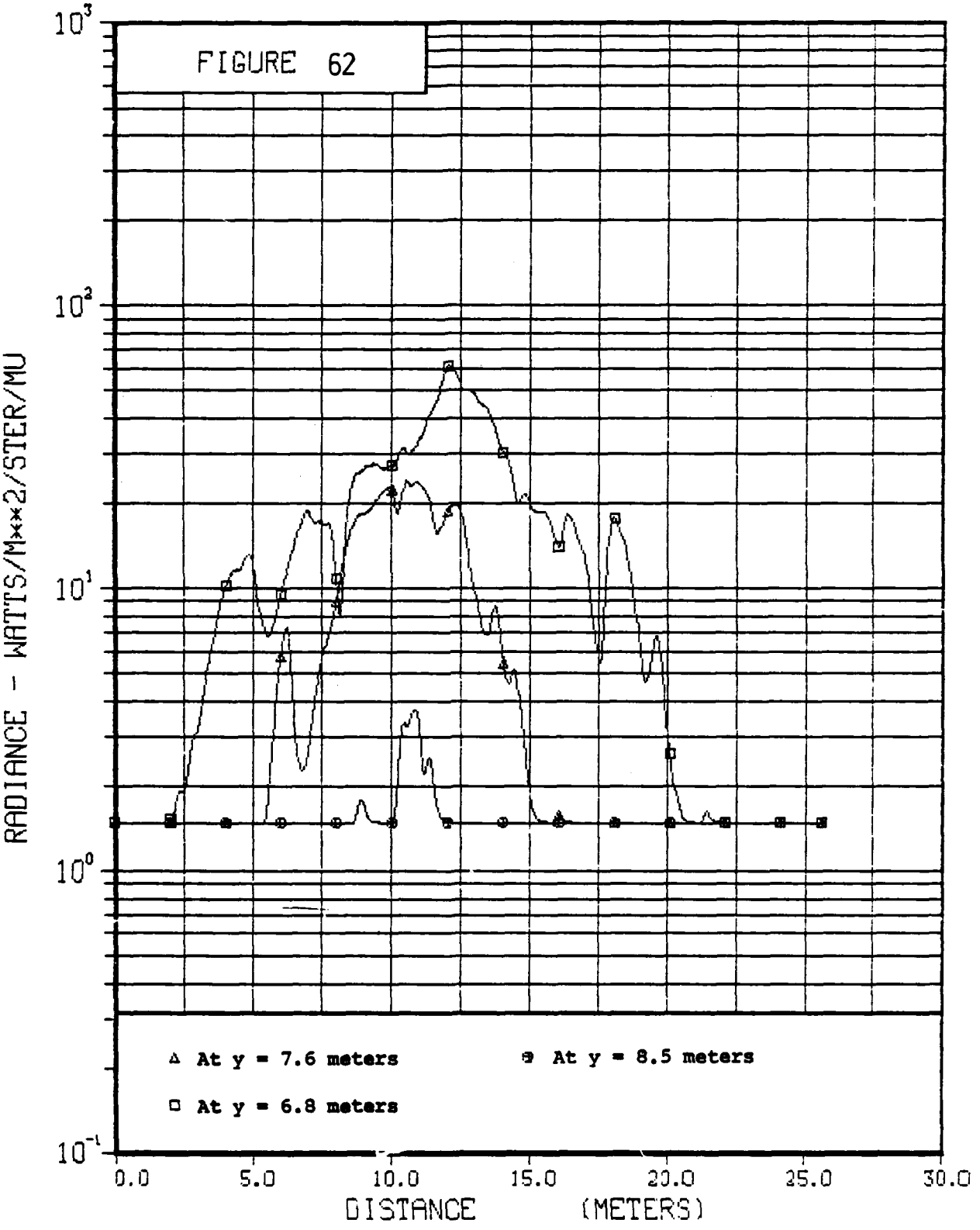

RADIANCE VS VERTICAL DISTANCE

FRAME 120 1.19 SECONDS

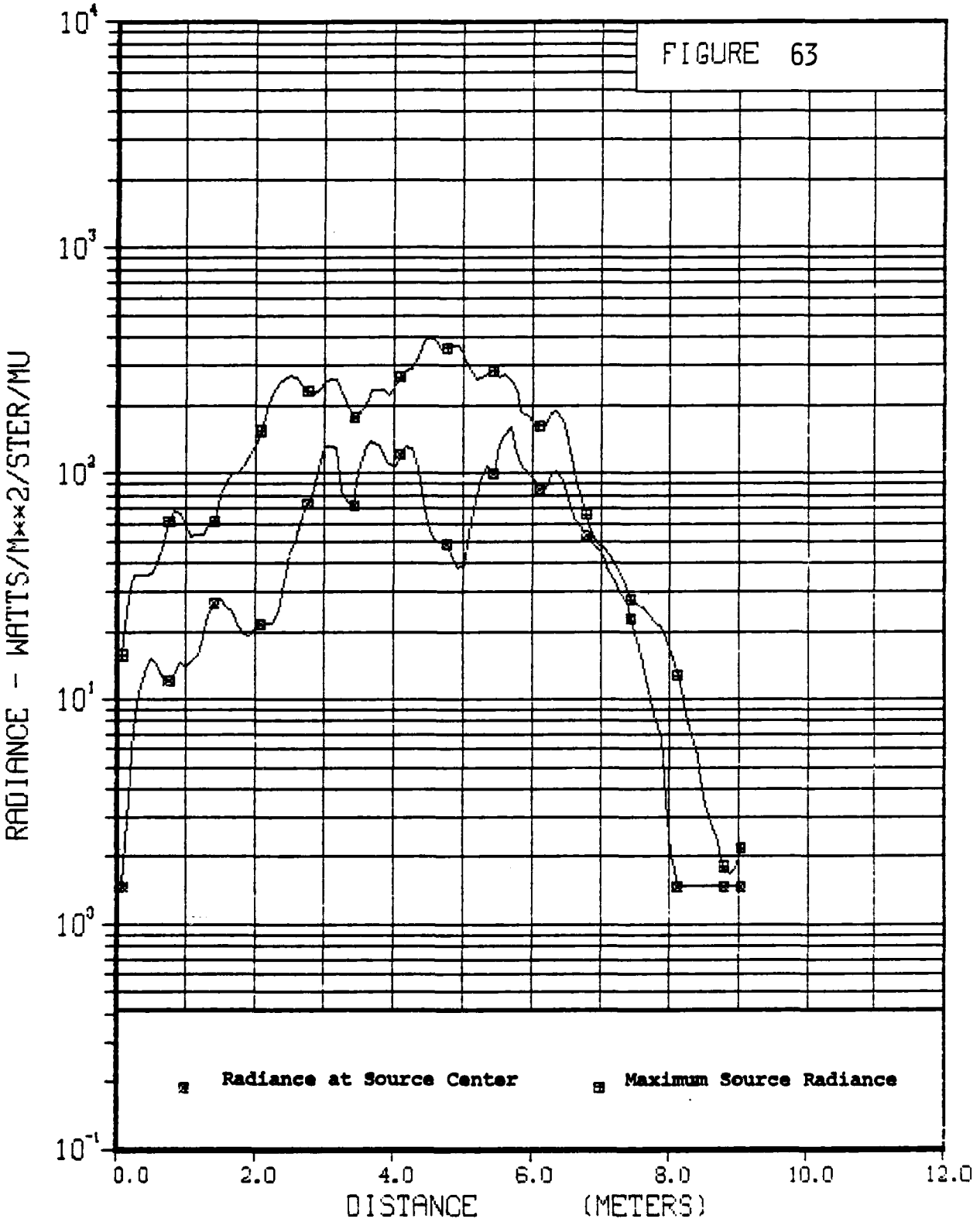

RADIANCE VS HORIZONTAL DISTANCE

FRAME 150 1.49 SECONDS

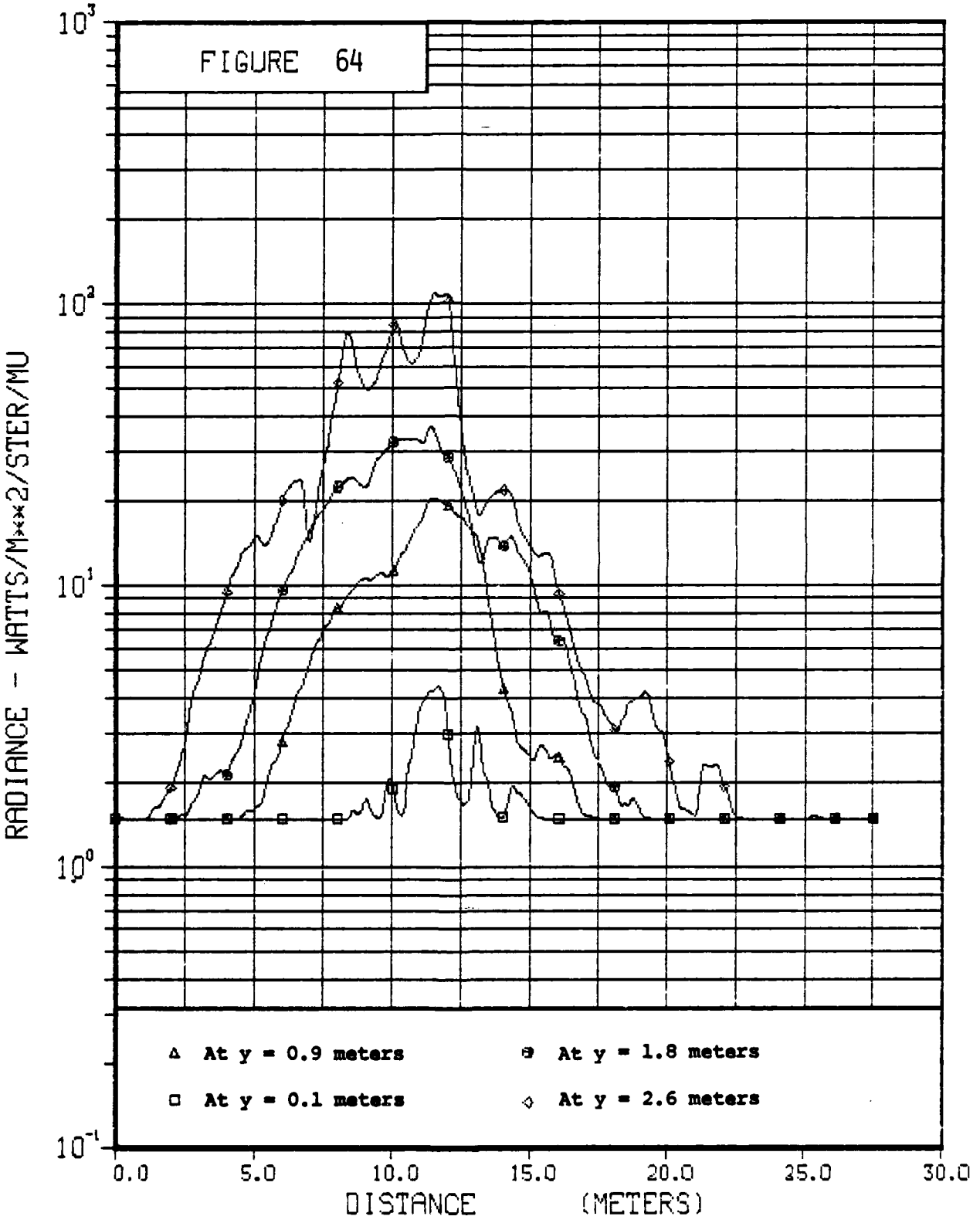

RADIANCE VS HORIZONTAL DISTANCE

FRAME 150 1.49 SECONDS

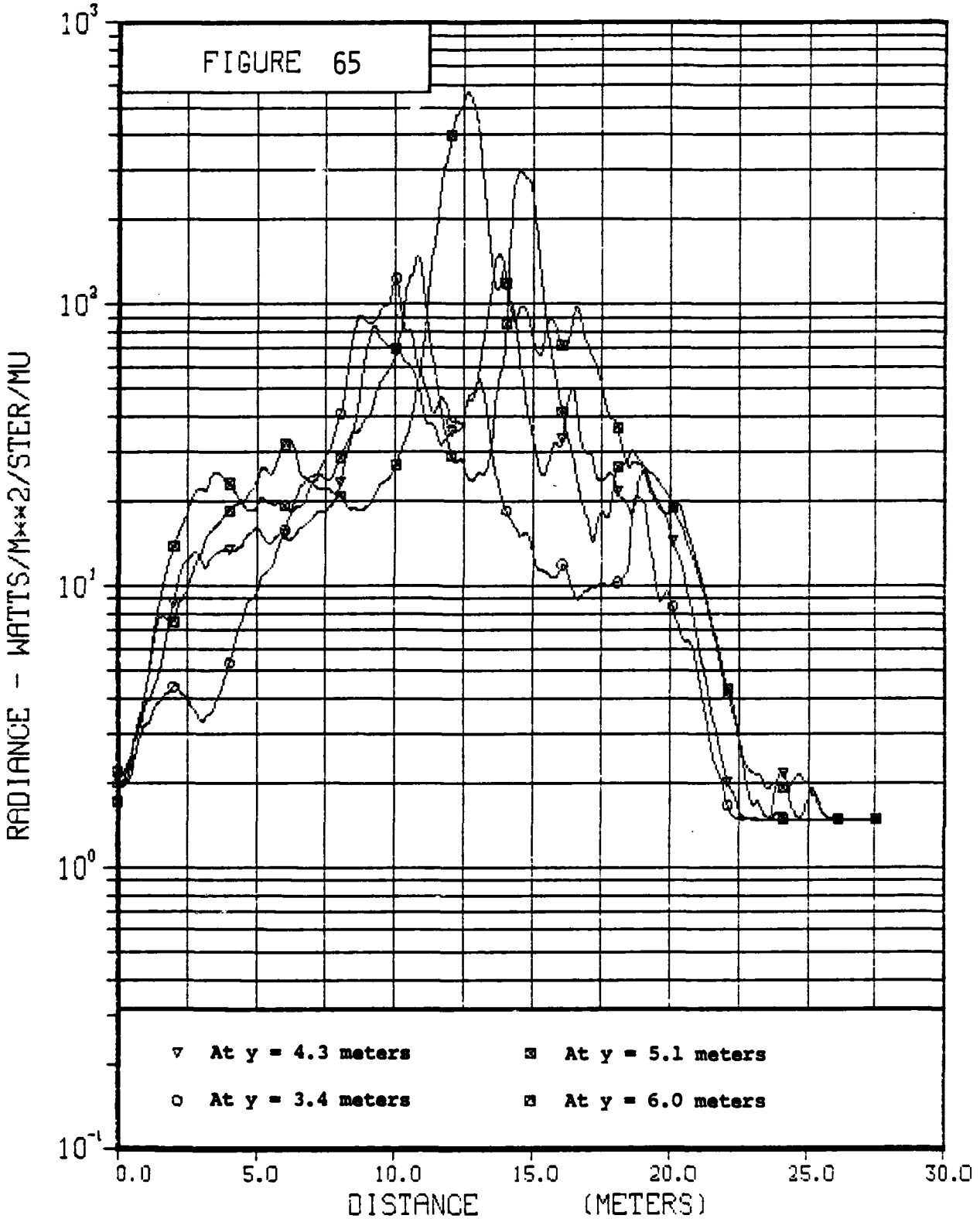

RADIANCE VS HORIZONTAL DISTANCE

FRAME 150 1.49 SECONDS

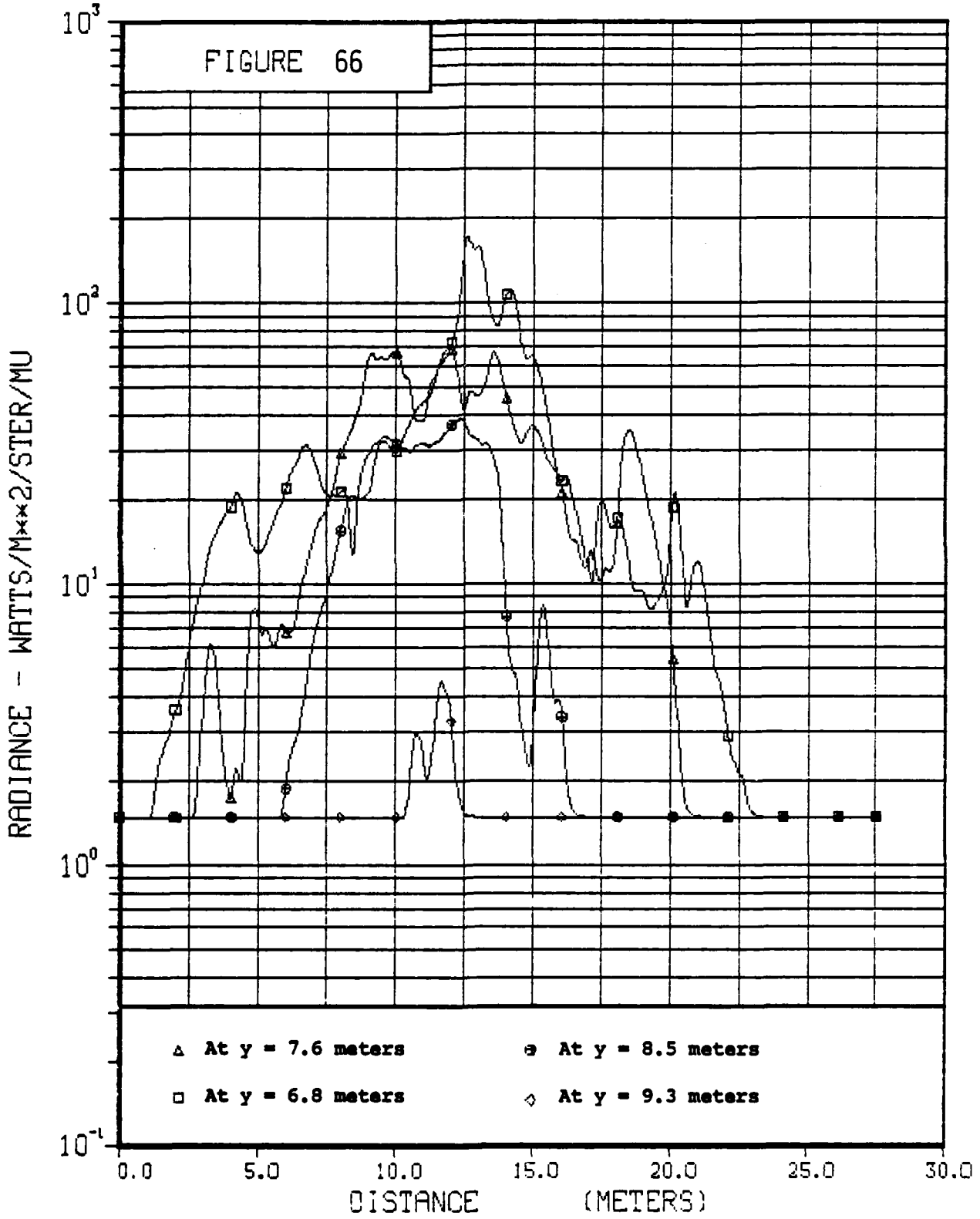

RADIANCE VS VERTICAL DISTANCE

FRAME 150 1.49 SECONDS

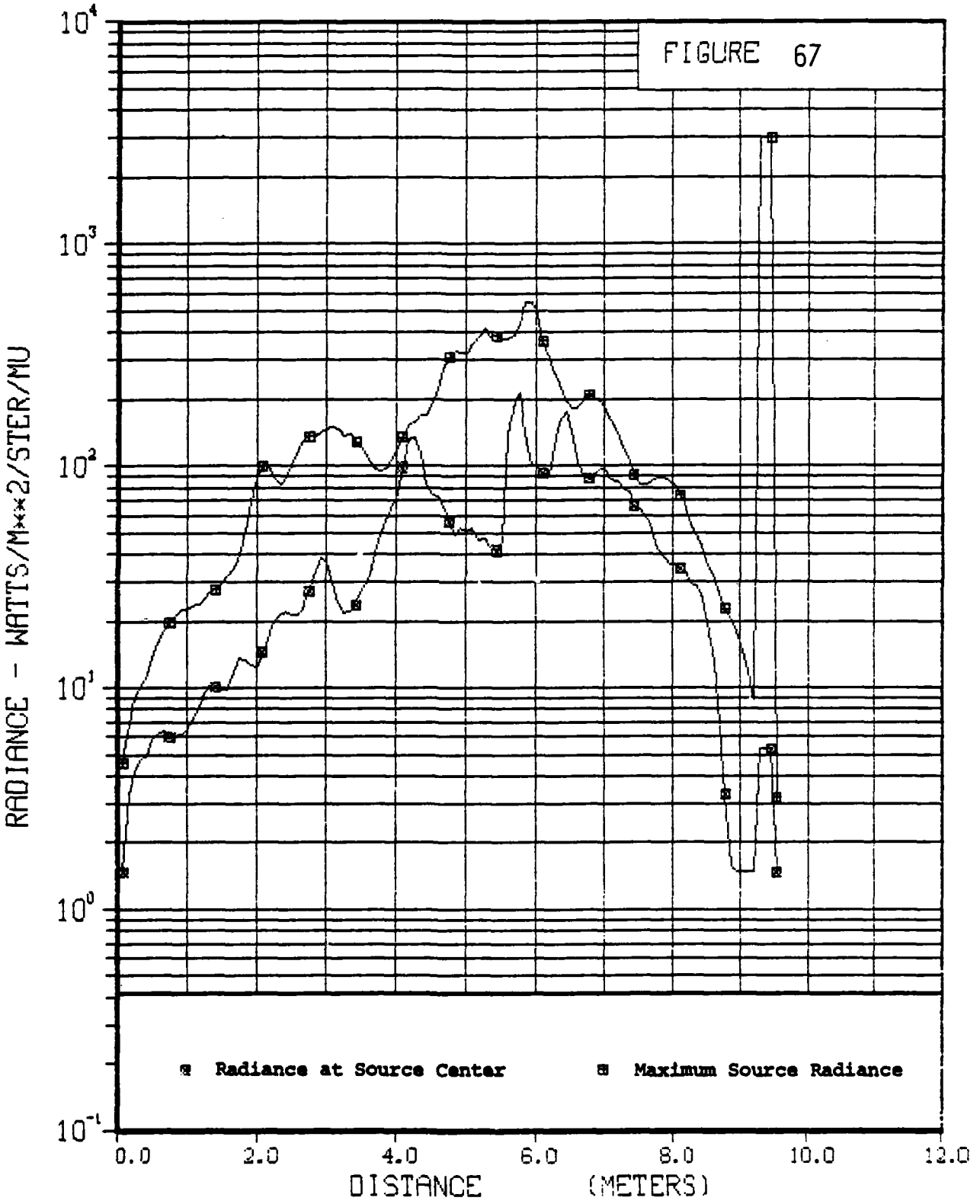

RADIANCE VS HORIZONTAL DISTANCE

FRAME 200 1.99 SECONDS

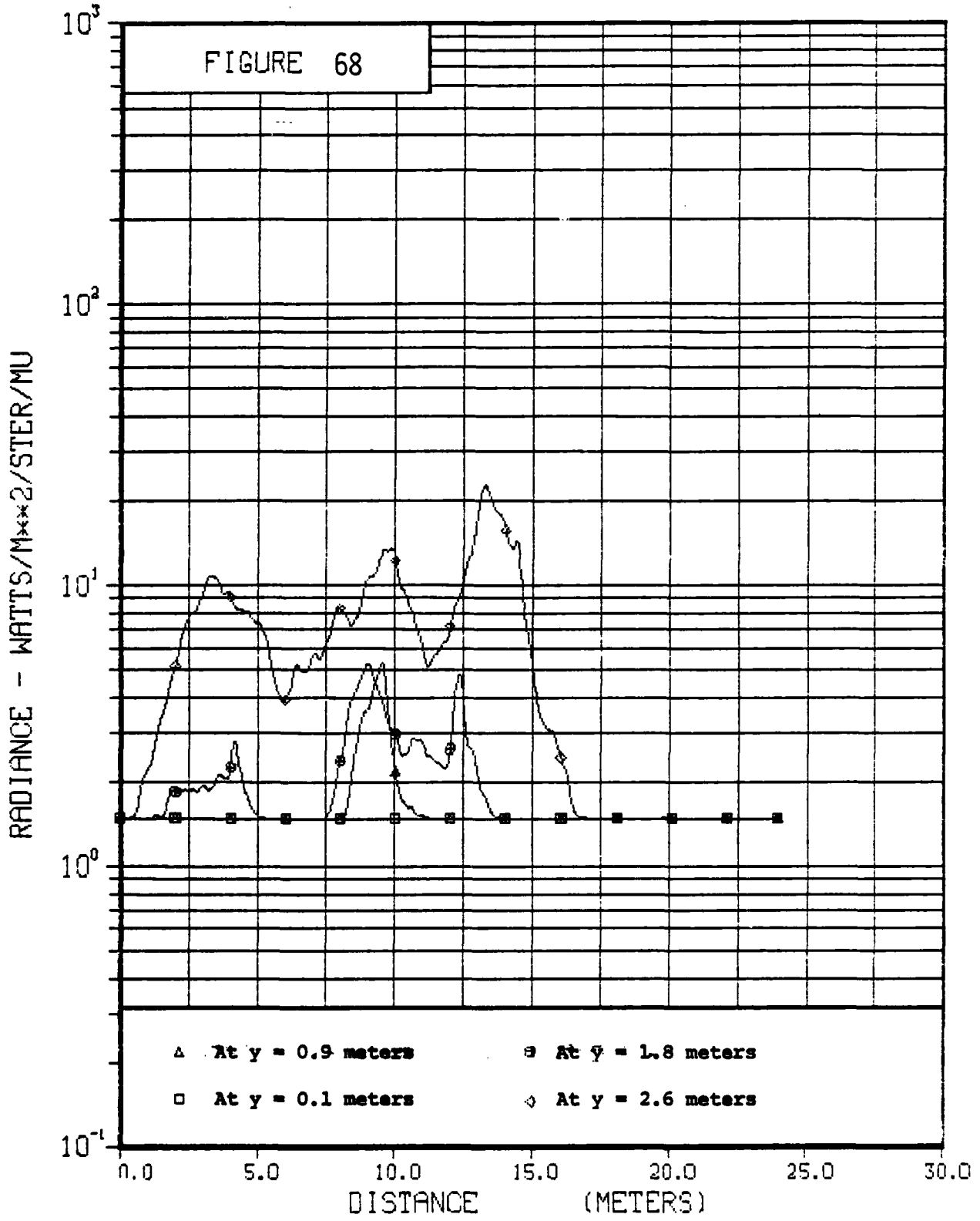

RADIANCE VS HORIZONTAL DISTANCE

FRAME 200 1.99 SECONDS

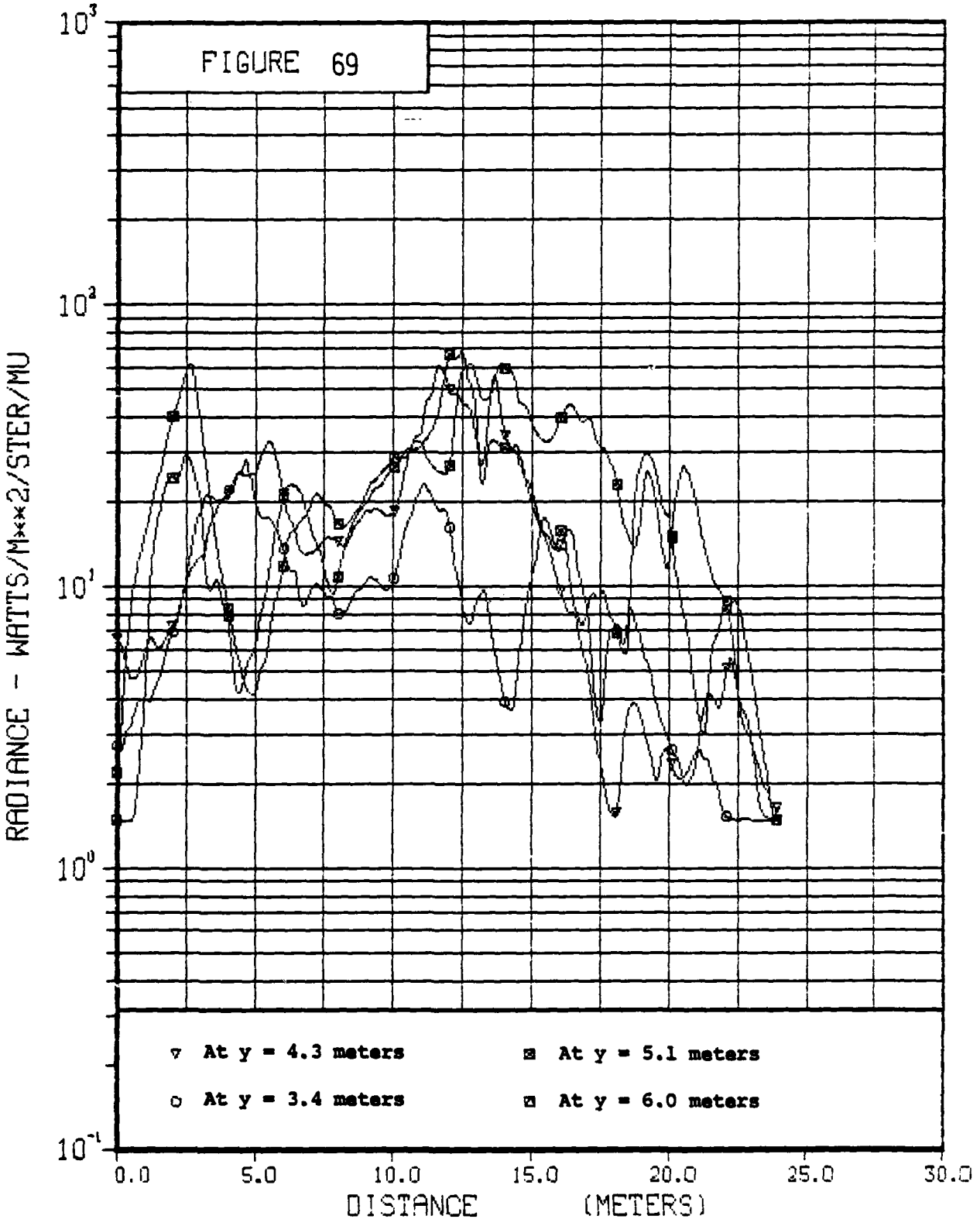

RADIANCE VS HORIZONTAL DISTANCE

FRAME 200 1.99 SECONDS

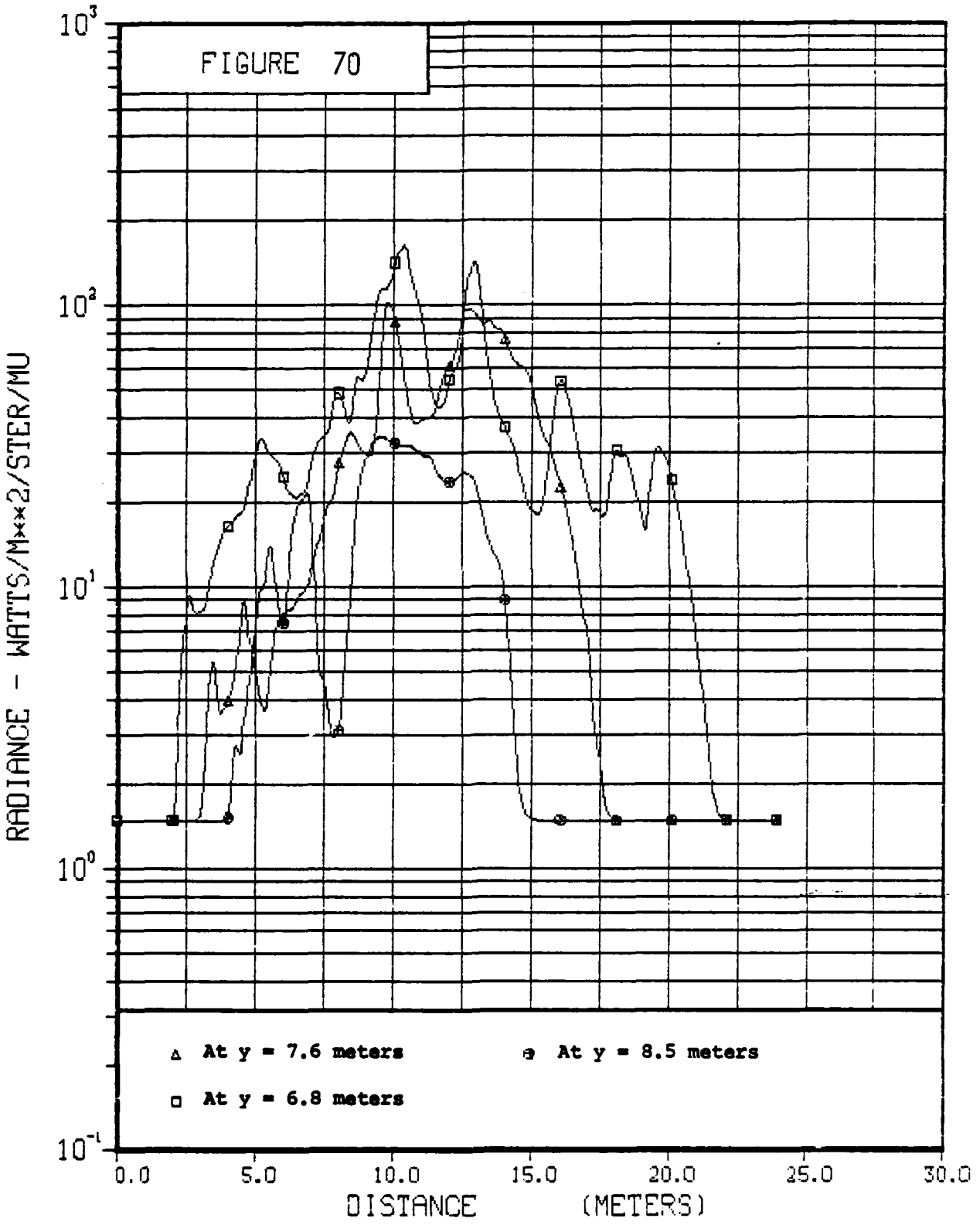

RADIANCE VS VERTICAL DISTANCE

FRAME 200 1.99 SECONDS

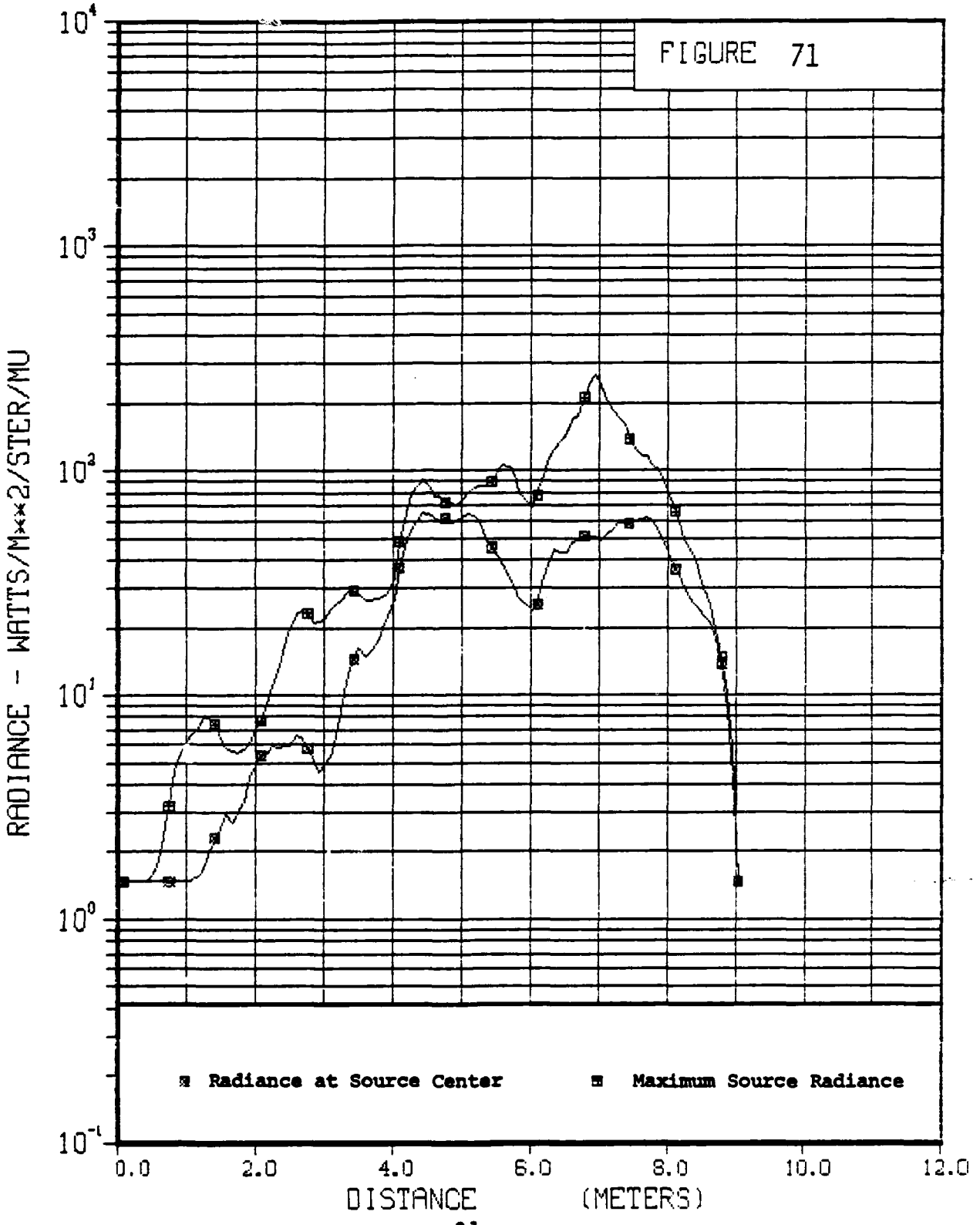

RADIANCE VS HORIZONTAL DISTANCE

FRAME 250 2.49 SECONDS

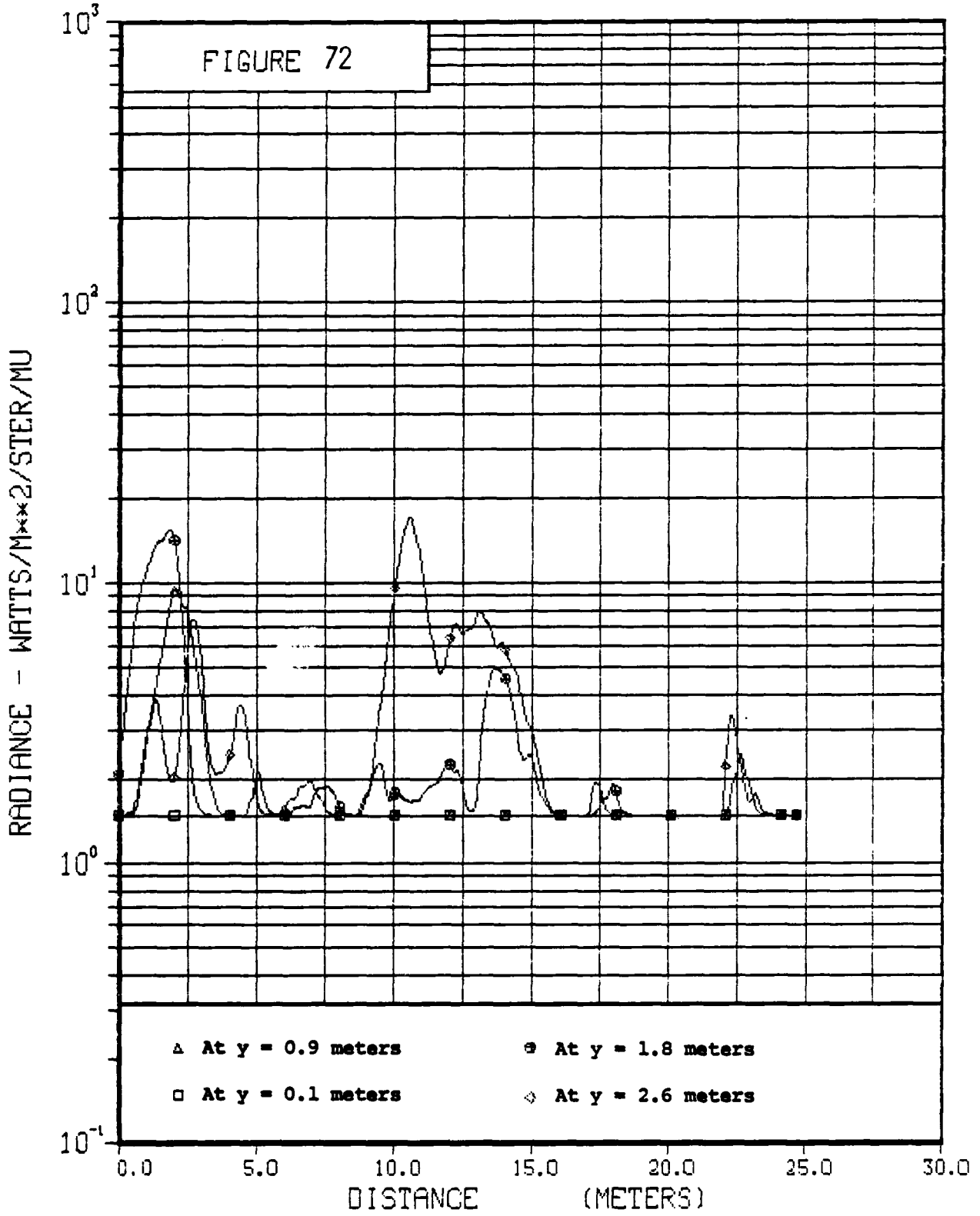

RADIANCE VS HORIZONTAL DISTANCE

FRAME 250 2.49 SECONDS

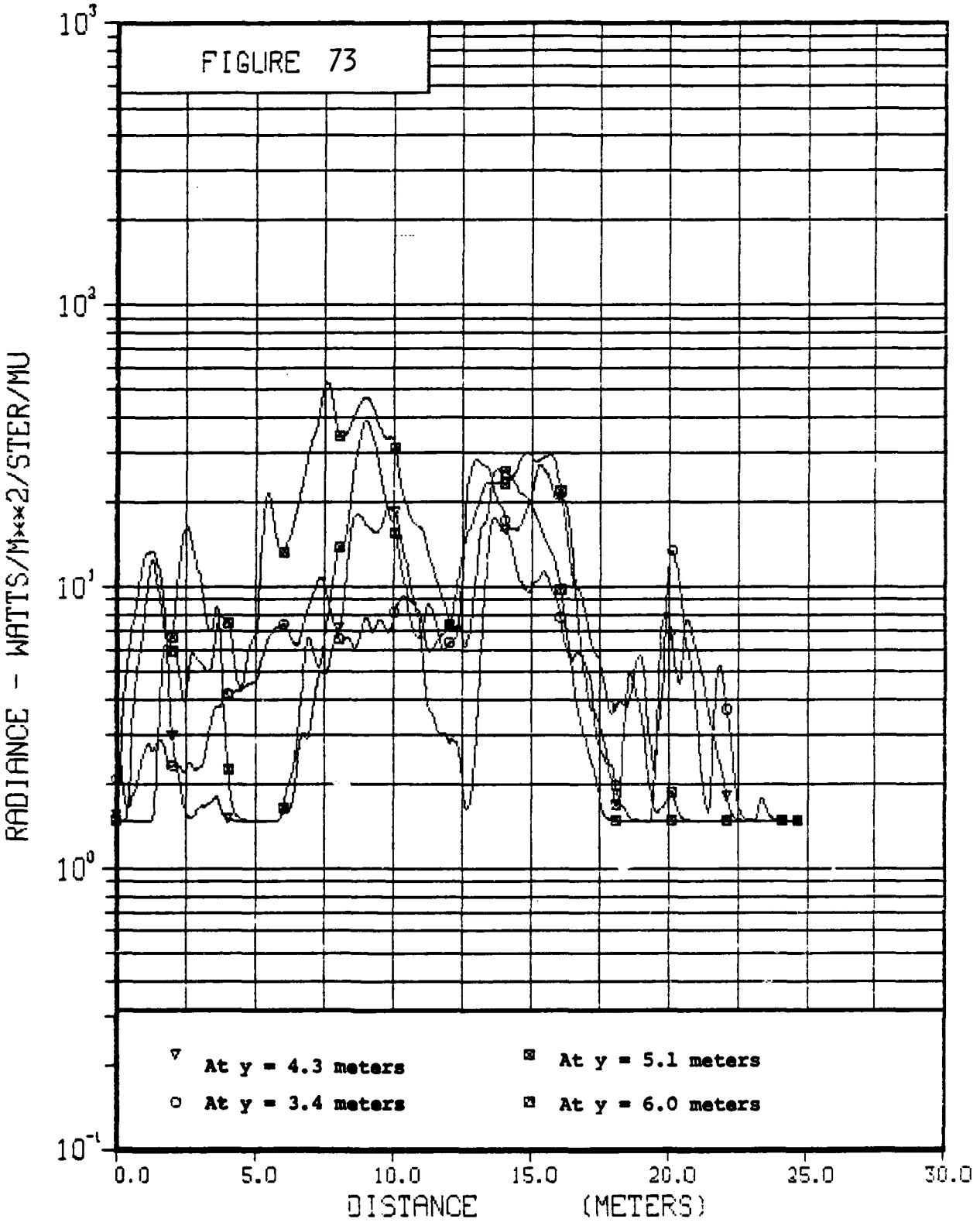

AD-A134 726 RADIATIVE PROPERTIES OF A NUCLEAR THERMAL SOURCE SIMULATOR(U) INFORMATION SCIENCE INC SANTA BARBARA CA W F DUDZIAK ET AL. 31 DEC 80 RM80-ISI101 DNA-5790F 2/2

UNCLASSIFIED DNA001-79-C-0393 F/G 14/2 NL

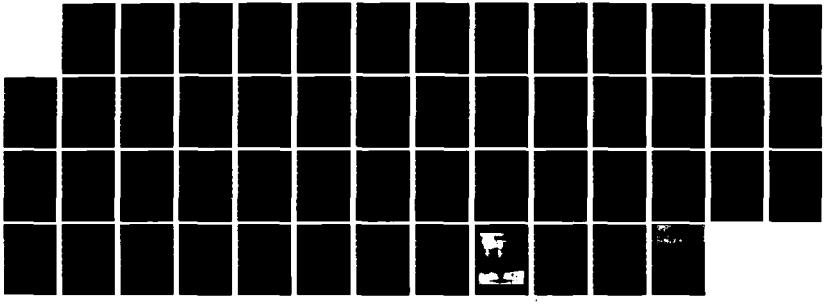

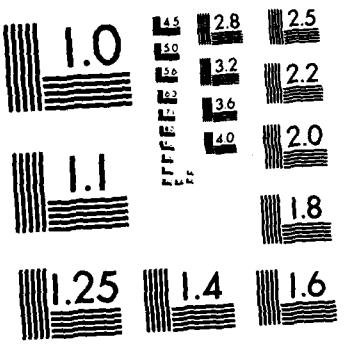

RADIANCE VS HORIZONTAL DISTANCE

FRAME 250 2.49 SECONDS

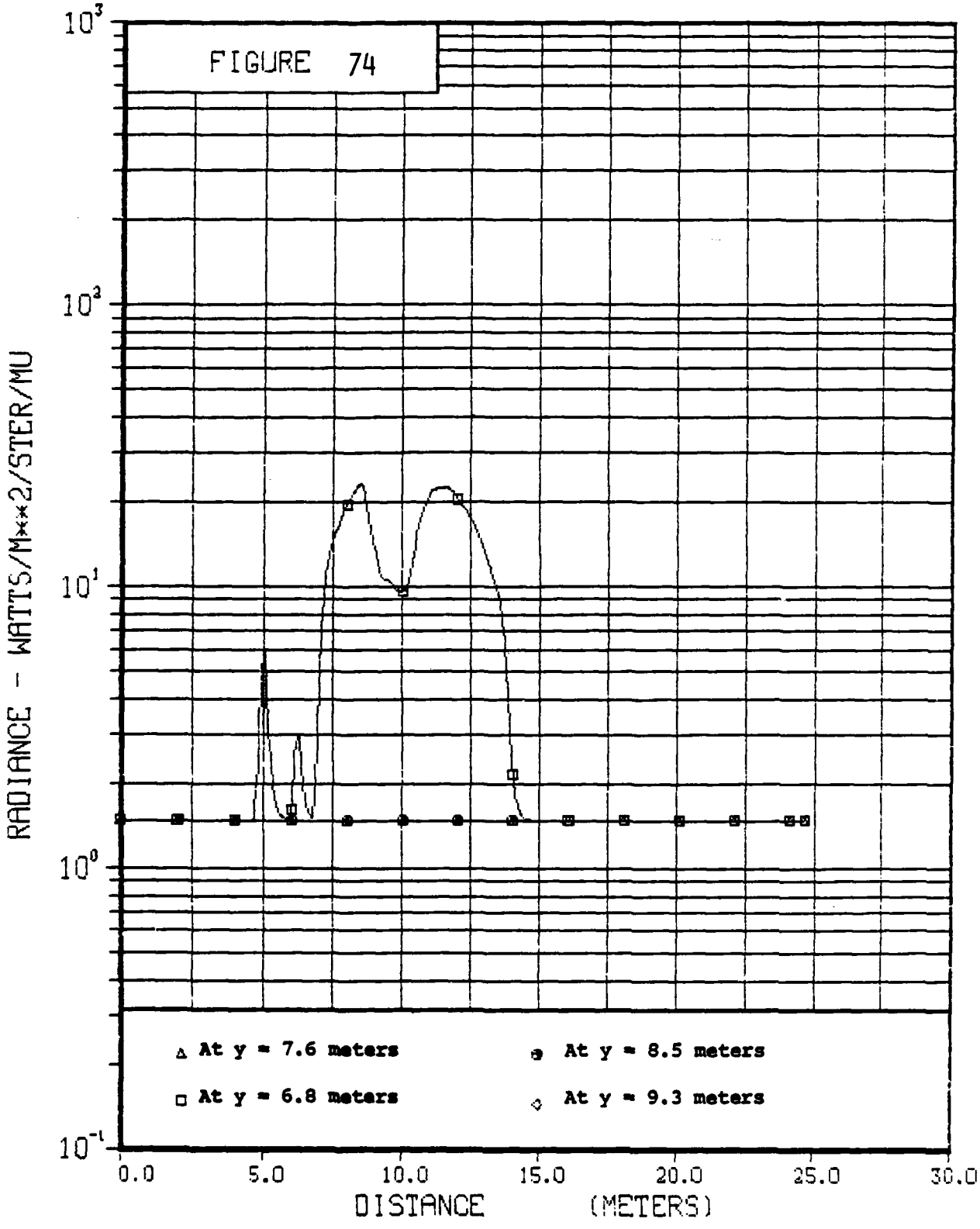

BLACK BODY TEMPERATURE VS RADIANCE

TEMPERATURE (DEGREES K) VS RADIANCE (WATTS/SQ.M-STER.-MU)

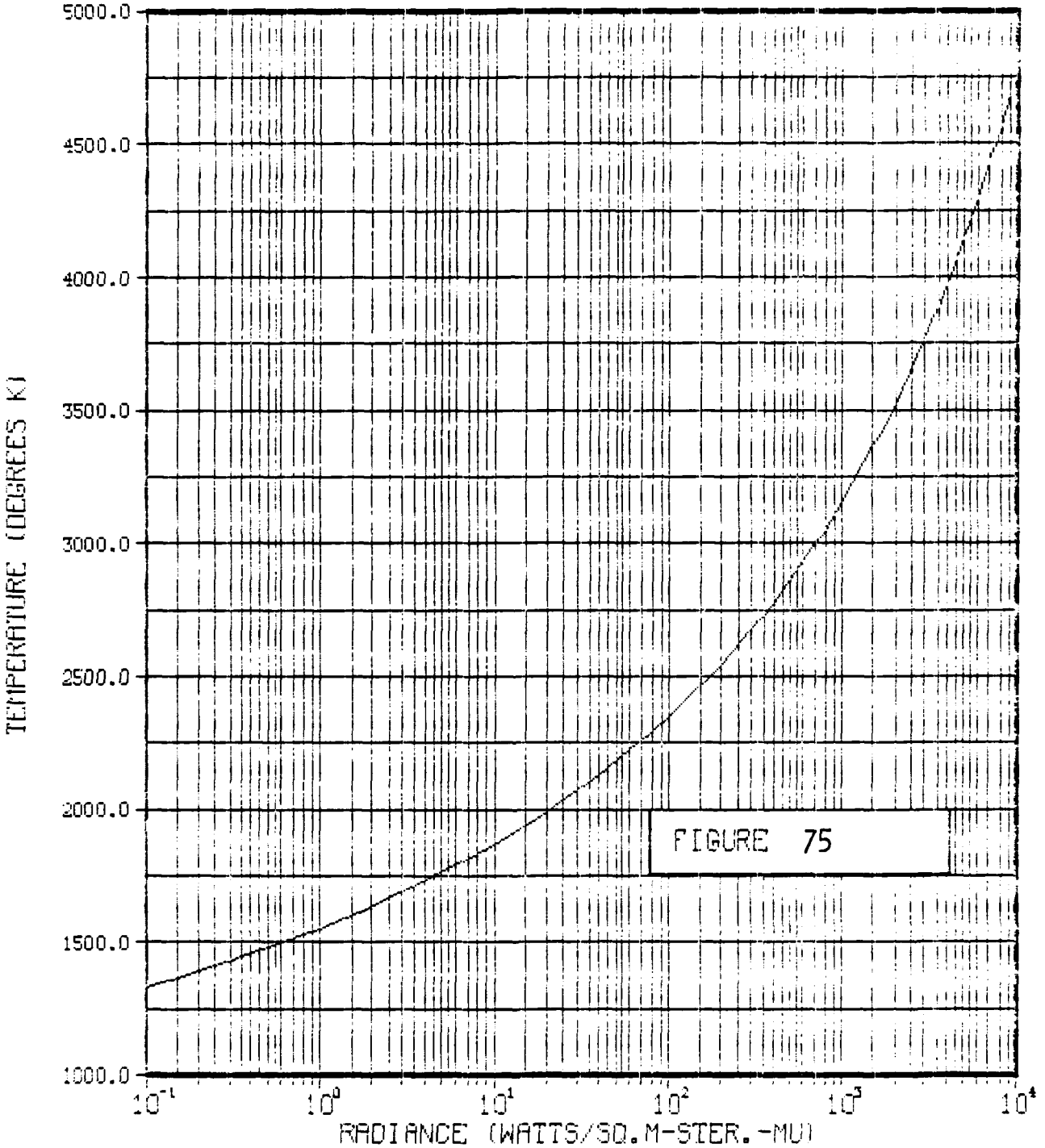


FIGURE 75

## SECTION 4

## 4.0 TRS SPECTRAL MEASUREMENTS

This section presents some of the spectral measurements that have been made from photographic film images. The location of this camera system was at the same optical station as the one described above. The optics system contained a high quality refraction grating as a spectral dispersing medium which was nearly wavelength independent as to dispersion and resolving power. The system also included a collimator with an accurate slit at its principal focus that acts as a TRS surface image forming element. The slit of this collimator was oriented with its long dimension parallel to the ground surface. The focus of this slit was such as to view the entire 16 modules of the TRS source at an elevation of 10.7 feet (3.3 meters). The narrow portion of this slit viewed 1.5 feet (0.46 meters) of the TRS source along the vertical direction at this height. The spectral content of this element of the TRS surface area was recorded with a framing camera.

In such a recording system, the image of the length of the slit is recorded from sprocket hole of the film to sprocket hole. The spectral information is recorded on the film perpendicular to this slit direction, with wavelengths in the red at the foot of the frame and wavelengths in the blue, toward the top of the frame.

The Kodak Tri-X panchromatic film (5063) which recorded the images was calibrated in a similar manner as previously discussed. In this calibration process the NBS standard source was likewise spectrally recorded. Also recorded was a laboratory mercury lamp standard with its four sharp lines (i.e., dominant spectral lines of 404.6, 435.8, 546.0, and 578.0 nanometers) in this (400- to 600- nanometer) waveband. This data served as a check on the calibration method. The data illustrating these calibration measurements that was used to transform digital film density into the summarized spectral information is not included in this report.

The spectral data is summarized in Figures 66 through 79. This data

does not necessarily represent the highest spectral radiance or temperature measurement. It represents data from a single scan line (from blue- to red) of digital density data obtained with a 50 by 50 micron aperture on each of the selected seven images of recorded data. Hence it represents information from a very small surface area (3.3 inch by 1.5 foot) of the TRS source roughly near the center of the 16 modules. Time did not allow analysis of a raster scan of the entire image from which maximum spectral radiance and temperature could be determined.

The data is presented in plot pairs. The first figure of such a pair presents a measure of spectral radiance in the selected wavelength passband of 400- to 600 nanometers. Its companion figure converts this measured radiance by equation 5, into temperature. The 2 to 5 percent scatter in the data arises from use of the small digitizing aperture. For ease of comparison a curve determined by the data is superimposed upon the data set smoothing out this data scatter.

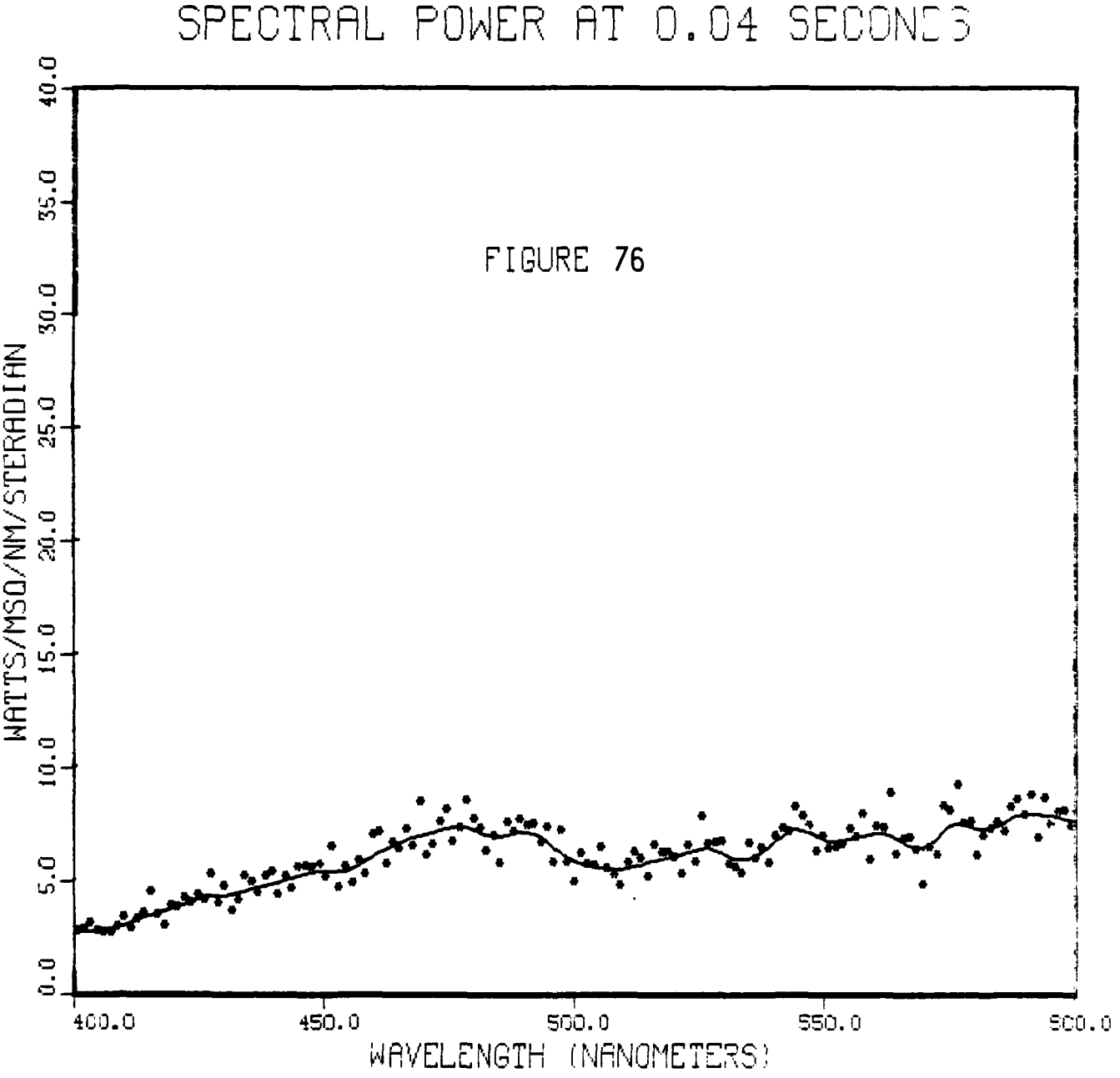
SPECTRAL POWER AT 0.04 SECONDS
WATTS/MSQ/NM/STERADIAN
0.0
5.0
10.0
15.0
20.0
25.0
30.0
35.0
40.0
400.0
450.0
500.0
550.0
600.0
WAVELENGTH (NANOMETERS)

FIGURE 76

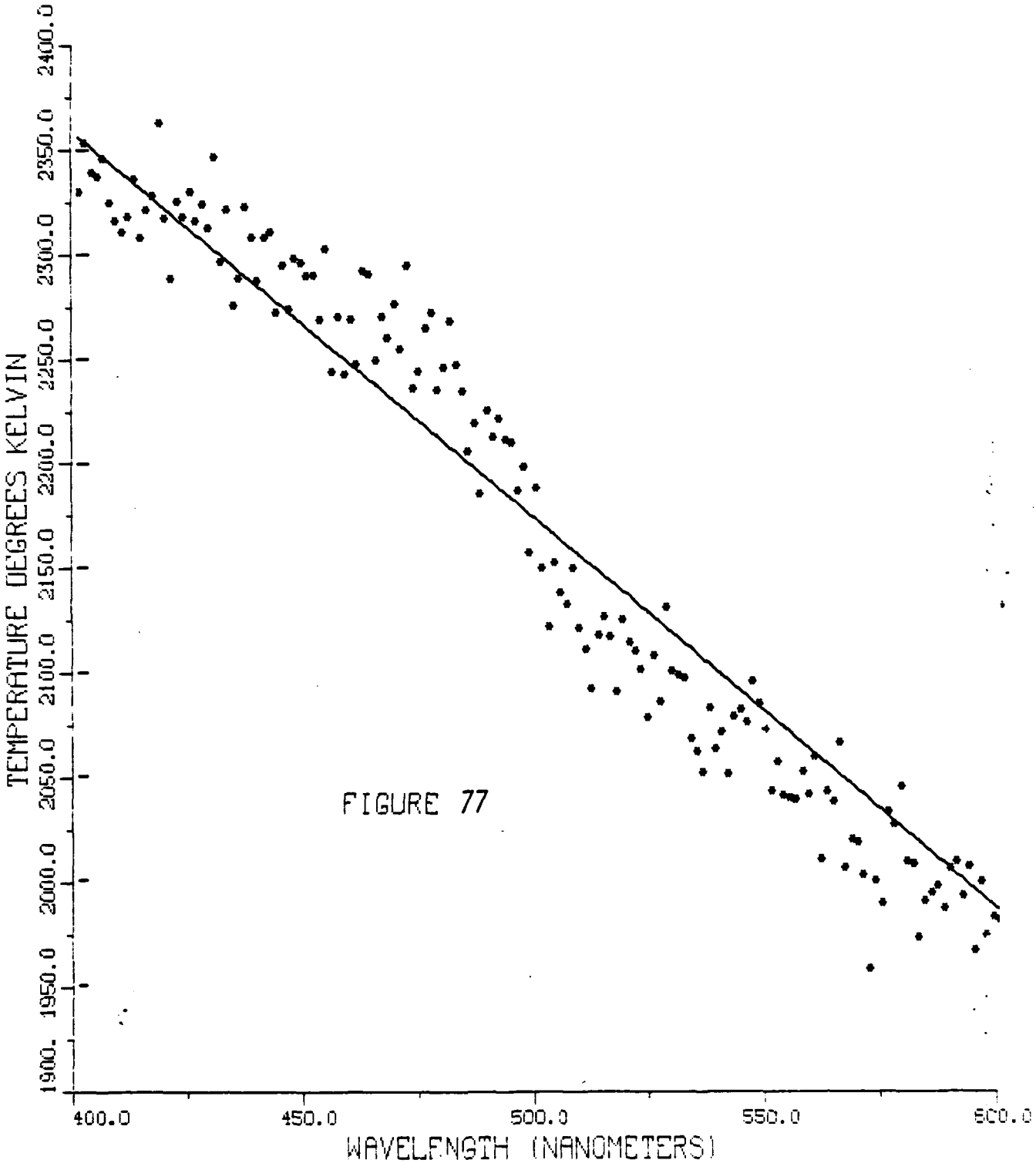
TEMPERATURE AT 0.04 SECONDS
TEMPERATURE DEGREES KELVIN
1900.
1950.0
2000.0
2050.0
2100.0
2150.0
2200.0
2250.0
2300.0
2350.0
2400.0
400.0
450.0
500.0
550.0
600.0
WAVELENGTH (NANOMETERS)

FIGURE 77

# SPECTRAL POWER AT 0.33 SECONDS

FIGURE 78

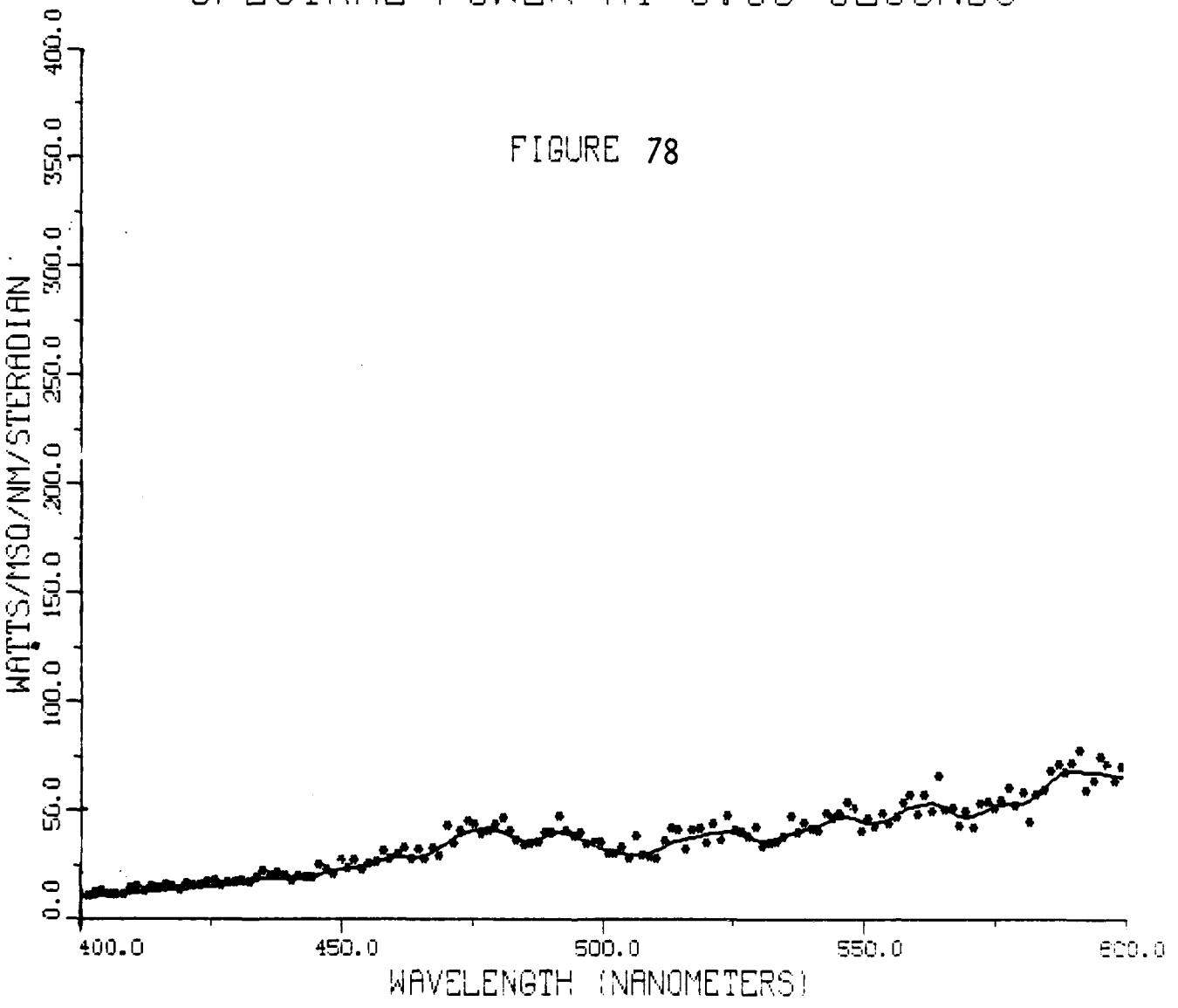

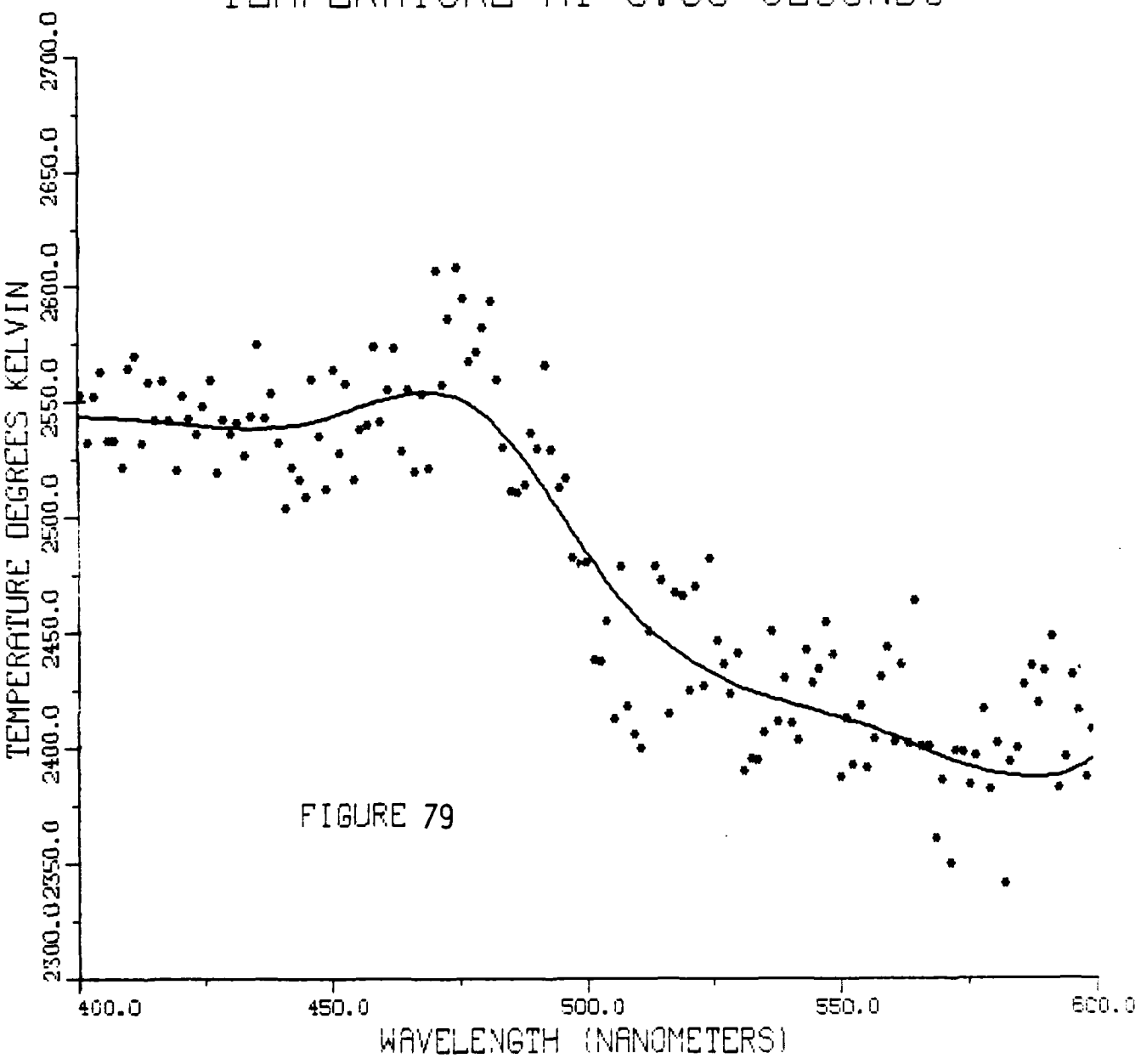
TEMPERATURE AT 0.33 SECONDS
TEMPERATURE DEGREES KELVIN
2300.0
2350.0
2400.0
2450.0
2500.0
2550.0
2600.0
2650.0
2700.0
400.0
450.0
500.0
550.0
600.0
WAVELENGTH (NANOMETERS)

FIGURE 79

# SPECTRAL POWER AT 0.62 SECONDS

FIGURE 80

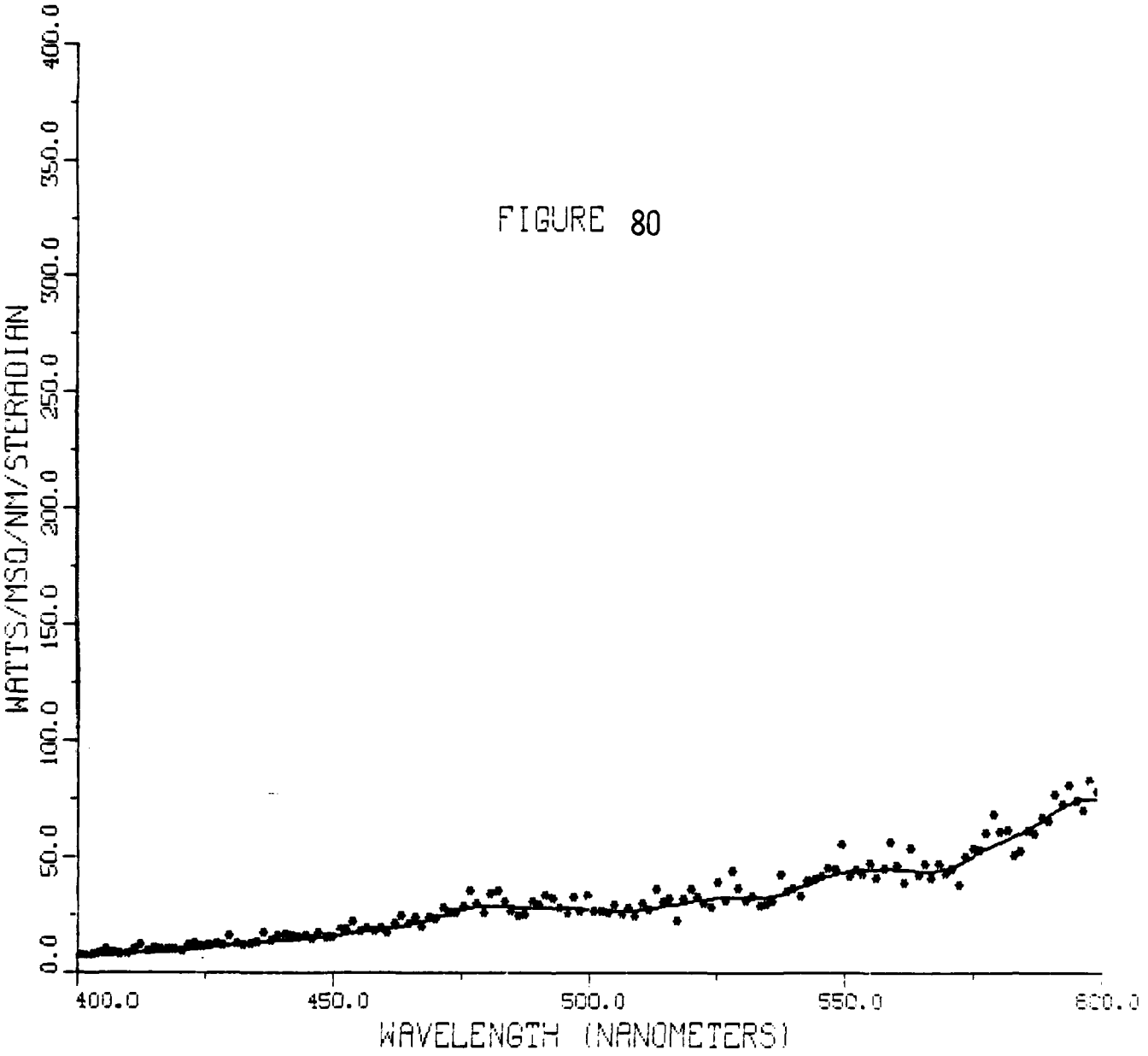

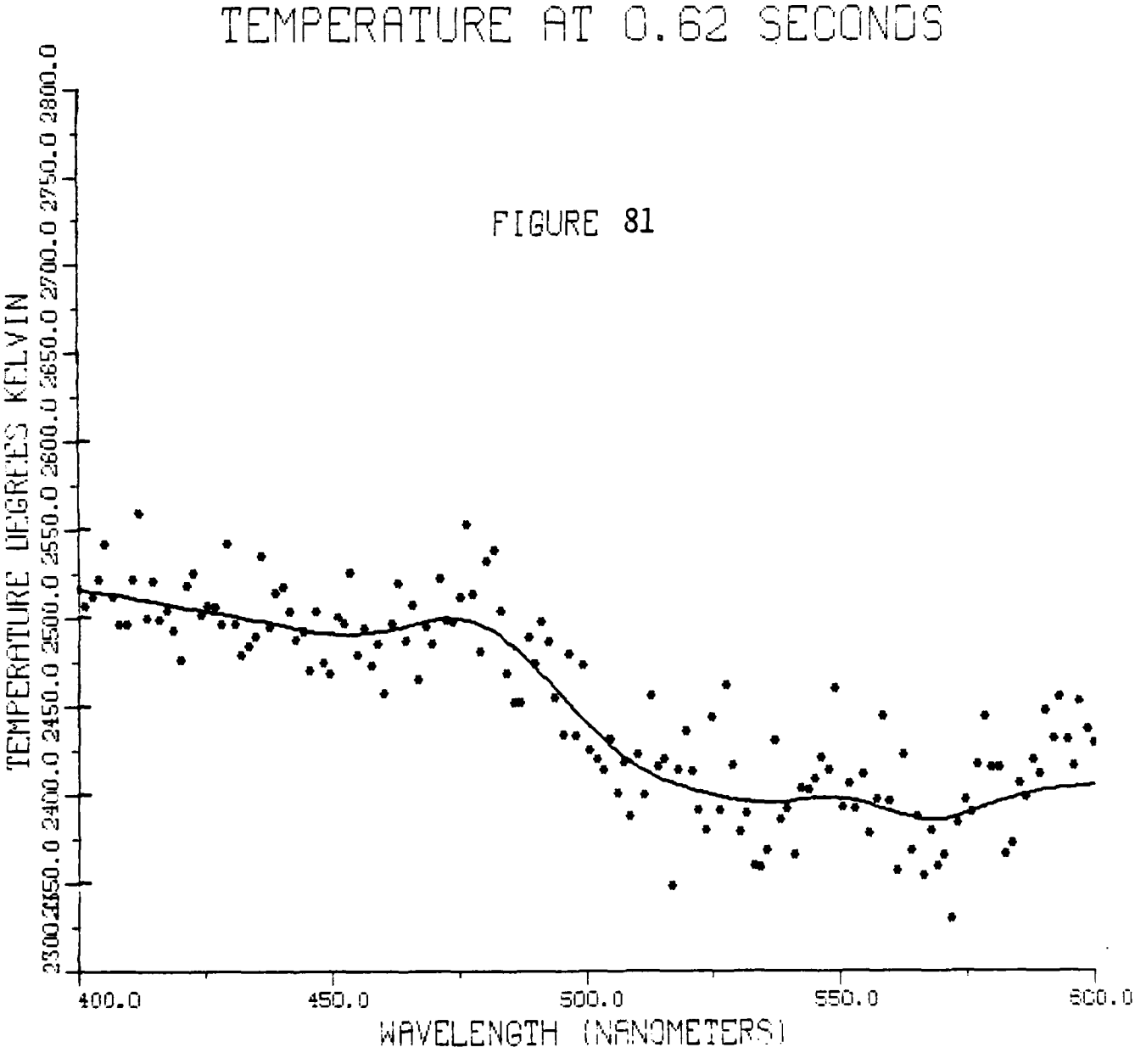
TEMPERATURE AT 0.62 SECONDS
TEMPERATURE DEGREES KELVIN
2300.0 2350.0 2400.0 2450.0 2500.0 2550.0 2600.0 2650.0 2700.0 2750.0 2800.0
400.0
450.0
500.0
550.0
600.0
WAVELENGTH (NANOMETERS)

FIGURE 81

# SPECTRAL POWER AT 0.92 SECONDS

FIGURE 82

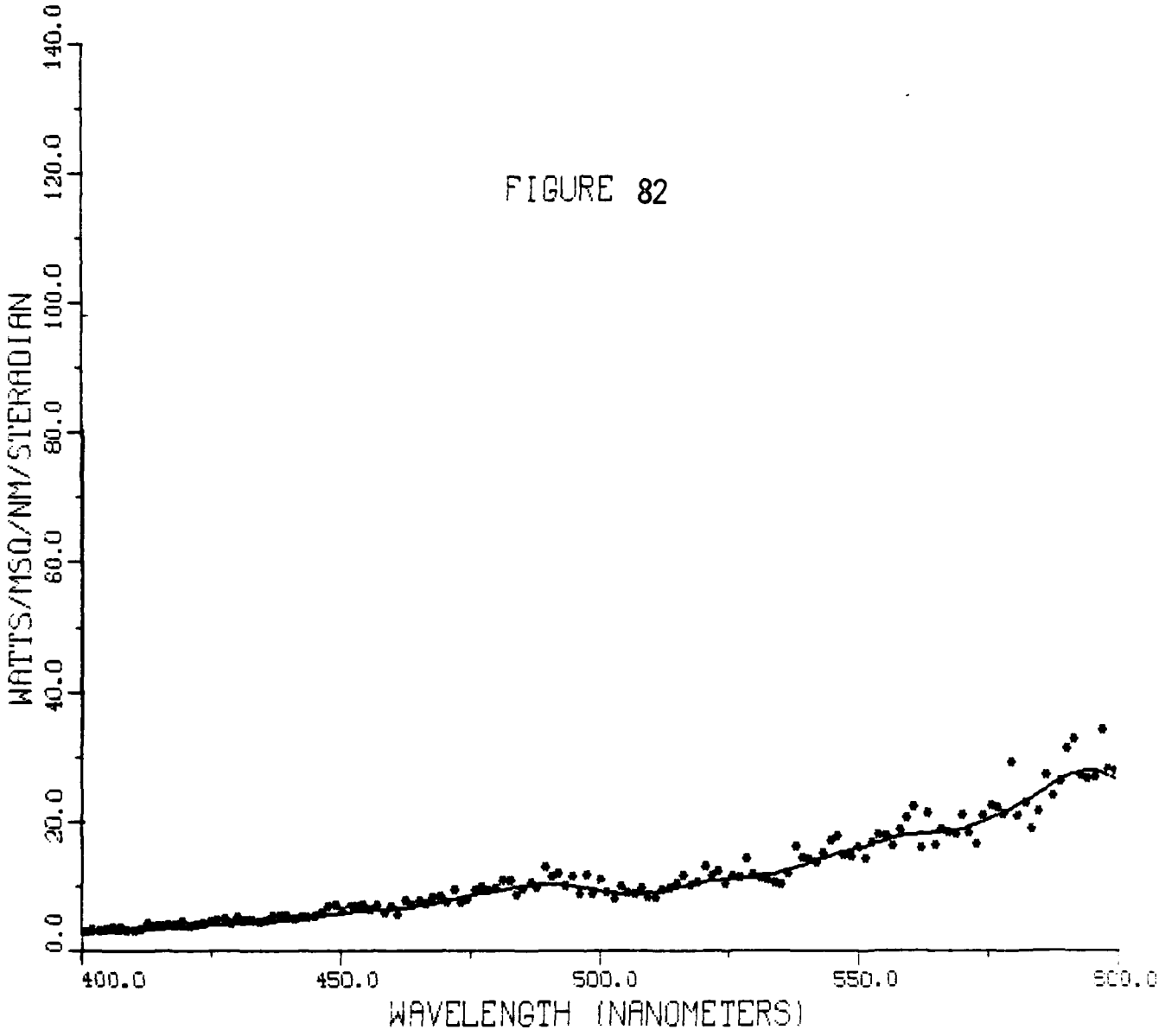

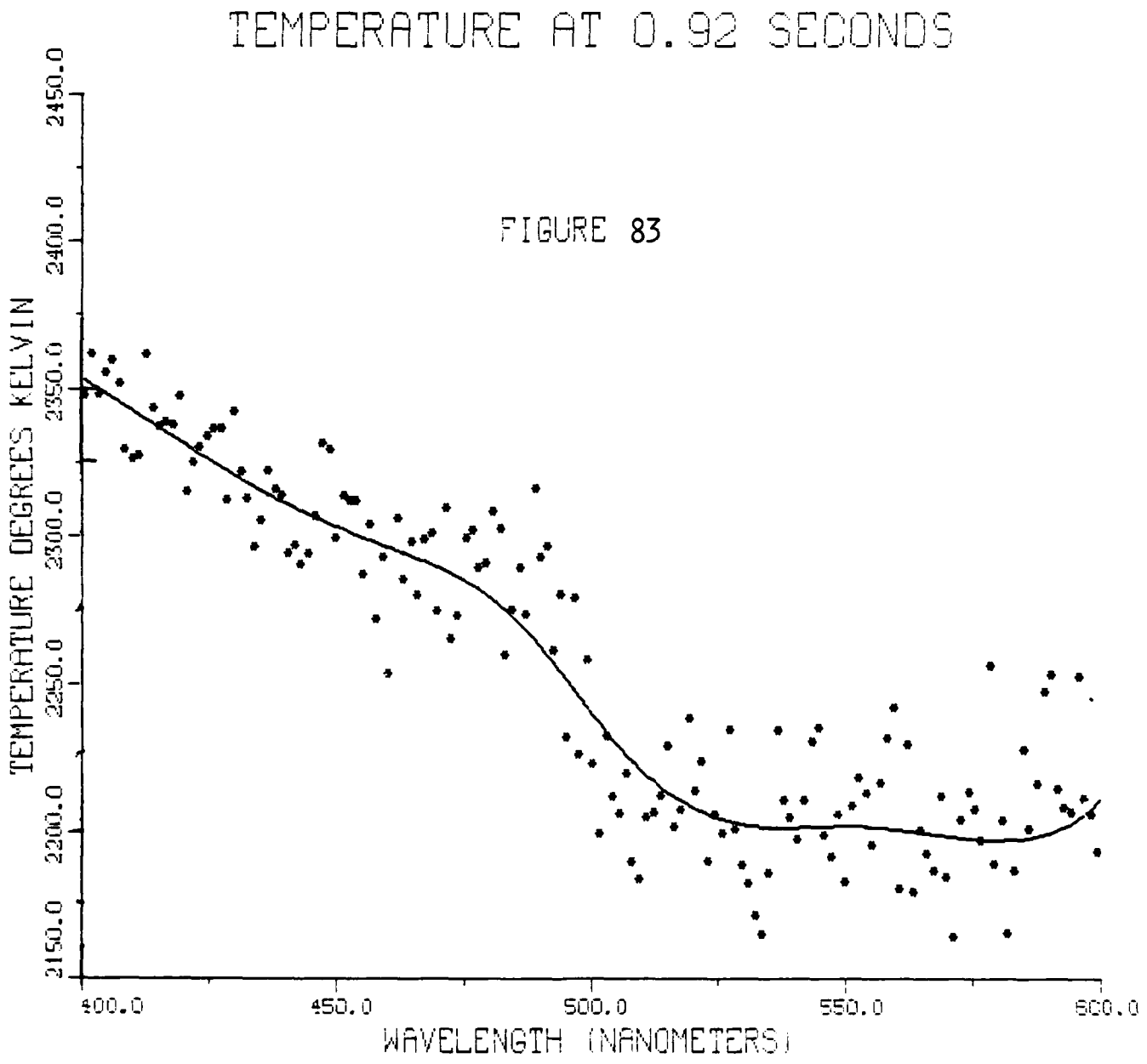
TEMPERATURE AT 0.92 SECONDS
TEMPERATURE DEGREES KELVIN
2450.0
2400.0
2350.0
2300.0
2250.0
2200.0
2150.0
400.0
450.0
500.0
550.0
600.0
WAVELENGTH (NANOMETERS)

FIGURE 83

# SPECTRAL POWER AT 1.20 SECONDS

FIGURE 84

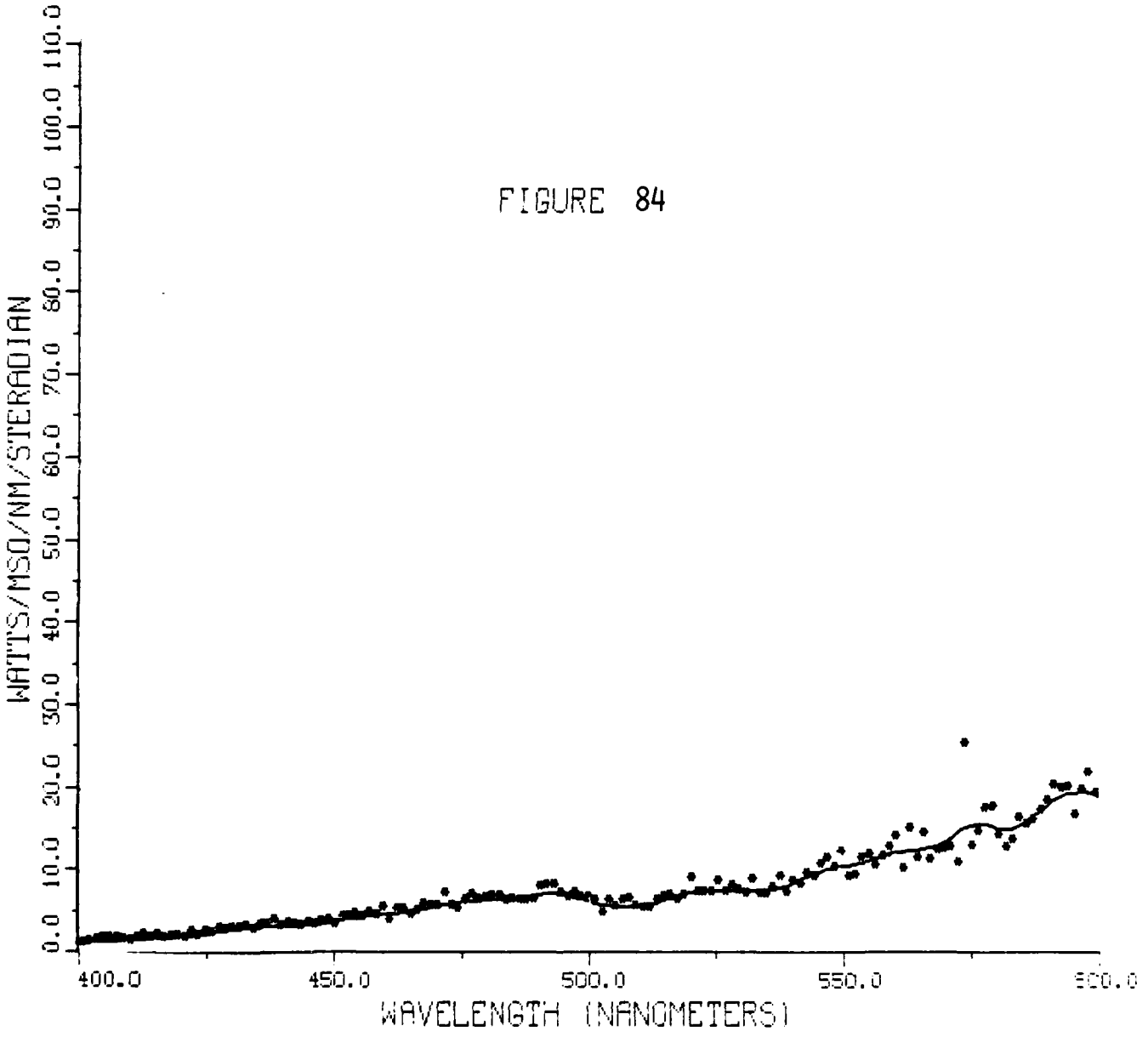

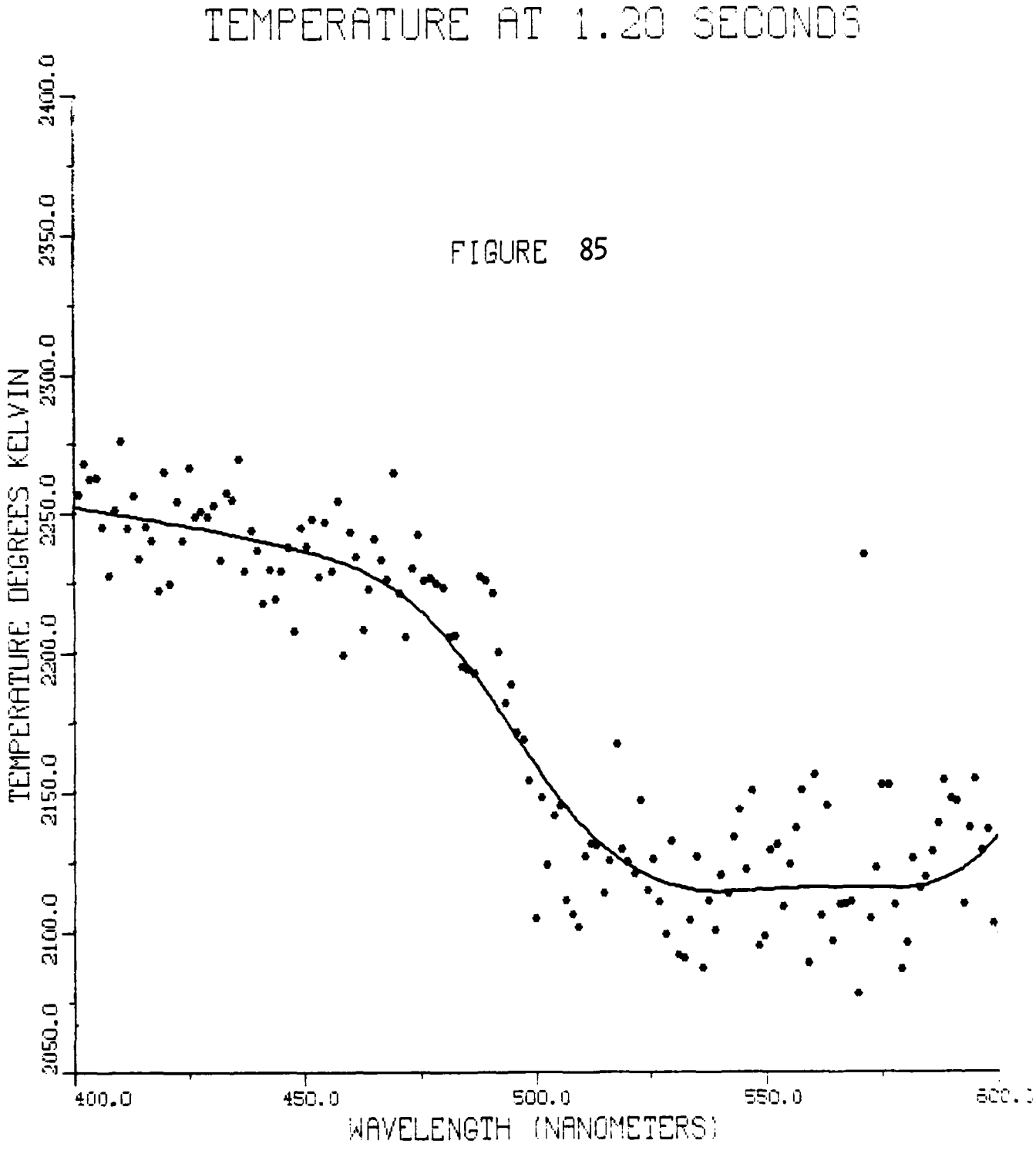
TEMPERATURE AT 1.20 SECONDS
TEMPERATURE DEGREES KELVIN
2400.0
2350.0
2300.0
2250.0
2200.0
2150.0
2100.0
2050.0
400.0
450.0
500.0
550.0
600.0
WAVELENGTH (NANOMETERS)

FIGURE 85

# SPECTRAL POWER AT 1.50 SECONDS

FIGURE 86

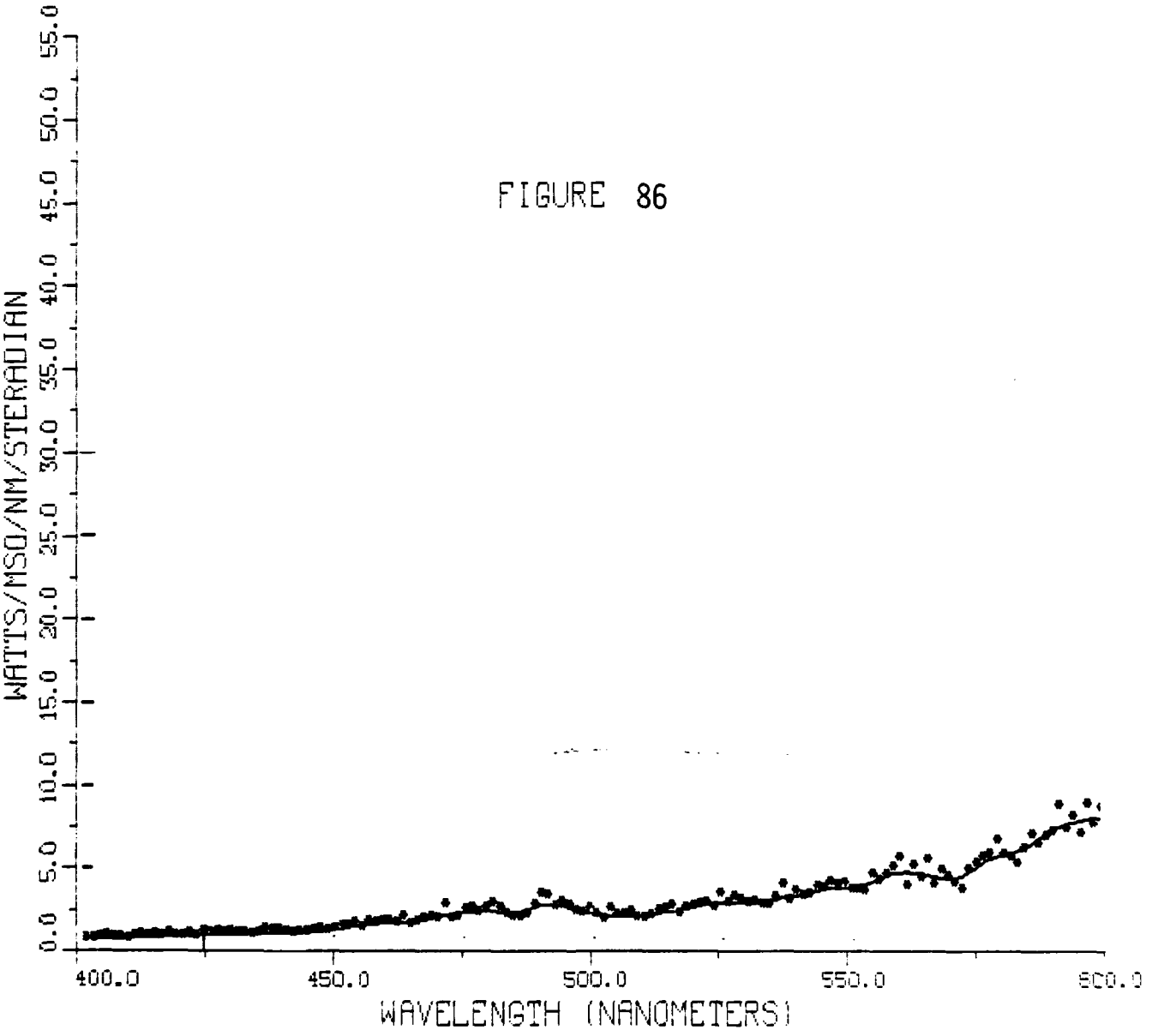

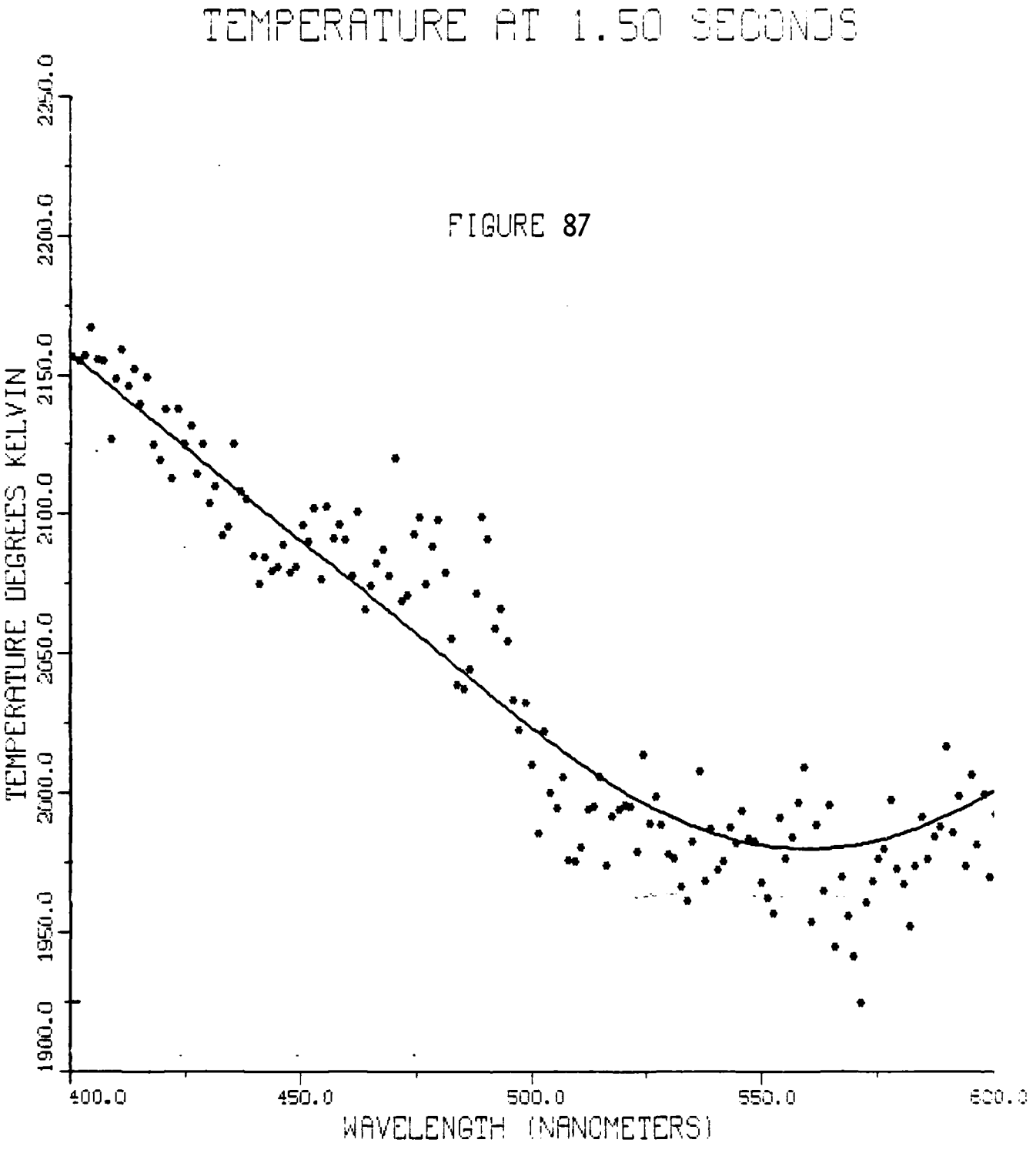
TEMPERATURE AT 1.50 SECONDS
TEMPERATURE DEGREES KELVIN
1900.0
1950.0
2000.0
2050.0
2100.0
2150.0
2200.0
2250.0
400.0
450.0
500.0
550.0
600.0
WAVELENGTH (NANOMETERS)

FIGURE 87

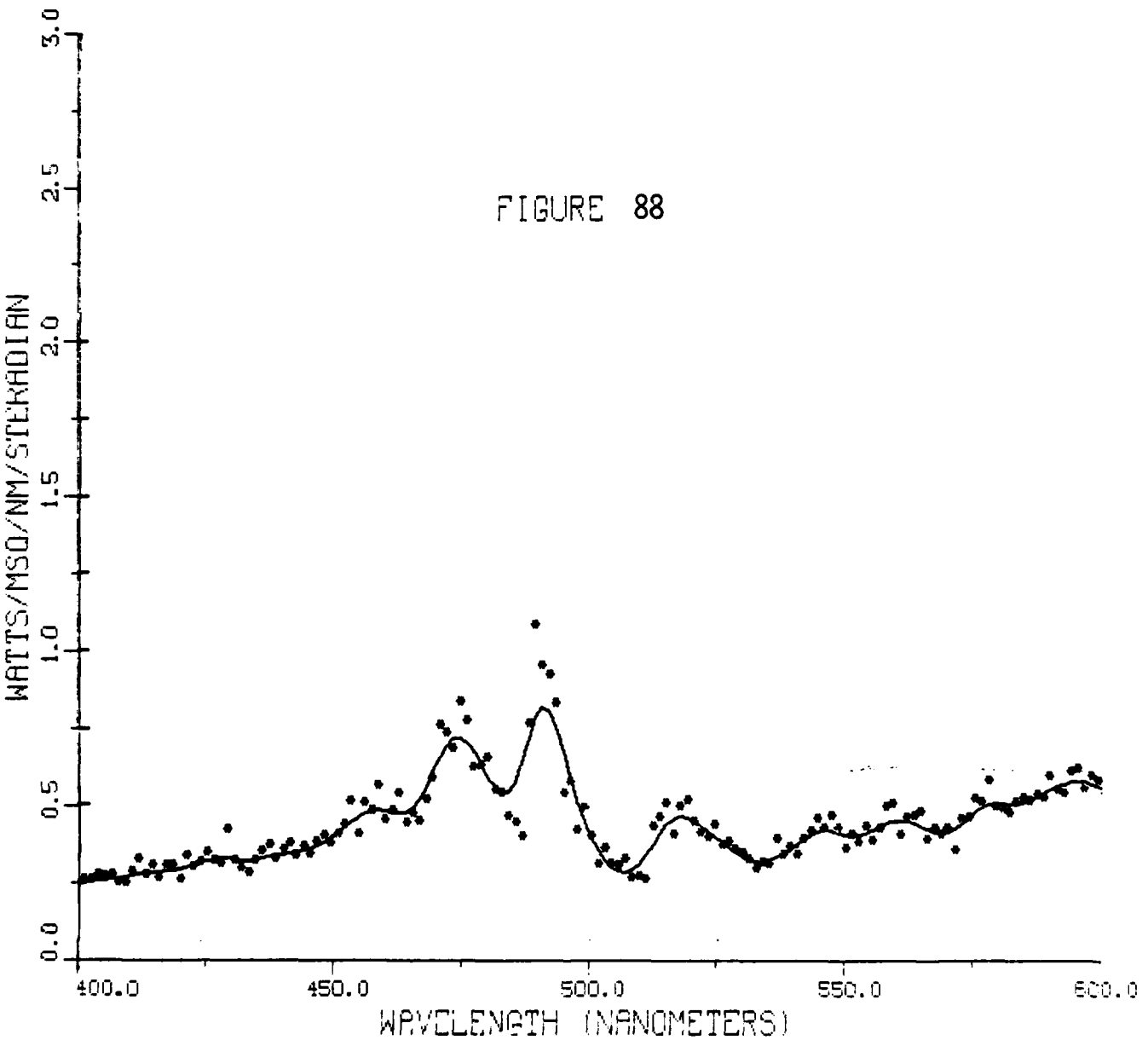
SPECTRAL POWER AT 3.40 SECONDS
WATTS/MSQ/NM/STERADIAN
0.0
0.5
1.0
1.5
2.0
2.5
3.0
400.0
450.0
500.0
550.0
600.0
WAVELENGTH (NANOMETERS)

FIGURE 88

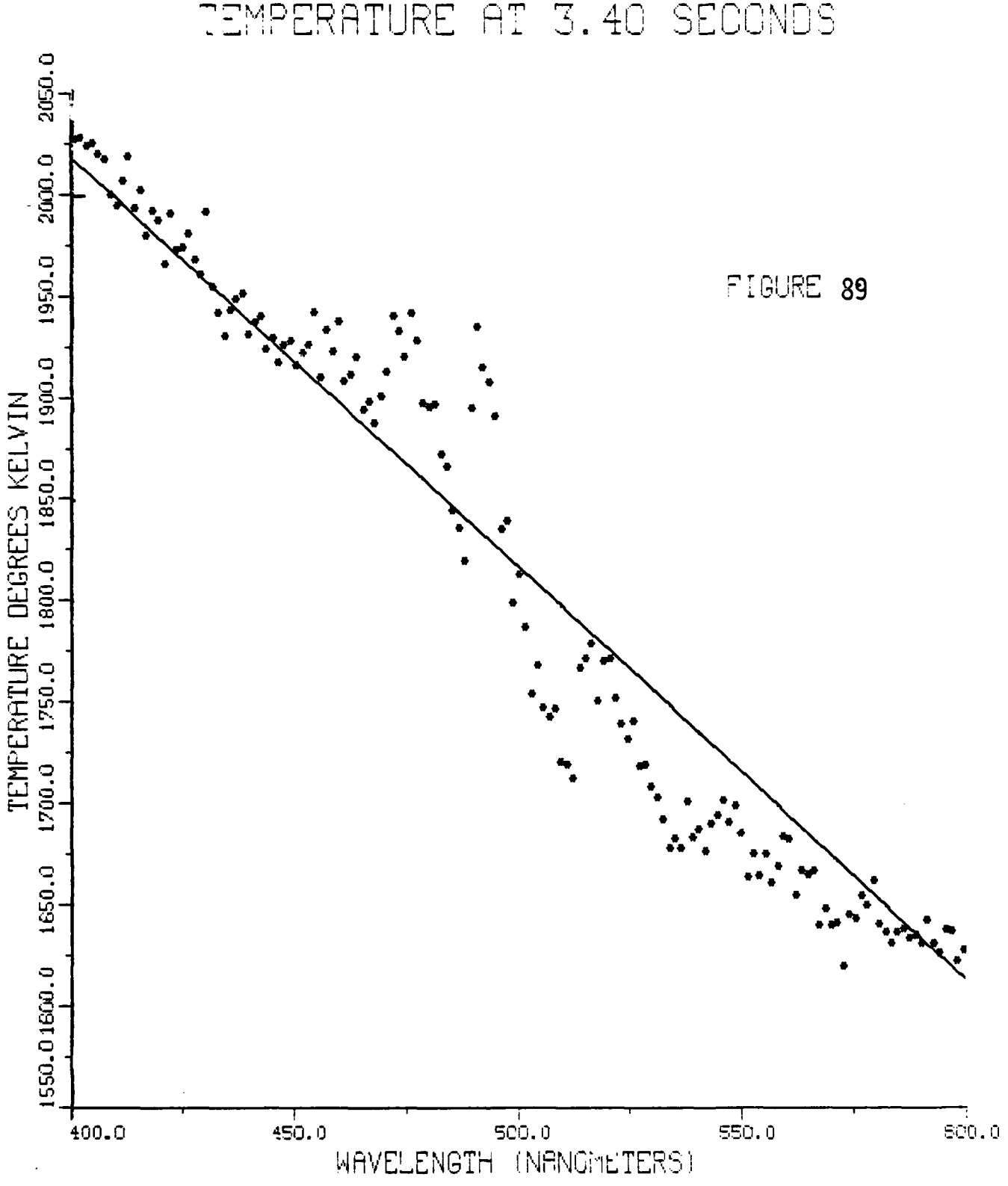
TEMPERATURE AT 3.40 SECONDS
TEMPERATURE DEGREES KELVIN
1550.0
1600.0
1650.0
1700.0
1750.0
1800.0
1850.0
1900.0
1950.0
2000.0
2050.0
400.0
450.0
500.0
550.0
600.0
WAVELENGTH (NANOMETERS)

FIGURE 89

SECTION 5

## 5.0 Conclusions

The purpose of this report has been to present in as much detail as possible, previously unreduced data of a TRS nuclear thermal soure simulator and to perform basic measurements on this data which may be useful to the Defense Nuclear Agency community.

Brightness time histories show that peak radiance values of small (3.3- by 3.3 inch) surface areas of the gas module source can reach as high as 6000 watts/$m^2$/ster/nm which corresponds to a black body temperature of 4300$^0$K. The large uneven chemical burning creates significant radiance fluctuations over the TRS surface. Averaging out these fluctuations over the total area of the ignited TRS surface indicates that the highest average radiance value of 266.3 watts/$m^2$/ster/nm at 660 nanometers is achieved at 0.85 seconds. This corresponds to a black body temperature of 2630$^0$K. The 0.85 seconds to reach this peak radiant power indicates that this thermal pulse very poorly simulates the rise rate of the main (second) power pulse of a nuclear device. The TRS rise rate is approximately 10 times too slow to simulate for example a 60 kt nuclear device.

Although emissivities of the TRS device are as yet unknown it can be said that the thermal output as determined by temperature measurements, of the LOX TRS device (see Annex A) is significantly greater than that achieved by the gas module TRS device.

## REFERENCES


1. Dishon, J.,"The Thermal Radiation Simulator Development Program", DNA Nuclear Blast And Shock Simulation Symposium, 28-30 November 1978.

2. Chambers,III,B,S, and Hasdal,J.A.,"Estimates Of Thermal Radiation Environments For Planning A Thermal Simulation On A He Test", DNA5073F, March 1979.

3. (a) Dudziak,W.F., et. al."Photographic Atlas Event WASP PRIME", DNA3576F, May, 1975: (b) Anderson, J., et.al., "Radiometric Data Reduction For Black and White and Color Film", ISI, TN022572, February 1972.

4. Buckner, J.K.,"Radiometric Data Reduction For Photographic Film", EG&G-1183-414B-3600,1967.

5. Larrabee, R.D.,"The Spectral Emissivity And Optical Properties Of Tungsten" Mass. Inst. of Technology Tech Report 328, May 1957.

6. Randolp and Overholzer,"Typical Total Emissivities Of Various Solids", Phys. Rev., 2:144(1913)

# APPENDIX

## SPECTRAL MEASUREMENTS ON A LOX TRS SOURCE

The LOX TRS thermal source replaces the gas bag modules with a structure composed of a set of nozzles that allow simultaneous ejection, under pressure, of liquid oxygen (LOX) and a liquid nitrogen - aluminum powder mixture. These jets, on evaporation, allow a higher concentration of the oxidation components described in equation 1.

During 24 December 1980 there were a few LOX TRS development experiments in Albuquerque. Presented here are some spectral measurements made on two of these experiments. Figure 24A illustrates a LOX TRS source ignition.

The measurements were made with a special camera electro- optical computer recording system. The heart of this electro optical system is a multi-spectral analyzer (OMA). It possesses a vidicon image scanning system that records in real time, spectral information on a random access memory (RAM) of a computer system located in a mobile van. The size of the RAM limited the spectral sampling to 512 pixels on each vidicon scan line over the selected wavelength interval. The spectral resolution of each recorded point is determined by the setting of the wavelength pass band of the spectrometer. For these two experiments, the spectral pass band ranged from 500 to 700 nanometers. This setting allowed wavelength variation measurements of less than 0.4 nanometer by adjacent pixels.

The optical system of the OMA was pointed so that its slit would be aligned vertically at the thermal source. The optics magnification was adjusted so that the imaging slit had a field of view on the source surface of one inch in the horizontal and four feet in the vertical direction. The bottom of this vertical slit was positioned at the expected hottest region (i.e., very near the nozzle outlet).

For these two experiments the OMA was programmed to sample six times the spectral content from the TRS surface defined by this slit. Each of the six scans were separated in time by 0.25 seconds. Thus spectral measurements

were made during the first 1.25 seconds of the thermal flash.

Fifteen seconds prior to thermal flash noise background information was recorded by the OMA system within this slit. This spectral background was subtracted from the raw thermal flash data during analysis. For each experiment the OMA was activated at the instant of observed visible light for data collected from the thermal source.

Figure 9A and Figure 17A illustrate graphically the raw data from the two OMA 1.25 second data collection operations. These figures give an overview of relative radiance as a function of wavelength and as a function of time. Scan 0 is the first scan at approximately zero time, that is, at the instant of observed visible light; Scan 1 is the second OMA spectral scan 0.25 seconds after scan 0 and so on. Thus in these figures one minus the number (n - 1) of "bell shaped" figures multiplied by 0.25 seconds indicates the time after ignition. Within each "bell shaped" figure the wavelength increases from left (500) to right (700). The height of the "bell shaped" figure illustrates the relative intensity variation within the slit every 0.25 seconds. Figure 9A illustrates data from an event classed as a "misfire" while Figure 17A illustrates the time intensity variations within the slit for a "good event" fire.

Prior to transforming the raw data presented in these two figures to spectral radiance and black body temperature, the OMA data obtained from the NBS calibration tungsten source will be presented. This will illustrate the the proper data analysis procedure.

Figure 1A presents the raw, relative intensity OMA signals from six scans of the NBS standard tungsten light source set at a temperature of 2600$^{0}$K as recorded in the laboratory with the same OMA field optics system. Figure 2A illustrates the highly amplified OMA background in the laboratory when the calibration light source is turned off. As seen, the six scans report the same relative intensity for each scan in both Figure 1A and Figure 2A.

Subtracting the background data (Figure 2A from Figure 1A) and using the OMA spectral response calibration curve determined in the laboratory with

a monochrometer, one obtains Figure 3A. This figure presents the spectral source radiance for scan 0 of the calibration light source. Since all "bell shape" scans are the same (computer determined to be within 0.1% of each other) it also represents the results for the other scans.

The spectral radiance, Figure 3A, is transformed to spectral temperature, Figure 4A, by equation 5. As observed Figure 4A shows a spectral temperature variation (from 2410$^0$K to 2310$^0$K) and that the maximum temperature is 200$^0$ lower than the temperature setting of the NBS source standard.

What has been overlooked in the data analysis which led to Figure 4A was the spectral emissivity for tungsten[5]. This temperature dependent spectral emissivity is reproduced in Figure 5A. Applying this emissivity correction transforms Figure 3A to Figure 6A and Figure 4A to Figure 7A.

For ease of comparison, Figure 8A, illustrates the meaning of this spectral emissivity correction. Here unsmoothed data from Scan 5 is used. As shown, this emissivity correction raises and straightens out the curve yielding a constant temperature with wavelength. Thus, it indicates that a tungsten radiator, when properly analyzed, radiates as a black body.

Figures 10A and Figures 12A through 16A present the analyzed data for the LOX TRS2 ("misfire") thermal source as temperature versus wavelength plots. Figure 11A illustrates typical radiance variation with wavelength for this source as obtained from Figure 9A. Similarly Figures 18A to 23A present similar temperature versus wavelength data in the selected spectrometer slit of the LOX TRS3 ("good fire") source as a function of time. Since the spectral emissivities of the LOX TRS source are as yet unknown, the emissivity was assumed as 1 (black body) in the analysis of this data. In these figures the nomenclature 12-24-80 refers to the date of the experiment, while TRS2,0 is read as Scan 0 of source TRS2.

It is important to note the shape of the temperature versus wavelength curves presented in Figures 10A through 23A, with Figure 8A as a reference. With emissivity equal to 1 (no correction), Figure 8A shows that as wavelength increases into the red, the temperature curve drops. This tempera-

ture wavelength dependence is also observed for the TRS gas bag source in Section 4. For the LOX TRS source the reverse seems to be indicated.

A review of the field data collection components showed that some decrease in this rise was achieved by study of the wavelength and brightness transmission dependence of the "spectrally flat" (non-sensitive to these parameters) inconel filters used in the field to screen out "blue sky" background from the OMA system. As illustrated by Figure 21A, this correction did not remove this reversal in wavelength dependence. The observed peculiarity in the LOX TRS spectral temperature dependence, as well as, emissivity measurements, will require future additional data collection and analysis.

FIGURE 1A

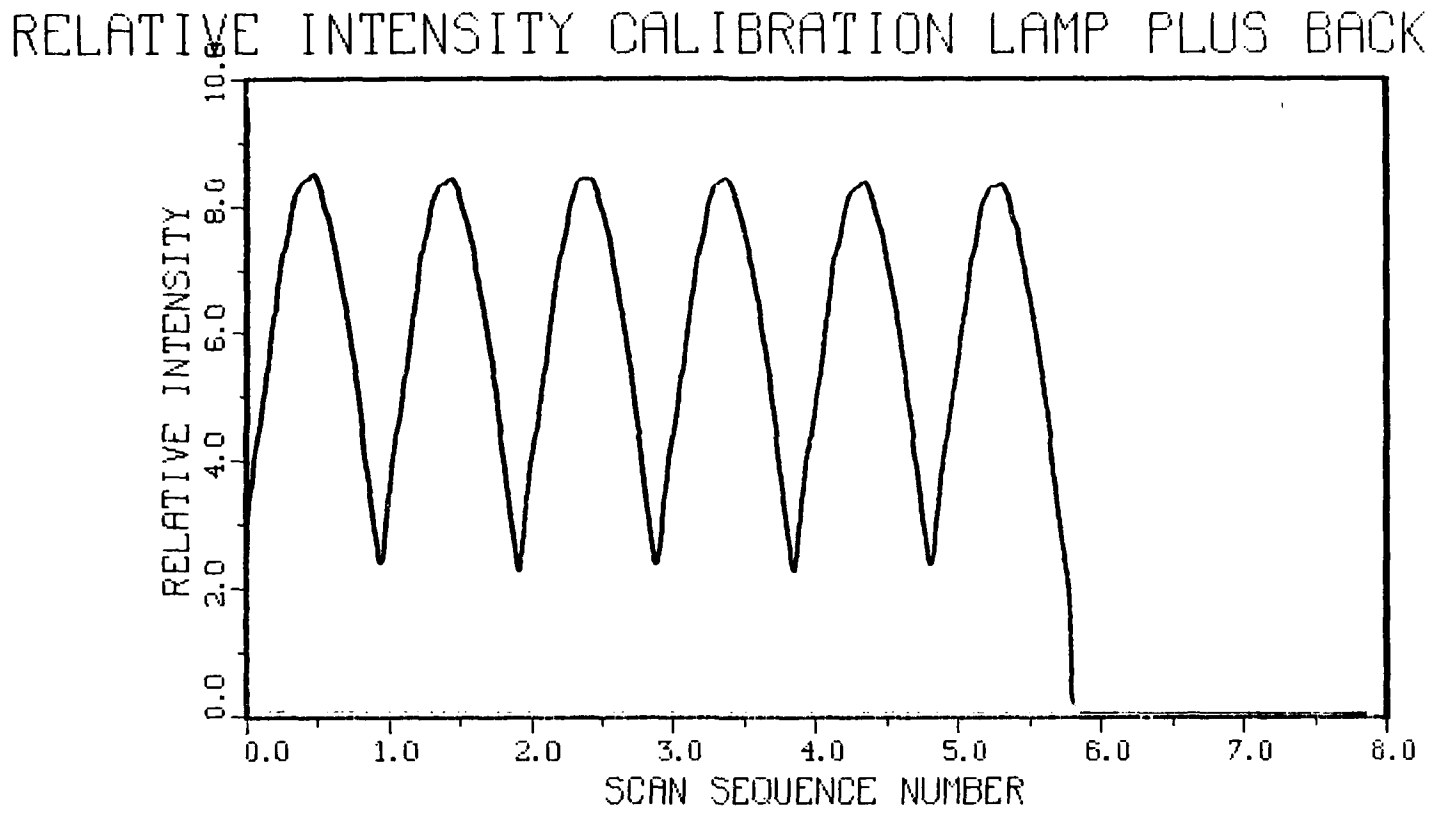
RELATIVE INTENSITY CALIBRATION LAMP PLUS BACKGROUND
RELATIVE INTENSITY
0.0
2.0
4.0
6.0
8.0
10.0
0.0
1.0
2.0
3.0
4.0
5.0
6.0
7.0
8.0
SCAN SEQUENCE NUMBER

FIGURE 2A

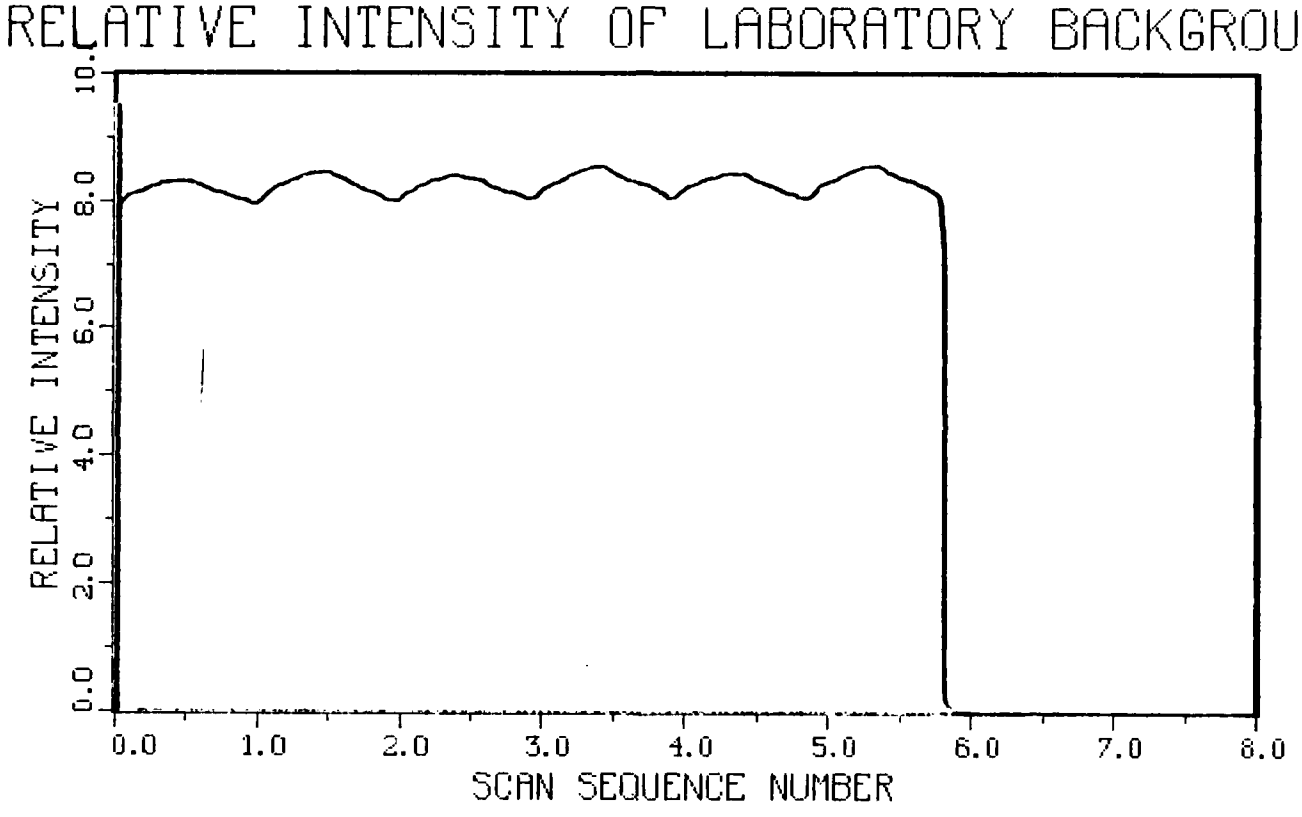
RELATIVE INTENSITY OF LABORATORY BACKGROUND
RELATIVE INTENSITY
0.0
2.0
4.0
6.0
8.0
10.
0.0
1.0
2.0
3.0
4.0
5.0
6.0
7.0
8.0
SCAN SEQUENCE NUMBER

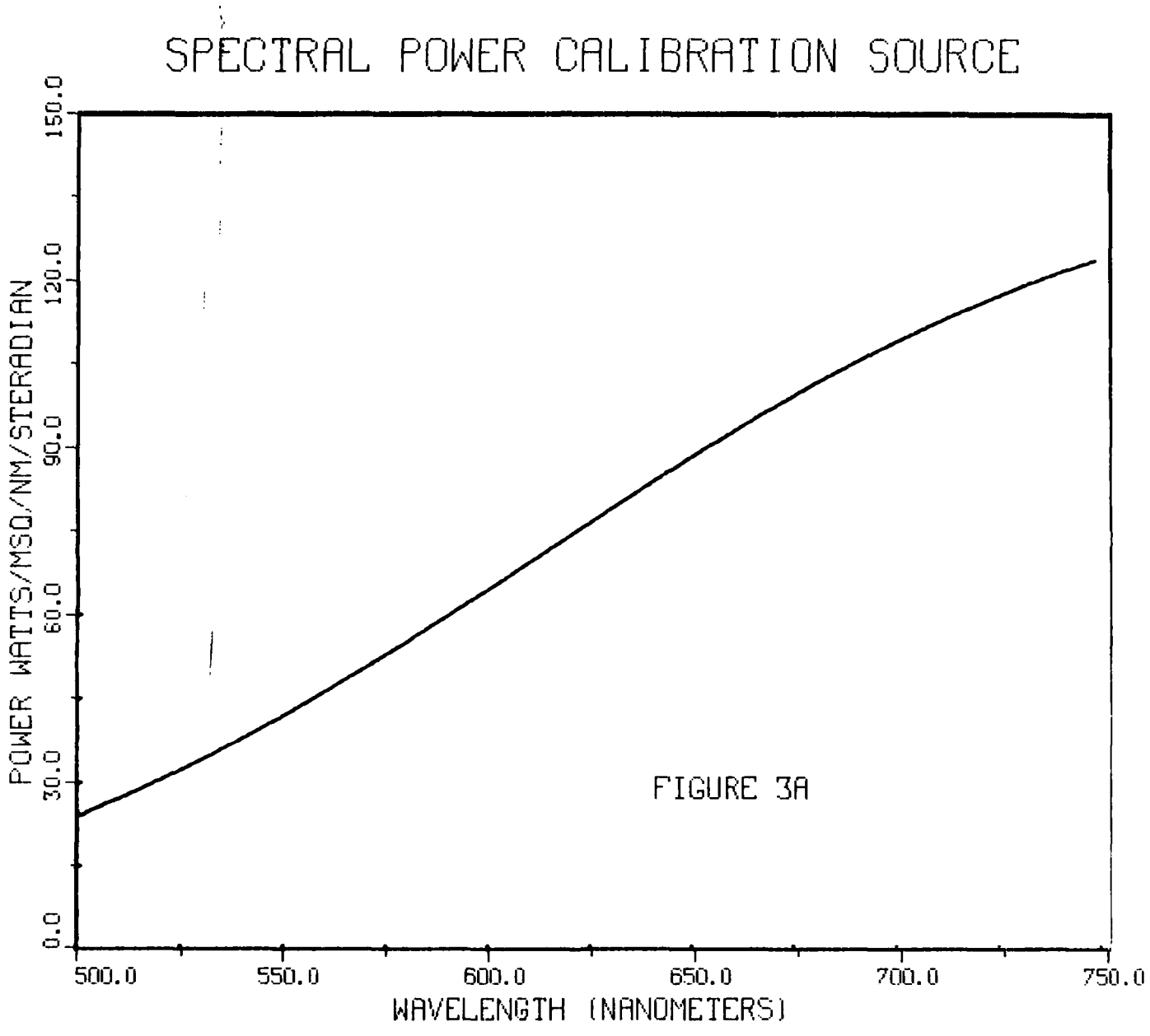
SPECTRAL POWER CALIBRATION SOURCE
POWER WATTS/MSQ/NM/STERADIAN
150.0
120.0
90.0
60.0
30.0
0.0
500.0
550.0
600.0
650.0
700.0
750.0
WAVELENGTH (NANOMETERS)

FIGURE 3A

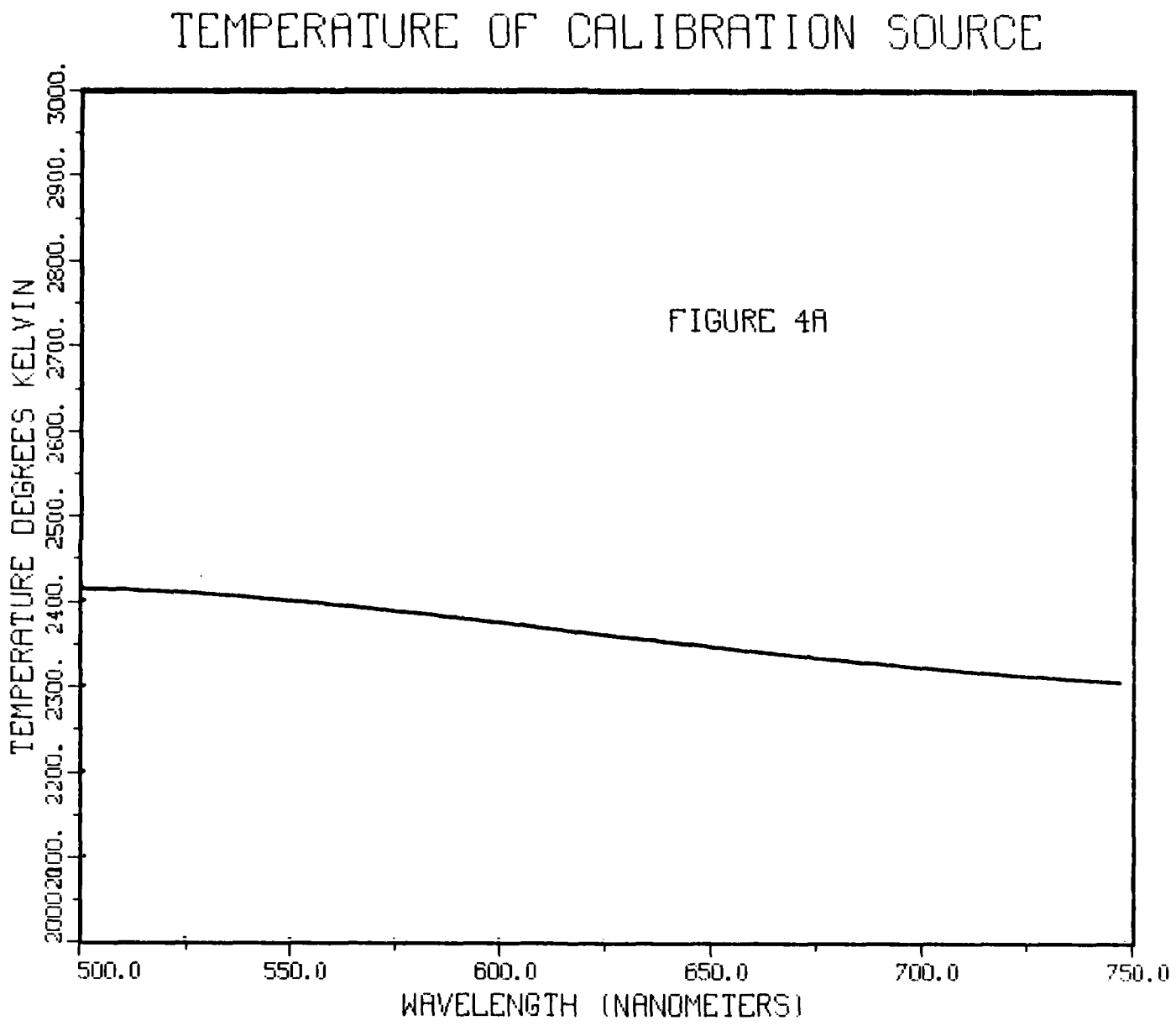
TEMPERATURE OF CALIBRATION SOURCE
TEMPERATURE DEGREES KELVIN
2000 2100. 2200. 2300. 2400. 2500. 2600. 2700. 2800. 2900. 3000.
500.0
550.0
600.0
650.0
700.0
750.0
WAVELENGTH (NANOMETERS)

FIGURE 4A

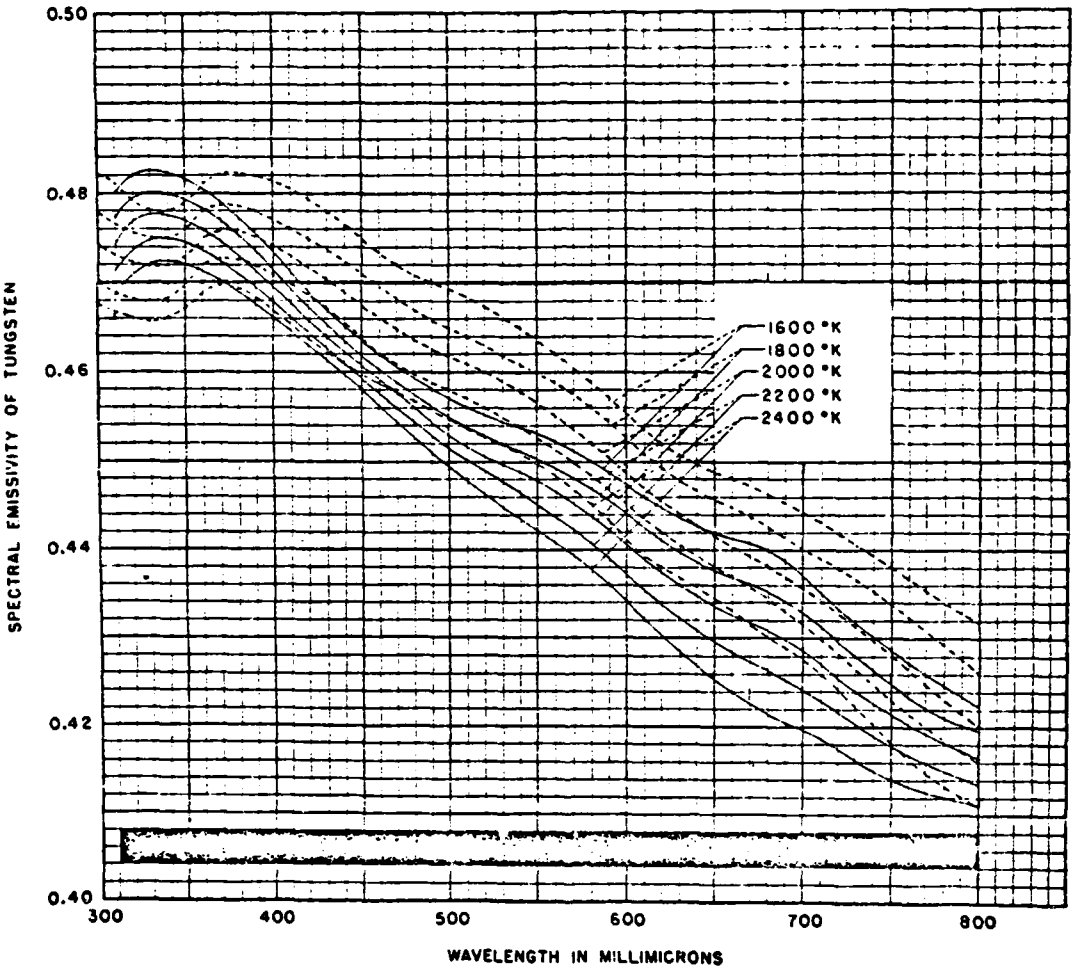


Fig. 5A The spectral emissivity of tungsten
— present experiment
-- J. C. De Vos, Physica 20, 690 (1954)

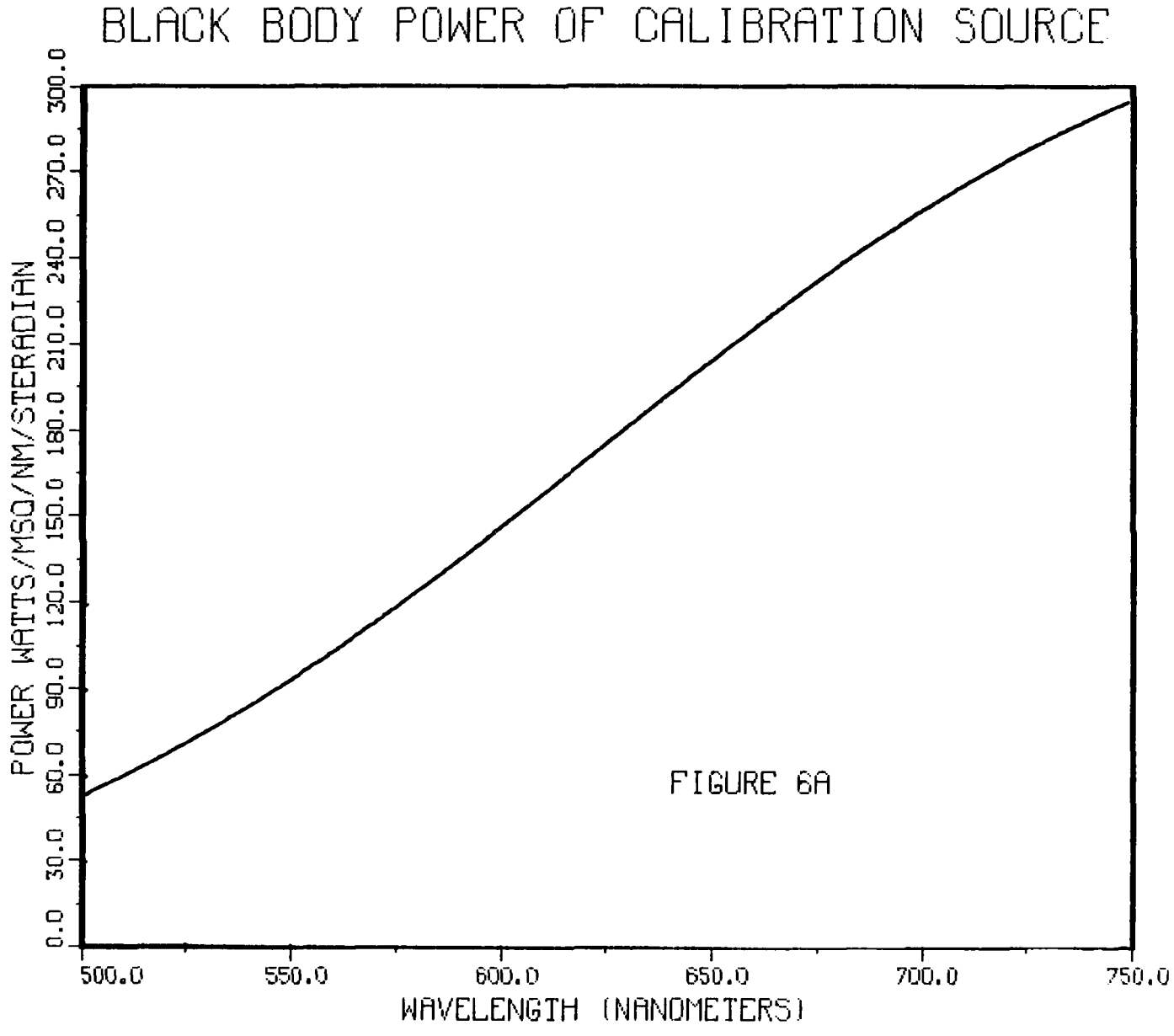
BLACK BODY POWER OF CALIBRATION SOURCE
POWER WATTS/MSQ/NM/STERADIAN
0.0
30.0
60.0
90.0
120.0
150.0
180.0
210.0
240.0
270.0
300.0
500.0
550.0
600.0
650.0
700.0
750.0
WAVELENGTH (NANOMETERS)

FIGURE 6A

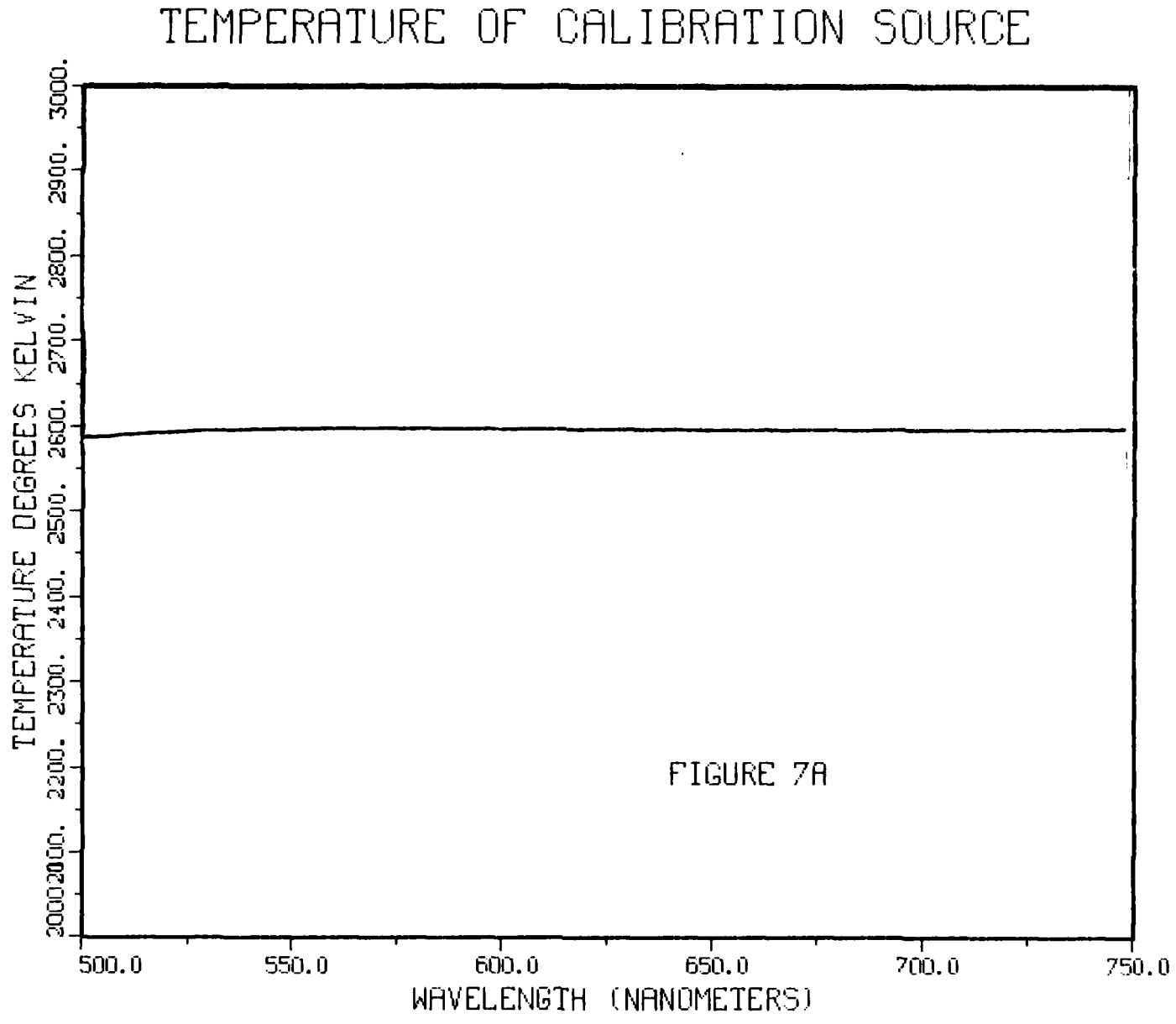
TEMPERATURE OF CALIBRATION SOURCE
TEMPERATURE DEGREES KELVIN
2000. 2100. 2200. 2300. 2400. 2500. 2600. 2700. 2800. 2900. 3000.
500.0
550.0
600.0
650.0
700.0
750.0
WAVELENGTH (NANOMETERS)

FIGURE 7A

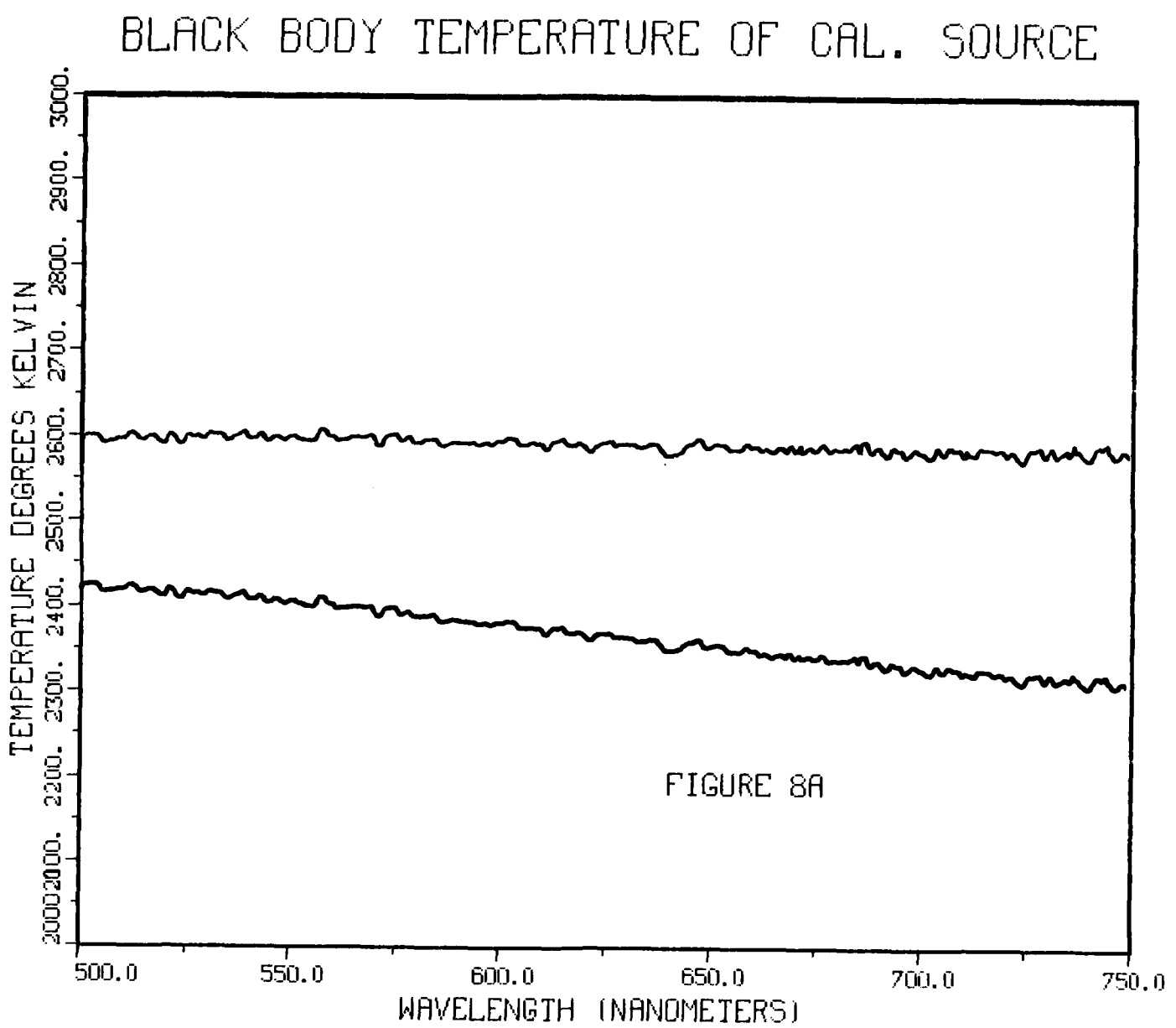
BLACK BODY TEMPERATURE OF CAL. SOURCE
TEMPERATURE DEGREES KELVIN
2000
2100.
2200.
2300.
2400.
2500.
2600.
2700.
2800.
2900.
3000.
500.0
550.0
600.0
650.0
700.0
750.0
WAVELENGTH (NANOMETERS)

FIGURE 8A

FIGURE 9A

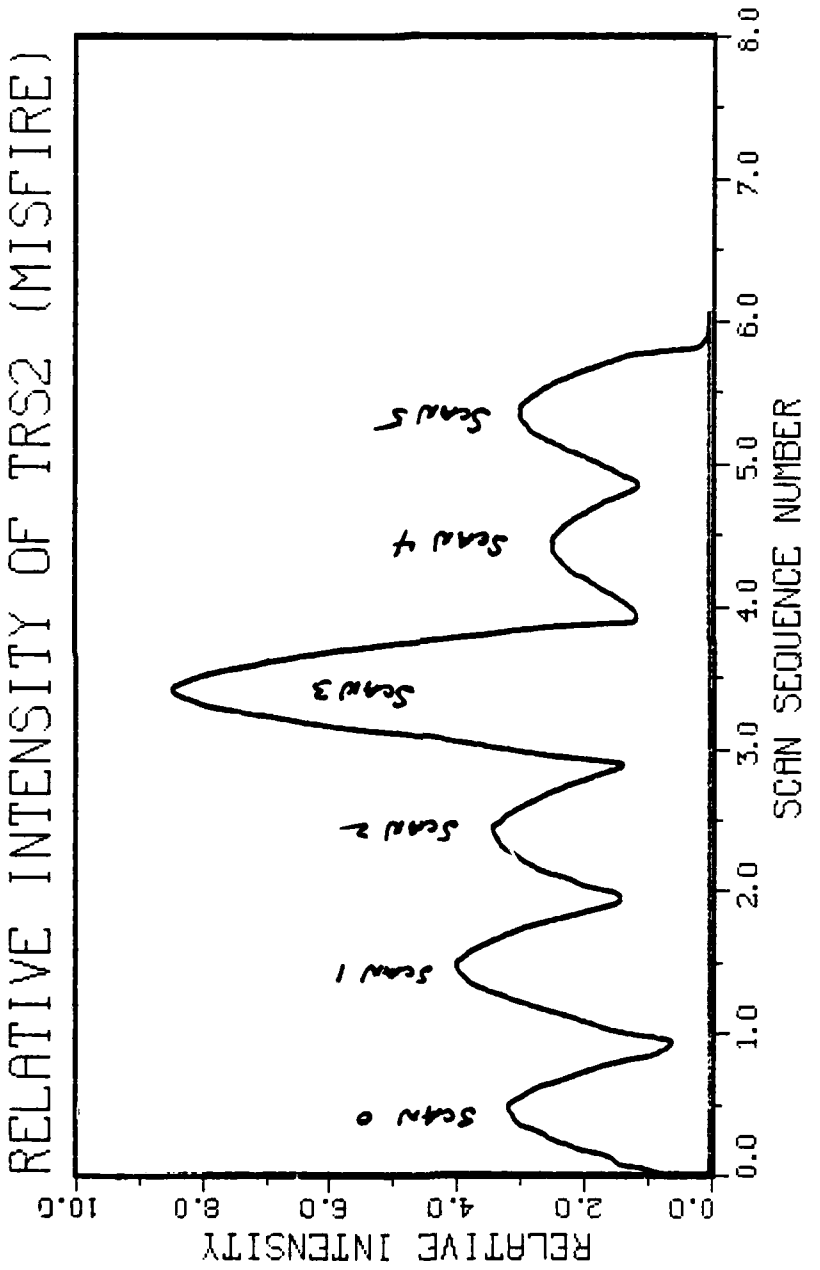
RELATIVE INTENSITY OF TRS2 (MISFIRE)
RELATIVE INTENSITY
SCAN SEQUENCE NUMBER
0.0
2.0
4.0
6.0
8.0
10.0
1.0
3.0
5.0
7.0

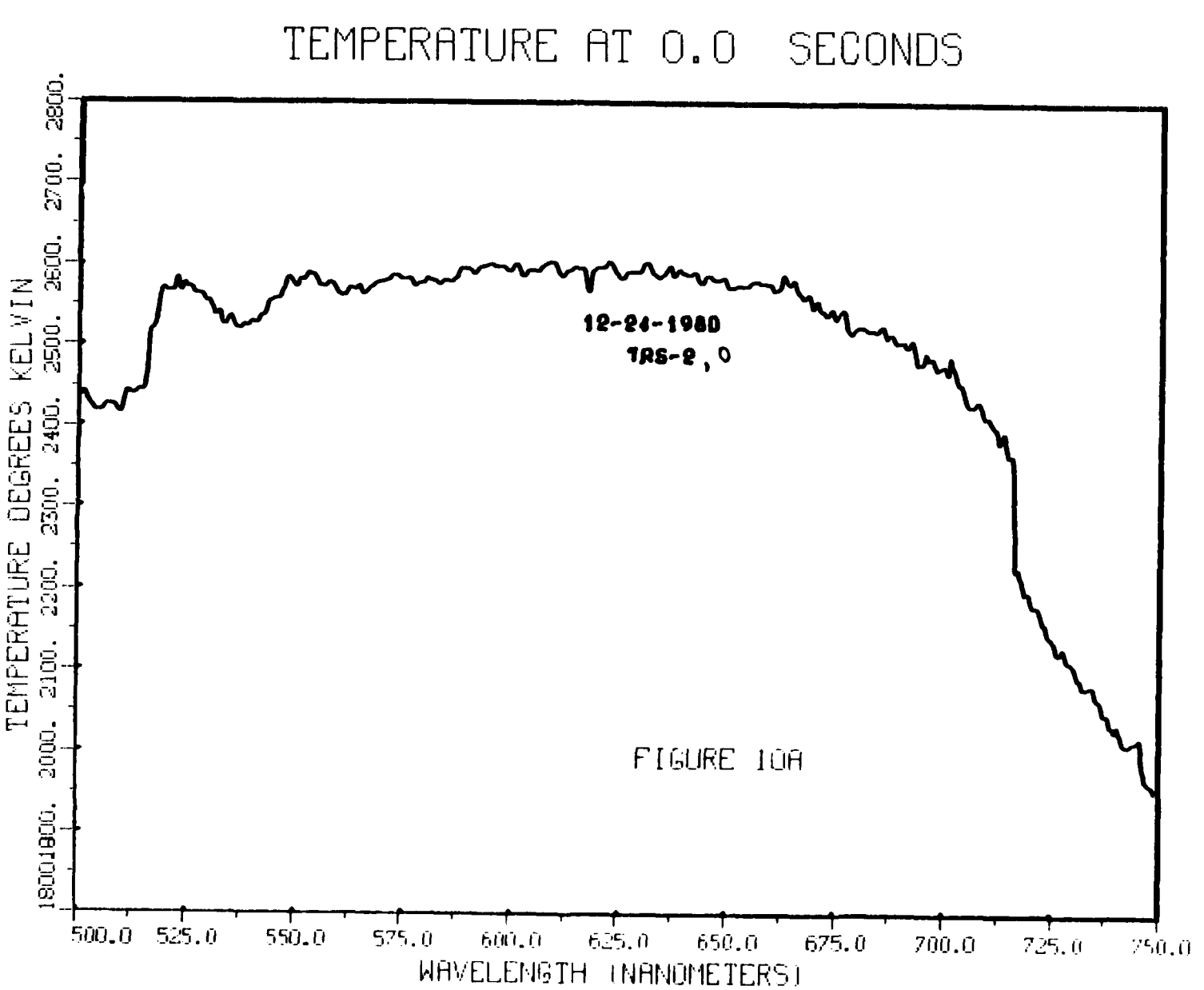
TEMPERATURE AT 0.0 SECONDS
TEMPERATURE DEGREES KELVIN
1800 1900. 2000. 2100. 2200. 2300. 2400. 2500. 2600. 2700. 2800.
12-24-1980
TRS-2, 0
500.0 525.0 550.0 575.0 600.0 625.0 650.0 675.0 700.0 725.0 750.0
WAVELENGTH (NANOMETERS)

FIGURE 10A

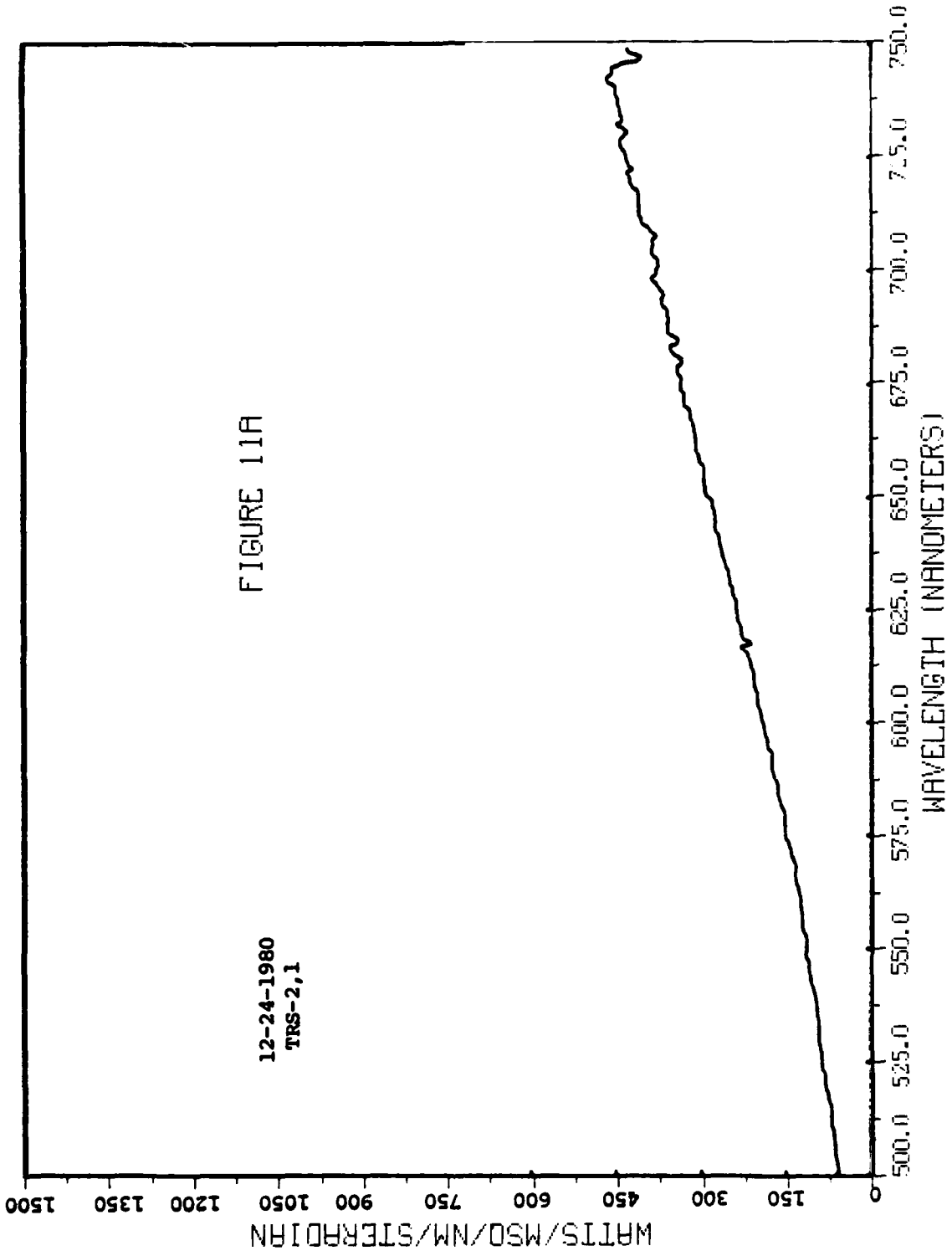
SPECTRAL POWER AT 0.25 SECONDS
FIGURE 11A
12-24-1980
TRS-2,1
WATTS/MSQ/NM/STERADIAN
0
150
300
450
600
750
900
1050
1200
1350
1500
500.0
525.0
550.0
575.0
600.0
625.0
650.0
675.0
700.0
725.0
750.0
WAVELENGTH (NANOMETERS)

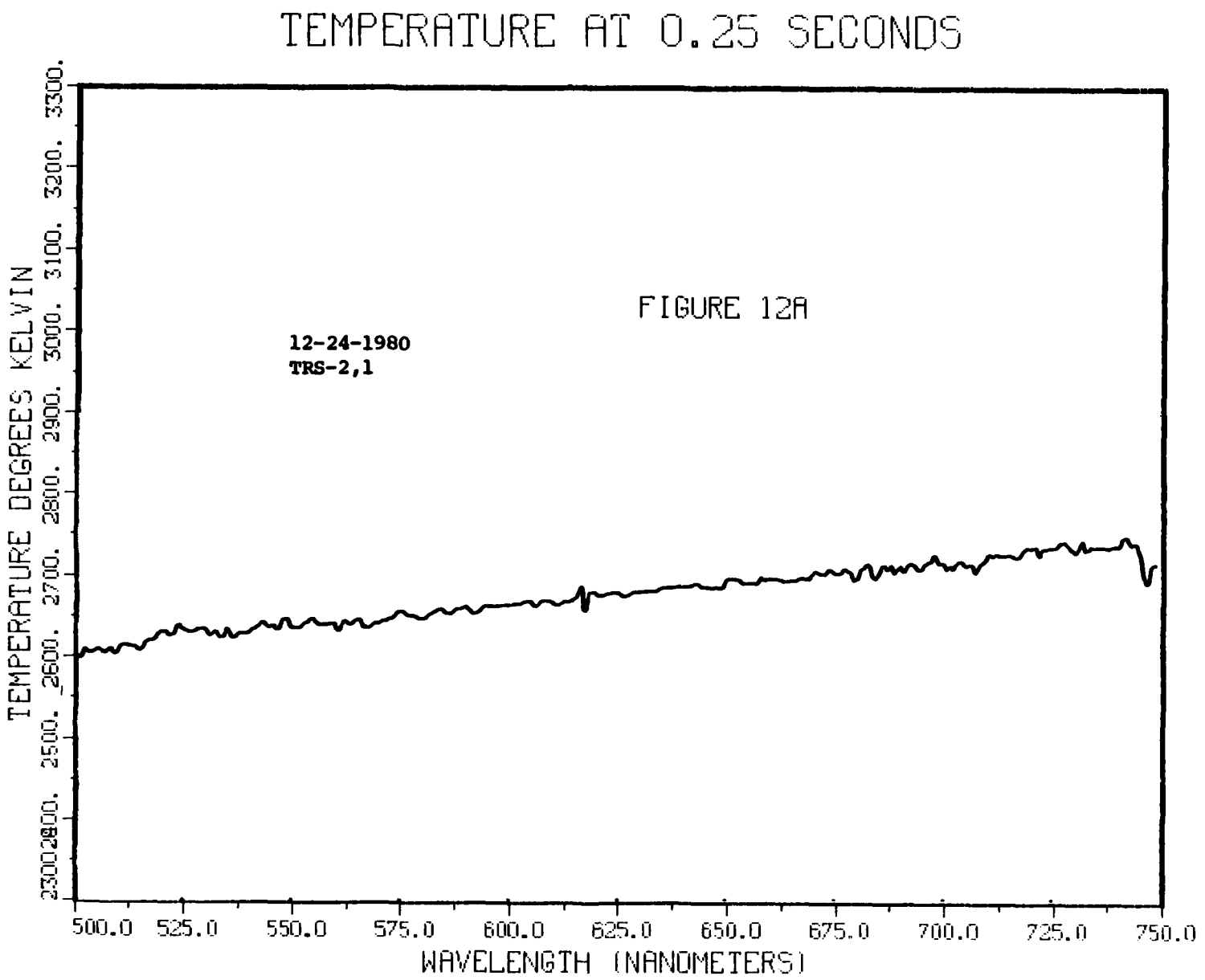
TEMPERATURE AT 0.25 SECONDS
FIGURE 12A
12-24-1980
TRS-2,1
TEMPERATURE DEGREES KELVIN
2300. 2400. 2500. 2600. 2700. 2800. 2900. 3000. 3100. 3200. 3300.
500.0 525.0 550.0 575.0 600.0 625.0 650.0 675.0 700.0 725.0 750.0
WAVELENGTH (NANOMETERS)

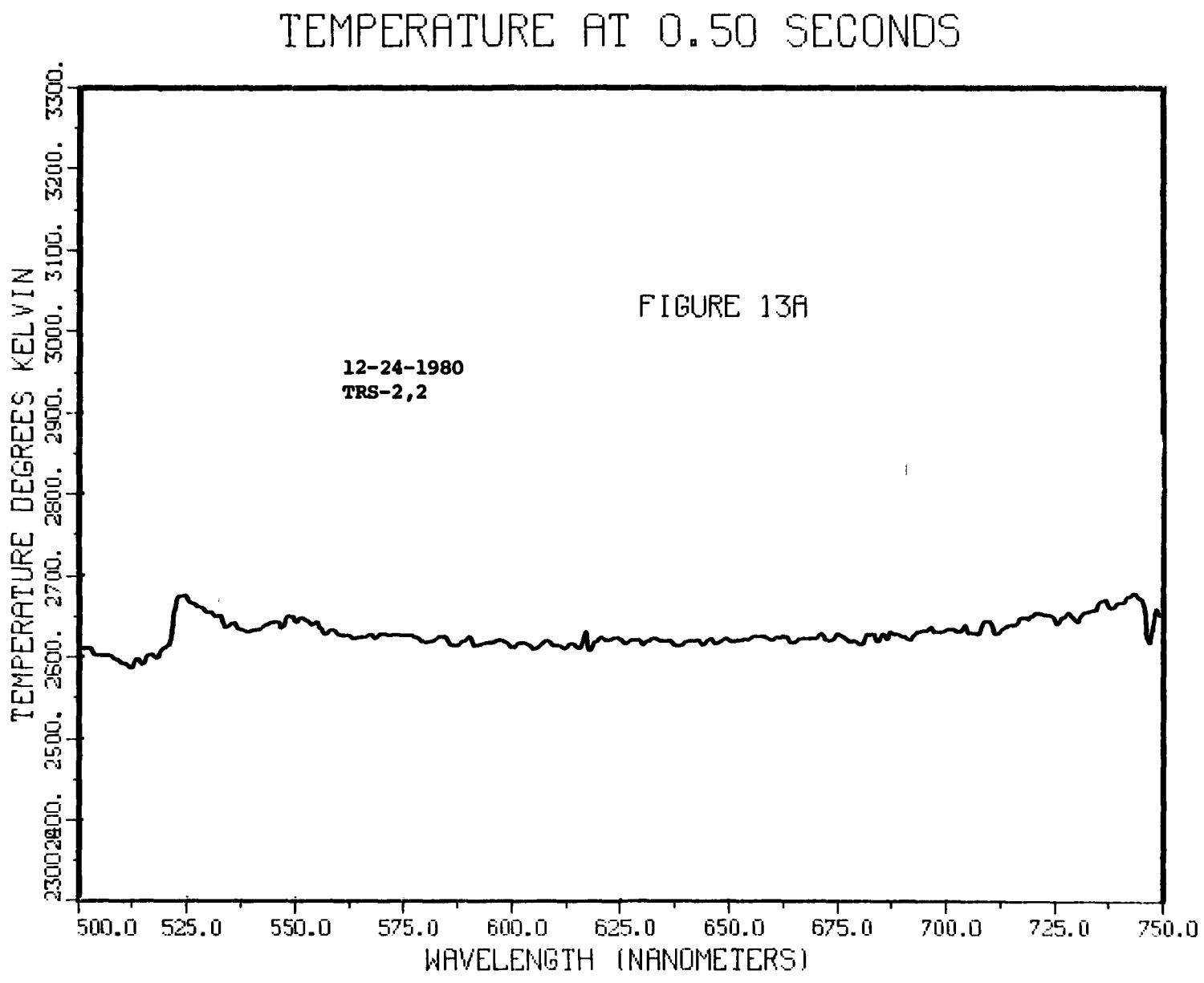
TEMPERATURE AT 0.50 SECONDS
TEMPERATURE DEGREES KELVIN
2300. 2400. 2500. 2600. 2700. 2800. 2900. 3000. 3100. 3200. 3300.
FIGURE 13A
12-24-1980
TRS-2,2
500.0 525.0 550.0 575.0 600.0 625.0 650.0 675.0 700.0 725.0 750.0
WAVELENGTH (NANOMETERS)

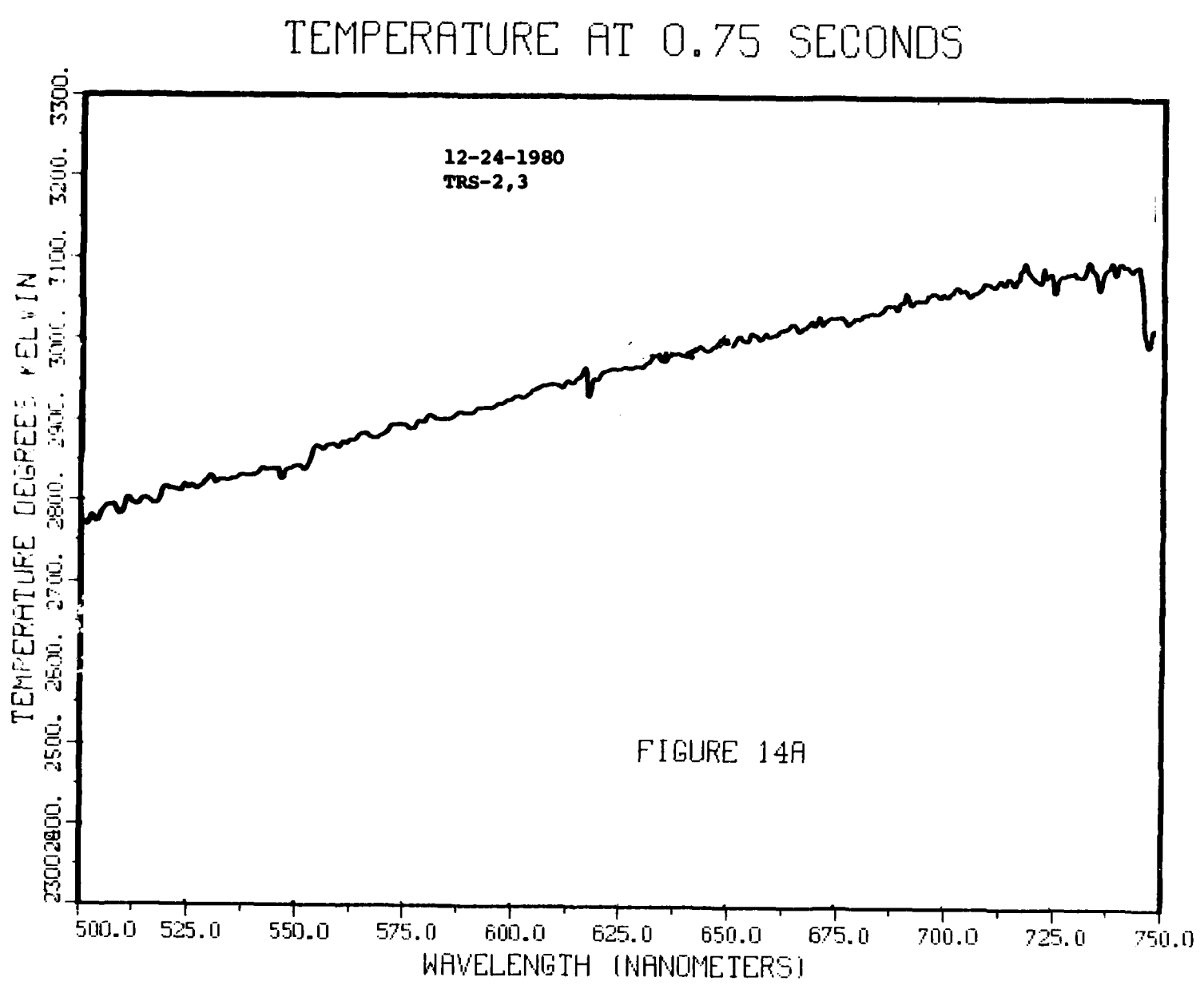
TEMPERATURE AT 0.75 SECONDS
12-24-1980
TRS-2,3
TEMPERATURE DEGREES KELVIN
2300. 2400. 2500. 2600. 2700. 2800. 2900. 3000. 3100. 3200. 3300.
500.0 525.0 550.0 575.0 600.0 625.0 650.0 675.0 700.0 725.0 750.0
WAVELENGTH (NANOMETERS)

FIGURE 14A

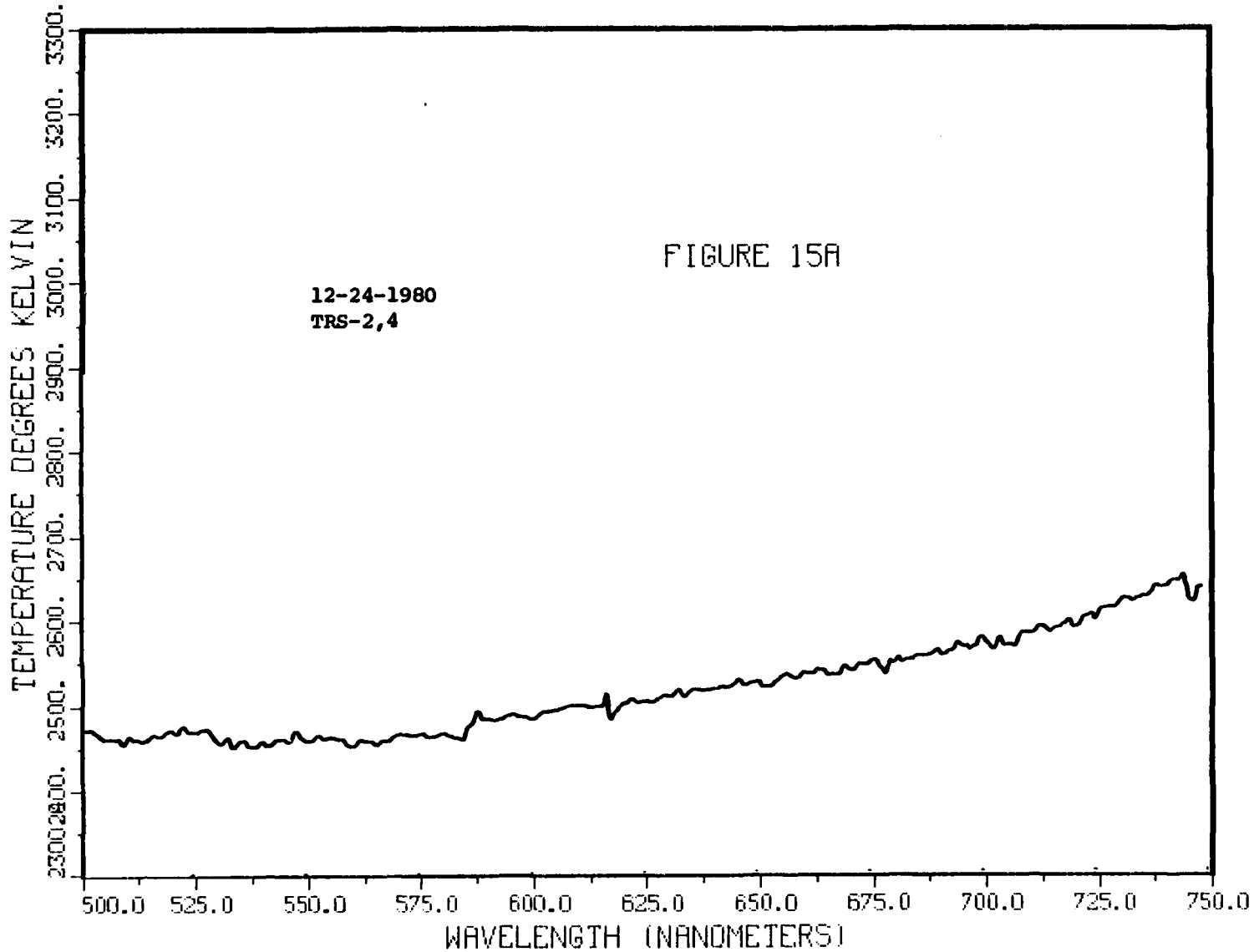
TEMPERATURE AT 1.00 SECONDS
FIGURE 15A
12-24-1980
TRS-2,4
TEMPERATURE DEGREES KELVIN
2300. 2400. 2500. 2600. 2700. 2800. 2900. 3000. 3100. 3200. 3300.
500.0 525.0 550.0 575.0 600.0 625.0 650.0 675.0 700.0 725.0 750.0
WAVELENGTH (NANOMETERS)

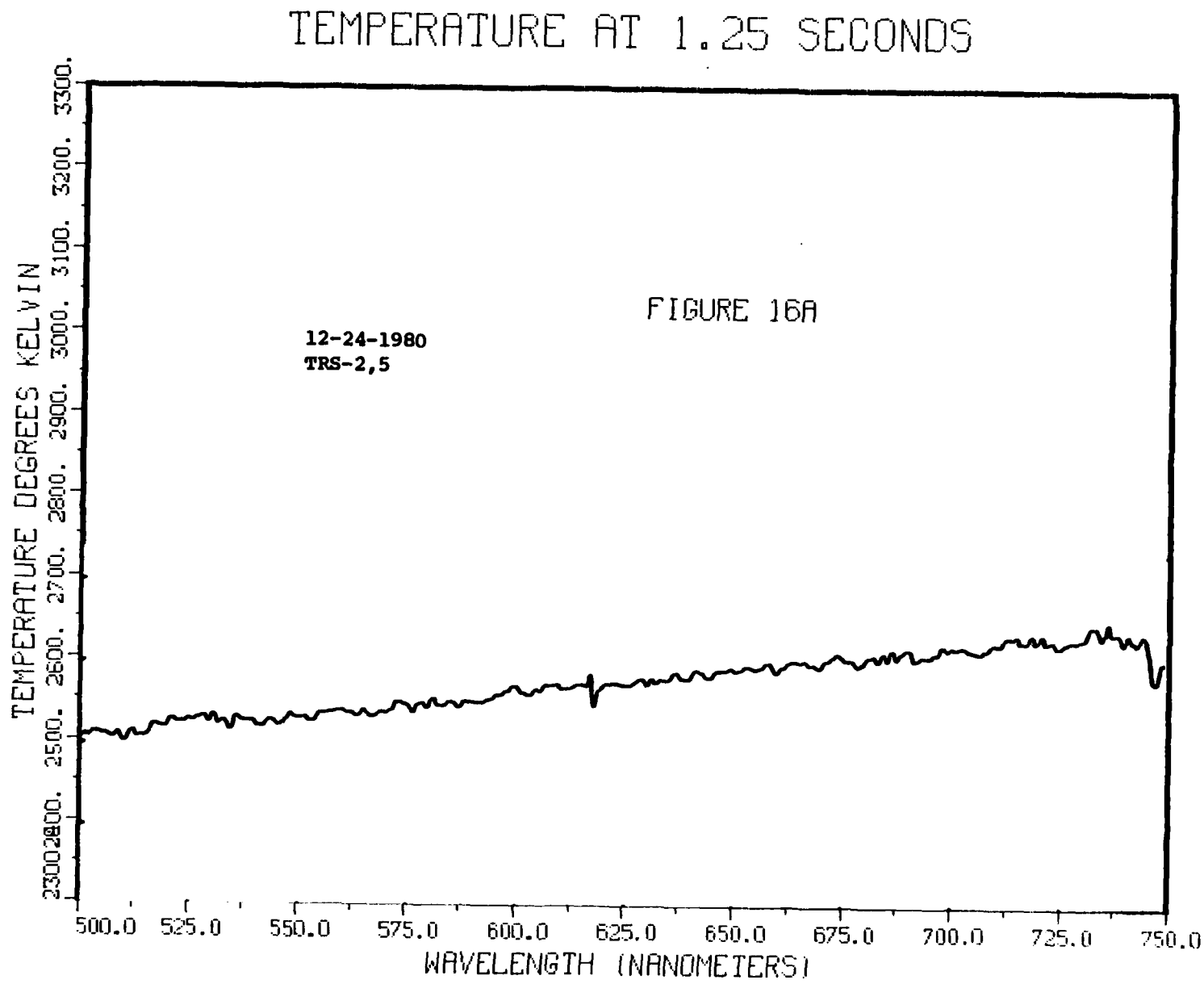
TEMPERATURE AT 1.25 SECONDS
FIGURE 16A
12-24-1980
TRS-2,5
TEMPERATURE DEGREES KELVIN
2300. 2400. 2500. 2600. 2700. 2800. 2900. 3000. 3100. 3200. 3300.
500.0 525.0 550.0 575.0 600.0 625.0 650.0 675.0 700.0 725.0 750.0
WAVELENGTH (NANOMETERS)

FIGURE 17A

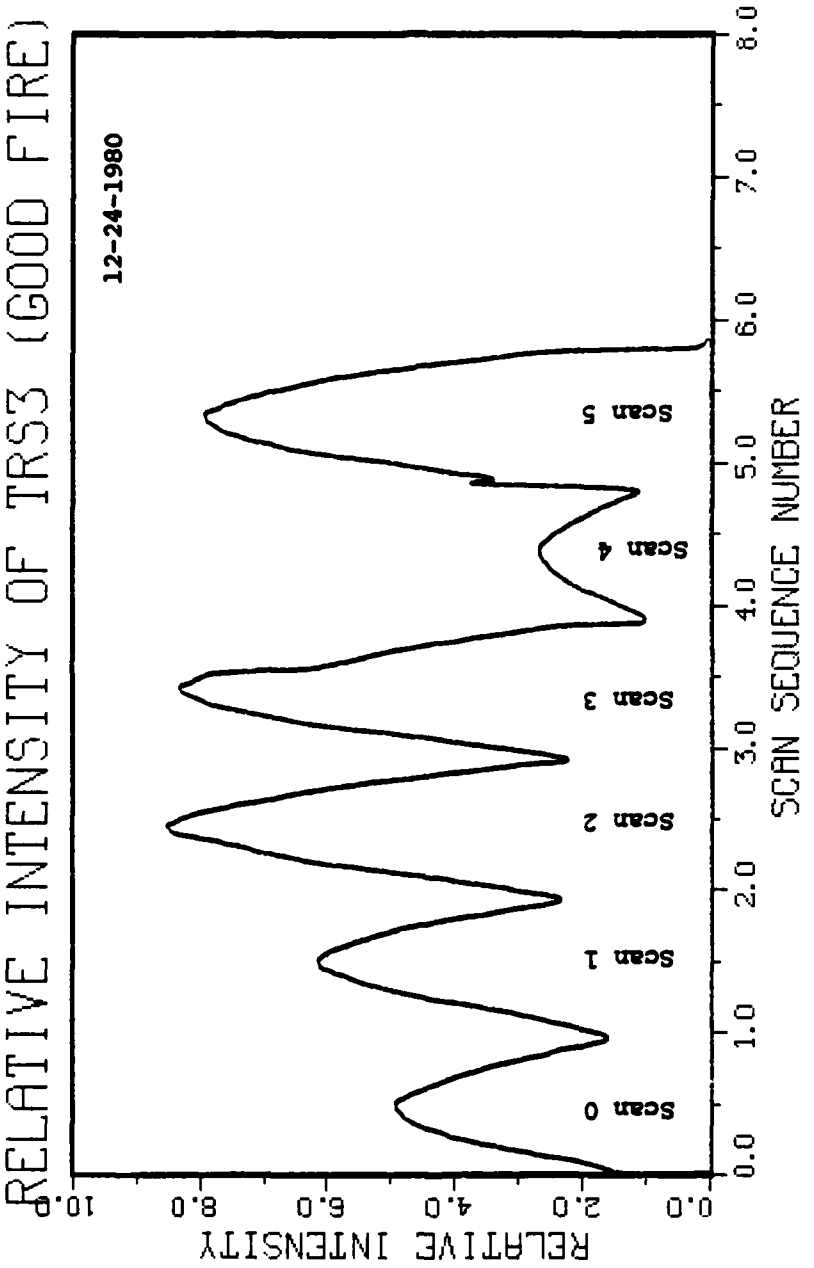
RELATIVE INTENSITY OF TRS3 (GOOD FIRE)
12-24-1980
Scan 0
Scan 1
Scan 2
Scan 3
Scan 4
Scan 5
RELATIVE INTENSITY
0.0
2.0
4.0
6.0
8.0
10.0
SCAN SEQUENCE NUMBER
0.0
1.0
2.0
3.0
4.0
5.0
6.0
7.0
8.0

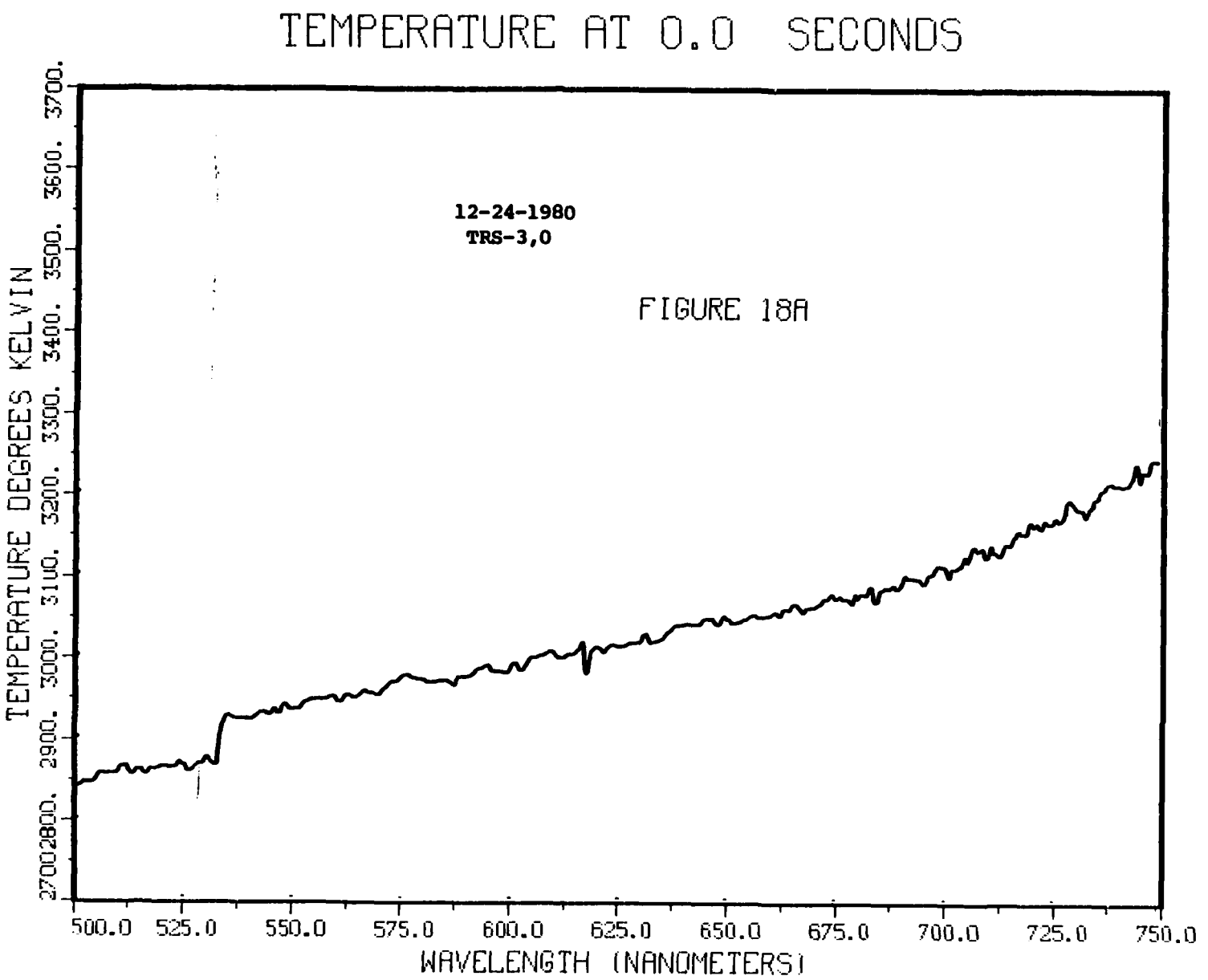
TEMPERATURE AT 0.0 SECONDS
12-24-1980
TRS-3,0
FIGURE 18A
TEMPERATURE DEGREES KELVIN
2700 2800. 2900. 3000. 3100. 3200. 3300. 3400. 3500. 3600. 3700.
500.0 525.0 550.0 575.0 600.0 625.0 650.0 675.0 700.0 725.0 750.0
WAVELENGTH (NANOMETERS)

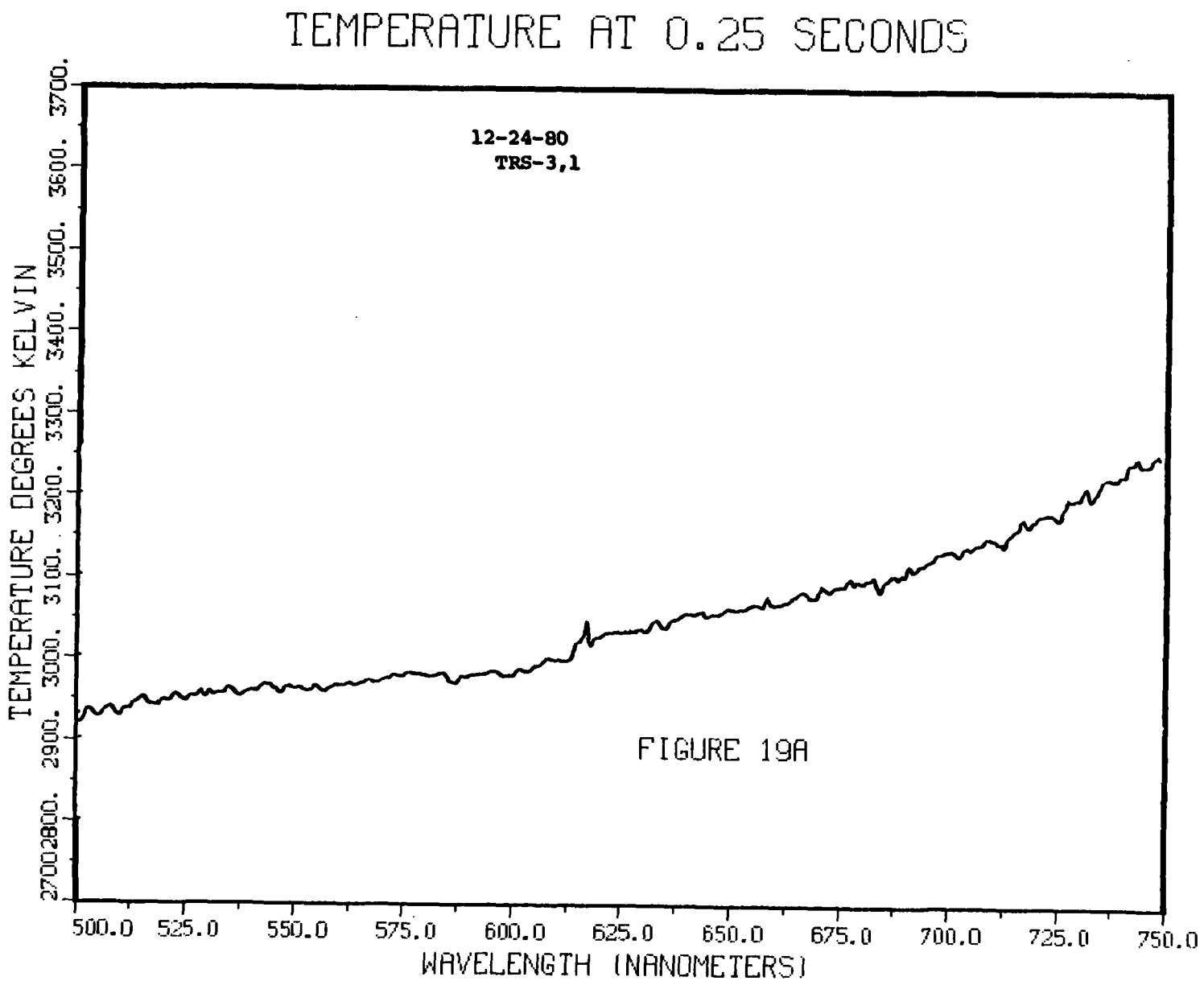
TEMPERATURE AT 0.25 SECONDS
12-24-80
TRS-3,1
TEMPERATURE DEGREES KELVIN
2700
2800.
2900.
3000.
3100.
3200.
3300.
3400.
3500.
3600.
3700.
500.0
525.0
550.0
575.0
600.0
625.0
650.0
675.0
700.0
725.0
750.0
WAVELENGTH (NANOMETERS)

FIGURE 19A

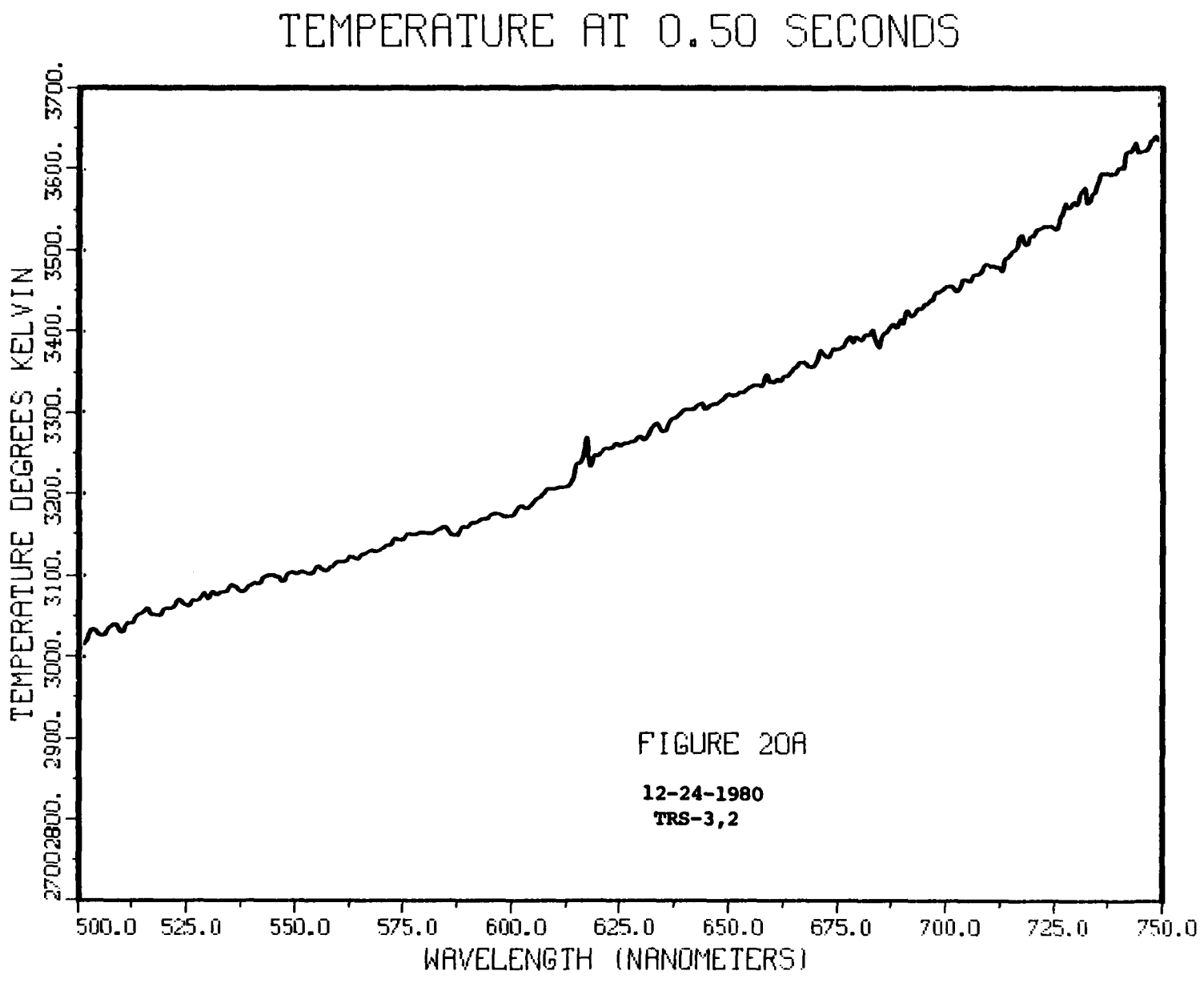


FIGURE 20A

12-24-1980
TRS-3,2

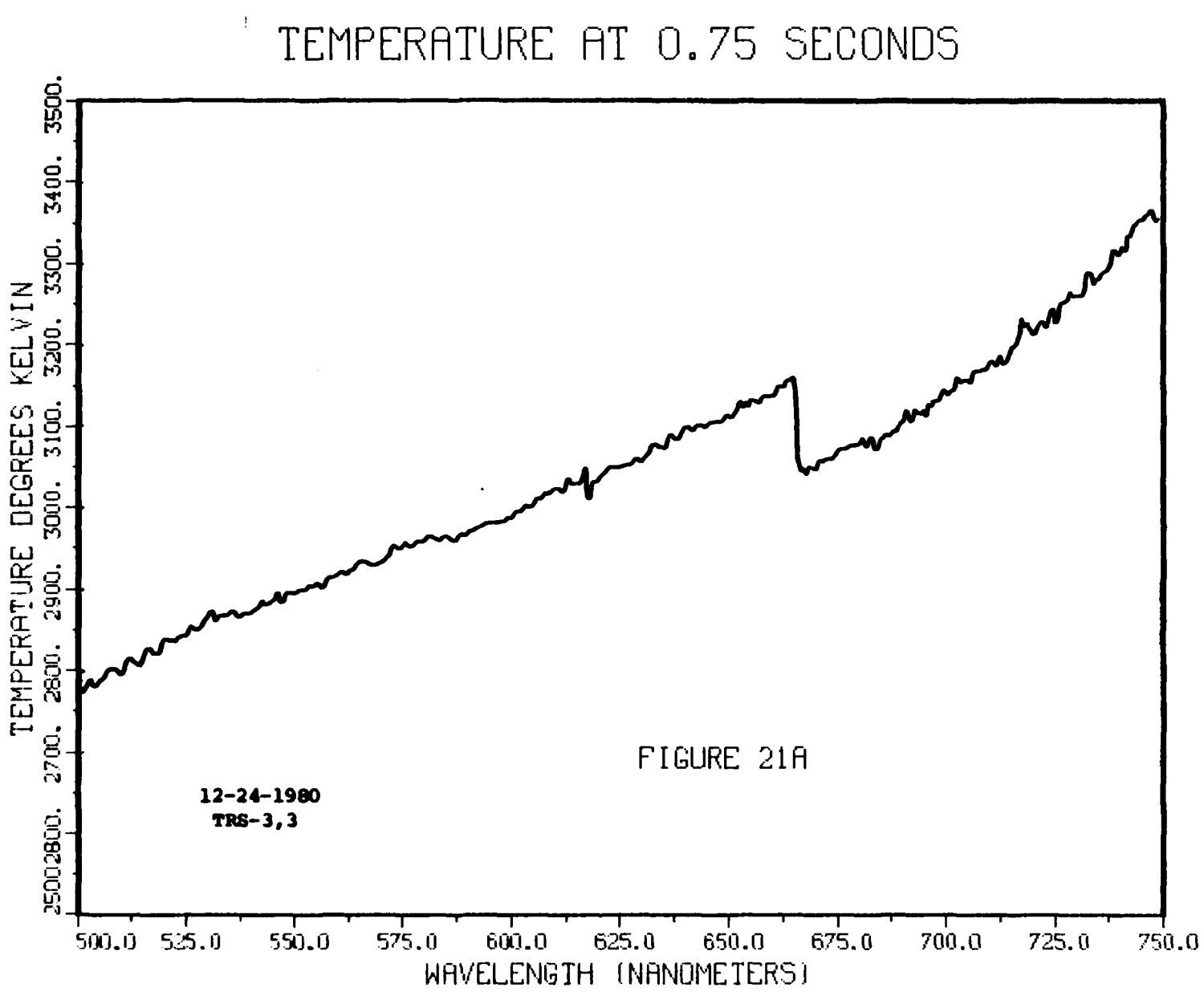
TEMPERATURE AT 0.75 SECONDS
TEMPERATURE DEGREES KELVIN
2500 2800. 2700. 2800. 2900. 3000. 3100. 3200. 3300. 3400. 3500.
500.0 525.0 550.0 575.0 600.0 625.0 650.0 675.0 700.0 725.0 750.0
WAVELENGTH (NANOMETERS)
12-24-1980
TRS-3,3

FIGURE 21A

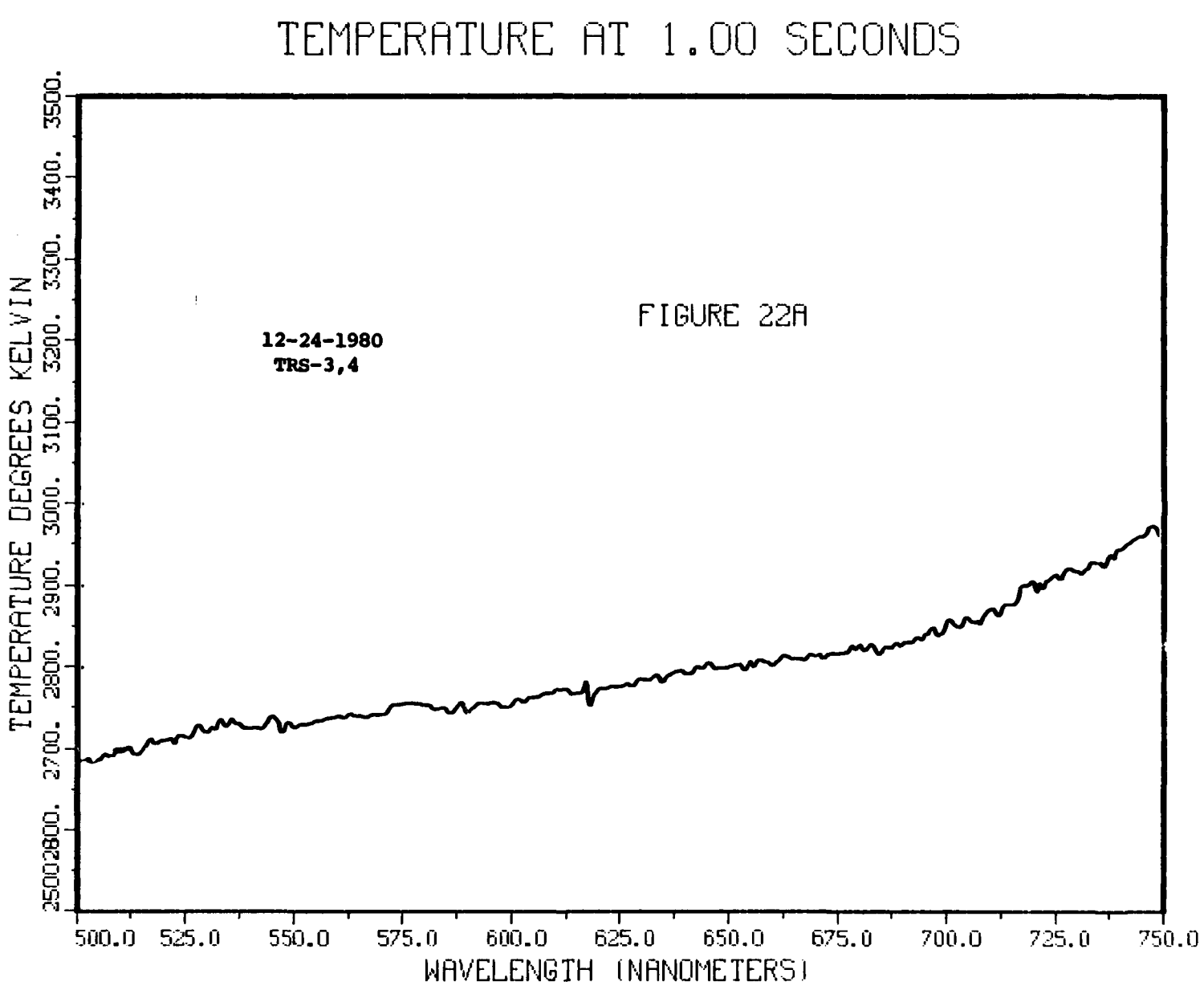
TEMPERATURE AT 1.00 SECONDS
FIGURE 22A
12-24-1980
TRS-3,4
TEMPERATURE DEGREES KELVIN
2500 2800. 2700. 2800. 2900. 3000. 3100. 3200. 3300. 3400. 3500.
500.0 525.0 550.0 575.0 600.0 625.0 650.0 675.0 700.0 725.0 750.0
WAVELENGTH (NANOMETERS)

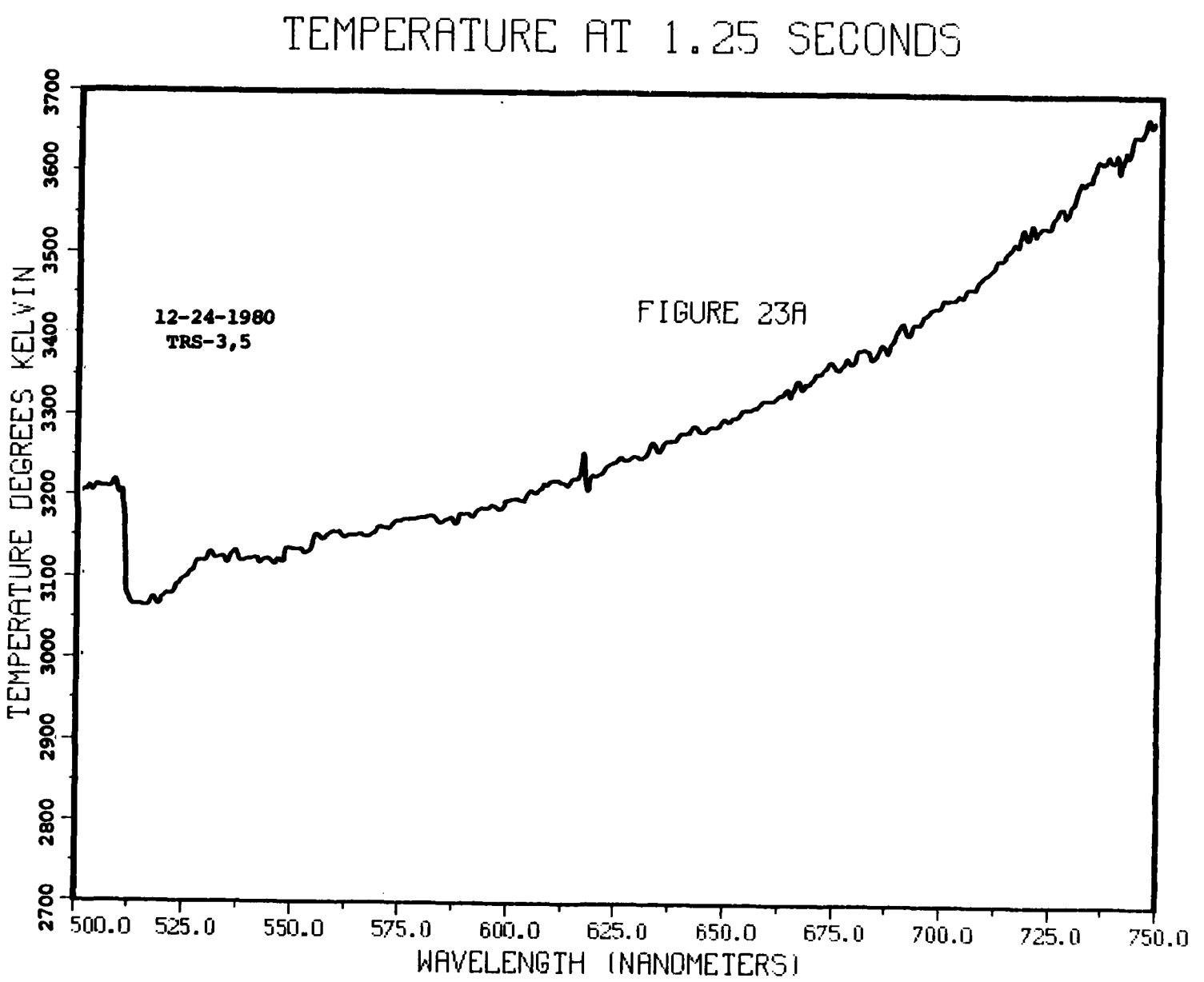
TEMPERATURE AT 1.25 SECONDS
12-24-1980
TRS-3,5
FIGURE 23A
TEMPERATURE DEGREES KELVIN
2700
2800
2900
3000
3100
3200
3300
3400
3500
3600
3700
500.0
525.0
550.0
575.0
600.0
625.0
650.0
675.0
700.0
725.0
750.0
WAVELENGTH (NANOMETERS)

FIGURE 24A. Ignited Single LOX TRS Source

# DISTRIBUTION LIST

DEPARTMENT OF DEFENSE

Defense Nuclear Agcy
ATTN: SPSS, G. Ullrich
ATTN: SPSS, T. Deevy
4 cy ATTN: TITL

Defense Tech Info Ctr
12 cy ATTN: DD

Under Secretary of Defense For Rsch & Engrg
ATTN: Strat & Space Sys (OS)

DEPARTMENT OF THE ARMY

BMD Systems Cmd
ATTN: BMDSC-HW
ATTN: BMDSC-HLE, R. Webb

USA Ballistic Rsch Labs
ATTN: ORDAR-BLT, J. Keefer
ATTN: ORDAR-BLA-S

DEPARTMENT OF THE AIR FORCE

Air Force Wpns Lab
ATTN: NTEO
ATTN: NTE, M. Plamondon
ATTN: NTES-S
ATTN: NTED-I
ATTN: NTED-A
ATTN: NTES-G
ATTN: SUL

Ballistic Missile Office
ATTN: ENSN, E. Furbee

DEPARTMENT OF ENERGY CONTRACTOR

Los Alamos National Lab
ATTN: M. Sanford
ATTN: R. Whittaker

DEPARTMENT OF DEFENSE CONTRACTORS

Acurex Corp
ATTN: C. Wolf

Aerospace Corp
ATTN: Tech Info Svcs
ATTN: H. Mirels

California Rsch & Tech, Inc
ATTN: Library
ATTN: M. Rosenblatt

University of Denver
ATTN: Sec Ofcr for J. Wisotski

Information Science, Inc
4 cy ATTN: W. Dudziak
4 cy ATTN: P. Lad

DEPARTMENT OF DEFENSE CONTRACTORS (Continued)

Kaman AviDyne
ATTN: R. Ruetenik

Kaman Sciences Corp
ATTN: D. Sachs

Kaman Tempo
ATTN: DASIAC

Kaman Tempo
ATTN: DASIAC

McDonnell Douglas Corp
ATTN: R. Halprin
ATTN: D. Dean
ATTN: H. Herdman

Pacific-Sierra Rsch Corp
ATTN: H. Brode, Chairman SAGE

R&D Assoc
ATTN: Tech Info Ctr
ATTN: J. Carpenter
ATTN: A. Kuhl
ATTN: P. Haas

S-CUBED
ATTN: C. Needham

S-CUBED
ATTN: J. Barthel
ATTN: Library
ATTN: K. Pyatt

Science & Engrg Assoc, Inc
ATTN: B. Chambers, III

Science Applications, Inc
ATTN: J. Cockayne
ATTN: W. Layson

Science Applications, Inc
ATTN: J. Dishon

SRI International
ATTN: G. Abrahamson
ATTN: Library
ATTN: J. Colton

TRW Electronics & Defense Sector
ATTN: T. Mazzola
ATTN: N. Lipner
ATTN: Tech Info Ctr

TRW Electronics & Defense Sector
ATTN: E. Wong
ATTN: G. Hulcher

H-Tech Labs, Inc
ATTN: B. Hartenbaum

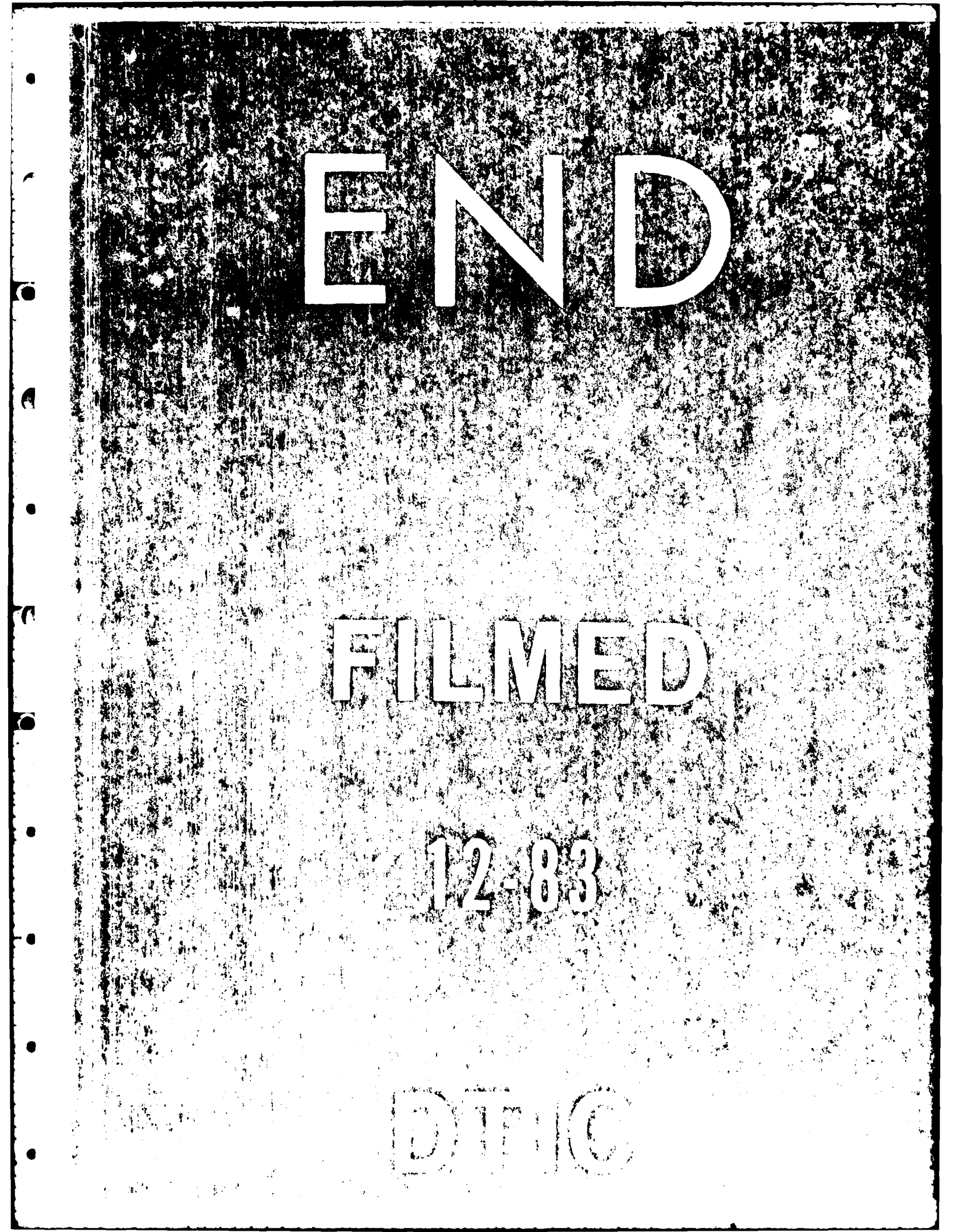
END
FILMED
12-83
DTIC